AN ABSTRACT OF THE THESIS OF

Frederick G. Thrall for the degree of Doctor of Philosophy

in Civil Engineering presented on May 1, 1981

Title: GEOTECHNICAL SIGNIFICANCE OF POORLY CRYSTALLINE SOILS DERIVED FROM VOLCANIC ASH

Redacted for Privacy

Abstract approved: J. R. Boll

Poorly crystalline soils derived from volcanic ash under moist climatic conditions develop unique engineering properties which significantly depend on their weathering and drying histories. These soils occur in many areas of the world associated with volcanic activity. Though volcanic ash soils have been related to engineering problems in Alaska, Hawaii, and Oregon, their presence has largely been ignored by the engineering profession.

Sampling of disturbed and undisturbed specimens from specific sites in Oregon and Alaska was conducted. These samples were studied using electron microscopy, infrared spectroscopy, and X-ray diffraction analysis to determine mineralogical and structural composition. Atterberg limits, moisture-density characteristics, specific gravity, grain size and strength behavior were investigated. Characterization tests were also conducted on air and oven dried soils to determine irreversible changes which occur with drying.

A literature review oriented to obtain all available geotechnical data on soils derived from volcanic ash is included as an integral part of the study. Geotechnical data, from this review, gathered for volcanic ash soils from around the world, are presented in summary form.

Correlations between engineering and index properties for poorly crystalline soils derived from volcanic ash are investigated for the combined literature and laboratory studies. A guide which geotechnical engineers can use to recognize these soils in the field is proposed.

Results indicate that engineering and index properties can be divided into three statistically separate groups which may be distinguished by specific physical characteristics such as color, mineral content, and drying history. Correlation studies show that values for effective angle of internal friction (ϕ'), undrained shear strength (c), and compression index (Cc) can best be estimated from insitu void ratio (e_o) as the predictor property.

The major difference in engineering behavior between crystalline soils and poorly crystalline soils derived from volcanic ash results from the presence of saturated amorphous materials within the soil matrix. These materials appear to have an unusual distribution of small pores within their structure which make them sensitive to remolding and/or drying.

Geotechnical Significance of Poorly Crystalline Soils Derived from Volcanic Ash

by

F. G. Thrall

A THESIS

submitted to

Oregon State University

in partial fulfillment of
the requirements for the
degree of

Doctor of Philosophy

June 1981

APPROVED:

Redacted for Privacy

Professor of Civil Engineering
in charge of major

Redacted for Privacy

Head of Department of Civil Engineering

Redacted for Privacy

Dean of Graduate School

Date thesis is presented May 1, 1981

Typed by Lyndalu Sikes for F. G. Thrail

ACKNOWLEDGEMENTS

I would like to thank Dr. W. L. Schroeder for help in financing this project, Dr. Benno Warkentin for providing his much needed expertice, and in particular, my major professor Dr. J. R. Bell, for seeing me through from beginning to end.

Special thanks are due to Lyndalu Sikes who re-typed the manuscript over a period of three days to meet my graduation deadline.

TABLE OF CONTENTS

Table of Contents (Continued)

Table of Contents (Continued)

Table of Contents (Continued)

LIST OF FIGURES

List of Figures (Continued)

List of Figures (Continued)

List of Figures (Continued)

List of Figures (Continued)

List of Figures (Continued)

LIST OF TABLES

List of Tables (Continued)

List of Tables (Continued)

GEOTECHNICAL SIGNIFICANCE OF POORLY CRYSTALLINE SOILS DERIVED FROM VOLCANIC ASH

I. INTRODUCTION

Engineering problems of soils derived from volcanic ash have puzzled geotechnical engineers for many years. Terzaghi (1958) in his report on the "Design and Performance of the Sasumua Dam," Africa, investigated the special properties of these soils. He states: "The unusual properties of the soils gave rise to doubts as to whether or not the soils could be used safely as a constructional material for the bulk of an earth dam." Near Hilo, Hawaii, Hirashima (1948) described problems in roadbuilding on these materials. He states: "In the natural state they possess the stable properties of a solid although the moisture contents are in excess of the liquid limit and many times in excess of the plastic limit. When remolded by construction traffic these soils become plastic or even semi-liquid." After a period as short as 1 day, these soils harden enough to support construction traffic until remolding again liquifies the soil.

A few investigators have more recently documented engineering problems with soils derived from volcanic ash. At Oregon State University, soil scientists have shown that the presence of landslides in the Cascade Mountains is associated with the presence of volcanic

ash soils. Numerous engineering problems have been reported for volcanic ash soils in Southeast Alaska. Landslides are prevalent and the soil liquifies when disturbed creating severe problems in hauling and placing excavated materials. Difficulty in pioneering roads by conventional methods have also been reported (Hirashima, 1951; Personal Communication, J. R. Bell). Landslides in New Zealand have been attributed to the presence of these materials (Fred Swanson, Personal Communication). Pope and Anderson (1960) say of the volcanic soils of the Pacific Northwest Cascade Mountain Range: "Research is needed in order to develop more reliable methods of testing and more economical designs in and of such soils."

Geologically young soils derived from volcanic ash parent material are commonly found to contain a confusing, ill-defined array of poorly crystalline clay minerals including mixtures of poorly formed halloysite or kaolinite, bundles of small diameter (10-20 A) imogolite tubes, conglomerates of small diameter (35-55 A) spherical allophane, and masses of gel-like amorphous materials. The soils may contain any one or all of these constituents plus well-formed crystalline clay and non-clay minerals as well.

Among soils derived from volcanic ash, those containing significant amounts of allophane or imogolite seem to present the most difficult problems in geotechnical engineering. Although the presence of allophane or imogolite in a particular soil mixture might

be inferred by clues given from various physical and chemical tests, their complex association with other poorly formed gels or amorphous minerals, precludes easy identification. Soils containing allophane and/or imogolite are generally referred to simply as allophane soils. This practice is followed in this report.

Allophane soils usually have very high natural water contents, high liquid limits and plastic limits, and low plastic indices and plot below the A-line on the Casagrande Plasticity Chart. These soils exhibit an irreversible loss in plasticity upon drying. Allophane soils also show a large irreversible volume decrease upon drying (Maeda, et al., 1977; Yong and Warkentin, 1966; Gradwell and Birrell, 1954). Further, these soils show different moisture density curves before and after drying. The position of the moisture density curves depend upon the initial water content and the amount of remolding produced during testing. Optimum water contents for these soils are usually below natural water contents (Newill, 1961; Willis, 1946; Hirashima, 1948). Particle size determinations for most poorly crystalline volcanic ash soils are almost always unreliable. Investigators have reported that grain size depends heavily upon treatment of the soil before and during testing (Birrell, 1966).

Apparent overconsolidation pressures commonly exceed insitu pressures even though evidence suggests no overburden pressures

have been applied. In most cases a wet climate suggests dessication has not taken place. Apparent overconsolidation is probably due to cemented bonds between the particles (Wallace, 1973).

Water content is not reliable indication of the stress history of a deposit. Gradwell and Birrell (1954) state that the compression index for most samples appears to vary less than the liquid limit so that the usual correlation between compression index and liquid limit (Terzaghi and Peck, 1967) is not valid. Compressibility tests have shown that laboratory results tend to underestimate field compression (Matyas, 1969).

Poorly crystalline soils derived from volcanic ash are, as a consequence of formation, residual soils. Thus, when characterizing geotechnical properties such as strength or compressibility, mode of formation must be taken into account.

Mitchell (1976) states that when crystalline soils are weathered in-place, the resulting texture and fabric is much like that of the parent materials. Soils derived from volcanic ash also develop features of parent ash materials. Volcanic ash as a parent material is uniquely different from crystalline parent materials in that each ash grain is loose, very fine, and occurs as an uncrystalized fragment at the time of eruption. Each particle has a large portion of surface area exposed to weathering solutions. Volcanic ash deposits

are very porous from top to bottom, permeability is high, and weathering progresses to the deep stratum in a short period of time.

It is easy to imagine that a soil with unusual properties might result from the weathering of parent materials which are radically different than their crystalline counterparts.

Allophane soils are common in many deposits which geotechnical engineers might encounter during site investigation. These soils characteristically have a greasy-waxy feel. When disturbed they release large amounts of water, and when dried show significant irreversable changes.

Soils derived from volcanic ash have often times been referred to simply as halloysites in the geotechnical literature. This characterization is not entirely incorrect since halloysite has been shown to occur with non-crystalline components. However, the effects of other important soil components which may constitute a significant part of minerals suites containing halloysite, have not been acknowledged. The complex nature of soils derived from volcanic ash has not generally been recognized in the engineering literature, possibly because of the many and varied names and definitions which have been applied to these soils.

Residual soils, when encountered under moist climatic conditions, provide a variety of unpredictable behaviors irrespective of mineralogy (Terzaghi and Peck, 1967). Careful study is required

if residual soils are encountered during site investigation. Poorly crystalline components derived from volcanic ash complicate the behavior of the residual soil structure. The complex engineering behavior of allophane soils is relatively unrecognized by geotechnical engineers, and poorly understood by soil scientists.

Available data characterizing the engineering behavior of volcanic ash soils have been derived from a wide variety of testing procedures which may or may not be standard. These varying studies have been conducted on volcanic ash soil deposits from many parts of the world. In many instances overall mineralogical composition and engineering character have not been investigated in a uniform manner. Thus, there is a need to summarize the results of geotechnical testing reported in the literature so that systematic analysis can be performed.

Objectives

The purposes of this study are to summarize reported mineralogical and engineering results from all parts of the world, and to study these materials in the field and laboratory by combining mineralogical data with conventional soil engineering testing.

The specific objectives of this research are to:

1. Report the existence and special properties of poorly crystalline volcanic ash soils in terms familiar to geotechnical engineers.

2. Formulate a guide, based on engineering behavior, with which the soils engineer can easily recognize soils which might contain significant amounts of poorly crystalline (allophanic) material.
3. Identify the effects of certain physical-chemical properties on the engineering properties of poorly crystalline volcanic ash soils so that these engineering properties may be more readily understood.
4. Determine what effects the presence of poorly crystalline soils derived from volcanic ash has on correlations with typical index properties used for crystalline soils.

Scope

The geotechnical properties of non-crystalline soils have not, in general, been studied by the engineering profession, and soil scientists have only made a few studies of limited engineering index properties. Therefore, this investigation first develops a broad based overview of these materials and their engineering properties to provide a basis for more detailed studies. Second, detailed mineralogical information is combined with soil engineering material behavior. Finally, since volcanic ash soils of the United States have not been systematically investigated, this study provides data on selected United States soils.

This report is composed of five parts as follows:

Phase I - Literature Review

A review of all available published and unpublished geotechnical data on soils derived from volcanic ash is included as an integral part of the study. From this review, geotechnical data, gathered for volcanic ash soils from around the world, are presented in summary form. This review also includes a report on the mineralogical composition, chemical and physical behavior, and structure of soils derived from volcanic ash.

Phase II - Field and Laboratory Study Results

This phase provides additional data on soils derived from volcanic ash from the northwestern United States and Alaska. This includes the sampling of disturbed and undisturbed specimens from specific areas in Oregon and Alaska.

All samples were analyzed using electron microscopy, X-ray diffraction, and infrared spectroscopy to determine mineral composition and structural arrangement. Engineering characterization tests were conducted to determine Atterberg limits, moisture density relationships, grain size, and strength behavior. Several tests were also performed to determine percentage and presence of allophane.

Phase III - Organization of Data from Literature Review and Laboratory Study

Data from the literature search and laboratory study are summarized and cataloged to show trends, similarities or differences among soil samples.

Phase IV - Correlation Among Geotechnical Properties

Correlations among the index properties for these soils are developed. Examples are the possible relationships that might exist between liquidity index and sensitivity or compression index and void ratio, for soils derived from volcanic ash.

The majority of correlations are constructed using regression analysis. The resulting correlations for non-crystalline volcanic ash soils are compared to the usual correlations for crystalline soils.

Phase V - Guide for Geotechnical Engineers

An identification method is presented for use by geotechnical engineers to identify and characterize volcanic ash soils.

II. BACKGROUND

Definition of Materials

Soil allophane through the years has been assigned a number of definitions in the soil science literature. Each succeeding definition has become increasingly specific as more advanced techniques for measuring the physical and chemical properties became available and the level of understanding advanced. However, in the engineering literature, the existence of these poorly crystalline soils has hardly been recognized.

Soils formed from volcanic ash make up a series which ranges from totally amorphous volcanic glass to crystalline clays. The soil constituents which lie between these series end members represent an ill-defined intermediate stage through which many soil types pass during the weathering process on their way to stability and crystalinity.

Soil constituents which are amorphous to X-rays will be termed 'amorphous materials'. Allophane is defined as an amorphous material which has a distinctive hollow spheroidal shape 35-50A in diameter (Wada and Wada, 1977; Fields and Claridge, 1975; Wada and Harward, 1974). Amorphous materials which are bundles of fibers or tubes with approximately 20A separation and 10-20A in

diameter are called imogolite (Yoshinga and Aomine, 1962b; Cradwick, 1972; Wright, 1964). Figures 1a and 1b show typical electron micrographs of allophane and imogolite.

Those amorphous substances intermediate between parent unweathered materials (most likely volcanic ash) and crystalline soils will be termed poorly crystalline soils. Poorly crystalline soils derived from volcanic ash exhibiting the special properties outlined in Chapter I, will be described as having allophanic character. Most natural deposits of weathered volcanic ash soils contain various mixtures of glass, allophane, imogolite, indistinct amorphous inclusions, crystalline, and organic components. Those poorly crystalline soils which contain significant amounts of amorphous materials with allophanic character will be termed allophane soils.

Occurrence

Allophane soils occur abundantly in many parts of the world. They have been reported in Japan, Indonesia, New Zealand, the Phillipines and other Pacific islands, Africa, many countries in Central and South America, Hawaii, and the Northwestern United States, including Alaska. The terminology applied to these soils varies from country to country. In Japan, soils which contain allophane are known as "humic allophane soils" or "andosols". In New Zealand they are referred to as "yellow-brown loams",

"yellow-brown pumice soils", or "alvic" soils. In Chile and Argentina, "trumao" or "allophanic" describes them. In the United States the term "andept" or "andosol" is most commonly applied.

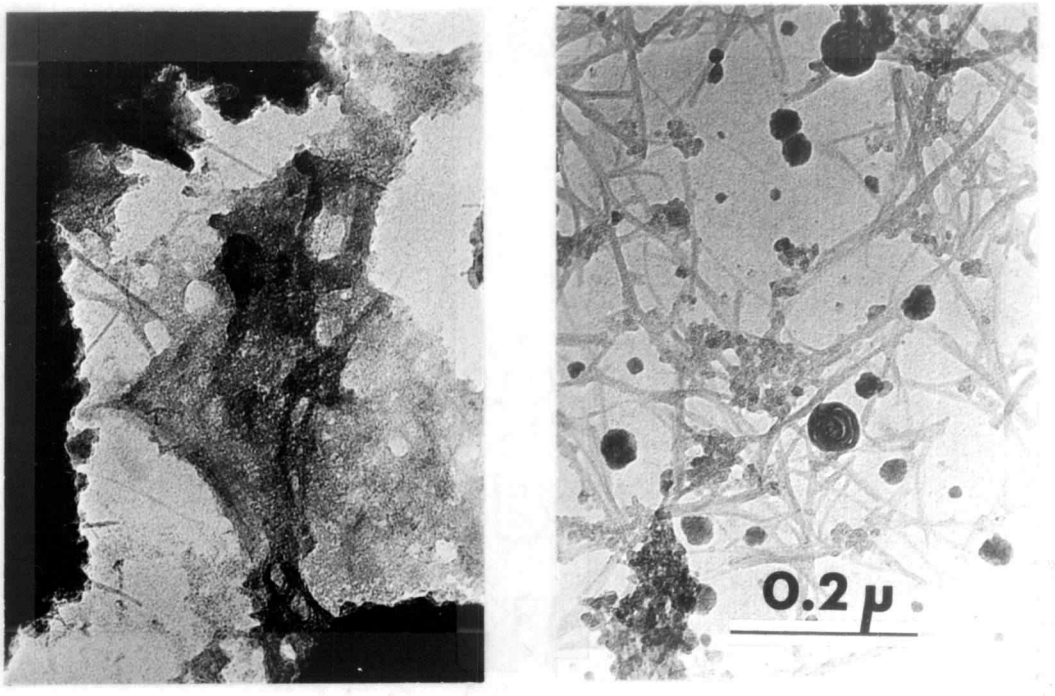

(a) (b)

Figure 1. Electron Micrographs of (a) Allophane from Alaska and (b) Imogolite from Japan. Scale is the same for both photos. (Photos from Moyle Harward, Oregon State University, Department of Soil Science.)

Since allophane soils are primarily formed from weathered volcanic ash deposits, their occurrence is usually associated with active or recently active volcanoes. Figure 2 shows areas of major

distribution for soils derived from volcanic ash.

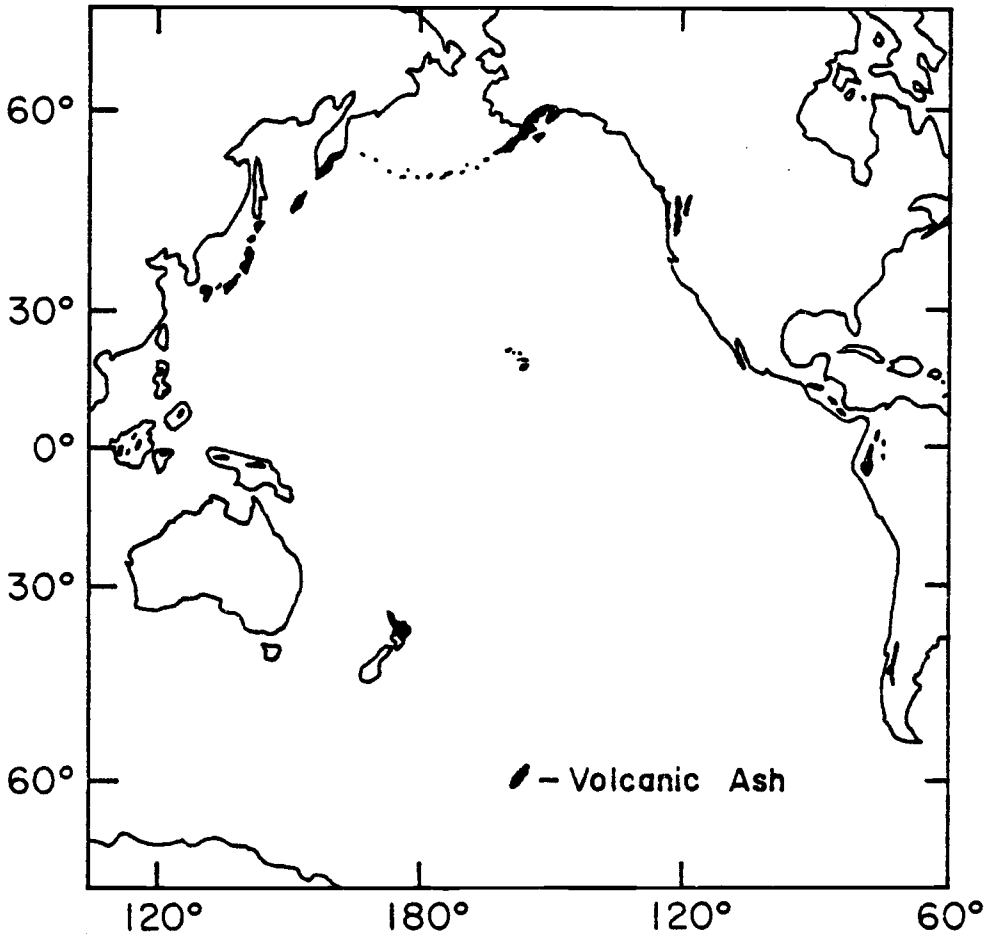

Figure 2. Areas of Major Distribution for Soils Derived from Volcanic Ash (Adopted from Dudal (1964)).

Allophane has been reported in several types of deposits including some of marine or lacustrine origin. On the west coast of the United States, soils containing allophane are usually not pure ash deposits. Some occur in alluvium which contains material eroded from old weathered volcanic ash (Flach, 1964). Soils formed from pure volcanic ash may, however, occur in small

pockets at high altitudes. In New Zealand, volcanic ash soils are described as being spread evenly over an undulating countryside, and are near saturation though above the water table (Gradwell and Birrell, 1954).

In South America (Yong and Warkentin, 1975) and Java, Indonesia (Wesley, 1973), two distinct soils of volcanic origin are described. A yellow-brown soil ("andosol") occurs above elevations of 1000 meters, associated with the temperate climate at those altitudes. A red soil ("latosol") occurs on the lower slopes, from sea level to approximately 1000 meters in elevation. At about the 1000 meter elevation there is a gradual transition from red to yellow-brown soil. The red soil is thought to have higher crystal order and thus, represents a more advanced stage of weathering.

In Hawaii (Hirashima, 1948) and in several South American countries (Flasch, 1964), soils derived from volcanic ash occur both in tropical and semi-arid regions. Ash exposed to great amounts of rainfall weathers to soils much different than the same ash on the leeward slopes which get much less rainfall. Volcanic ash soils occurring in regions of low humidity do not develop the unique features of allophane soils.

Formation

Allophane soils are formed primarily from the weathering of well-drained volcanic ash under conditions of moderate to high rainfall. Several investigators have reported the formation of allophanes from parent materials such as massive basalt in Ireland, massive dunite in New Zealand (Fields and Claridge, 1975), and sedimentary rock from New Zealand (Wada and Harward, 1974). However, Wada and Harward (1974) point out that conclusive evidence has not been found which confirms the formation of allophane soils from parent materials other than volcanic ash.

Allophane soils do not appear at the very early or the very late stages of weathering of a volcanic ash deposit. Wada and Harward (1974) found that these soils appear at an age approximately 1000 to 2000 years after deposition in tropical climates and later in less humid climates. In silica-rich, poorly-drained environments, allophane and imogolite continue to weather to halloysite, in well-drained environments, the allophane soils transform to gibbsite.

Henmi and Wada (1976) found halloysite, imogolite and allophane co-existing in deposits of volcanic ash. These materials constitute a "mineral series" representing various stages of weathering.

Allophane, imogolite, and halloysite are only the easily recognizable end members. Much of the allophanic material in the deposit is in the developmental stages between allophane, imogolite and higher-ordered halloysite. This coexistence suggests some sort of heterogeneous weathering within a single soil deposit. These types of residual deposits are normally very heterogeneous. Wallace (1973) describes an allophane soil in which six measurements of the natural moisture content of parts of a two inch soil lump range from 108% to 146%. Gradwell and Birrell (1954) suggest that the extreme inhomogeneity attributed to these types of deposits is due mainly to "erratic movements of water which tend, on elevated sites, to seep in channels rather than to permeate the soil uniformly as it would below the water table."

Allophane soils from different areas of the world all have different deposition and weathering histories, however, the general particle shapes and characteristics seem to be essentially the same.

Structure of Imogolite

Electron micrographs of imogolite indicate that it consists of hollow tubes with outside and inside diameters of 20 and 10A , respectively (Figure 1b). Figure 3 shows the structure of imogolite as postulated by Cradwick, et al. (1972) and visualized by Wada and Wada (1977).

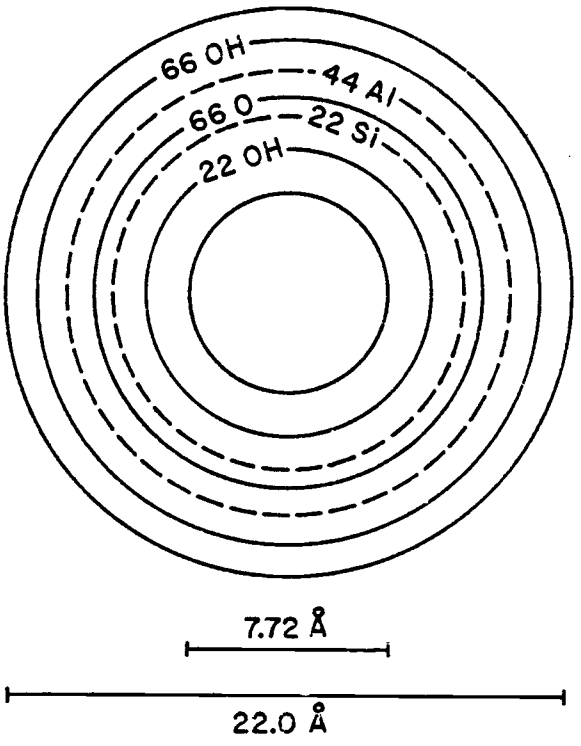

Figure 3. Postulated structure of imogolite in cross-section (after Wada and Wada (1977)).

Results from density tests (Wada and Wada, 1977) yield measured specific gravities averaging 2.7 for imogolite which are measurably greater than calculated specific gravities of 2.65 based on the postulated structure. In this model there are vacant sites at the inner SiOH sheet. Water molecules can penetrate into these sites making the measured densities higher than the calculated density. Wada

and Wada (1977) also report that float-sink density tests performed with different organic liquids indicate that the hollow spaces within the imogolite tubes are filled with strongly bound water. Assuming a density of 2.70 g/cm^3 for the tube wall and 1.0 g/cm^3 for the bound water, the amount of retained water in imogolite is approximately 10% by weight of oven dried soil. The volume of this much water is compatible with the dimensions of the postulated structure if water molecules are assumed to occupy the vacant sites in the inner SiOH sheet.

Structure of Allophane

Electron micrographs of allophane indicate that it consists of hollow spheres with outside diameters of 35 to 55A (Figure 1a). The wall of this sphere has thicknesses ranging from 7 to 10A (Wada and Wada, 1977). Figure 4a shows a schematic cross-section of the allophane structure.

Henmi and Wada (1976), Udagawa, et al. (1969) and others relate the allophane structure to a curved "defective structure" of kaolinite. Kaolinite consists of three layers of molecules--oxygen, oxygen hydroxyl and hydroxyl. The total thickness of these layers is 7A which is consistent with the 7 to 10A thickness of the allophane sphere walls. Figure 4b shows a possible structure for allophane.

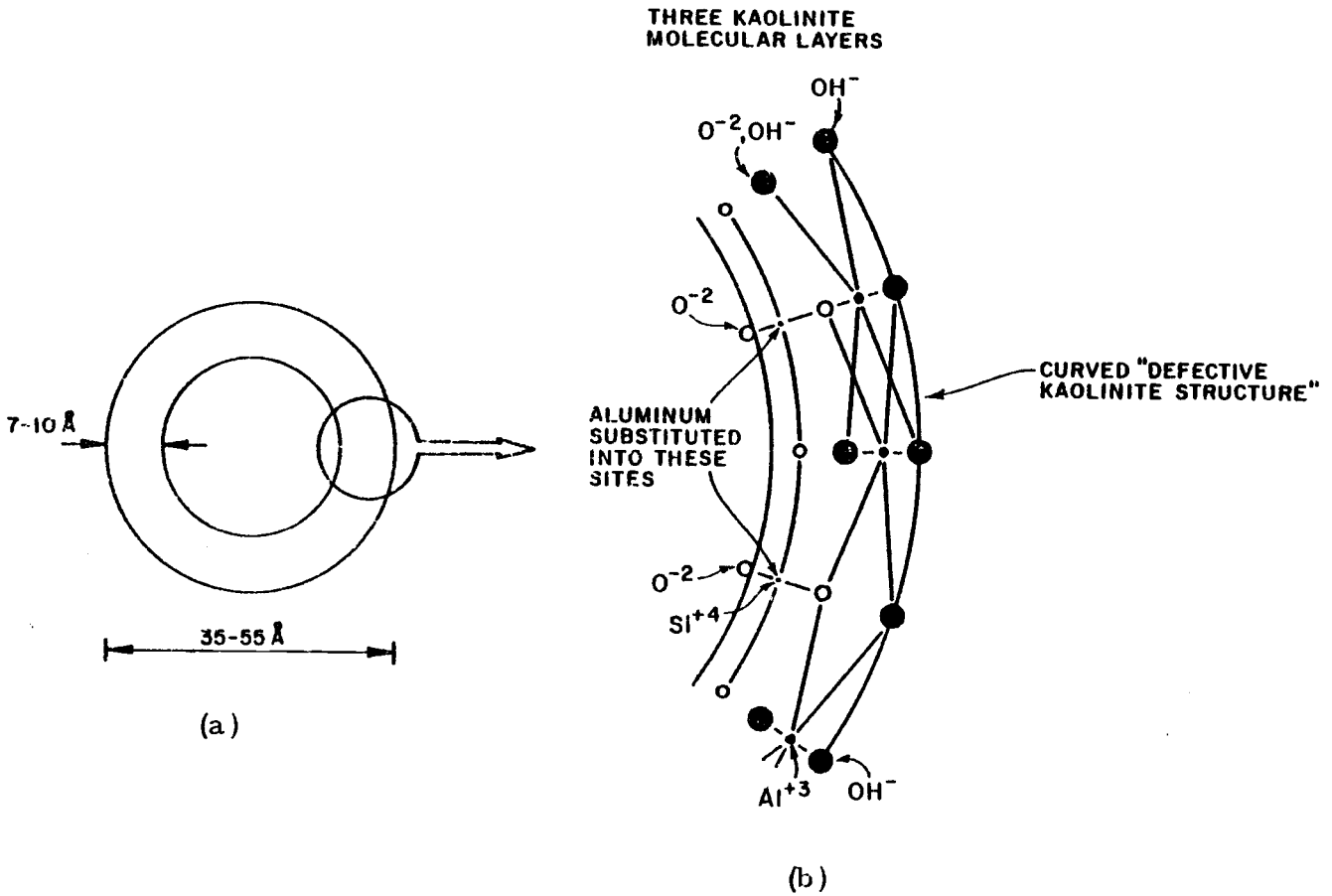

Figure 4. (a) Schematic cross-section of allophane sphere; (b) possible molecular arrangement for allophane (adapted from Wada and Wada (1977); and Udagawa (1969).

The measured density of allophane (2.75 g/cm^3) is, as previously mentioned with imogolite, higher than calculated densities based on the postulated structure. Again this can be explained by assuming that water molecules pass through the kaolinite-like structure of allophane filling the void space inside the sphere as well as vacant sites in the structure itself.

Physical Properties

There are several measurable physical properties of poorly crystalline soils which distinguish them from the more ordered crystalline clays. Some of the more diagnostic properties are discussed below.

X-Ray Diffraction

X-ray diffraction uses Bragg's Law to arrive at characteristic diffraction maxima for different substances. A beam of monochromatic X-rays is focused on a specially prepared sample of clay. For each family of atomic planes with characteristic d-spacing, there are many particles whose orientation is such that they make the proper θ angle with the incident X-rays to satisfy Bragg's Law, $n\lambda = 2d \sin \theta$. If the resulting diffraction maxima are very small or nonexistent, the sample is said to be amorphous to X-rays.

In general, the finest fraction ($< .1\mu$) of poorly crystalline soils are X-ray amorphous and the coarser fines show diffraction maxima. This indicates that the smaller fines are composed of poorly crystalline minerals (Iamura, 1969). An example of the X-ray diffraction pattern for this finer fraction as compared to crystalline kaolinite is shown in Figure 5. Several maxima appear in kaolinite but the X-ray power diffraction patterns show no pronounced maxima for the allophane soil, indicating its amorphous nature.

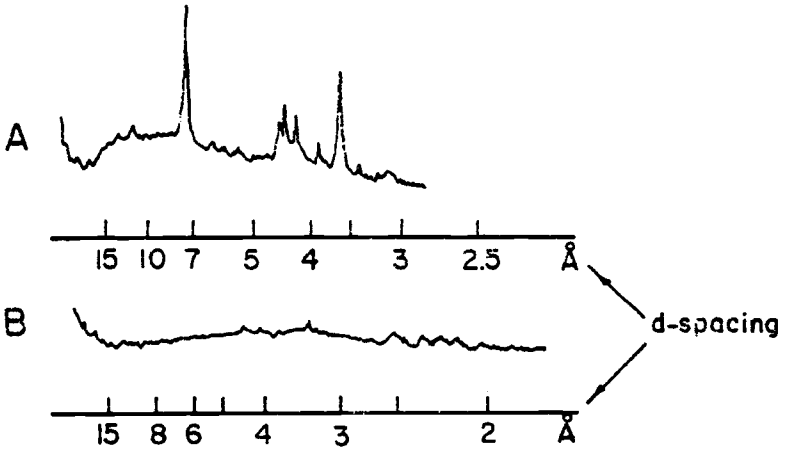

Figure 5. X-ray Powder Diffraction Patterns of A. kaolinite and B. allophane from Imaichi (Japan) surface soil (After Iamura (1969)).

Cation Exchange Capacity

Most soils retain and are able to exchange positively charged ions associated with their surfaces. This capacity for cation exchange is different for different soil minerals. Each soil mineral shows inherent affinities for specific cations, but these affinities may change with soil pH.

The soil system must be electrically neutral. This means that the sum of exchangeable cation charges must equal the negative charge of the soil at a given pH. In the soil system, the distribution of cations has been shown to grade continuously from a high concentration at the particle surface to a much lower concentration in the porewater between grains.

Some cations are more strongly adsorbed than others by a specific clay mineral. This is due to variations in ion radius, ion valence, and the attraction a particular soil colloid might have for a particular cation. In general, for a given valence, large ions are more easily replaced. For ions of the same size, a higher valence ion will replace a lower valence ion.

Charge on a soil particle surface often varies with pH. This is known as pH-dependent charge. In the case of poorly crystalline volcanic ash soils, the primary source of pH-dependent charge is thought to be the gain or loss of hydrogen ions from hydroxyl groups

on the edges of the soil particles (Bohn, et al., 1979).

Wada and Harward (1974) and others have found that the ion exchange capacities of "amorphous clay materials" are not constant, but depend upon environmental conditions such as concentration of the leaching solution, the cations in solution, and especially the pH of the solution. For allophane soils, the surface charge is more strongly pH-dependent than for most crystalline soils, and in general, cation exchange capacities for poorly crystalline soils are higher than for crystalline soils.

Differential Thermal Analysis

Differential thermal analysis measures the temperatures at which changes take place in a soil subjected to continuous heating. Clays lose water or go through phase changes which either give off or absorb heat (exothermic or endothermic reactions) at specific temperatures. These temperatures are characteristic of the mineral structure and, therefore, can be used to identify specific clay types.

For poorly crystalline clays the differential thermal analysis curves show:

1. a strong endothermic peak between 100 and 200°C attributed to the loss of adsorbed water.

2. an exothermic peak between 400 and 700°C attributed to the removal of organic matter.

3. an exothermic peak between 840 and 940°C, attributed to crystallization of high temperature silicate minerals.

The intensity of the endothermic peak attributed to adsorbed water is related to the degree of crystallinity (Lai and Swindale, 1969). The larger peak indicates lower crystal order. Figure 6 shows differential thermal analysis curves for allophane and crystalline kaolinite.

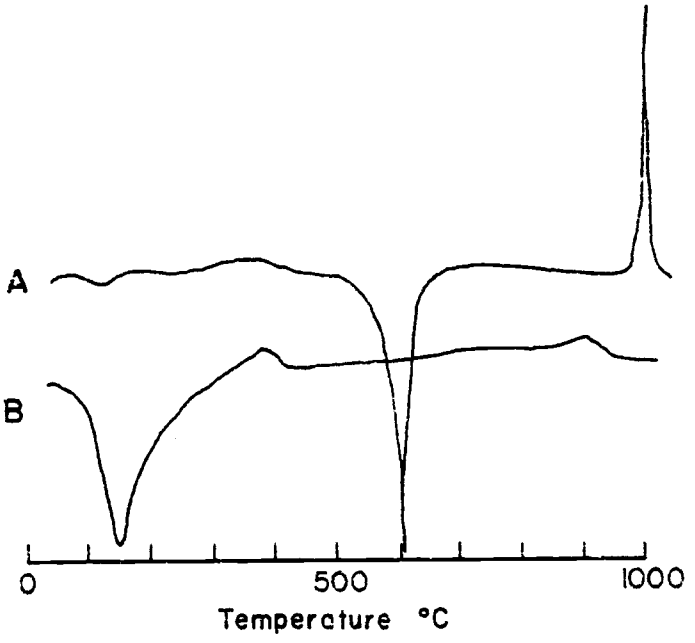

Figure 6. Differential Thermal Analysis Curves of A. kaolinite and B. allophane from Imaichi (Japan) surface soil (after Iamura (1969)).

Infrared Spectroscopy

Molecular vibrations are in the range of infrared radiation, and therefore tend to adsorb infrared radiation. Each particular molecular group will vibrate at characteristic frequences, and will adsorb characteristic radiated infrared frequencies. In this way, materials can be identified by the range of infrared frequencies they adsorb (Grim, 1953).

Infrared adsorption has an advantage over the use of X-ray diffraction in the case of poorly crystalline soils because specific information is gained for constituents amorphous to X-rays. In particular, the presence of allophane is indicated by peaks ranging from 1600 to 1650 cm^{-1} and 1020 to 1040 cm^{-1} if the organic matter has been removed (Fieldes, et al., 1972). These peaks are given by the water retained by allophane. Other water holding materials such as organic matter give the same peaks. The interference of organic matter with the allophane peaks may be corrected by prior treatment with hydrogen peroxide to destroy the organic matter.

Soil Grain Properties

Most allophane soils consist of aggregated masses or "clusters" of much smaller particles (Terzaghi, 1958; Foss, 1973). Some of the grains appear to be cemented together with gel-like coatings formed

from aluminum and iron oxides (Terzaghi, 1958). Wesley (1973) states that air drying irreversibly changes these very fine grained cohesive soils into non-plastic, very gritty sand-like materials. It has been shown that measured percentages of sand size particles increase and clay sizes decrease with drying (Martini and Palencia, 1975).

Many investigators have reported that the amount of measured fines also depends on the amount of dispersion and flocculation during the running of a hydrometer test for grain size distribution (Hannon, 1972; Maeda, et al., 1977; Wesley, 1973; Wells and Furkert, 1972; Foss, 1973; Warkentin and Maeda, 1974). Terzaghi (1958) reported that the "Java clay" used for Tjipanoedjang Dam in Indonesia had a clay content varying from 6 to 33% depending on the dispersing agent used.

Investigators have reported measured surface areas (specific surfaces) ranging from 104 to 400 m^2/g for allophane soils from the Caribbean, Japan and New Zealand (Lai and Swindale, 1969; Gradwell and Birrell, 1954). These values were obtained by the nitrogen adsorption method.

Atterberg Limits

Allophane soils in their natural condition have high liquid and plastic limits and a small range of water contents over which they

are plastic (Maeda, et al., 1977). Results from Figure 7 suggests that as the allophane content increases, natural water contents and Atterberg limit values increase. Liquid limits as high as 300 to 400% and plastic limits ranging from 180 to 200% have been reported (Warkentin, 1972).

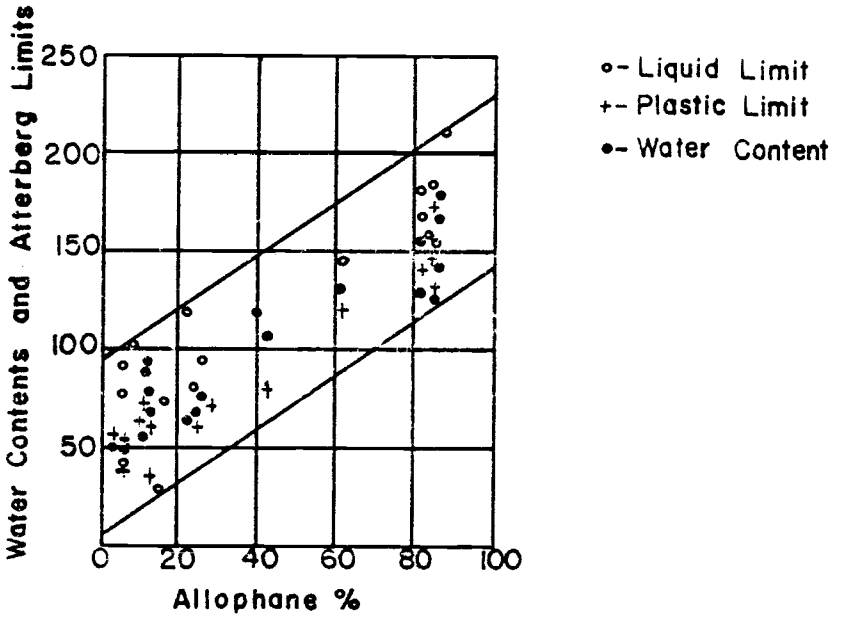

Figure 7. Increase in water content and Atterberg limits with increasing allophane content (after Wesley (1973)).

The Atterberg limits for allophane soils tend to fall below the A-line in the MH range on the Casagrande Plasticity Chart. Different samples from the same soil stratum plot on a straight line approximately parallel to the A-line (Maeda, et al., 1977). Warkentin (1972) and McNabb (1979) suggest that the presence of amorphous materials in soils may be inferred from the position of the Atterberg limits of air dried soil on the Casagrande Plasticity Chart, and that the allophane percentage or "allophanic character".

Drying or allophane soils decreases the liquid and plastic limits irreversibly. Hirashima (1948) observed that dried allophane soil lumps, continuously immersed in water in the laboratory for two years showed no signs of regaining their original plastic state.

The presence of organic matter in allophane soils greatly affects the Atterberg limits. Studies show that the liquid limit increases 1.5 to 3% for every 1% increase of organic matter content (Maeda, et al., 1977).

The liquid limits have been found to vary greatly within a few inches in the same soil deposit. They may vary by as much as 30% on samples four inches apart (Gradwell and Birrell, 1954).

Activity

In general, activities ranging from less than 0.6 for the yellow brown soils of Indonesia to 1.2 to 1.5 for the allophane soils of New

Zealand have been reported (Northey, 1966; Wesley, 1974). Values for activity are very uncertain due to the difficulty of determining the percentage of clay size particles less than 2 μm and the effects of other minerals mixed with the allophane.

Natural Water Contents

Natural water contents for allophane soils in general seem to be high and variable in comparison with their crystalline counterparts. Water contents also seem to be larger for those soils with higher allophane percentages (Wesley, 1973).

Hirashima (1948) reports that numerous moisture content samples taken from various depths indicate exceedingly high natural moisture contents for Hawaiian allophane soils. Figure 8 shows large scatter between moisture contents at various depths up to 20 feet.

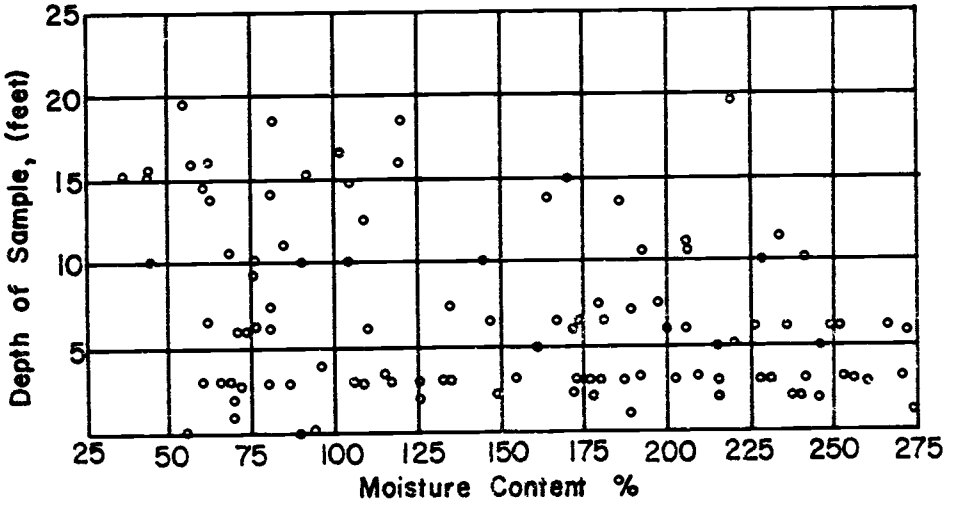

Figure 8. Scatter diagram showing moisture contents of samples, and depths taken (after Hirashima (1948)).

No apparent correlation seems to exist between water content and depth for this soil. These large variations in water content are also reported for soils from New Guinea and New Zealand (Wallace, 1973; Gradwell and Birrell, 1954).

In New Guinea, investigators have reported natural water contents of 80 to 190% (Wallace, 1973). In Hawaii, values as high as 560% have been reported (Hirashima, 1948). Moisture contents for allophane soils in New Zealand may be comparable with those of highly organic topsoils of non-volcanic origin (Birrell, 1964).

In Japanese allophane soils, moisture contents in the natural state are higher than the liquid limits. This indicates an unstable situation, namely that these soils will liquefy when disturbed (Warkentin and Maeda, 1974). Though the natural water contents are far in excess of the plastic limit and usually greater than the liquid limit, the material in its natural undisturbed state has the characteristics of a brittle solid rather than a liquid (Hirashima, 1948). Though some Hawaiian allophane soils have natural moisture contents in excess of 200%, and liquefy under the kneading action of construction traffic, they do not liquefy under earthquake shaking (Nielsen, 1977).

Density

In general, allophane soils are described as having low insitu

bulk densities. Several typical values for bulk dry density are presented in Table 1.

Table 1. Typical values of bulk dry density.

Location	Density (g/cm^3)	Unit Weight lb/ft^3	Reference
Japan	0.3-0.89	18.7-49.9	Maeda, et al., 1977
Sumatra, Indonesia	0.86	53.8	Hill, et al., 1975
New Guinea	0.56-0.88	35-55	Wallace, 1973
Central America	0.50-1.0	31.2-62.4	Martini and Palencia, 1975

Compaction - Moisture-Density Relationships

Compacted allophane soils have low maximum dry densities and unit weights (0.80 to 1.30 g/cm^3; 49.9 to 81.1 lb/ft^3) and high optimum water contents. Optimum water contents are usually much below the natural water contents (Maeda, et al., 1977). Compaction test results for soils with the high allophane contents are unusual in that maximum dry densities are not well defined. Figure 9 shows moisture-density curves for allophane from Indonesia at varying initial moisture contents. For this soil in its natural condition, there is a very flat curve and poorly defined optimum water content approximately equal to 160% (Wesley, 1973).

Hill, et al. (1975) reports that the optimum water content equals the plastic limit for a soil from Sumatra, Indonesia. The maximum dry density for this soil is 1.03 g/cm^3 (64.0 lb/ft^3). Optimum water contents for moisture-density curves determined by the Standard AASHTO method on Indonesian allophane soils are in most cases found to be close to the plastic limit. This assumes that the treatment of the soil prior to testing for both tests is the same. Figure 10 indicates that a drop in plastic limit on air drying is accompanied by an almost identical drop in the optimum water content (Wesley, 1973).

With allophane soil samples a range of optimum water contents or maximum dry densities can be obtained depending on the treatment of the sample prior to testing. Figure 9 shows that drying will generally reduce the optimum water content and increase the maximum dry density. At lower water contents, a much more pronounced peak is evident.

For soils which change irreversibly upon drying, it is necessary to carry out compaction tests at the natural soil moisture content, wetting and drying to obtain a curve which represents field conditions. Wesley (1973) reports that adequate field compaction can be obtained for water contents up to 10 to 15% on either side of optimum.

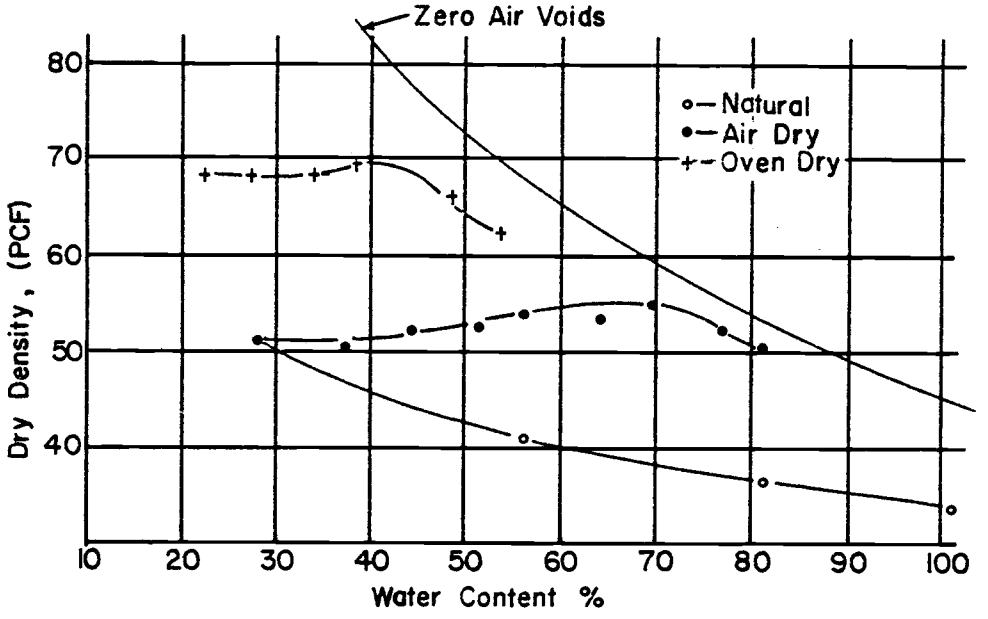

Figure 9. Moisture density curves for allophane soils from Indonesia (after Wesley (1974)).

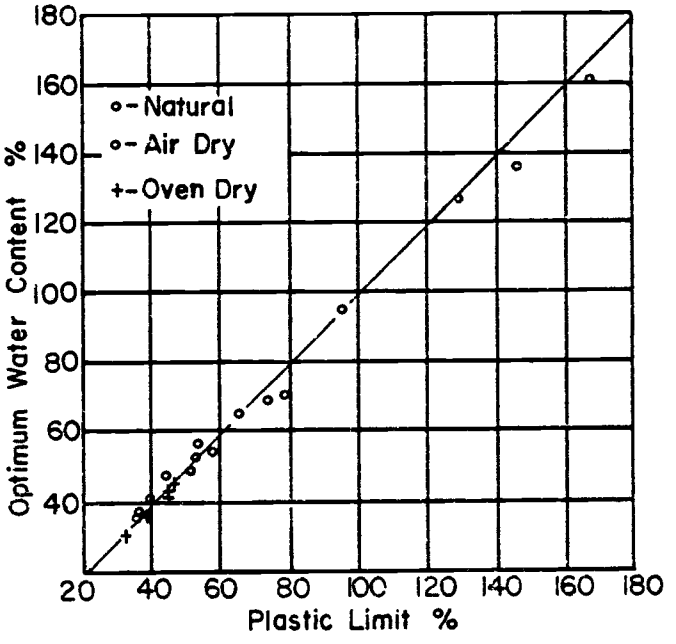

Figure 10. Relationship between optimum water content and plastic limit (after Wesley (1973)).

Compressibility

Allophane soils are fairly compressible once the apparent preconsolidation pressure has been exceeded. The consolidation curves of undisturbed allophane soils characteristically show a sharp change in slope, thus estimation of the apparent preconsolidation pressure is easily made. Disturbed e-log p curves show a smooth decrease in void ratio. Figure 11 shows an e-log p curve for Indonesian allophane. Field measurements have shown that laboratory compression tests tend to underestimate field compression (Matyas, 1969).

Compressibility tests from New Guinea, Indonesia, New Zealand, and other locations show that apparent preconsolidation pressures determined from these tests are much greater than the overburden pressures. Tests on soils in these areas indicate overconsolidation, however, there is no geologic evidence which suggests overconsolidation due to overburden or dessication has taken place (Hill, et al., 1975; Wallace, 1973; Birrell, 1952). This apparent overconsolidation pressure may be due to cemented bonds between the particles (Wallace, 1973). Investigators have reported apparent overconsolidation pressures ranging from 1 to 3 kg/cm^2

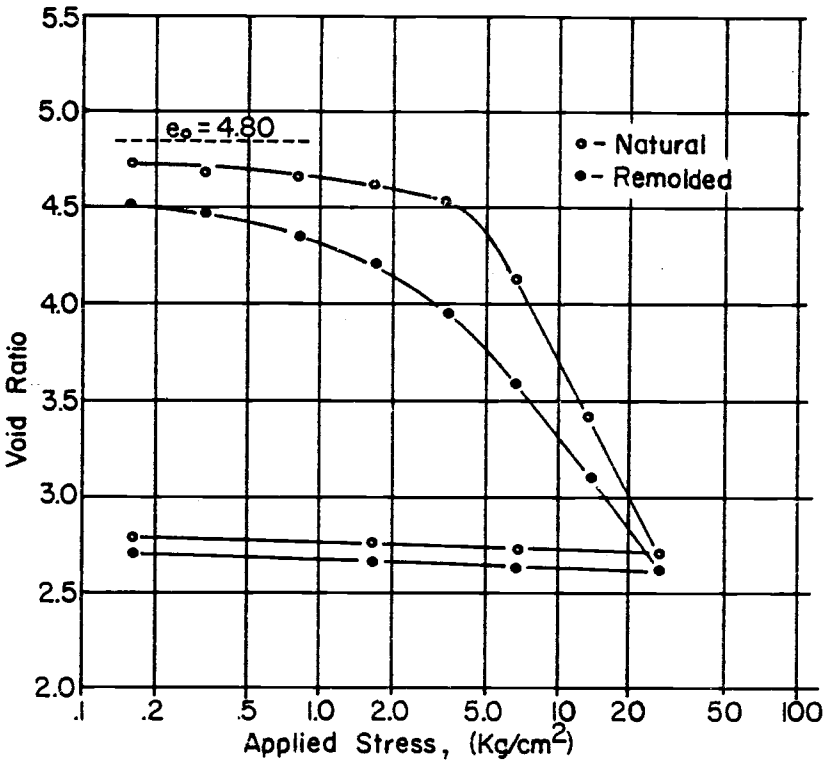

Figure 11. Consolidation curve for allophane from Indonesia (after Wesley (1974)).

for Japanese soils and 1 to 2 kg/cm^2 for New Zealand soils (Wallace, 1973; Birrell, 1952). Overburden pressures were not reported.

Compression index (Cc) values for two New Zealand allophane soils are presented in Table 2. These are compared with Cc values for typical crystalline clays, calculated from Cc = 0.009 (LL-10), where LL = Liquid Limit (Terzaghi and Peck, 1967).

Table 2. Typical compression index values for New Zealand allophane soils (after Gradwell and Birrell (1954)).

Sample	Cc determined from e-log p	Cc calculated from Cc = 0.009 (LL-10)
309	1.73	1.08
301	1.53	1.99

The liquid limits for allophane soils appear to vary much more than the corresponding Cc values. Thus the divergence between the usual correlation between liquid limit and Cc is much greater for allophane soils than for crystalline soils (Gradwell and Birrell, 1954). Wallace (1973) has shown that a relationship exists between Cc and void ratio (e_o) for Indonesian allophane soils such that $Cc = ae_o - b$, where a and b are regression coefficients equal to 0.6 and 0.7, respectively. A typical relationship between Cc and e_o for crystalline clays is: $Cc = 1.15 (e_o - 0.35)$ (Bowles, 1979).

Researchers have reported that rebound for the unloaded portion of the e-log p curve is small for both disturbed (remolded)

and undisturbed allophane soils. This behavior is much like that of conventional crystalline soils.

Permeability

Allophane soils do not have exceedingly low permeabilities in spite of their very fine particle size. For allophane in general, the coefficient of permeability (k) is smallest near the natural water content and gradually increases upon drying. Investigators have noted that allophane soils aggregate upon drying, thus increasing k by as much as one hundredfold (Maeda, et al., 1977; Gradwell and Birrell, 1954; Wallace, 1973). Table 3 presents typical values of k for various allophane soils.

Table 3. Coefficient of permeability for allophane soils.

Location	Coefficient of Permeability k (cm/sec)	Reference
Hawaii, Paaloa	1.47×10^{-6}	Andrews, 1936
Africa, Sasamua Dam		
insitu	3.0×10^{-7}	
compacted	2.0×10^{-7} to 6.0×10^{-8}	Terzaghi, 1958
Japan	1.0×10^{-5} to 2.5×10^{-8}	Matuo, et al., 1953

Strength and Sensitivity

In general, allophane soils in the undisturbed state are very stable, often occurring in free standing slopes of 45 to 70° (Maeda, et al., 1977; Wesley, 1973). Unconfined compressive strengths (q_u) of 1.0 to 2.3 kg/cm^2 and vane shear strengths of 0.7 to 1.0 kg/cm^2 have been reported for Japanese allophane soils (Wells and Furkert, 1972). Hoshino (1953) states that for Japanese Kanto Loam, values of q_u can be computed from:

$$q_u = (\sqrt{1 + \tan \phi} + \tan \phi)$$

The shear strengths of Japanese allophane soils decrease with increasing amounts of organic matter but do not increase with increasing overburden pressure. Shear strength also is not related to void ratio. Samples with the same shear strengths have void ratios varying from 1.9 to 5.1 (Maeda, et al., 1977; Wesley, 1974).

Many investigators observed that the effective angle of internal friction (ϕ'), and c' effective cohesion intercept varied over a wide range of values depending on the moisture content and density at which the tests were run (Willis, 1946; Terzaghi, 1958; Foss, 1973). Table 4 presents reported values of c' and ϕ' for various soils containing allophane.

Table 4. Typical reported values of effective strength parameters, cohesion (c') and angle of internal friction (ϕ').

Location	Angle of Internal Friction ϕ'	Cohesion c'(kg/cm^2)	Reference
New Zealand	0 to 8^o	0.2 to 0.4	Maeda, et al. 1977
New Zealand, Egmont	"a few degrees"	0.28 to 0.42	Gradwell and Birrell, 1954
Africa, Sasamua Dam	30 to 36^o	0.3	Terzaghi, 1958
Hawaii	0 to 49	0.2 to 1.2	Willis, 1946

Strain at failure for most allophane soils is about 2 to 3% compared with 2 to 6% for most crystalline clay soils (Maeda, et al., 1977; Gradwell and Birrell, 1954).

Investigators seem to agree that allophane soils have some degree of sensitivity. Most report moderate sensitivities on the order of 1 to 12 (Maeda, et al., 1977; Lohnes and Handy, 1968; Wallace, 1975). Wells and Furkert (1972) postulate that the large quantities of water present in natural allophane is held in hydrogen bonded clusters of water molecules. Mechanical working breaks these clusters and distributes the water evenly over the clay surface. Water released during this process explains the "greasy" feel when working the soils with the fingers.

Compacted allophanes from Indonesia seem to have about the same shear strengths as insitu soils (Wesley, 1974). Placement water contents do not have a large effect on ϕ'. The cohesion intercept is affected by both placement water content and dry density. Residual strengths are consistent and independent of placement conditions (Matyas, 1969).

Visco-Elastic Properties

Investigators have reported large ranges of values describing the elastic behavior of allophane soils. Some typical values are reported in Table 5.

Table 5. Values of elastic constants for various allophane soils.

Location	Youngs Modulus $E(kg/cm^2)$	Poissons Ratio μ	Reference
Japan			
Iwate	600 to 900 depending on the time of year		Gradwell and Birrell, 1954
Kanto Loam	15	0.1 to 0.2	Gradwell and Birrell, 1954
New Zealand			
Egmont	42	--	Gradwell and Birrell, 1954
Fernando Poo Island			
Compacted	150 to 400 depending on the molding water content	--	Salas, 1963

For insitu materials, Youngs modulus (E) is sensitive to the time of year (natural water content of the soil). For compacted samples, E decreases greatly with increasing molding water contents. High density, compacted samples also are much more brittle than low density materials. Uriel and Serrano (1973) report for an allophane soil in the Canary Islands that the stress-strain response is elastic and linear below a critical stress. E is high and failure strains are less than 1%. Upon reaching the critical stress, a sudden change (decrease) in the modulus is caused by destruction of the natural soil structure.

Summary

Allophane soils have unique engineering properties which depend in varying degrees on the amount of drying they have experienced. Due to variations in drying in the field, and during testing and sampling, standard soil testing methods may not accurately predict field performance.

Though these soils occur abundantly in the Western Cascades of Oregon and Washington, Alaska, and Hawaii, their presence has been largely ignored by the engineering profession. During the last several years, development and logging pressures have forced construction activity into areas containing these soils, thus it is important that geotechnical engineers be made aware of the many engineering problems associated with allophane soils.

III. SOIL ENGINEERING PROPERTIES

Introduction

This chapter describes engineering data taken from the literature. A tabular summary of these data plus brief soil descriptions are presented in Appendix A. From this summary, it is obvious that large gaps exist in the geographic distribution of reported geotechnical data on soils derived from volcanic ash. One large gap is for the United States. In an effort to fill this informational void, engineering laboratory testing was performed on several soils from the Pacific Northwest and Alaska. This chapter summarizes these laboratory test results, and discusses the combined results of geotechnical data from the literature and determined by the laboratory study.

Selection of Engineering Data from Literature

Several hundred references thought to contain geotechnical data on soils derived from volcanic ash were searched. Many relatively large blocks of data were initially screened out. One of these related to latterites derived from volcanic ash. As a group, latterites were found unsuitable for inclusion as allophane soils, because as a consequence of their age and mode of formation (severe leaching of silica), they cannot assemble the Si-Al-OH combinations required to form the

poorly crystalline components of allophane clays. Mexico City clays were also eliminated. These clays have many of the same geotechnical properties as poorly crystalline allophane clays. The Mexico City clays however, are composed primarily of diatoms (Mesri, 1975). Unweathered ash deposits were also rejected since they have not yet formed the special constituents required of an allophane soil.

Appropriate references for review were chosen based on three important considerations. First, geographic location of the materials described was of prime importance. Any country or region in the vicinity of geologically recent volcanic activity most likely has at some time experienced significant ashfall. For example; many countries surrounding the Pacific Ring of Fire have soils derived from volcanic ash. Second, geologic origin of the materials, though inseparably linked to geographic location, was important because ash accumulations may have been carried by winds, away from the immediate vicinity of volcanic activity. For example; allophane soils in Ireland are thought to be derived from ash accumulations brought from Iceland (Wada and Harward, 1974). Climate was also an important consideration. Allophane soils do not form from ash deposits in arid or semi-arid regions. Ash accumulated on the windward and leeward slopes in Hawaii develop different soil types due to differences

in weathering intensities. Volcanic ash soils found on windward slopes develop the special properties of allophane soils while those on the leeward side stay relatively ash-like (Hirashima, 1948).

In addition to these three major considerations, a key for identifying allophane soils was developed to further identify desirable soil data. This key was developed based on known physical-engineering properties of allophane soils. Engineering index properties in the key are placed in order of importance, as determined by this investigator. Table 6 presents the key used.

Any soils encountered in the literature which fit the criteria outlined in Table 6, were included in the tabular summary in Appendix A. Often not all of the key properties were reported, and judgements were made based on a few of the properties. In all cases, Atterberg limits and/or natural water contents were used as the main indicators. Other engineering properties are harder to measure and are not reported as often. Any soil encountered in the literature which indicated the presence of allophane or imogolite by name was included.

Location of Soils Selected

Approximately 200 soils which fit the required criteria outlined in Table 6 were identified from the literature. The soils were

Table 6. Key for identifying probable allophane soils.

Index or engineering property	Typical behavior as compared with crystalline soil behavior
Atterberg limits	High liquid limit and low plasticity index. Upon drying a significant decrease in the liquid limit takes place, with the liquid limit decreasing more than the plastic limit. These changes are irreversible.
Natural water content	Usually high and variable.
Grain size	Upon drying, an irreversible increase in average grain size occurs.
Moisture-density relationships	Low maximum dry densities and high optimum water contents. Upon drying, $\gamma_{d\ max}$ increases and w_{opt} decreases. These changes are irreversible.
Insitu dry density	Usually low and variable.
Sensitivity	Moderate; strength gradually recovers with time if disturbed.
Permeability	High relative to other fine grained soils. k is a minimum near the natural water content and increases with drying.

cataloged as a group according to country or region. These groups were placed in alphabetical order, in the tabular summary in Appendix A. Included are soils from Africa, Australia, The Carribean, Central America, Indonesia, Japan, The Canary Islands, New Guinea, New Zealand. South America, Hawaii and the north western United States.

A large percentage of the soil data reported in Appendix A is from New Zealand. Extra emphasis is also placed on volcanic ash soils in Japan. Only very sketchy information is available for a few soils from the Pacific Northwest, and one soil is reported from Alaska.

Discussion of Data from Literature Review

The geotechnical data as presented in the literature has several defects. Very few reported soils are presented with full sets of data. Quite often, Atterberg limits are reported without accompanying natural water content, grain size or strength data. Strength data may be reported without density or specific gravity information. Many times, overconsolidation pressures are given without accompanying overburden pressures.

Non-uniform methods for conducting tests or presenting data were followed. This may be expected for references collected from

several countries. A significant number of authors did not adequately outline test methods used. In many cases, Φ and/or c were presented, but the test methods were not. Thus, it is unknown if strength parameters were from vane shear, unconfined compression, direct shear, or triaxial tests. Strengths of most New Zealand soils were based on Proctor needle testing (New Zealand Soil Bureau, 1968).

An important consideration when interpreting test results from allophane soils is the drying history. Surface or cutbank soils have usually experienced some degree of drying. Northfacing or south-facing slopes may experience different degrees of drying. Sampling, transport, and storage techniques are also important. Gidigasu (1976) and others suggest that these soils may change crystal-structure if disturbed, exposed to drying, or transported and stored for relatively short periods of time.

Comparison and interpretation of test results performed on fragile soils is a very difficult and complex task. Conclusions drawn from such comparisons must be carefully constructed and thoroughly thought out.

Most important in characterizing volcanic ash soils taken from the literature, is the determination of clay mineral type and proof that these 200 $\pm$ soils included in the summary are actually allophane soils. In many cases, the soils were defined as, or indicated to

contain allophanic constituents which impart special engineering behavior to the soils. Often thought, only parent materials were mentioned, with no specific reference to clay mineral type. This was especially true for the engineering literature. Sometimes, in the engineering literature, soils which appeared to exhibit some of the special engineering properties were collectively referred to as halloysites (Terzaghi, 1958; Pope and Anderson, 1960). For these cases, the use of the term halloysite by its strictest definition was ignored, and applied to those soils previously defined as allophane soils.

Appendix A contains a tabular summary of data from the literature review. Most of the soils presented in Appendix A have corresponding soil and parent material descriptions keyed to soil members in the table.

Figures 12-18 summarize some of the data presented in Appendix A. From Figure 12 note that reported water contents range from 8 to 180%. Natural water contents up to 313% were reported. Of course, since the drying history of many of the samples are unknown, the average of these data may be lower than actual field conditions might show.

Figures 13, 14 and 15 present reported Atterberg limits for the natural, air dry, and oven dry cases respectively. Most of the

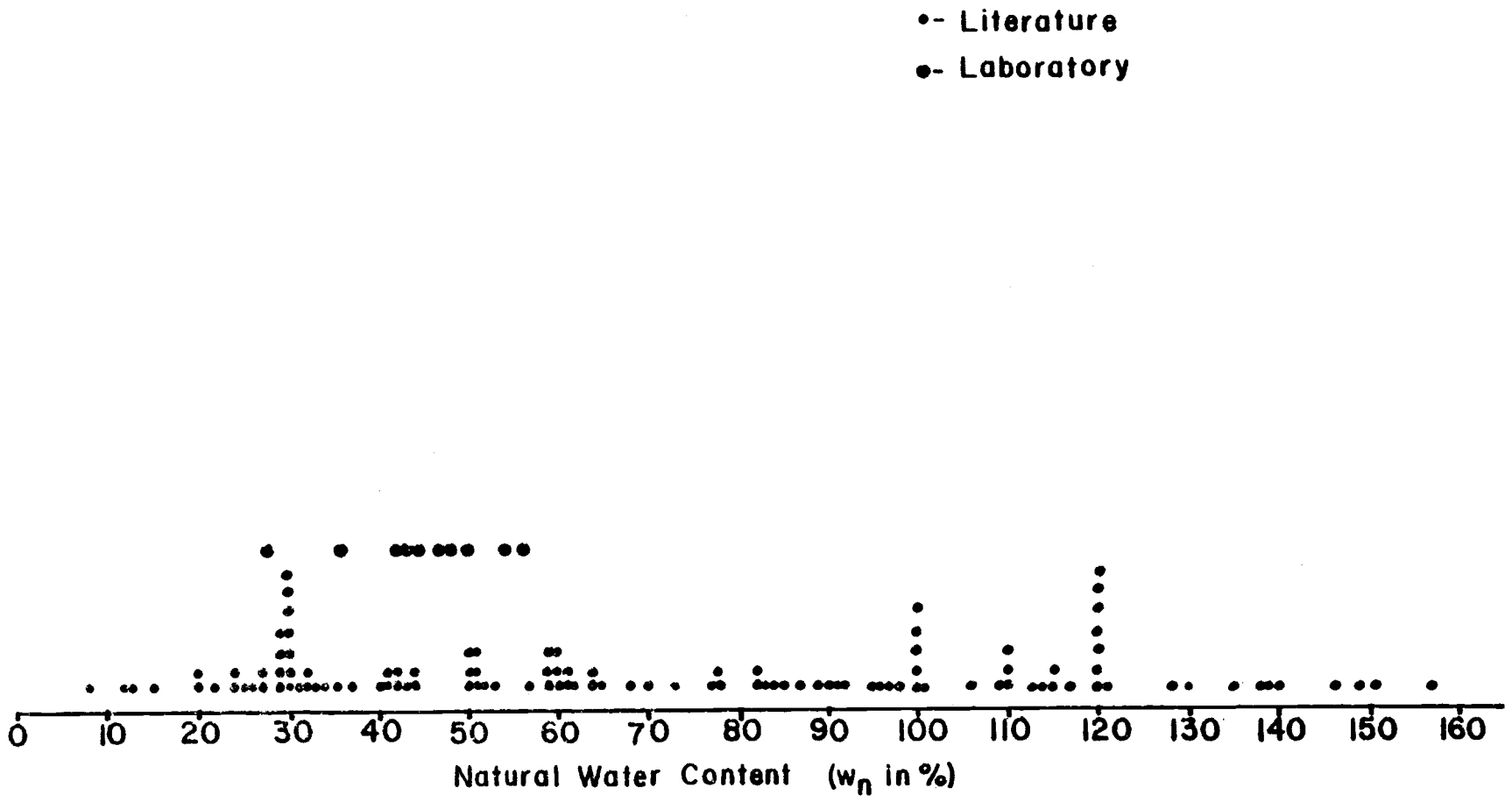

Figure 12. Distribution of natural water contents.

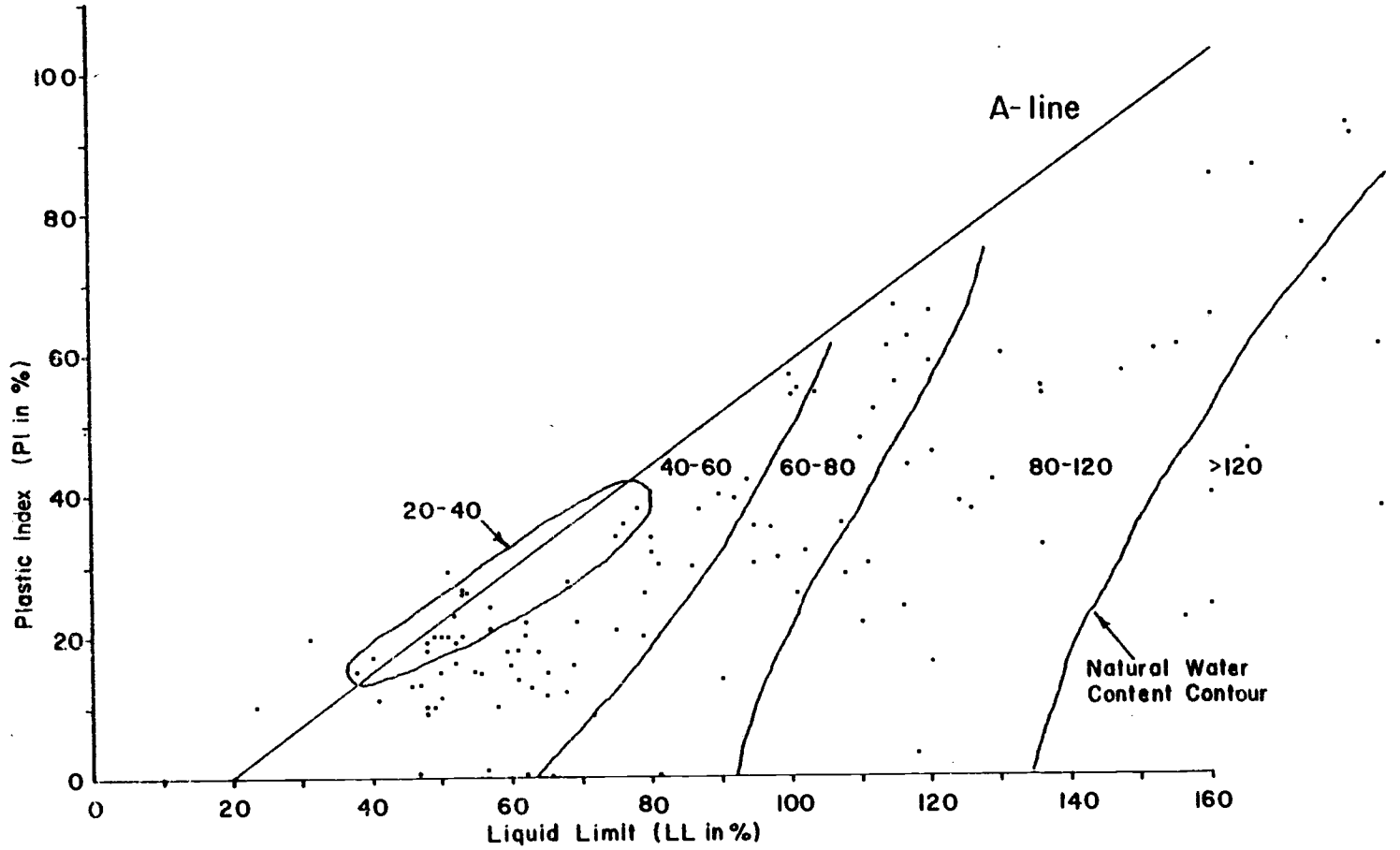

Figure 13. Distribution of Atterberg limits, in the natural state.

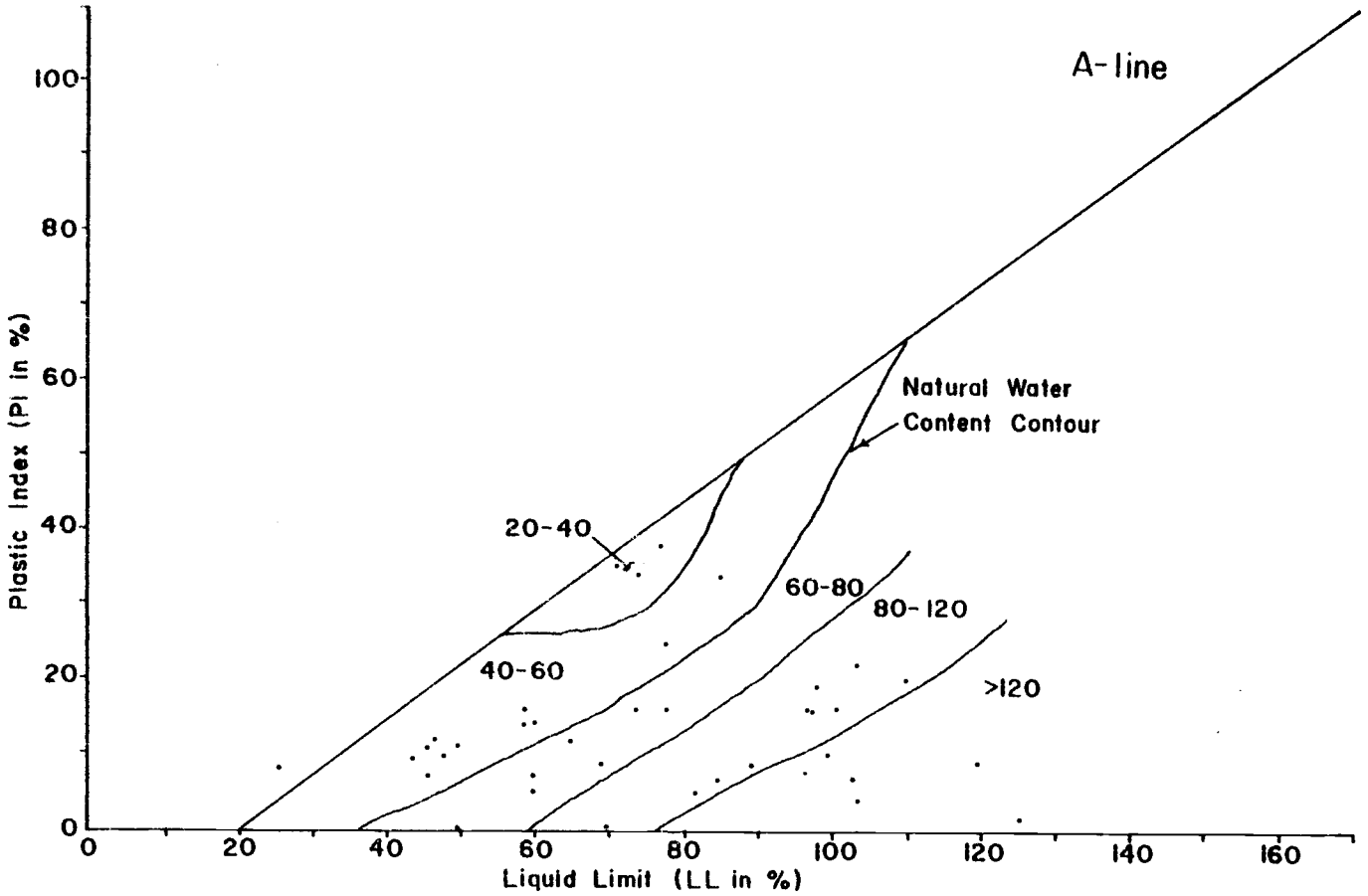

Figure 14. Distribution of Atterberg limits, in the air-dry state.

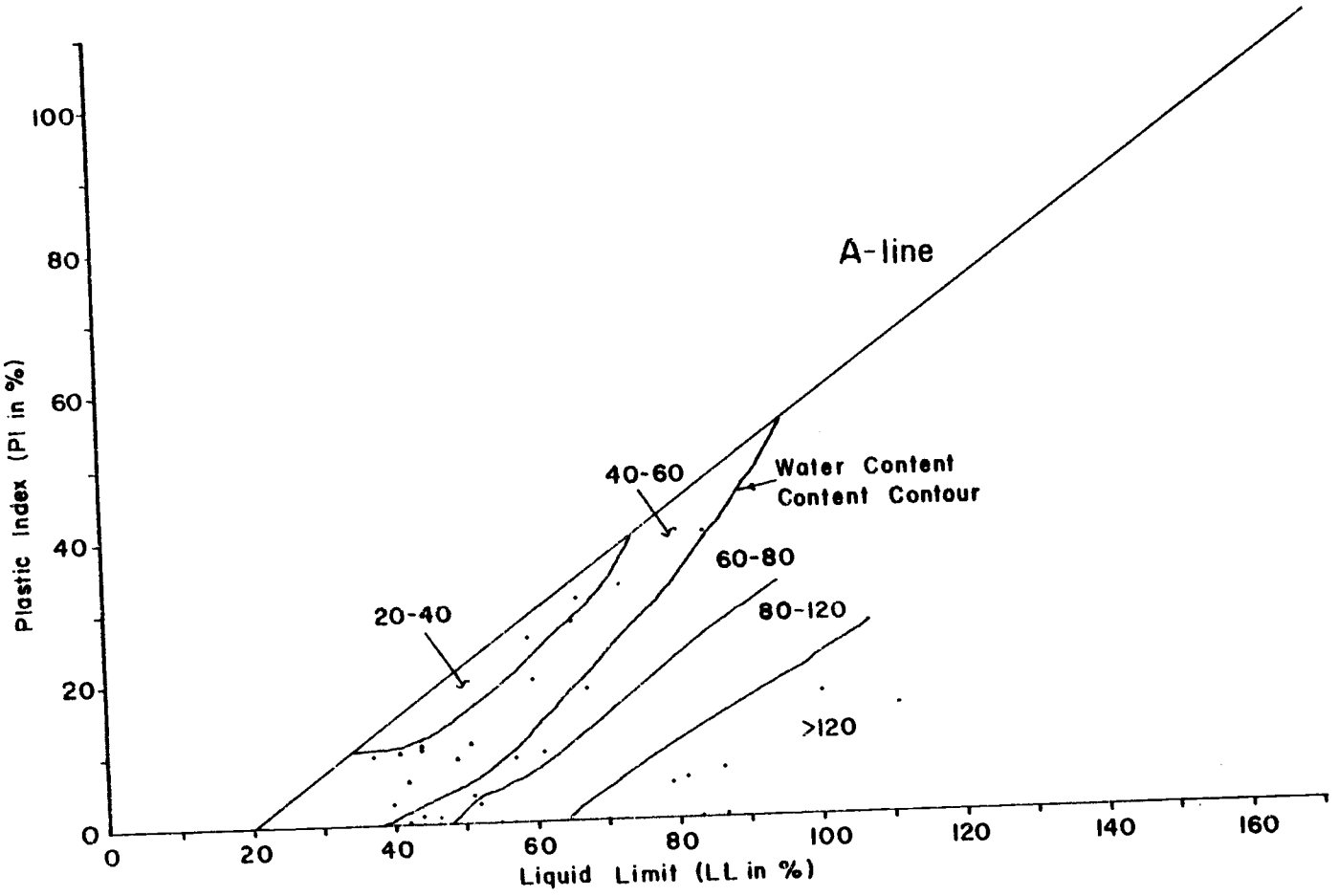

Figure 15. Distribution of Atterberg limits, in the oven dry state.

data plot well below the A-line. Liquid limits range from 23 to 350% for the natural condition, 26 to 125% for air dry conditions and 40 to 111% for oven dry samples. These results show in general, that plasticity is greatly reduced upon drying and that the amount of plasticity lost depends upon the degree of drying. In the air dry and oven dry cases, the values plotted on the Casagrande Plasticity Chart seem to group themselves into three areas, with the oven dry area more compact and distinct. Water content contours can be drawn on the plasticity chart for all three cases. Soil Atterberg limits, and corresponding natural water contents, seem to arrange themselves along contours as shown in Figures 13, 14 and 15. For example, in the air dry case, a soil with a liquid limit (LL) of 75% and a plastic index (PI) of 15% will most likely have a natural water content ranging from 60-80%. Those soils with relatively low natural water contents plot closer to the A-line than those with higher natural water contents.

Figures 16, 17 and 18 show plotted optimum water content values for the natural, air dry, and oven dry case respectively. It is evident that irreversible changes with drying occur, and the magnitude of these changes depends on the amount of drying. In general, optimum dry density ($\gamma_d$max) increases with drying and

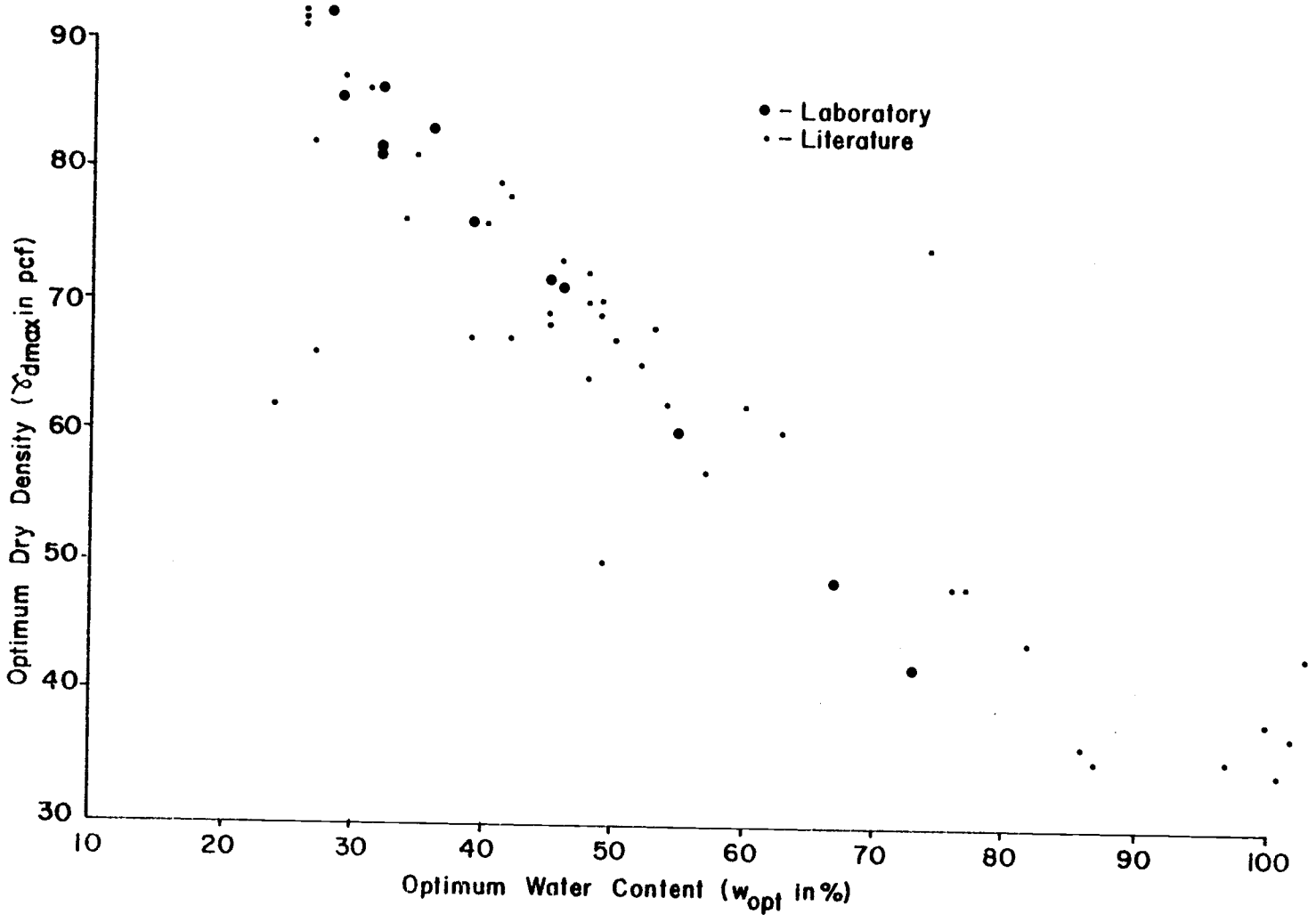

Figure 16. Optimum dry density vs. optimum water content, undried.

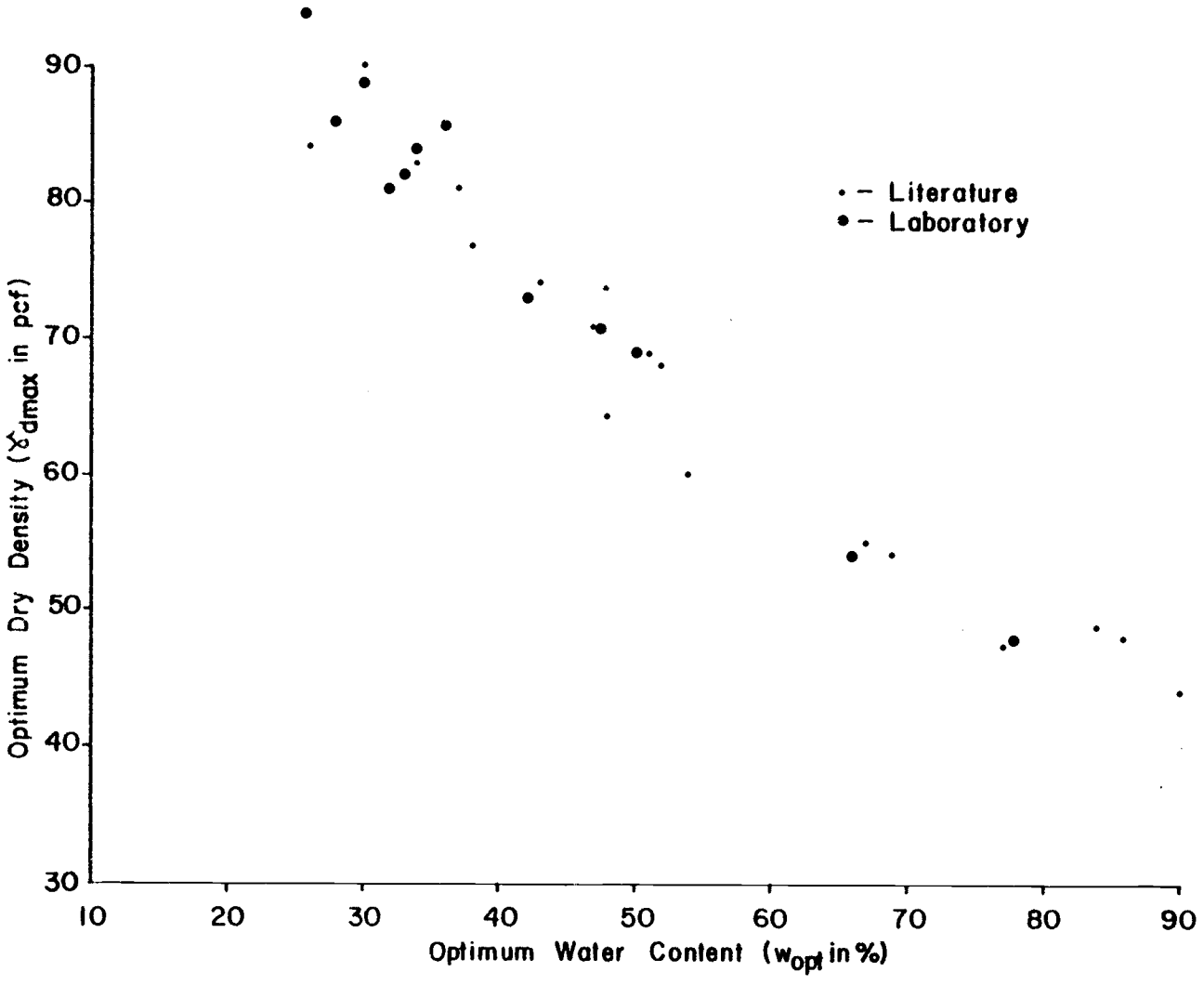

Figure 17. Optimum dry density vs. optimum water content, air dried.

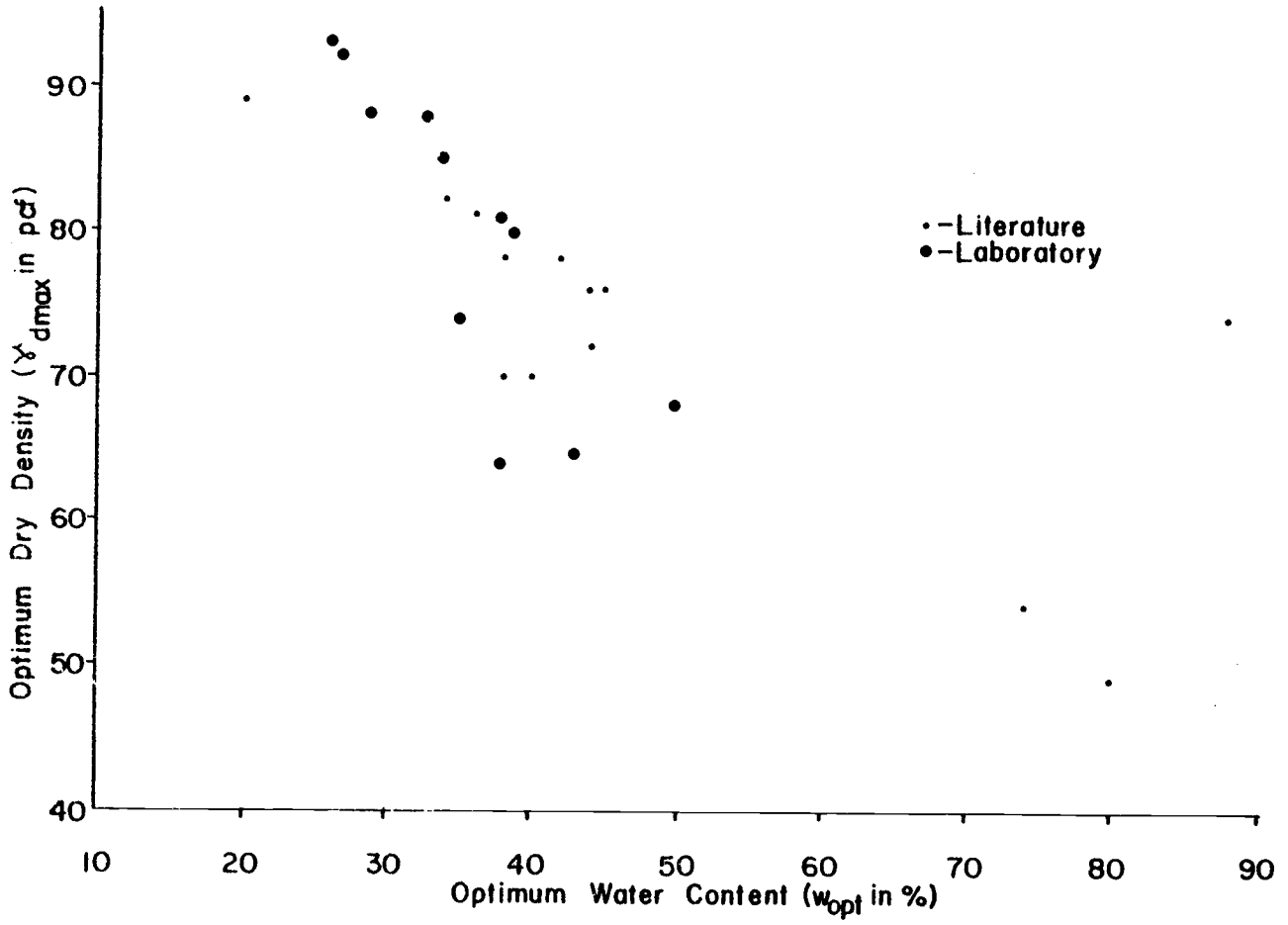

Figure 18. Optimum dry density vs. optimum water content, oven dried.

optimum water content (w_{opt}) decreases. Also with drying, the results appear less scattered. Table 7 presents a summary of ranges of moisture-density optimum water content values for all three cases.

Table 7. Range of moisture-density optimum values.

	Drying History		
	Natural	Air Dry	Oven Dry
Maximum dry unit weight (γ_d max in pcf)	101-34	94-44	96-49
Optimum water content (w_{opt} in %)	20-103	26-90	20-80

Warkentin (1972) and McNabb (1979) suggest that the presence of amorphous materials in soils may be inferred from the position of the Atterberg limits of air dried soil on the Casagrande chart. The allophane percentage or "allophanic character" corresponds to a higher angle on the plasticity chart measured from horizontal and revolving around the liquid limit equal to 20%. Further analysis of soils from the literature indicates that this may be true for most soils containing allophane (wet or dry). In Figure 19a, the dark lines define the boundaries of samples containing 6 to 30%, and greater than 30% allophane on the Casagrande Plasticity Chart. The extent and location

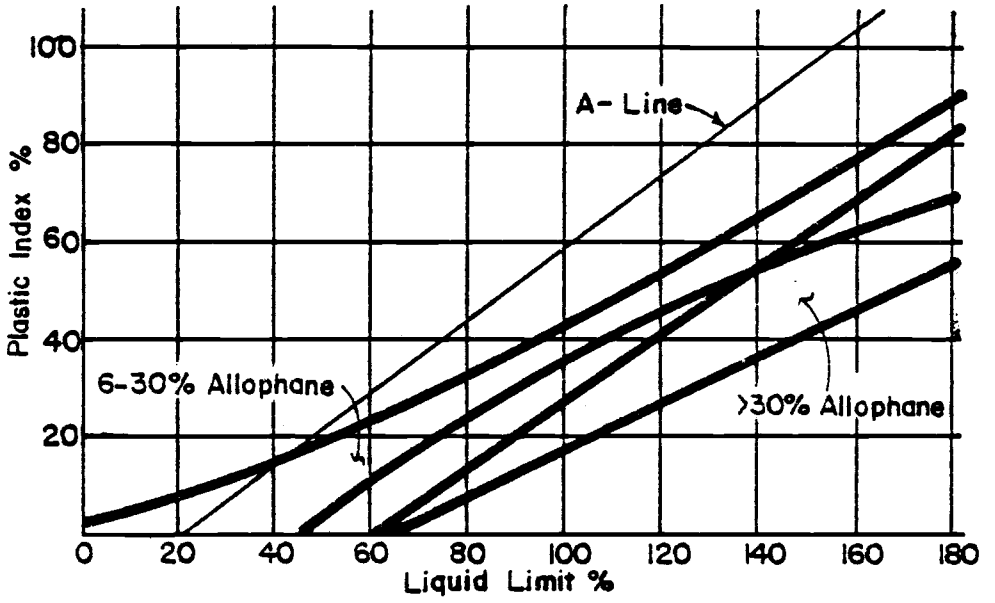

(a)

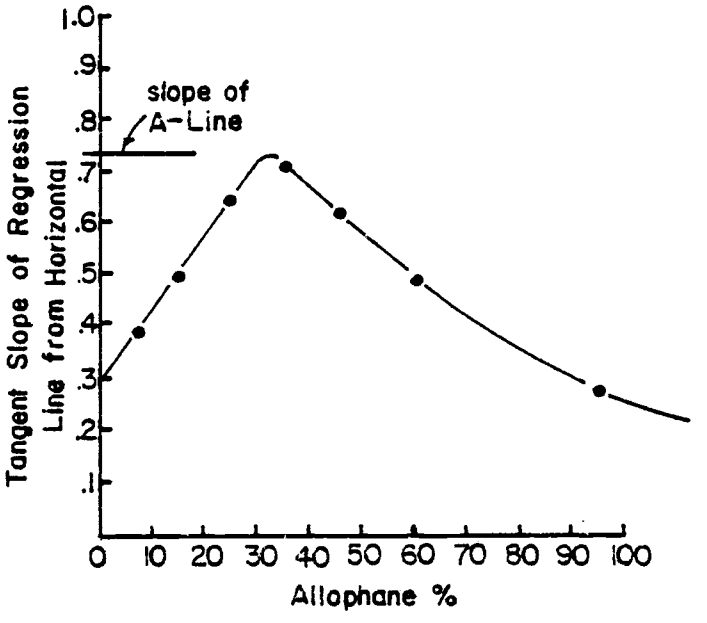

(b)

Figure 19. (a) Percent allophane vs. position on the Casagrande Plasticity Chart; (b) Tangent slope of regression line vs. percent allophane.

of these areas were determined using linear regression analysis of 106 samples reported in the literature. Figure 19b shows the relationship between the angle of lines for varying allophane percentages measured from horizontal versus, percent allophane. For lower allophane percentages, the slope is much less than that of the A-line slope. This slope increases with increasing allophane percentage. At 32% allophane, the tangent of the slope angle equals 0.73 (36.1°) which is approximately equal to the slope of the A-line. For allophane percentages greater than 32%, the slope decreases asymptotically to the value of 0.15 (8.5°). As the percentage of allophane increases, the position on the plasticity chart moves further away from the A-line into the high liquid limit and low plastic index range. Higher slopes measured from horizontal indicate less change in plastic limit with decreasing liquid limits. At 32% allophane, the rate of change of plastic limit with liquid limit is a minimum. This information may be useful in predicting allophane percentages on the basis of the Atterberg limits.

Laboratory - Sampling

Disturbed and undisturbed samples were taken from nine sites on the Middle Fork Willamette, Middle and North Santiam, and McKenzie River drainages of the Cascade Mountain range, west central

Oregon. Surface soils were also sampled from two sites in southeast Alaska.

Table 8 summarizes sample site names, numbers, number and type of samples taken at each site, and a general description of the site soils. Appendix B provides site and sample information. Data presented in Appendix B include; parent materials, general site descriptions, aspect, elevation and soil profile logs outlining sample type, depths, and soil description. Figures 20, 21 and 22 give locations for each site in Oregon and Alaska.

Most samples were taken from areas of easy accessibility; road cuts, or slump headwalls. The cutbanks or headwalls sampled were shaded so that soils near the surface were moist. Sites were chosen so that minimal drying had occurred in the past. The Dome Creek Slide (Site 1), was directly southfacing so that some drying probably occurred.

Sample Site Selection

Sampling sites in the Oregon Cascades were chosen based on parent materials and x-ray diffraction patterns reported by Taskey (1978) in his thesis titled "Relationships of Clay Mineralogy to Landscape Stability in Western Oregon". Taskey (1978) presented mineralogical, X-ray diffraction, and descriptive results for

Table 8. Summary of sampling site information.

Site Number	Site Name	Type and Number of Samples	General description of soils
1	Dome Creek Slide	2 - bag 2 - jar 2 - shelby tube	Brown-red moist friable silt, basalt chip float.
2	Dome Creek Cutbank	2 - bag 2 - jar	Red-brown clayey-silt
3	Buck Creek	2 - bag 3 - jar 2 - shelby tube	Moist red-brown friable silt with basalt-cobble float
4	Pyramid Creek Cutbank	1 - bag 1 - jar 2 - shelby tube	Moist grey-brown clayey silt.
5	Batchellor Creek Cutbank	1 - bag 1 - jar 2 - shelby tube	Moist yellow-brown silt, some 1/4 inch sand. Soil stiffens noticeably with depth.
6	Box Canyon Creek Slump	1 - bag 1 - jar 2 - shelby tube	Moist yellow-tan slightly plastic clayey silt with variable coloring and stiffness

Table 8. Continued

Site Number	Site Name	Type and Number of Samples	General description of soils
7	Quartzville Creek Cutbank	1 - bag 1 - jar 2 - shelby tube	Moist light brown clayey silt with occasional cobbles.
8	Fritz Creek Slump	1 - bag 1 - jar 2 - shelby tube	Moist yellow-brown gravelly, sandy friable silt; inhomogeneous with some cobbles.
9	Lookout Creek Cutbank	2 - bag 2 - jar 2 - shelby tube	Moist dark brown mottled sand silt with cobbles.
10	Alaska-4 Shelikof	2 - bag 1 - jar 3 - shelby tube	Orange brown and gray medium plastic sandy-silty clay
11	Slaska-5 Sitka	2 - bag 1 - jar 3 - shelby tube	Orange-brown sandy silty clay.

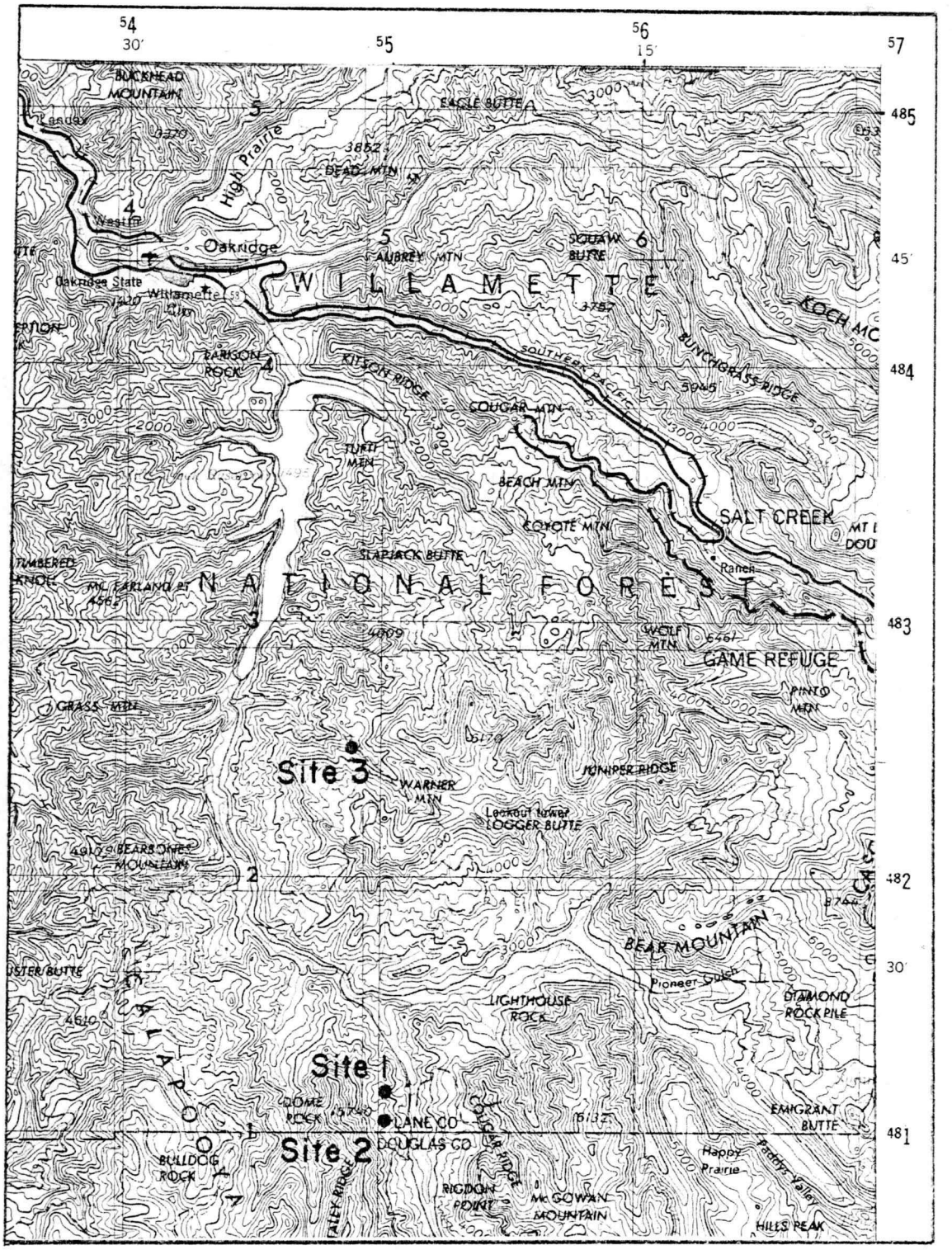

Figure 20. Sample site locations--Oakridge area of the Oregon Cascades.

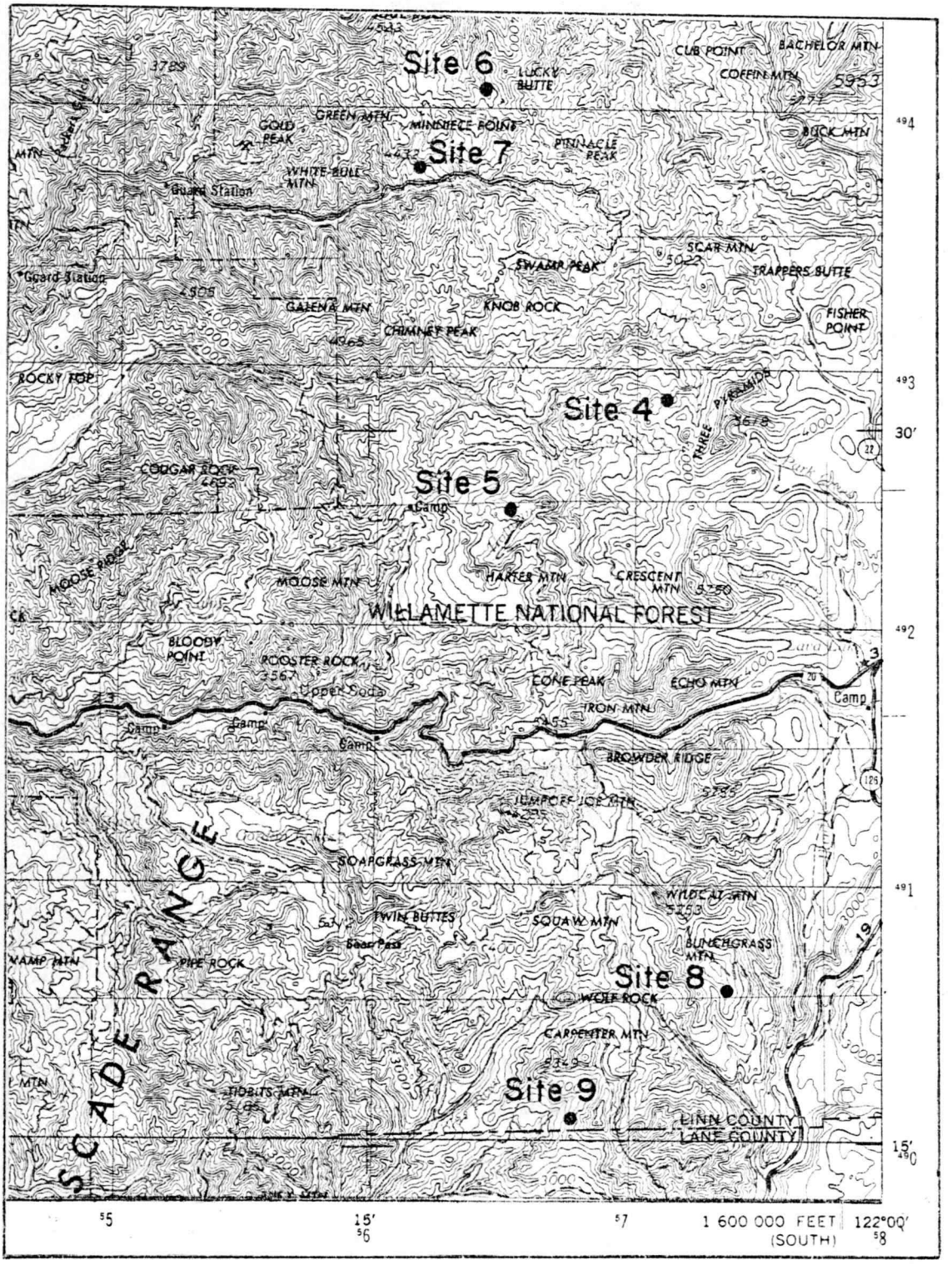

Figure 21. Sample site locations--Detroit to Cougar Reservoir area of the Oregon Cascades.

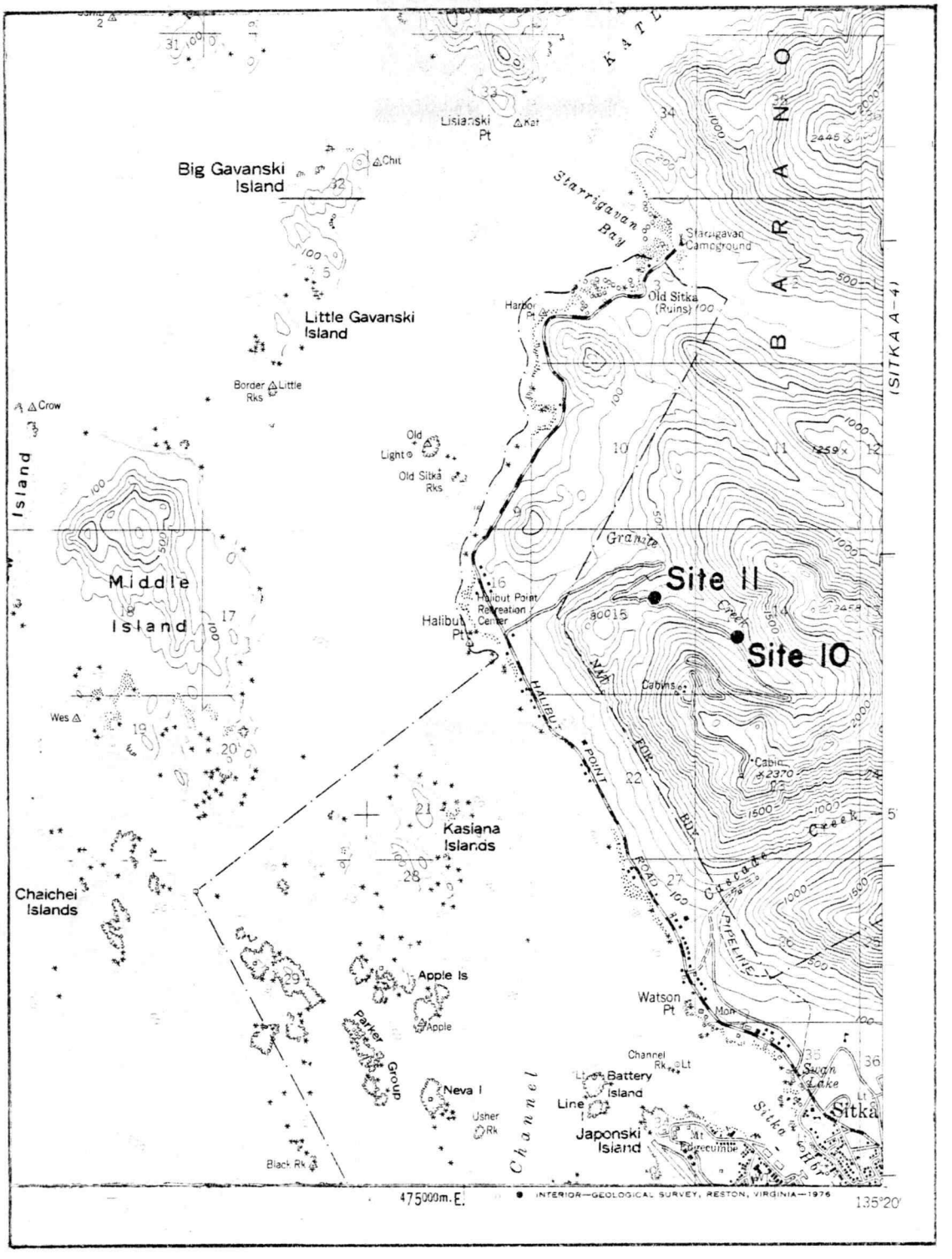

Figure 22. Sample site locations--south east Alaska.

many sites in the Oregon Cascades. Nine sites which showed X-ray diffraction patterns indicating the presence of amorphous materials and soils derived from volcanic ash, were chosen for sampling. Soil sampling sites in Alaska were located in areas of geologically young volcanic ashfalls.

Sampling and Transport Methods

Disturbed and undisturbed samples were taken at depths dictated by the specific sampling site. Usually the surficial 1 to 4 feet were sampled with the upper few inches to 1 foot of organic litter being avoided. Care was taken to obtain samples which represented average visual characteristics of soils in and around the surrounding area. Site data such as parent material, average soil depths, elevation, slope shape, average slope angle, land use, and general site descriptions were recorded at each site location.

Disturbed samples were excavated over the cross-sectional depth desired. In this way bulk samples representing cross-sections of 1 to 2 feet were taken. Twenty to forty pounds of this excavated material was placed in plastic lined canvas bags. Small amounts were stored in quart jars for transport to the laboratory humid room. All samples were carefully labeled. Soil descriptions, and corresponding depths were recorded. Water contents for each site were determined

for the jar samples immediately upon arrival in the laboratory.

Undisturbed specimens were sampled with short (2. 5 ft.) thin wall shelby tubes. The shelby tubes were supported by a special frame designed for sampling in shallow soils. Depending on the site, the tubes were pushed, trimmed, or lightly driven into the soil mantle. At least two 2. 5 ft. tubes were filled at each site. Upon removal from the ground, each tube was immediately sealed with wax, capped, and sealed with tape, for transport to the laboratory. Appendix C describes these sampling procedures in detail.

Laboratory Methods - Engineering Testing

Seven conventional soil characterization tests were conducted on samples from each site. These tests were performed according to ASTM standards and conventional engineering practice except where special information was required. Deviations from standard test methods are noted where appropriate. Appendix C describes all test procedures in detail.

Natural Moisture Content

Natural water contents in percentage of dry weight were determined for each sample. These were for the whole soil, taken from

jar samples which represent 1 to 2 foot sections in the soil profile. Natural water contents were also determined for undisturbed samples, when removed from the tubes for strength testing. In addition, natural water contents were determined for soils separated for grain size analysis. Several water contents from the same deposit allowed some comparisons as to vertical variation in water contents over shallow depths.

Atterberg Limits

Three sets of Atterberg limit tests were performed on each sample. These were conducted under natural moisture, air dry, and oven dry conditions. For the natural water content case, the minus number 40 standard sieve size soil particles were separated by wet sieving. Excess water was evaporated from the minus 40 material in a plaster of paris bowl coated with filter paper. The minus 40 slurry material was dried to approximately the liquid limit then tested for Atterberg limits using the standard method. For air dry and oven dry cases, standard ASTM method D423 for determination of Atterberg limits was used. The samples were air dried to equilibrium with laboratory atmosphere (approximately 23^{o}C at low humidity). The oven dry samples were dried at 110^{o}C for 24 hours.

Specific Gravity

Specific gravity was determined for each whole soil sample by standard ASTM method D854. Three separate tests were run on about 50 g of dried soil which had been gently ground with a motor and rubber-tipped pestle. Specific gravity was determined by displacement in de-aired distilled water.

Grain Size

A partial grain size distribution was determined by wet sieving soil initially at the natural water content, through the number 40 and number 200 mesh sieves. Grain sizes are reported as percent retained on the number 40 sieve, percent retained on the number 200 sieve and percent passing the number 200 sieve. It has been well documented that grain size distributions are extremely dependent on sampling and testing variables for allophane soils (Wesley, 1973; Maeda, et al., 1977). For this reason, detailed grain size distributions were not determined for all samples. Standard mechanical grain size distributions were determined by ASTM standard method D422; for sites 10 and 11.

Moisture-Density

Moisture-density relationships for each sample were determined for natural field conditions, air dry conditions, and oven dry conditions. These curves were established using standard ASTM D698 compactive effort. The curves at field moisture were dried from the natural water content to obtain a range of points. The air dry curves were wet from the air dried initial water content. The oven dry samples were dried at 105°C for 24 hours, then wet until several points past the optimum values were recorded.

Insitu Unit Weight

Insitu unit weight was determined for undisturbed samples by measuring the volume and weight of undisturbed specimens extracted and cut from the shelby tubes.

Strength

Three or four consolidated undrained triaxial tests with pore pressure measurements were conducted on undisturbed samples over a range of low confining pressures. Each sample was extracted from the shelby tube directly into the testing apparatus without major trimming. The samples were then saturated under incremented backpressure to approximately 50 psi, consolidated to equilibrium

at the desired effective confining pressure, and failed undrained under strain controlled conditions at approximately 0.6 percent strain per minute. The tests were run to strains of 20%. Effective and total stress failure envelopes were determined for each field sample site. Appendix C describes test procedures in detail.

Presentation of Geotechnical Data

Atterberg Limits and Natural Moisture Contents

Table 9 summarizes natural moisture content and Atterberg limit results for all sites. The liquid limit and plastic index for natural, air dry and oven dry conditions are plotted for Sites 1-9 in Figure 23.

Soils from the Oregon Cascades (Sites 1 through 9) have much lower natural moisture contents, and Atterberg limit values than those from Alaska (Sites 10 and 11). Natural moisture contents for the Cascade soils appear to average about 40-50% in most cases. For Alaska soils, this average is about 150%.

Figure 23 indicates that the Atterberg limit appear to group themselves into four distinct areas progressively further from the A-line. The groupings by increasing distance from the A-line are: Sites 8 and 9; Sites 3, 4, 6 and 7; Sites 1, 2 and 5; and Sites 10 and 11.

Table 9. Atterberg limits and natural water contents.

Site Number	Natural Moisture Content %	Atterberg Limits								
		Natural			Air Dry			Oven Dry		
		LL* %	PL* %	PI* %	LL %	PL %	PI %	LL %	PL %	PI %
1	36.5	47.8	50.6	N.P.	50.3	56.5	N.P.	41.5	Ø	N.P.
1b	44.0	72.5	49.8	22.7	78.3	53.6	24.7	56.7	Ø	N.P.
2	56.0	63.0	50.2	12.8	69.0	60.0	9.0	50.9	47.0	3.9
3	42.6	48.8	38.8	10.0	44.2	39.3	4.9	40.5	37.4	3.1
4	46.9	60.8	46.6	14.2	58.8	43.2	15.6	48.7	39.5	9.2
5	42.3	69.0	52.7	16.3	63.6	50.6	13.0	57.2	48.2	9.0
6	49.6	59.7	41.5	18.2	48.4	38.8	9.6	44.3	33.8	10.5
7	48.5	60.0	44.0	16.0	59.7	45.8	13.9	51.2	39.7	11.5
8	53.7	46.3	33.4	12.9	46.4	35.3	11.1	41.3	31.0	10.3
9	28.2	50.3	35.3	15.0	47.2	34.9	12.3	44.0	32.7	11.3
10	135.3	160.5	95.3	65.2	104.0	100.0	4.0	86.8	86.8	N.P.
11	160.3	233.9	119.3	114.2	125.0	125.0	N.P.	84.0	86.7	N.P.

* LL = Liquid Limit

PL = Plastic Limit

PI = Plastic Index

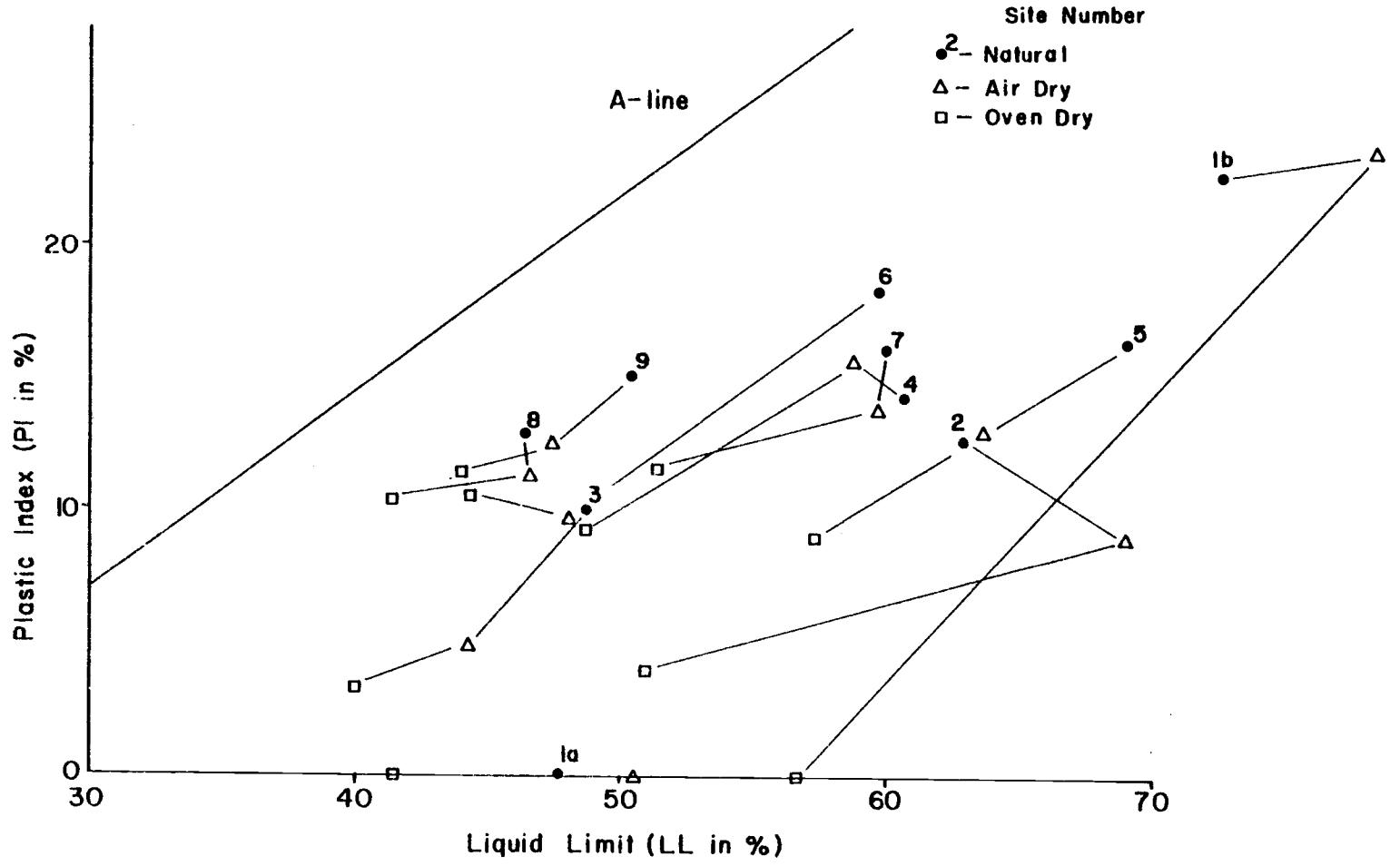

Figure 23. Atterberg limits for Sites 1 thru 9.

Grain Size

Table 10 summarizes grain size results. Samples from Sites 10 and 11 show a marked decrease in plus 40 material upon drying. This probably results from grinding of the air dried sample. The minus 40 plus 200 material percentages also increase considerably upon drying. Site 10 fines decrease upon drying but, Site 11 fines increase upon drying. The percent change in fines content with drying is small for both sites, when compared with the plus 40 and minus 40 plus 200 percentage changes.

Moisture-Density and Specific Gravity

Table 11 summarizes specific gravity and moisture-density relationships for all sites. Moisture-density curves from each site are plotted for natural, air dry, and oven dry conditions. All optimum values are determined from these curves.

In general, $\gamma_{d\ max}$ (maximum dry unit weight) increases and w_{opt} (optimum moisture content) decreases with drying. For natural conditions, $\gamma_{d\ max}$ and w_{opt} are variable between sites. $\gamma_{d\ max}$ ranges from 42 to 92 lb/ft^3. w_{opt} ranges from 28 to 73% moisture. G_s (specific gravity) also varies between sites ranging between 2.65 and 2.88.

Table 10. Summary of grain size results.

Site Number	Retained #40 %	Passing #40 Retained #200 %	Passing #200 %
1	56.8	21.8	21.4
1b	33.3	22.3	44.4
2	17.4	15.9	66.7
3	33.0	19.3	47.7
4	38.3	19.6	42.1
5	46.1	25.2	28.7
6	38.2	22.7	39.1
7	24.0	18.4	57.6
8	48.9	12.8	38.3
9	41.6	13.1	45.3
10	43.7	12.9	43.4
10 (air dry)	32.0	32.0	36.0
11	54.7	20.8	24.5
11 (air dry)	23.0	42	35

Table 11. Summary of specific gravity and moisture density optimum values.

Site Number	Specific Gravity	Moisture Density Optimum Values					
		Natural		Air Dry		Oven Dry	
		$\gamma_{d\ max}$ * lb/ft^3	w_{opt} * %	$\gamma_{d\ max}$ lb/ft^3	w_{opt} %	$\gamma_{d\ max}$ lb/ft^3	w_{opt} %
1	2.78	71.5	45.0	72.8	42.0	79.8	39.0
1b	2.88	60.0	55.0	69.0	50.0	67.5	50.0
2	2.87	71.2	46.5	70.9	47.0	81.0	38.5
3	2.86	85.9	31.7	88.8	30.5	92.4	27.0
4	2.71	81.2	32.5	84.0	33.5	87.8	29.2
5	2.67	81.2	32.0	81.2	32.0	74.5	35.0
6	2.79	83.5	35.5	86.3	35.5	88.3	32.8
7	2.80	76.5	39.0	81.5	33.0	85.0	33.5
8	2.68	92.0	28.0	94.5	26.0	96.5	24.0
9	2.67	85.5	29.5	85.5	28.5	93.0	25.5
10	2.67	48.5	67.0	54.0	66.0	64.5	38.0
11	2.65	42.0	73.0	48.0	78.0	64.5	43.0

* $\gamma_{d\ max}$ = Maximum dry unit weight

w_{opt} = Optimum moisture content

Strength and Insitu Density

Table 12 summarizes effective stress strength parameters for all sites except Site 2, for which undisturbed samples were not taken. Table 12 presents strength parameters for three interpretations of failure point for the same strength data. These are:

1. Maximum Deviator Stress-strain
2. Maximum Stress Ratio
3. Effective Stress Path

Values of c' and ϕ' for the maximum stress-strain case were determined by assuming deviator stress and strain at failure to be the maximum deviator stress point of the deviator stress-strain curve, or that portion of the curve at which a definite or abrupt change in slope occurs. Porewater pressure at failure was taken at the same failure strain. The effective stress Mohr envelope was constructed by linear regression analysis.

For the maximum stress ratio case, values of c' and ϕ' were determined by assuming failure strain to occur at the maximum point of the effective major principal stress ratio versus strain curve. Failure deviator stress and failure pore pressures were taken at this strain, and plotted at a Mohr envelope using linear regression analysis.

For the effective stress path case, a 'best fit' effective stress path failure envelope was determined by linear regression analysis

Table 12. Summary of effective stress strength parameters.

Site Number and Name	Effective Stress Strength Parameters					
	Maximum Stress-strain		Maximum Stress Ratio		Effective Stress Path	
	ϕ' (degrees)	c' (kg/cm^2)	ϕ' (degrees)	c' (kg/cm^2)	ϕ' (degrees)	c' (kg/cm^2)
1 - Dome Creek	49.7	-0.14	57.3	-0.15	56.1	-0.12
3 - Buck Creek	35.9	0.03	42.7	0.04	42.1	0.01
4 - Pyrimid Creek	42.3	-0.07	52.5	-0.08	46.9	-0.09
5 - Batchellor Creek	28.9	0.11	28.9	0.11	32.1	0.08
6 - Box Canyon Creek	46.1	-0.10	46.1	-0.08	46.7	-0.10
7 - Quartzville Creek	24.8	0.11	37.1	0.03	38.1	0.0
8 - Fritz Creek	45.8	-0.03	56.3	-0.26	50.3	-0.11
9 - Lookout Creek	36.7	-0.01	43.1	-0.01	43.3	0.01
10 - Alaska	18.7	0.15	11.8	0.19	20.1	0.14
11 - Alaska	41.5	0.11	51.4	0.04	43.2	0.10

on the appropriate points for each set of stress paths. This envelope was then adjusted so that a Mohr envelope was constructed. This was accomplished by noting that;

$$\sin \phi' = \tan \phi_{sp}$$

and

$$c' = d \frac{\tan \phi'}{\sin \phi'} \quad ;$$

where: ϕ' = effective angle of internal friction

ϕ_{sp} = angle of stress path envelope from horizontal

d = c intercept of stress path envelope

c' = effective cohesion intercept

Table 13 summarizes insitu conditions for the undisturbed samples from each site. Note the large variations in moisture contents and unit weights. Degree of saturation ranges from 54 to 100% with the average approximately 80%.

Appendix D presents a summary of these data in detail. Appendix D also presents a summary of effective stress strength parameters for each site. Plots included in Appendix D for each site are:

Deviator Stress vs. Strain

Pore Water Pressure vs. Strain

Major Principal Stress Ratio vs. Strain

One Half Deviator Stress vs. Average Principal Stress (Stress Path)

Table 13. Summary of insitu conditions.

Site Number and Name	Insitu Values			
	Moisture Content w_n (%)	Wet Density γ (g/cm^3)	Dry Density γ_d (g/cm^3)	Degree Saturation S (%)
1 - Dome Creek	37.5	1.35	0.98	56.9
	42.6	1.44	1.01	66.2
	38.7	1.29	0.93	54.1
3 - Buck Creek	39.8	1.57	1.12	73.6
	39.6	1.66	1.19	80.6
	28.4	1.52	1.18	57.4
4 - Pyrimid Creek	48.0	1.58	1.07	84.6
	45.5	1.75	1.20	98.4
	51.0	1.43	0.95	74.2
	40.3	1.81	1.29	99.2
5 - Batchellor Creek	46.6	1.55	1.06	81.6
	48.8	1.52	1.02	80.7
	40.6	1.50	1.07	72.1
6 - Box Canyon Creek	42.1	1.57	1.10	77.0
	45.4	1.45	1.00	70.5
	45.0	1.51	1.04	75.0
7 - Quartzville Creek	42.5	1.44	1.01	67.2
	48.2	1.55	1.04	80.5
	40.2	1.48	1.06	68.1

Table 13. Continued.

Site Number and Name	Insitu Values			
	Moisture Content w_n (%)	Wet Density γ (g/cm^3)	Dry Density γ_d (g/cm^3)	Degree Saturation S (%)
8 - Fritz Creek	45.5	1.28	0.88	59.6
	40.0	1.14	0.81	46.8
	53.3	1.12	0.73	53.5
9 - Lookout Creek	31.5	1.59	1.21	69.6
	43.7	1.80	1.25	(103.1)
	32.6	1.91	1.44	(102.0)
10 - Alaska	151.5	1.33	0.53	99.9
	137.0	1.33	0.56	97.3
	144.8	1.27	0.52	93.2
11 - Alaska	190.7	1.25	0.43	97.3
	101.8	1.35	0.67	90.1
	169.0	1.29	0.48	98.2

Mohr Effective Stress Envelope - Maximum Deviator Stress-Strain

Mohr Effective Stress Envelope - Maximum Stress Ratio.

The summaries of strength parameters in Appendix D presents deviator stress at failure, pore pressure at failure, axial strain at failure and A pore pressure parameter at failure for the maximum deviator stress-strain and maximum stress ratio cases. The A pore-pressure parameter was calculated using:

$$A = \frac{\Delta u_f}{\Delta \sigma_{1f}}$$

where Δu_f is the change in pore-pressure in kg/cm^2 at failure, and $\Delta \sigma_{1f}$ is the deviator stress at failure in kg/cm^2. This equation assumes that the sample was saturated and that the confining pressure is constant during the compression phase of the test.

The deviator stress-strain curves were derived from force-deflection data by calculating the sample area by the following equation:

$$\text{Area} = \frac{\text{Initial Sample Area}}{1 - \epsilon}$$

where ϵ is the strain.

Table 12 shows that the indicated angle of internal friction ranges from 18.7 to 57.3 degrees. Also, the indicated cohesion values are small, and many are negative. These results will be discussed further in Chapter V.

IV. TESTS DETERMINING SOIL MINERALOGY, SOIL STRUCTURE, AND PARTICLE SHAPE

Introduction

This chapter describes the mineralogical and structural properties of poorly crystalline volcanic ash soils reported in the literature review, and tested during the laboratory study. The laboratory resting program was designed to characterize structural and mineralogical properties of the soils sampled from Oregon and Alaska (see Chapter III for sample locations). This section outlines the laboratory testing program, and presents results from both the laboratory and literature studies.

Chapter II states that the detection of associated mineral suites found in weathered volcanic ash requires a combination of laboratory detection techniques which when added together give a comprehensive overview of soil structure and composition.

Typically, various combinations of allophane, imogolite, halloysite, kaolinite, and associated gels and cements occur together in volcanic ash deposits. The laboratory testing program was oriented towards detection of these mineral assemblages.

Constituents of Volcanic Ash Soils Reported in the Literature

Table 14 presents a summary of descriptions of soils derived from volcanic ash, as reported in the literature. Appendix A presents soil name, location and description information, in detail, for each reported soil.

The materials described in Table 14 are remarkably similar to each other considering the variety of investigators reporting a wide range of soil deposits from around the world. Similarities between locations include the distinctive yellow-brown color, granular-aggregated appearance of primarily fine grained soils, and the thixotropic behavior. Most of the soils were reported to contain allophane and related amorphous materials in combination with halloysites in various states of hydration. A variety of other minor constituents were also reported.

Laboratory Methods - Mineralogical Testing

Several mineralogical and structural characterization tests were conducted on samples from sites in the Oregon Cascades and Alaska. Sampling, transport, and sample storage procedures for samples from Sites 1 thru 11 were described in Chapter III.

The main objectives of these characterization tests were to estimate the type and relative amounts of clay minerals contained

Table 14. Summary of soil descriptions.

Africa	Coarse grained appearing red clay containing dehydrated halloysite allophane, and meta-halloysite. Sixty to seventy percent of the clay appears to be extremely small halloysite which may be allophane altering to halloysite.
Australia	Fine textured silty clay containing 85% dehydrated halloysite, and 9% free iron oxides.
Carribean	Residual soils containing allophane and hydrated halloysite. Amounts are approximately 55% hydrated halloysite, 28% dehydrated halloysite, and 17% goethite.
Central America	Thixotropic volcanic ash soils high in amorphous and organic content.
Hawaii	Thixotropic silty clay derived from volcanic ash. Moisture contents are in excess of the liquid limit, and upon drying the material irreversably becomes granular.
Indonesia	Yellowish-brown soils formed from volcanic ash parent materials. Soils are primarily allophane with halloysite and kaolinite.
Japan	Aggregated yellow-brown allophane with hydrated halloysite in the lower layers.
New Guinea	Moist yellow-brown silty composed of hydrated halloysite and allophane with moderate amounts of gibbsite and vermiculite.
New Zealand	Yellow-brown clay formed from andesitic and rhyolitic ash. These soils contain allophane as the principal mineral with some gibbsite, and small amounts of iron oxides.
North America	Fine clay-like soils with sandy appearance. Soils contain allophane and other amorphous constituents, hydrated halloysite, halloysite, chloritic intergrades and smectites.

Table 14. Continued

Phillipines	Hydrated halloysite formed in weathered tuffs and lavas.
South America	Soils of volcanic origin with high moisture holding capacity and high permeability.

in the samples with emphasis on detecting the presence and percentage of allophane and associated amorphous clay minerals. This required the following basic steps:

1. Determine if the sample contains allophane, imogolite, or related intermediate amorphous materials.
2. Estimate percentage of amorphous allophanic material in each sample.
3. Identify other amorphous constituents other than allophane, if present.
4. Estimate percentage of other amorphous materials.
5. Determine what crystalline constituents are present, if in significant amounts.
6. Estimate crystalline material percentages.

To best complete these objectives, several test methods were combined to satisfy several requirements for each step. These methods for each step were:

Step 1
- Infrared spectroscopy on whole sample
- visual electron microscope identification
- Phenolpthalein indicator paper method

Step 2
- Rehydration
- Infrared spectroscopy
- Electron microscope

Step 3 . Infrared spectroscopy

. Electron microscope

Step 4 . Infrared spectroscopy

. Electron microscope

Step 5 . Infrared spectroscopy

. Electron microscope

. Powder X-ray diffraction

Step 6 . Infrared spectroscopy

. Electron microscope

. X-ray powder diffraction

Infrared spectroscopy, electron microscopy, X-ray powder diffraction, rehydration, and phenolpthalein indicator method are discussed separately as follows:

Infrared Spectroscopy

Infrared absorption spectroscopy is performed on the minus #40 fraction from each site as outlined by Fieldes and Furkert (1972). If allophane is present, a key absorption peak appears near 1620 cm^{-1}. Clay mineral percentages may be determined from relative peak heights.

Sample preparation includes air drying, sample grinding, subsampling, mixing with KBr, and pressing into pellets under high pressures (10, 000 psi). The samples are scanned over ranges of

4000 to 700 cm^{-1} using a Beckman infrared absorption spectrophometer. Appendix E outlines laboratory procedures in detail. Two samples from each site are prepared. One is dry untreated whole soil, the other treated with hydrogen peroxide to remove organic matter. Organic matter may sometimes mask key allophane peaks.

X-ray Powder Diffraction

Air dried whole samples from each site were gently ground and randomly placed in an X-ray goniometer. These samples were scanned from 3 to 60 degrees$^{2\theta}$. d-spacings and peak heights were determined by conventional accepted methods.

Transmission Electron Microscope Identification

Separated clay samples from each site were viewed and photographed under the transmission electron microscope. Several photos representing the general soil matrix were taken at relatively low magnification (6500x). Subsequent areas of interest were identified in these photographs, and optically enlarged to various higher magnifications.

Sample preparation included the dispersion and separation of clays, and the preparation of microscope grids at three different soil-water dilutions to assure even sample spread over the grid

area. Appendix E describes these procedures in detail.

Taskey (1978) suggests that some features observed under the electron microscope beam may have been altered during observation. In particular he suggests that tubular halloysite may have been partially formed, or altered due to instability under the electron beam. Radical changes were not observed for the samples reported here, however, some burning of amorphous material was observed. To prevent such changes, all samples were observed under low magnification for short periods of time.

Scanning Electron Microscope

Whole freeze dried samples from each site were viewed and photographed under the scanning electron microscope (SEM). Photos representing the intact soil matrix were taken at various degrees of magnification.

Sample preparation involved the freeze drying of intact whole samples initially at the natural moisture content. The freeze dried sample was placed onto metal stubs and photographed under the SEM by conventional methods.

Percent Allophane by Rehydration

Percent allophane in a particular sample has been correlated to regain of moisture content in an oven dried soil sample (Warkentin

and Maeda, 1974). Specifically, a small sample of soil was dried at 300° C for 24 hours. The dried sample was then placed into a controlled atmosphere at 56.5% relative humidity for 30 days. The moisture content after 30 days was then correlated to the percentage of allophane for the whole sample.

Rapid Field and Laboratory Test for Allophane

A portion of soil on phenolphthalein paper treated with 1 m NaF turns the paper red if the allophane content is significant (Fieldes and Perrott, 1966). This treatment, as described by Fieldes and Perrott (1966) was applied to soils from each sample site. This test was conducted with samples at natural moisture conditions, air dry conditions, and air dry with organic matter removed with hydrogen peroxide. Possible reactions are; no reaction, less than 5% allophane; paper turns pink, 5-7% allophane; paper turns red, greater than 7% allophane. The reactions as described in Fieldes and Perrott (1966) are more specifically referred to as measurements of allophanic activity. Appendix E describes the test procedure in detail.

Presentation of Mineral Constituent Characterization Data

Infrared Spectroscopy

Figure 24 shows infrared absorption curves for samples 1 thru

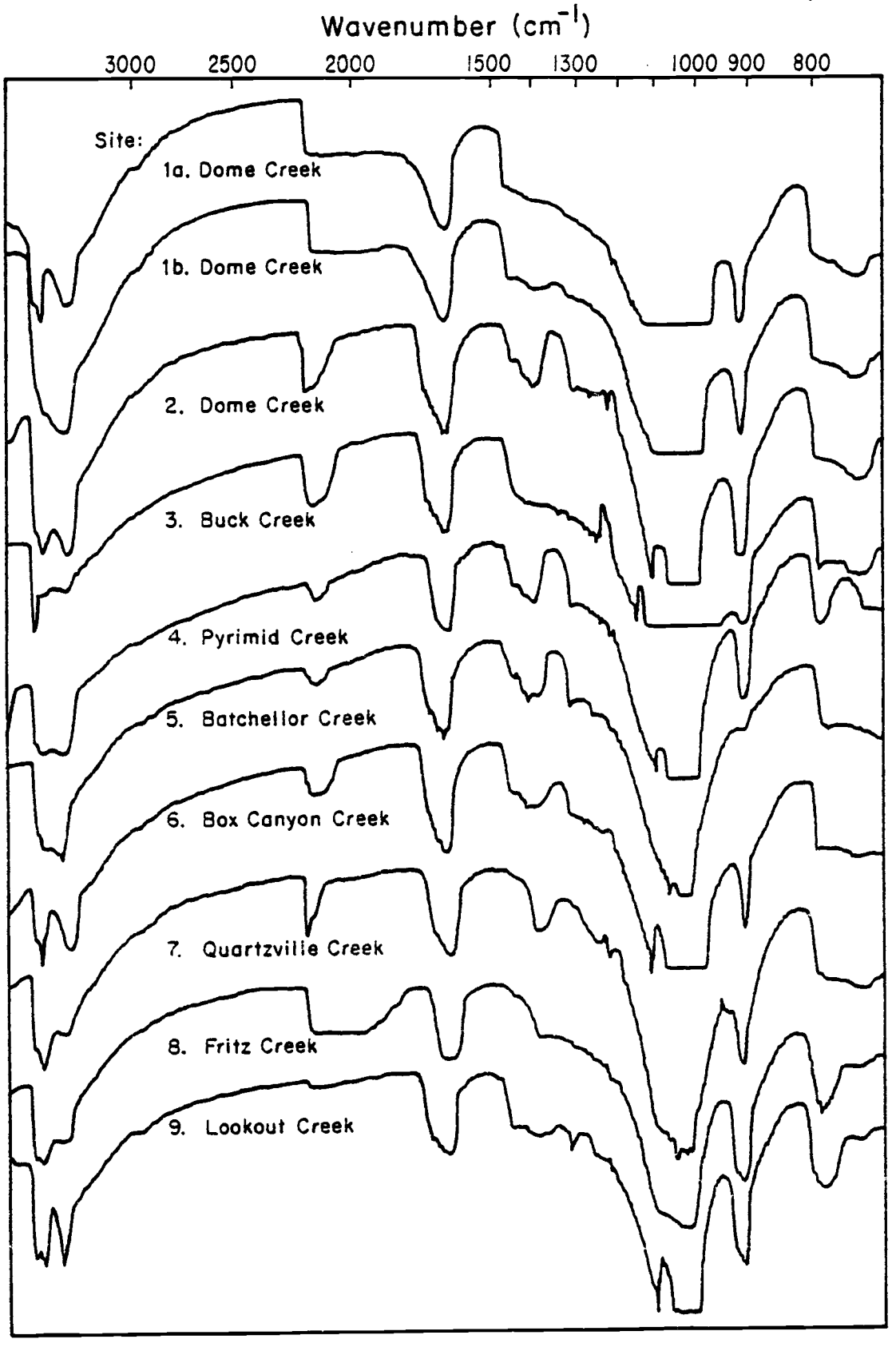

Figure 24. Infrared adsorption curves.

9. Table 15 summarizes the analysis of these curves by procedures outlined in Fieldes and Furkert (1972).

Three major constituents indicated by these results are halloysite, allophane and quartz. Halloysite produces distinctive double peaks at 3720 and 3630 cm^{-1}, respectively, with the 3630 peak sharper and more pronounced. Allophane is indicated by the 1620 cm^{-1} peak. The allophane peaks in Figure 24 are considerably larger than example peaks shown in Fieldes and Furkert (1972). The quartz peak is evidenced by an abrupt change in slope at 800 cm^{-1}. Peaks in the 1450 cm^{-1} and 2200 cm^{-1} range are thought to be due to the presence of carbonate and nitrogen compounds, respectively.

The curves shown in Figure 24 are of samples treated with hydrogen peroxide. Comparison with curves run on untreated samples show that hydrogen peroxide had little or no affect on the major peaks, and only changed those portions of the adsorption curve associated with organic matter.

Mineral percentages shown in Table 15 indicate that allophane dominates the soil constituents, ranging from 16 to 53 percent by weight. Halloysite and quartz are also present in smaller amounts averaging about 15 and 10 percent respectively. Kaolinite makes up 8.3% of the sample from Site 3, and illite is present in the soils from Sites 4, 7 and 8.

Table 15. Minerals and mineral percentages of the minus #40 fraction as determined by infrared spectometry.

Site Number	Site Name	Minerals Present	Mineral; Percent Whole Sample
1	Dome Creek	Halloysite	8
		Allophane	27
		Quartz	8
1b	Dome Creek	Allophane	52
		Quartz	14
2	Dome Creek	Halloysite	16
		Allophane	53
		Quartz	12
3	Buck Creek	Kaolinite	8
		Allophane	45
		Quartz	13
4	Pyrimid Creek	Illite	3
		Metahalloysite	21
		Allophane	29
		Quartz	6
5	Batchellor Creek	Halloysite	7
		Allophane	37
		Quartz	8
6	Box Canyon Creek	Halloysite	13
		Allophane	38
		Quartz	9
7	Quartzville Creek	Halloysite	27
		Illite	7
		Allophane	31
		Quartz	9
8	Fritz Creek	Metahalloysite	17
		Illite	16
		Allophane	16
		Quartz	6

Table 15. Continued.

Site Number	Site Name	Minerals Present	Mineral; Percent Whole Sample
9	Lookout Creek	Metahalloysite	12
		Allophane	34
		Quartz	11

Table 16. Summary of major peak d-spacings for X-ray powder diffraction.

Site 1 Dome Creek		Site 1b Dome Creek		Site 2 Dome Creek		Site 3 Buck Creek		Site 4 Pyrimid Creek		Site 5 Batchellor Creek	
16.5*	(10)**					15.9	(13)			15.9	(7)
								14.6	(4)		
						9.98	(12)*				
7.96	(6)			7.92	(3)						
						7.40	(10)*				
										6.8	(6)
4.52	(18)									4.56	(19)
		4.39	(11)	4.35	(20)	4.42	(26)*	4.45	(13)	4.41	(9)
								4.24	(6)		
4.13	(10)					4.13	(9)	4.13	(9)		
		4.01	(8)					4.04	(12)		
3.82	(10)							3.88	(5)		
						3.76	(13)	3.76	(7)		
		3.34	(12)					3.33	(12)		
3.26	(20)	3.19	(14)			3.23	(29)	3.21	(18)		
		3.11	(9)								
				2.92	(6)	2.93	(20)				
2.78	(12)										
		2.69	(7)	2.68	(6)	2.7	(22)				
2.55	(22)	2.51	(10)	2.50*	(20)	2.52	(38)	2.52	(11)	2.56	(17)
										2.24	(16)
										2.01	(7)

* d - spacing ** relative intensity

Table 16 Continued

Site 6 Box Canyon Creek		Site 7 Quartzville Creek		Site 8 Fritz Creek		Site 9 Lookout Creek		Site 10 Alaska		Site 11 Alaska	
13.9	(9)										
		8.6	(19)								
						7.43	(7)				
				7.2	(8)	7.19	(6)				
				4.79	(8)						
4.48	(30)										
		4.36	(15)	4.32	(17)	4.32	(19)				
		4.17	(7)								
4.06	(38)	3.96	(7)	4.02	(35)	4.01	(41)	4.09	(16)	4.02	(8)
								3.81	(12)		
										3.73	(11)
								3.67	(10)		
						3.56	(7)				
								3.46	(20)		
3.36	(30)	3.30	(32)	3.32	(29)	3.32	(27)	3.38	(19)	3.32	(8)
3.21	(14)	3.15	(8)					3.23	(38)	3.18	(18)
								3.04	(10)		
								2.96	(8)		
		2.86	(4)	2.84	(6)	2.86	(6)	2.87	(8)	2.87	(48)
		2.67	(7)								
2.55	(15)	2.50	(10)	2.51	(16)	2.50	(10)	2.54	(7)		
				2.48	(14)			2.45	(15)		
						2.34	(8)				
				2.22	(5)						
						2.12	(6)				

Mineral percentage by this method is tenuous at best, and these determinations can best be used to determine relative mineral contents between sites rather than absolute percentages.

X-ray Powder Diffraction

Table 16 presents a summary of major peak inter-planar d-spacings and relative intensities for each soil. These are arranged so that similar d-spacings appear on horizontal rows across the table, and site data are grouped in vertical columns.

Table 17 summarizes the interpretations of data. The data were analyzed by matching appropriate d-spacings and peak intensities to specific mineral types. A large variety of materials were indicated. The mineral fractions appear to be dominated by various feldspars, halloysite, and quartz. There is also evidence of illite, Al-Fe-Si compounds, chlorite, hematite, poorly formed gibbsite and kaolinites. Some evidence for imogolite and allophane is present (d-spacing about 16A for imogolite and 2.25A for allophane). These materials are difficult to detect with X-ray diffraction since they are amorphous.

Percent Allophane by Rehydration

Table 18 presents the results of this test. Calculated allophane percentage is twice the rehydration water content (B. Warkentin, personal communication).

Table 17. Minerals of the whole soil sample as determined by random powder x-ray diffraction.

Site Number	Site Name	Minerals Indicated
1	Dome Creek	Imogolite, Halloysite, Quartz, Feldspars, Al-Fe Oxides, Chlorite
1b	Dome Creek	Halloysite, Feldspars, Quartz, Hematite
2	Dome Creek	Halloysite, Feldspars, Hematite
3	Buck Creek	Imogolite, Halloysite, Quartz, Feldspars
4	Pyrimid Creek	Imogolite, Halloysite, Quartz, Feldspars, Allophane
5	Batchellor Creek	Halloysite, Illite, Allophane
6	Box Canyon Creek	Imogolite, Halloysite, Feldspars, Illite, Chlorite
7	Quartzville Creek	Halloysite, Feldspars, Al and Fe Oxides
8	Fritz Creek	Halloysite, poorly formed gibbsite, Feldspars, Illite, Quartz, Allophane
9	Lookout Creek	Halloysite, disordered kaolinite, Feldspars, Quartz
10	Alaska Shelikof	Quartz, Feldspars, Aluminum Silicate hydrate, Al-Si Oxide
11	Alaska Sitka	Feldspars, Quartz, Al-H silicates

Table 18. Percent allophane by rehydration.

Site Number	Site Name	Rehydration Water Content (%)	Calculated Allophane Percentage
1	Dome Creek	6.5	13
1b	Dome Creek	11.5	23
2	Dome Creek	9.1	18
3	Buck Creek	4.4	9
4	Pyrimid Creek	4.6	9
5	Batchellor Creek	6.6	13
6	Box Canyon Creek	8.3	17
7	Quartzville Creek	6.0	12
8	Fritz Creek	5.3	10
9	Lookout Creek	5.4	10
10	Alaska	4.2	8
11	Alaska	10.0	20

Rapid Field and Laboratory Test for Allophane

Results of the field and laboratory test, as outlined by Fieldes and Perrott (1966) are presented in Table 19. Each color reaction was graded on a scale from 0 to 10 with 0 being no reaction, and 10 being very positive dark purple. Intermediate numbers represent various shades of pink. Air drying without organic removal seems to dilute the reactions when compared with natural conditions. Air drying with the organics removed appears to increase the intensity of color reaction.

Electron Microscopy

Results from both the scanning electron microscope (SEM) and transmission electron microscope (TEM) studies are more appropriately presented in latter sections. The TEM results are presented in the discussion section of this chapter and the SEM results are presented in Chapter VI.

Discussion of Mineral Characterization Data -- By Site

Table 20 presents clay mineral compositions for each site as reported by Taskey (1978). As evidenced by the variety of materials reported in Tables 15, 17 and 20, reliable mineral determinations

Table 19. Summary of rapid allophane test results.

Site Number	Site Name	Natural Conditions	Air Dry with OM	Air Dry without OM	Percent Allophane
1	Dome Creek	3*	1	7	5 to 7
1b	Dome Creek	6	2	9	5 to 7
2	Dome Creek	10	10	10	more than 7
3	Buck Creek	5	2	7	5 to 7
4	Pyrimid Creek	1	0	1	less than 5
5	Batchellor Creek	1	0	5	5 to 7
6	Box Canyon Creek	1	0	1	less than 5
7	Quartzville Creek	4	3	4	5 to 7
8	Fritz Creek	4	0	3	5 to 7
9	Lookout Creek	5	1	4	5 to 7
10	Alaska	8	9	-	more than 7
11	Alaska	10	10	-	more than 7

* graded color reaction with 0 being no color reaction, and 10 a very positive dark purple. Intermediate numbers represent various shades of pink. Numbers 8, 9 and 10 correspond to more than 7% allophane; numbers 2 thru 8; 5 to 7% allophane; numbers 0 and 1 are below 5% (after Fields and Perrott, 1966).

for these soils are difficult. Best results are obtained when several determinative methods are used. Conclusions based on these different methods must take into account the reliability of each test, and its ability to detect specific minerals of interest.

For example; the presence or absence of amorphous materials is difficult to determine by X-ray analysis. The presence of other crystalline clay minerals can very reliably be predicted using the preferred orientation paste method with characterization treatments outlined by Taskey (1978). Other crystalline minerals may best be detected using the random powder mount method of X-ray diffraction analysis. It has been shown that amorphous materials adsorb characteristic portions of the infrared spectrum and therefore can be detected using infrared spectography. Electron microscopy can roughly show the presence and forms of minerals in the soil. It appears that this tool is best used to confirm and enhance the results of characterization tests by other methods when dealing with amorphous, poorly crystalline soils.

Mineral compositions for Sites 1 thru 11 are discussed based on results from infrared spectrography, X-ray diffraction, transmission electron microscopy, and results reported by Taskey (1978).

Table 20. Clay mineral composition as reported by Taskey (1978).

Site Number	Site Name	Clay Minerals Reported
1, 1b, 2	Dome Creek	amorphous material, well developed hydrated halloysite, spheroidal and tubular halloysite.
3	Buck Creek	amorphous material and poorly formed chloritic intergrade.
4	Phrimid Creek	spheroidals and tubular halloysite, amorphous material, chloritic intergrade, amorphous films and strands which resemble imogolite.
5	Batchellor Creek	amorphous components, halloysite in various hydration states and strong smectite.
6	Box Canyon Creek	amorphous material, poorly crystalline chloritic intergrade well developed gibbsite tubular and spheroidal halloysite.
7	Quartzville Creek	strong hydrated halloysite and amorphous material.
8	Fritz Creek	amorphous material, hint of chloritic intergrade.
9	Lookout Creek	amorphous material, halloysite with a range of hydration, and chloritic intergrade.

Site 1a - Dome Creek Slide

This material was sampled at a depth of 15 feet in a slide along Dome Creek. Characterization analysis indicates that major constituents present are halloysite, imogolite and allophane, quartz, and various feldspars. Taskey (1978) in his clay mineral analysis also reported that halloysite and amorphous materials were the major constituents of the clay fraction.

Transmission electron micrographs of the sample are shown in Figure 25a and b. This micrograph shows cloudy, mottled amorphous material (Figure 25b), rough edged 2 μm particles which appear to be agglomerations of smaller particles, and a long thin particle which appears to be a fibrous mass enclosed by gel-like material.

Site 1b - Dome Creek Slide

These materials were sampled 4 feet from the surface, just below the root zone. Characterization tests again indicate that large amounts of allophane are present. Accompanying minerals include halloysite, quartz, feldspar and some iron oxides. Taskey (1978) also reports the presence of tubular and spheroidal halloysite.

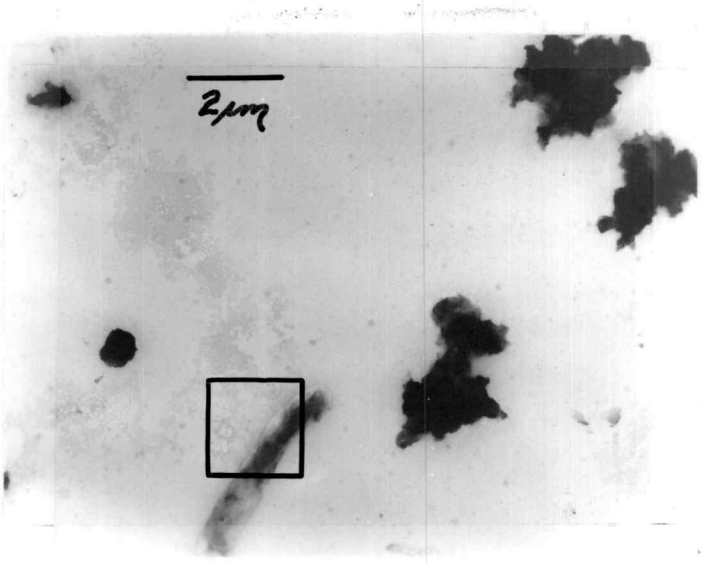

(a)

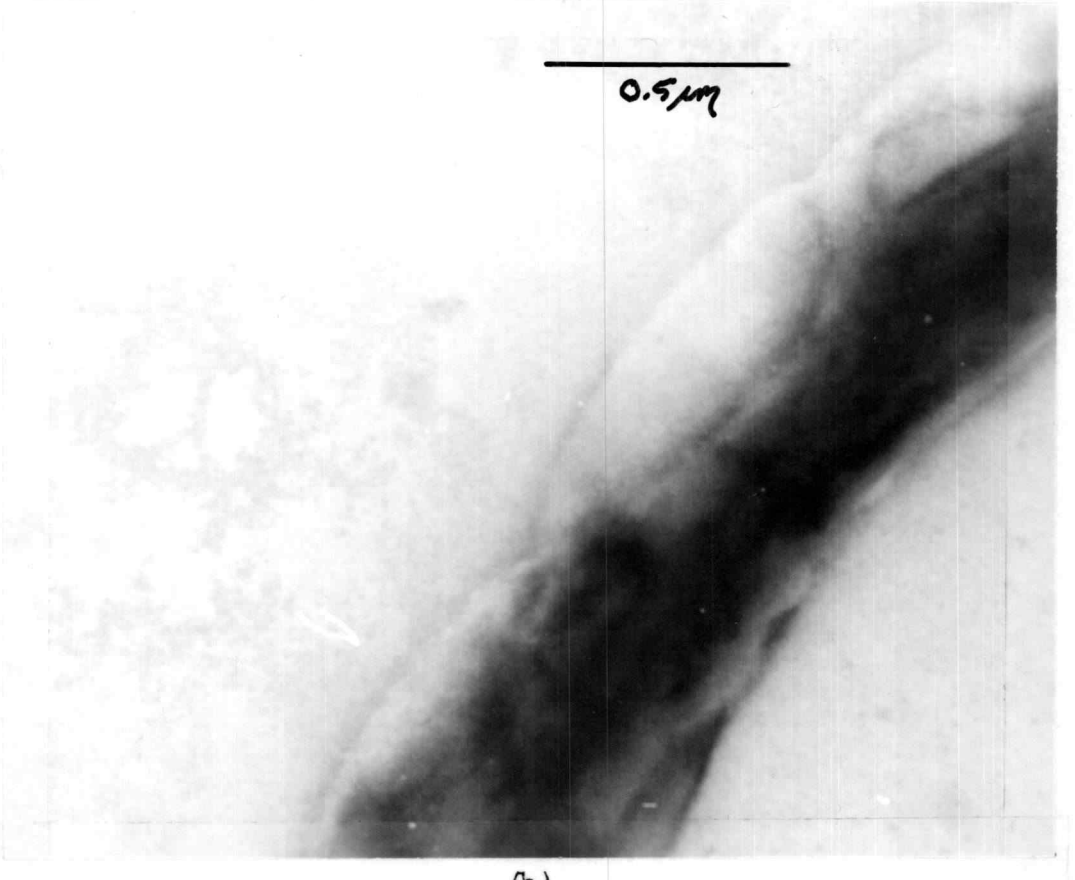

(b)

Figure 25. (a) TEM micrograph of Site 1a (6500x); (b) TEM micrograph of Site 1a (65000x).

Figures 26a and b shows typical particle shapes and arrangements. Figure 26b is an enlargement of the area shown in 26a. These electron micrographs show irregularly shaped solid particles, agglomerations of smaller particles arranged in circular type structures, and smatterings of spherical less distinct poorly formed materials. Figure 26b clearly shows a conglomerate of poorly formed metahalloysite structures arranged in star-like formations. This metahalloysite and other particles are held together by a mass of gelatinous amorphous material which seems to coat most of the particles.

Site 2 - Dome Creek Cutbank

X-ray and infrared spectograph results indicate that halloysite, allophane, quartz, feldspars and some iron oxides comprise most of the sample with allophane being especially prominent.

Figure 27a and b shows electron micrographs of a sample taken at the 5 to 6 foot depth in a shaded cutbank. Figure 27a shows some irregular distinct particles surrounded by clouds of indistinct materials of various shapes. Figure 27b is an enlargement of the area outlined in 27a, and shows evidence of very poorly formed tubular halloysite spherical halloysite, and fuzzy looking formless amorphous materials. Most of the indistinct but recognizable particles appear to be held in the formless amorphous substance.

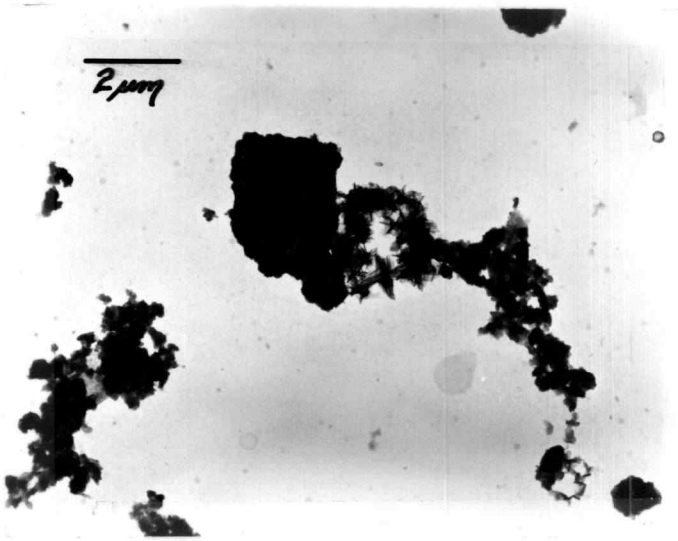

Figure 26. (a) TEM micrograph of Site 1b (6500x); (b) TEM micrograph of Site 1b (65000x).

Figure 26b.

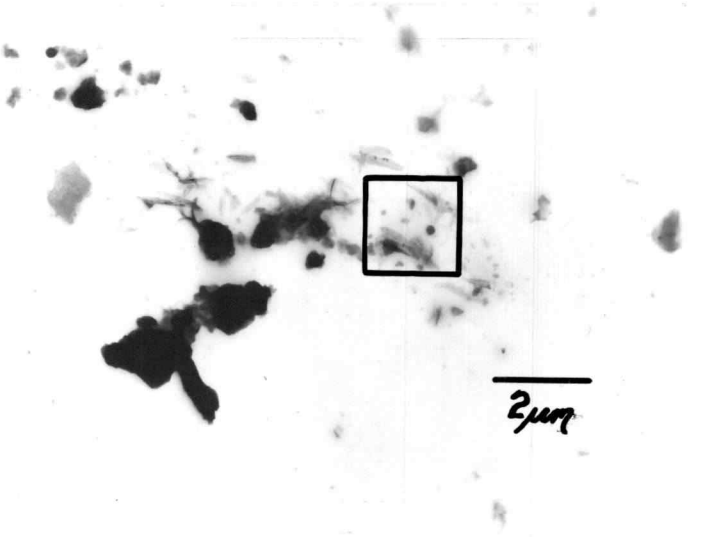

(a)

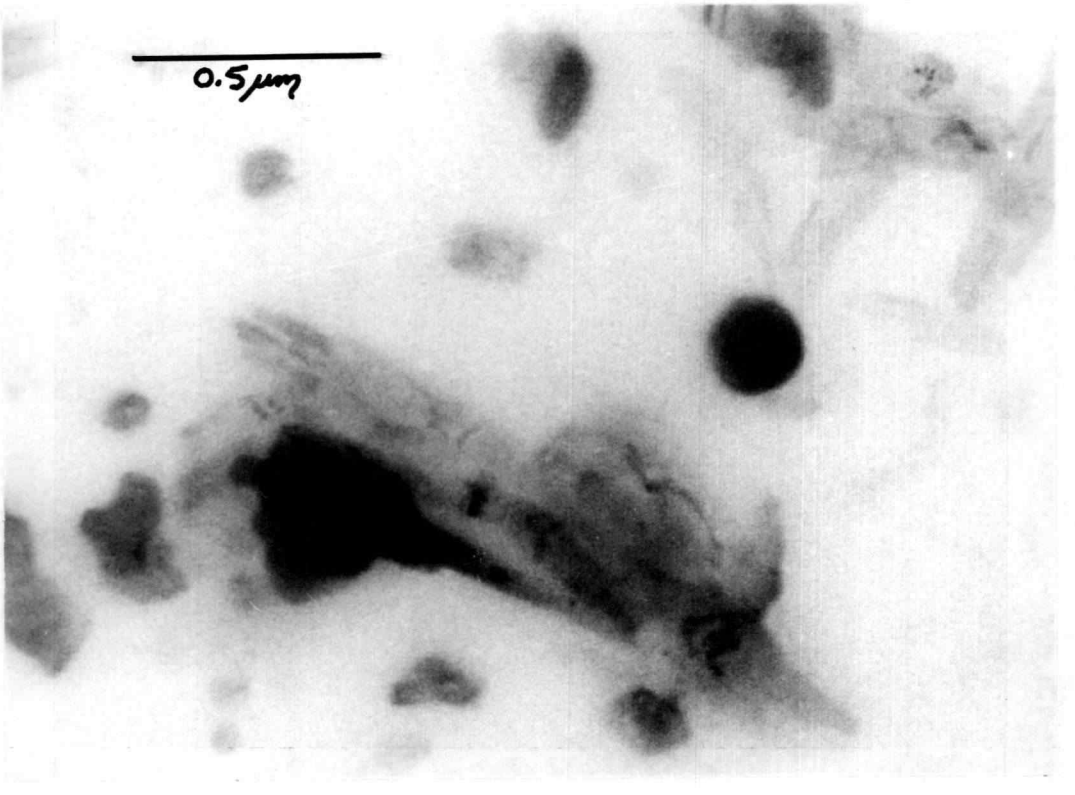

(b)

Figure 27. (a) TEM micrograph of Site 2 (6500x); (b) TEM micrograph of Site 2 (65000x).

Site 3 - Buck Creek

Mineral characterization tests indicate that soils sampled from Buck Creek are primarily composed of kaolinite, halloysite, allophane imogolite, quartz and various feldspars. The kaolinite peak, as indicated in its infrared spectrographs, is weak, indicating poorly formed kaolinite or metahalloysite.

Figures 28 and 29a and b show electron micrographs of samples from the clay fraction of Buck Creek. Figures 28b and 29b are enlargements of the areas shown in 28a and 29a. These photographs show agglomerations of distinct roughly surfaced particles intimately mixed with indistinct cloudy amorphous gel. In Figures 28a and 28b some hint of platelike kaolinite is evident, especially in the lower portion of Figure 28a. Figure 28b shows indistinct dark masses, some platelike, some rounded, and some with tubular shapes being held together in a gelatinous, webbed mass of amorphous material. Figures 29a and 29b show a characteristic strand of mixed, rounded particles and amorphous material.

Taskey (1978) reports that the Buck Creek clay fraction consists mostly of amorphous material with some poorly formed chloritic intergrades. He also detected the presence of small hollow spheres which were postulated to be spherical halloysite in the early stages of formation.

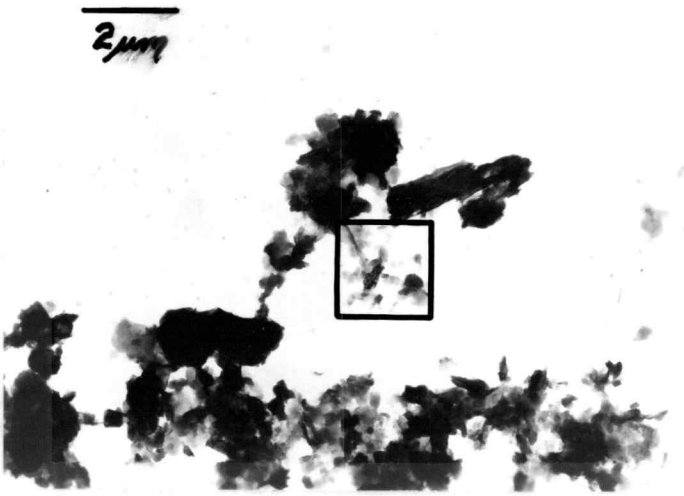

(a)

(b)

Figure 28. (a) TEM micrograph of Site 3 (6500x); (b) TEM micrograph of Site 3 (65000x).

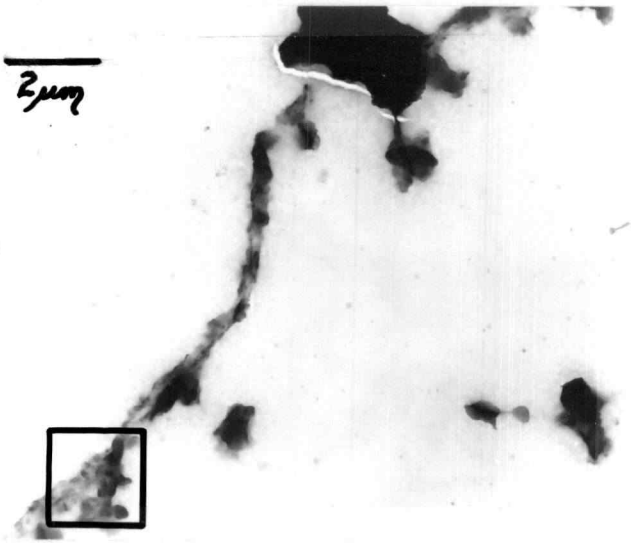

(a)

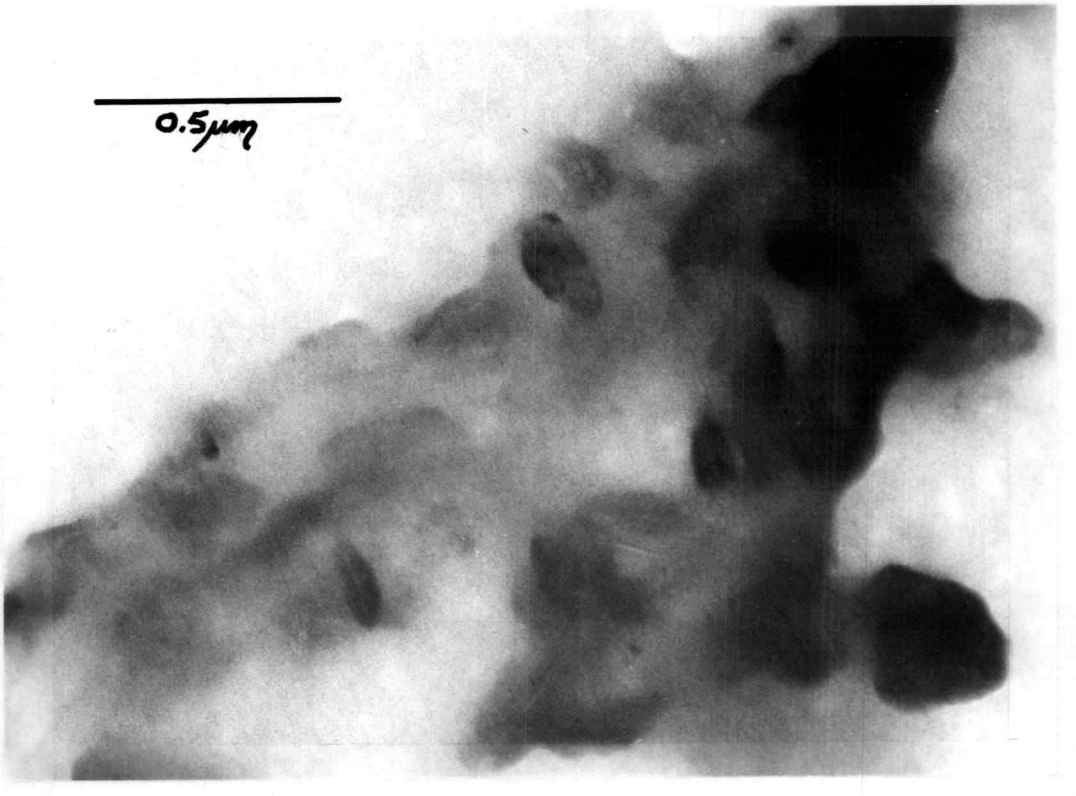

(b)

Figure 29. (a) TEM micrograph of Site 3 (6500x); (b) TEM micrograph of Site 3 (65000x).

Site 4 - Pyrimid Creek Cutbank

Characterization tests indicate that metahalloysite, halloysite, illite, allophane, imogolite, quartz and feldspars are present in the whole sample. Taskey (1978) reports the existence of tubular and spherical halloysite set in a matrix of "amorphous microaggregates, which are bound together by a network of amorphous films and strands which resemble imogolite."

Electron micrographs (Figures 30a and 30b) show the same structure with pieces of tubular halloysite, indistinct spheres, and platelike (illite) grains, floating in an amorphous matrix. Figure 30b is an enlargement of the area shown in 30a.

Site 5 - Batchellor Creek Cutbank

Test results on soils from Site 5 indicate the presence of halloysite, illite allophane, imogolite, feldspar and quartz with some chlorite.

Electron micrographs in Figure 31a and 31b show that very indistinct forms of halloysite are present with scattered and variable clouds of amorphous material. Figure 31a shows some irregularly shaped grains which may be some poorly formed halloysites. Figure 31b shows the indistinct boundary between the clay features, and the cloudy amorphous matrix material.

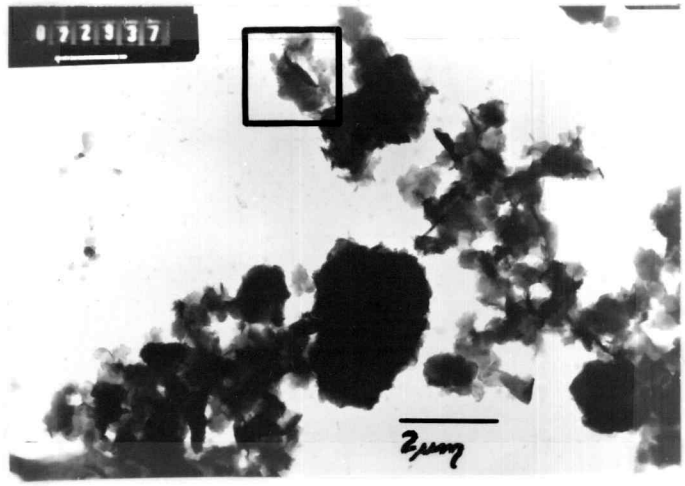

(a)

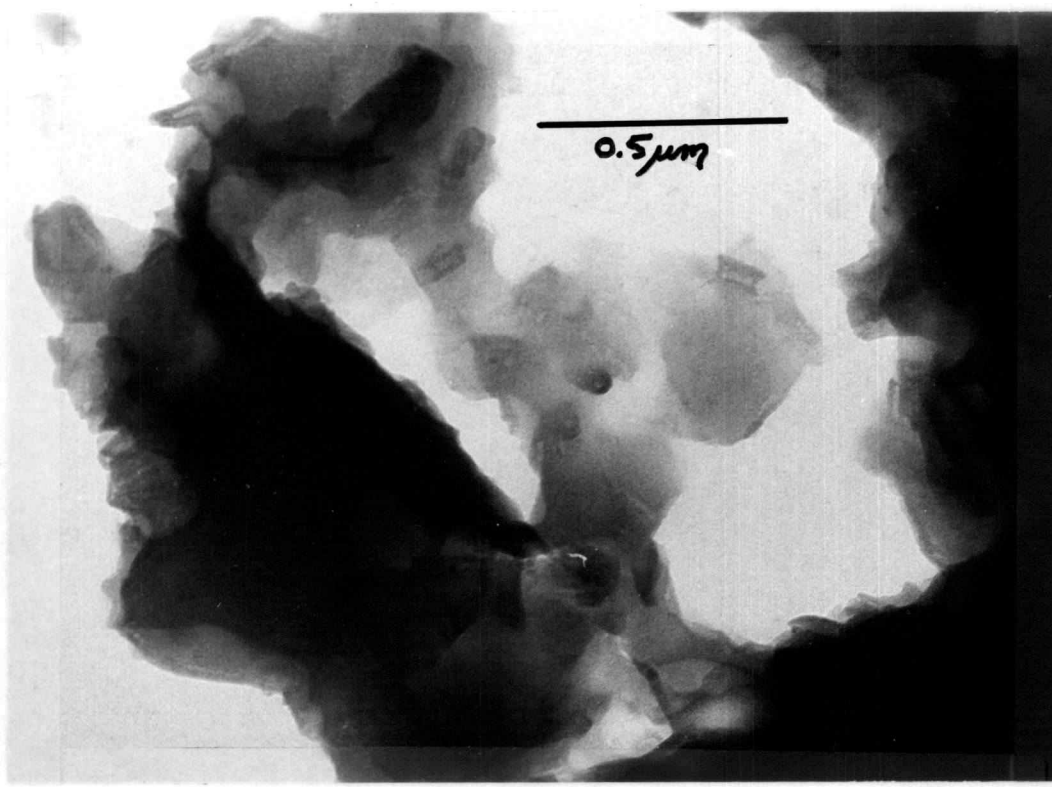

(b)

Figure 30. (a) TEM micrograph of Site 4 (6500x); (b) TEM micrograph of Site 4 (65000x).

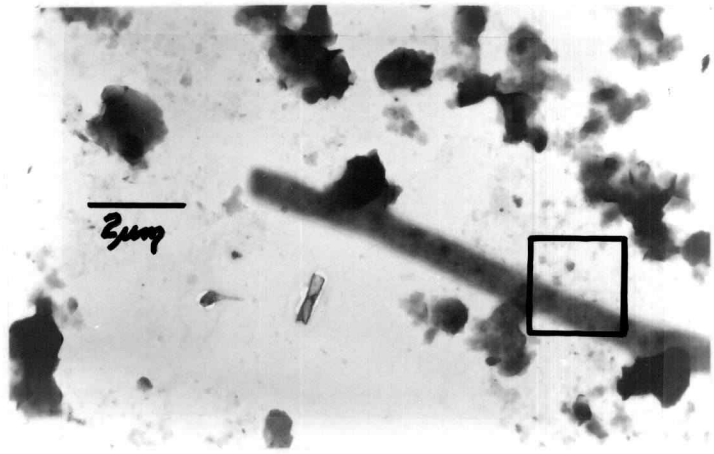

(a)

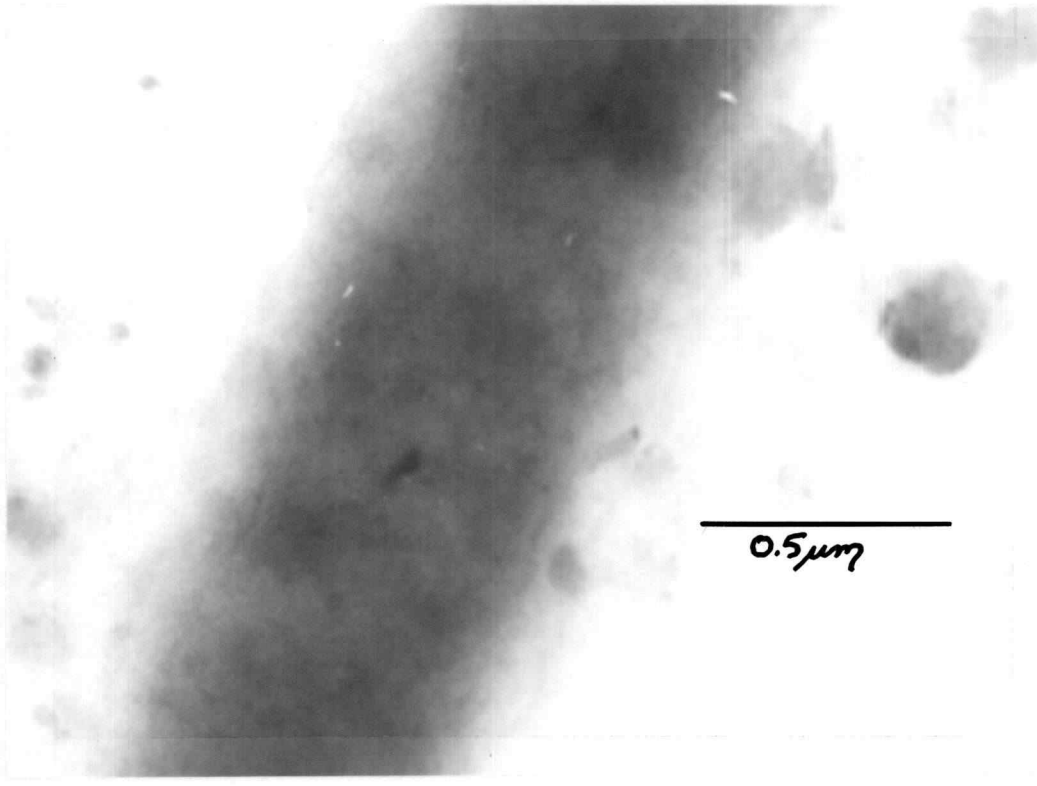

(b)

Figure 31. (a) TEM micrograph of Site 5 (6500x); (b) TEM micrograph of Site 5 (65000x).

Site 6 - Box Canyon Creek

Characterization test results show that the primary soil constituents of Box Canyon Creek soil are halloysite, allophane, imogolite, quartz, and feldspar with some illite and chlorite. Taskey (1978) describes the soil clay fraction as containing primarily amorphous materials with poorly crystaline chloritic intergrades, well developed gibbsite, and tubular and spheroidal halloysite. He also reported that electron microscope observations revealed small aggregated halloysite and other clay sized particles held together by strands and films of amorphous materials.

Figures 32a and 32b show indistinct grains set in an amorphous matrix much like that described in Taskey (1978) for Box Canyon Creek.

Site 7 - Quartzville Creek Cutbank

Infrared spectography and x-ray diffraction results show that these soils consist primarily of halloysite, illite, amorphous constituents, quartz and feldspar with some aluminum and iron oxides. Most of the sample consists of halloysite and amorphous material. Taskey (1978) reported that soils from this area contain strong evidence of hydrated halloysite and amorphous material.

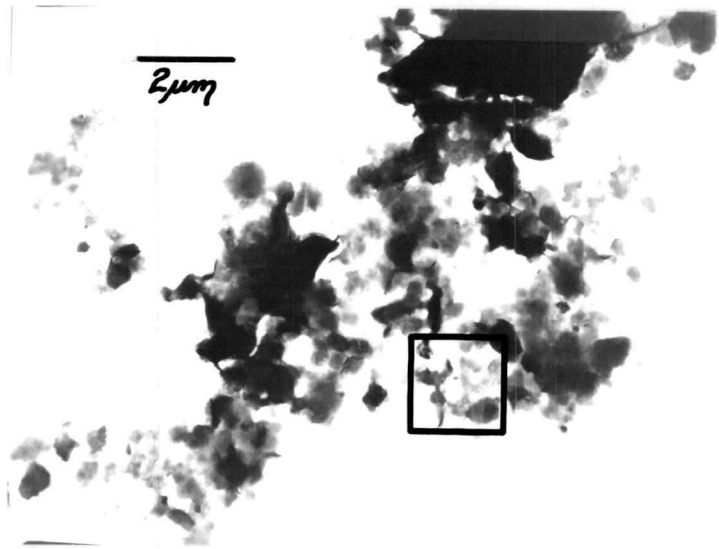

(a)

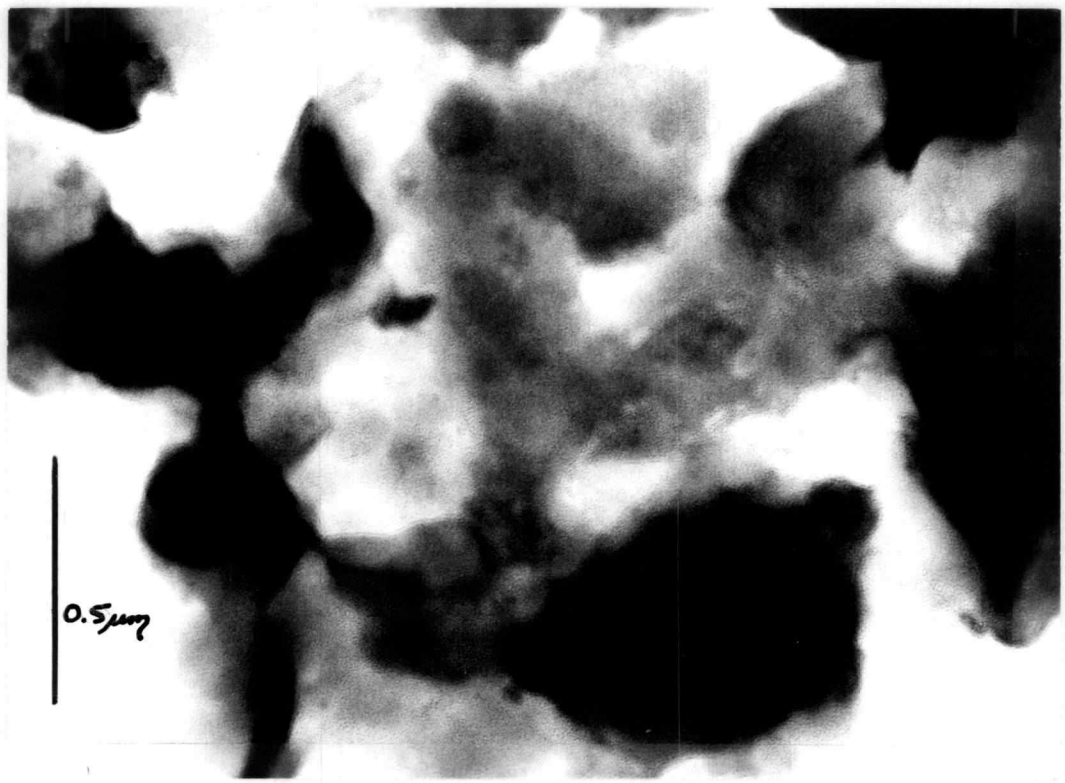

(b)

Figure 32. (a) TEM micrograph of Site 6 (6500x); (b) TEM micrograph of Site 6 (65000x).

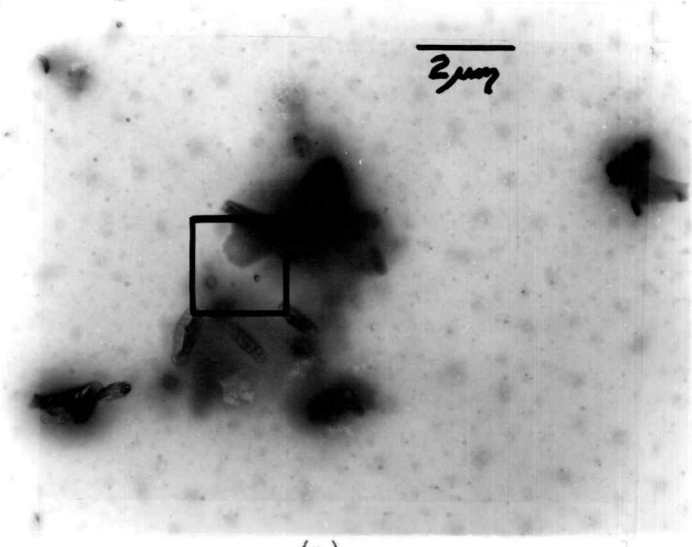

(a)

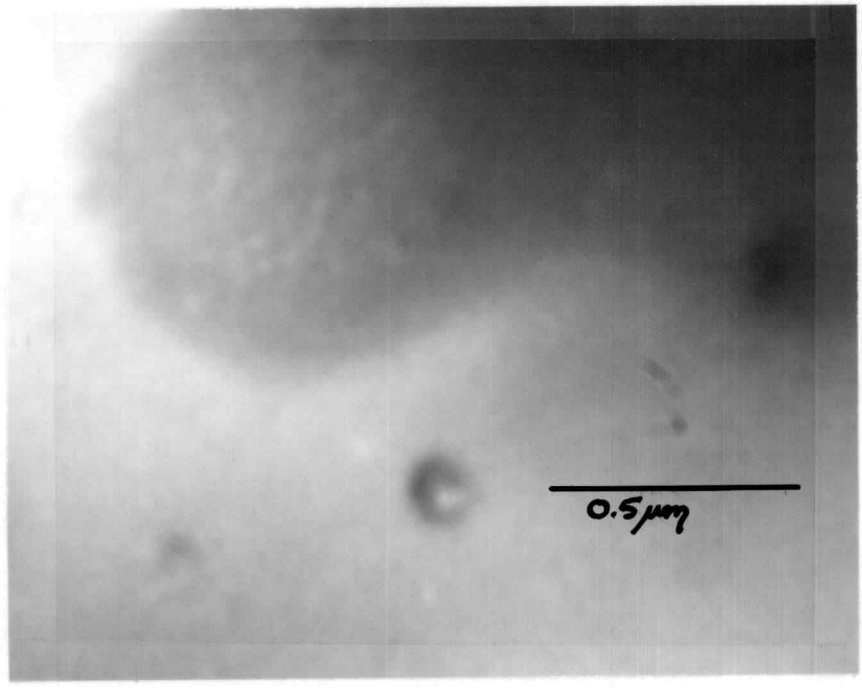

(b)

Figure 33. (a) TEM micrograph of Site 7 (6500x); (b) TEM micrograph of Site 7 (65000x).

Electron micrographs (Figures 33a and 33b) show some indistinct poorly formed halloysite tubes surrounded by a dense cloudy matrix of amorphous material. Figure 33b shows that boundaries between particles and amorphous matrix are poorly defined. Figure 33b is an enlargement of the area shown in Figure 33a.

Site 8 - Fritz Creek Slump

Characterization tests show that metahalloysite, halloysite, illite, amorphous constituents, poorly formed gibbsite, feldspars and quartz are present in these soils. Halloysite, illite and allophanic materials are the major constituents.

Electron micrographs (Figures 34a and b) show several features. Figure 34a shows large 2 μm particles surrounded by smaller agglomerates of distinct and indistinct particles. Figures 34b and 34a show that the particles and agglomerates are held together by webs of cloudily indistinct amorphous strands.

Site 9 - Lookout Creek Cutbank

Primary constituents of soils from Lookout Creek are halloysite, metahalloysite, disordered kaolinite, feldspar and quartz. Taskey (1978) reports that halloysite with a range of hydrations, amorphous

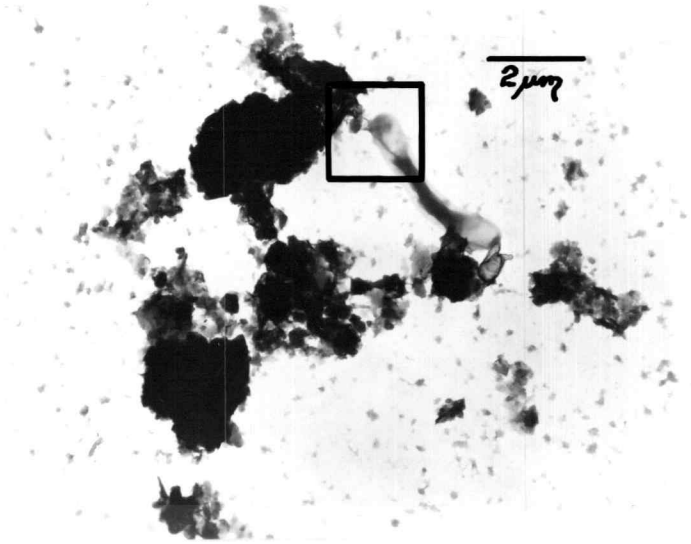

(a)

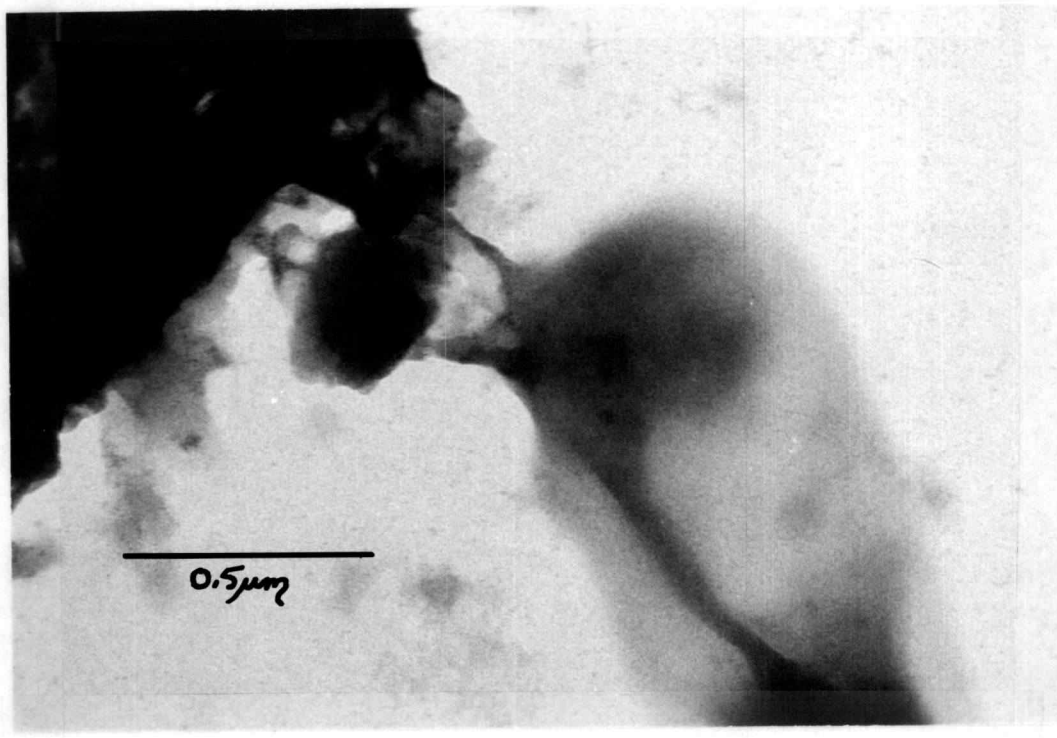

(b)

Figure 34. (a) TEM of Site 8 (6500x); (b) TEM of Site 8 (65000x); (c) TEM micrograph of Site 8 (65000x).

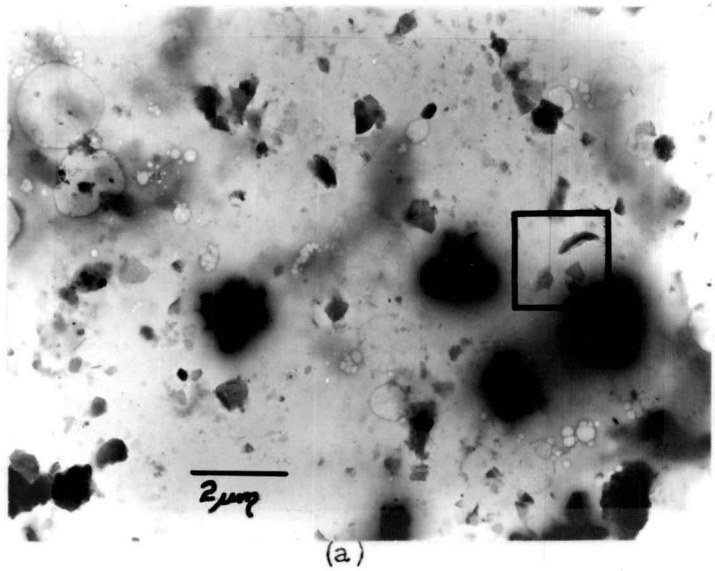

(a)

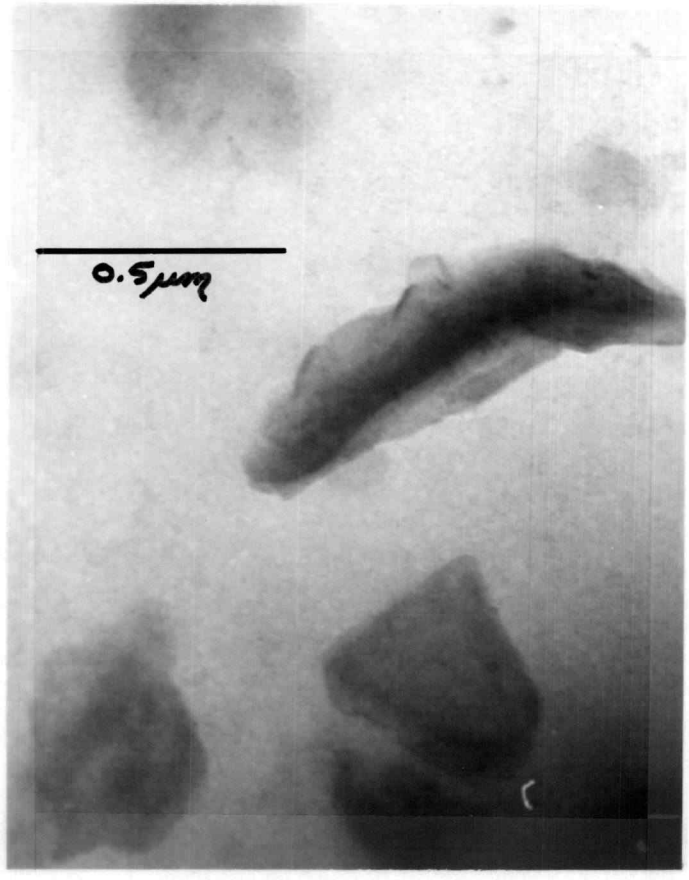

(b)

Figure 35. (a) TEM micrograph of Site 9 (6500x); (b) TEM micrograph of Site 9 (65000x).

materials, and chloritic intergrades, make up the bulk of the samples.

Figures 35a and 35b show typical forms and structures observed under the electron microscope. Figure 35a shows many distinct and indistinct particles set in a dense cloudy amorphous matrix. Note the evidence of 'burning' under the electron beam shown by the round bubbles. Figure 35b is an enlargement of the area shown in 35a, and shows a halloysite particle and a neighboring poorly formed kaolinite plate. All of these particles are set in a gel - like amorphous cloud.

Site 10 - Alaska Shelikof

Characterization tests indicate that site 10 consists primarily of amorphous constituents, quartz and feldspar.

Electron micrographs of the clay fraction (Figures 36a and 36b) support these results. Figure 36a shows some distinct particles (probably a quartz grain) surrounded by webbed poorly formed amorphous material. Figure 36b shows this amorphous material to consist of strand-like gel connecting indistinct particles much like imogolite and allophane type materials. Figure 36b is an enlargement of the area shown in Figure 36a.

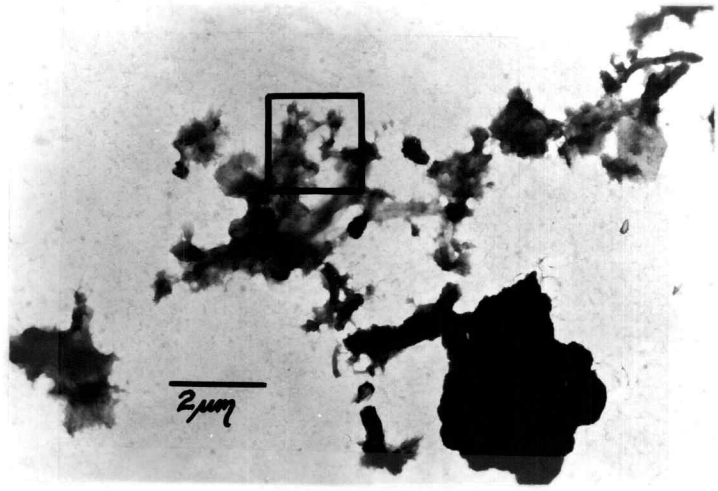

(a)

(b)

Figure 36. (a) TEM micrograph of Site 10 (6500x); (b) TEM micrograph of Site 10 (65000x).

Site 11 - Alaska Sitka

X-ray diffraction results indicate that primary constituents are amorphous materials quarts and feldspar.

Electron micrographs (Figures 37a and 37b) show an agglomeration of distinct and indistinct particles. Figure 37b shows that these particles are held together by characteristic imogolite strands and amorphous gel which make up a large portion of the sample.

Summary

In general, it appears that the soil deposits described consist primarily of various forms of halloysite, large amounts of various amorphous materials, quartz and feldspar. Mica type minerals (illite) are also reported for a large number of samples.

It has been shown that smectite, micas, quartz and feldspars are usually inherited in the parent ash. This is especially true for dacitic (high quartz content) ashes (Tokashiki and Wada, 1975). Based on this information, it is safe to assume that the illite and smectites are inherited by the parent materials and are not formed from volcanic ash as a consequence of special weathering conditions.

Halloysite has been reported to coexist with allophane, imogolite and other amorphous constituents in many geologically young volcanic ash deposits (Henmi and Wada, 1976). Halloysite

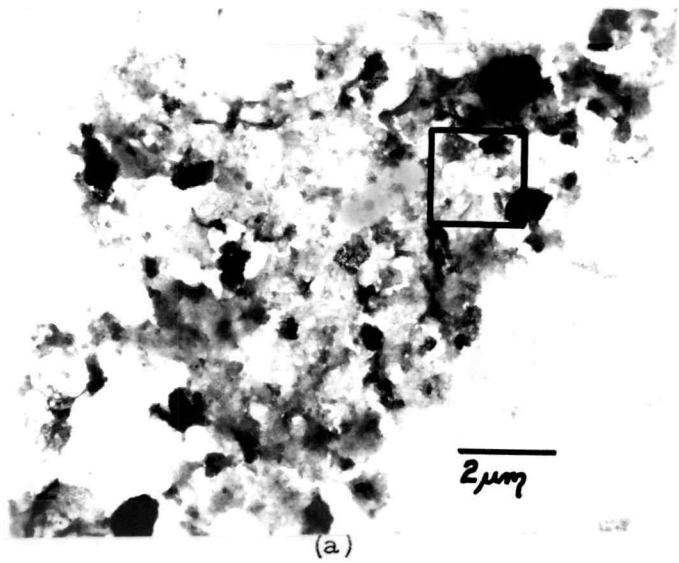

(a)

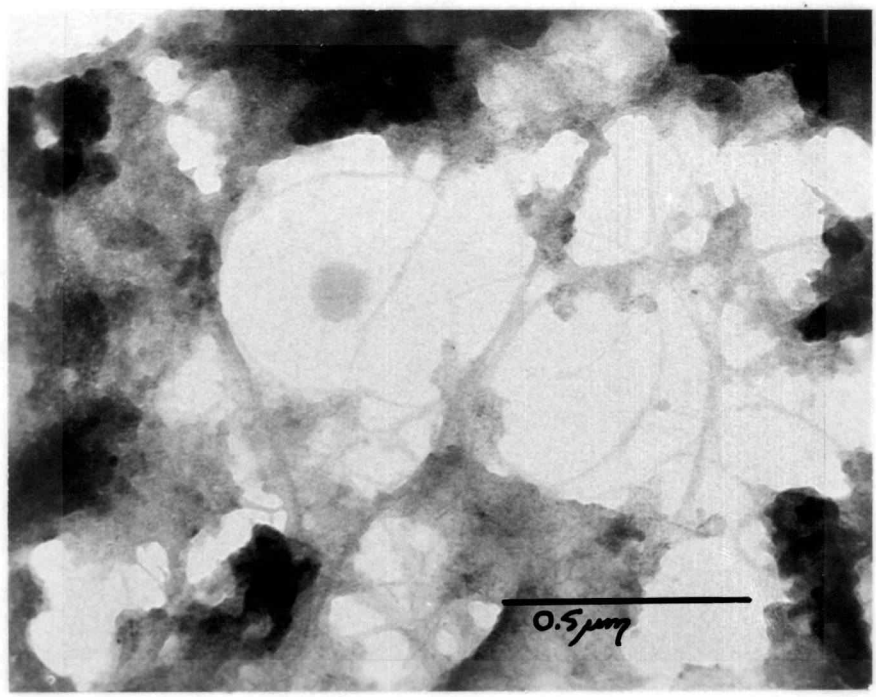

(b)

Figure 37. (a) TEM micrograph of Site 11 (6500x); (b) TEM micrograph of Site 11 (65000x).

may weather from allophanic constituents (Wada and Harward, 1974), or may form in the volcanic glass matrix as reported by Dixon (1977).

Electron micrographs of the soils from the Cascades and Alaska suggest that halloysite, allophane and imogolite are forming simultaneously in clouds of amorphous materials. This coexistence can be explained by heterogeneous weathering within the deposit where varying silica concentrations are present due to seepage of water through cracks and channels. This is a typical characteristic of deposits which are weathered in place.

The presence of significant amounts of poorly formed indistinct soil grains, along with large amounts of cloudy amorphous gels support the observation that the soils have undergone little soil development. These observations indicate that most of the soil deposits sampled are in the early stages of soil development.

V. DISCUSSION OF GEOTECHNICAL TEST RESULTS AND ENGINEERING CORRELATIONS

Introduction

This chapter discusses in detail, results obtained by geotechnical testing, and results presented in the tabular review of engineering test values reported in Appendix A.

Correlations between the index properties and engineering properties for these soils are developed. Results are presented such that engineering behaviors are correlated with key index properties. The majority of correlations were constructed using regression analysis. Statistical tests were run on engineering index properties so that statistical trends could be identified. The effects of relative allophanic/crystalline component percentage on engineering and index properties are also discussed.

Discussion of Engineering Test Results

Natural Moisture Contents

Natural moisture contents from laboratory testing are summarized in Table 21. Statistical analyses on these values suggest that all samples are not from the same group or population.

Table 21. Summary of natural water content for Sites 1 thru 11.

Site Number	Site Description	Natural Water Content (w_n in %)				
		Jar Samples	Grain Size Samples	Strength Samples		
1	Dome Creek	36.5	35.7	37.5	42.6	38.7
1b	Dome Creek	44.0	104.8	--	--	--
2	Dome Creek	56.0	59.4	--	--	--
3	Buck Creek	42.6	45.6	39.8	39.6	28.4
4	Pyrimid Creek	46.9	43.2	48.0	45.5	51.0
5	Batchellor Creek	42.3	27.2	46.6	48.8	40.6
6	Box Canyon Creek	49.6	40.6	42.1	45.4	45.0
7	Quartzville Creek	48.5	52.3	42.5	48.2	40.2
8	Fritz Creek	53.7	32.2	45.5	40.0	53.3
9	Lookout Creek	28.2	34.1	31.5	43.7	32.6
10	Alaska	143.0	135.3	151.5	137.0	144.8
11	Alaska	186.0	160.3	190.7	101.8	169.0

The statistical test used for this determination is an analysis of variance for one variable using the F statistic (Dixon and Massey, 1969). Results of the F tests indicate that natural water contents for Sites 1 thru 11 do not belong to the same normal distribution. Sites 1 thru 9 seem to group into one normally distributed population, and Sites 10 and 11 into another.

This hypothesis is further supported if the cumulative percentage of all water contents reported in the literature review and laboratory study are plotted on normal probability paper. This plot is shown in Figure 38. Normal probability paper is scaled so that any cumulative-normal-distribution plots as a straight line. Note that Figure 38 shows more than one straight line, indicating the presence of two and possibly three normal distributions.

Figure 39 shows a frequency histogram of water content observations. Normal distribution curves fitted to the frequency histogram have means of 37.8% and 110.6%. Standard deviations are 14.1% and 36.9% respectively. Another group is evident on the high end of the water content histogram. However, these represent a small number of samples.

Some reasons for the presence of two distince water content groups may be:

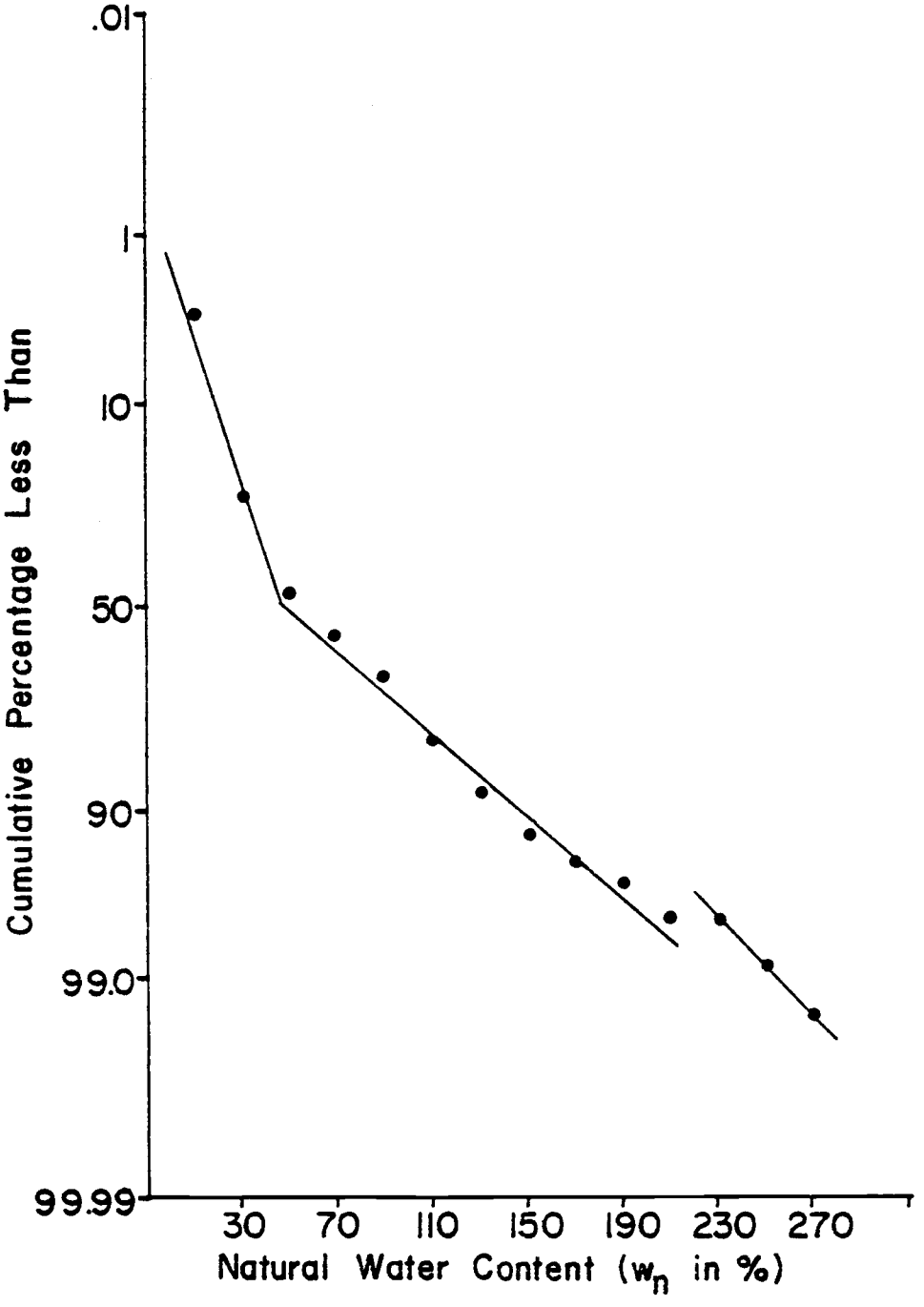

Figure 38. Cumulative normal distribution of natural water contents.

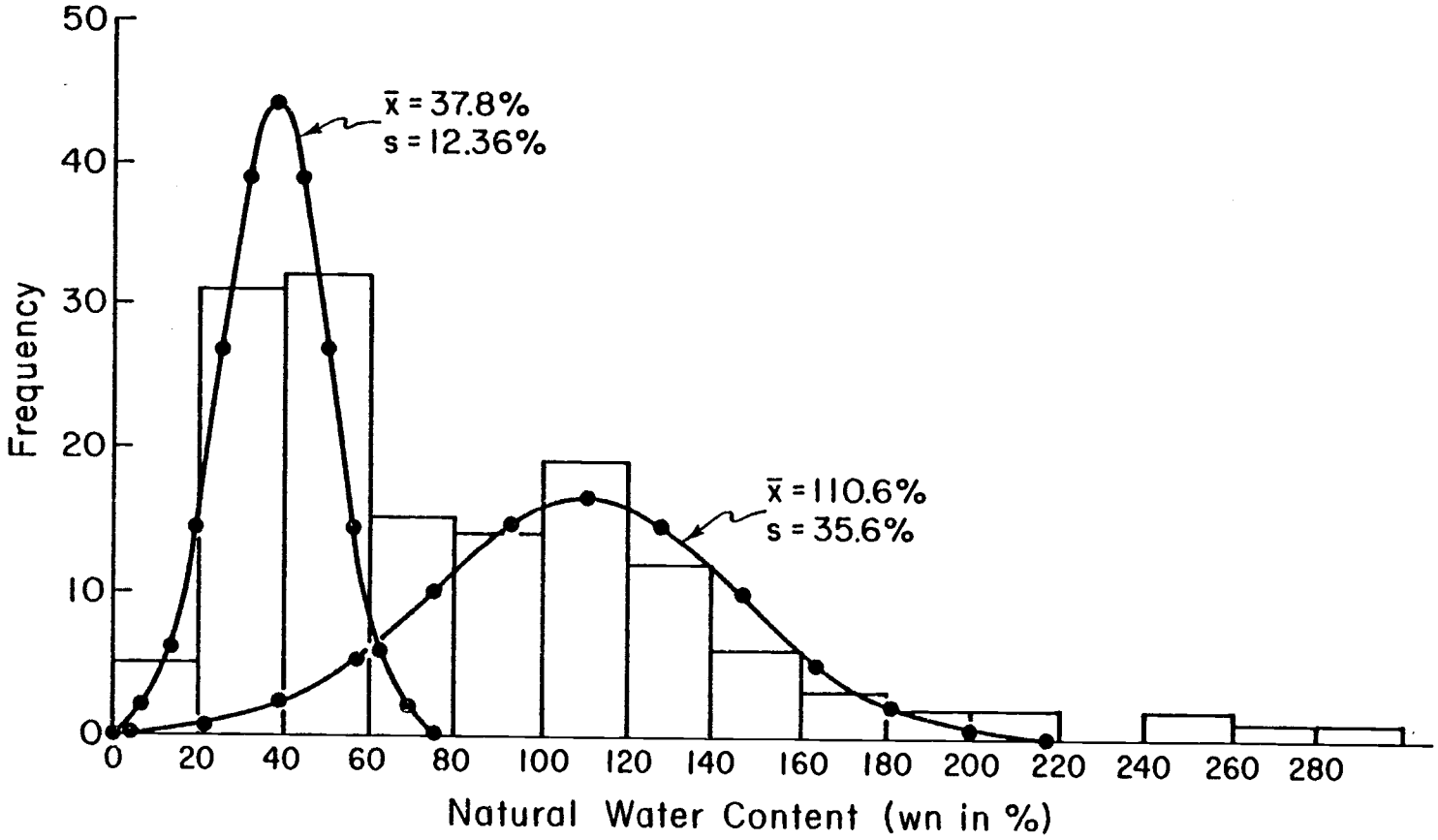

Figure 39. Frequency histogram of natural water content observations, and fitted normal distribution curves.

1. A distinct material difference exists between the two groups.
2. Soils undergo abrupt changes to a different average water content when irreversably dried by natural processes in the field.
3. Varying mineral percentages produce an abrupt change in water holding capacity.

To test these groupings, all reported soil water contents were divided into two groups based on specific characteristics which might indicate low or high water contents. Divisions of particular soils into a low or high water content group were based upon soil descriptions presented in Appendix A and B. Significant amounts of allophane, yellow-brown colors, and high clay percentages were used to characterize the high water content group. Possibility of previous drying, red colors, high silt-sand content, and high reported halloysite percentage characterized the low water content group. Statistical t-tests between the low and high groups indicated that average means for each group were not equal with 95% confidence ($\alpha = .05$). This finding statistically justifies dividing the reported natural water contents into two groups. This result also confirms that the soils have specific physical criteria by which the separation into low ($w_n < 60\%$) and high ($w_n > 60\%$) water content groups can be made.

The separated water content groups in Figure 39 assume natural water content distributions to be normal. Investigators have

shown this to be true. Warkentin and Maeda, 1981 state that natural water contents usually appear to be normally distributed for soils of similar origin and parent materials.

Atterberg Limits

Atterberg limits from the laboratory study and literature review are presented in Table 9 and Appendix A respectively. All undried Atterberg limit values are plotted on the plasticity chart in Figure 13. General trends and ranges of measurement are discussed in Chapter III.

Statistical tests on paired undried liquid limit and plastic index results indicate that these data, much like the natural water content results, are not from the same normally distributed statistical group. By the method described in Lumb (1966) these paired liquid limit and plastic index data were transformed to their standardized normal variate for each value. Average values for liquid limit and plastic index observations were 97. 9% and 35. 1% respectively. Standard derivations were 52. 0% and 25. 8% respectively.

These transformed variables were plotted on a scatter diagram and tested against a theoretical normal distribution using the chi-square statistic. Chi-square tests on the liquid limit and plastic index results show that more than one distribution of values must be

present with 99% confidence ($\alpha = .01$). Lumb (1966) reports that Atterberg limit observations from any similar soil type should be normally distributed. Thus, these results show that more than one normally distributed population must be present.

Figures 40 and 41 show frequency histograms for both the liquid limit and plastic index standardized normal variates. The presence of two and possibly three distributions are evident. Table 22 summarizes the mean for each of the reported distributions shown in the frequency histograms.

Table 22. Mean values for liquid limit and plastic index observations.

	Low Group	Intermediate Group	High Group
Liquid Limit (LL in %)	63.6	115.6	180.0
Plastic Index (PI in %)	14.7	33.8	64.2

These results, when combined with the water content analysis show that natural water contents averaging about 38% may be associated with low group Atterberg limits, water contents of about 111% with the intermediate group, and water contents of 200% or greater with the high group.

Lumb (1966) reports that the liquidity index for similar soils should be normally distributed. Figure 42 shows a cumulative

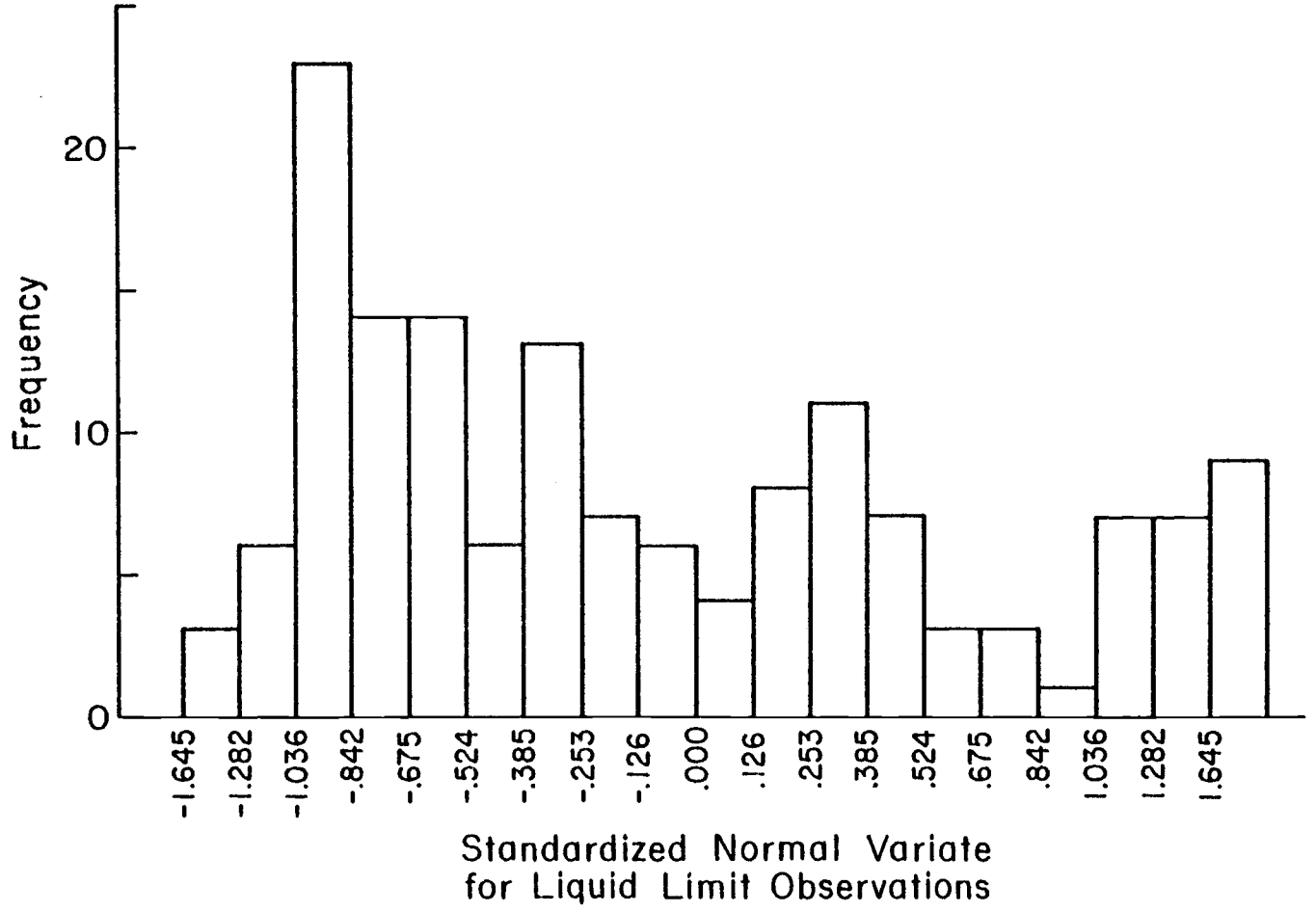

Figure 40. Frequency histogram of liquid limit observations.

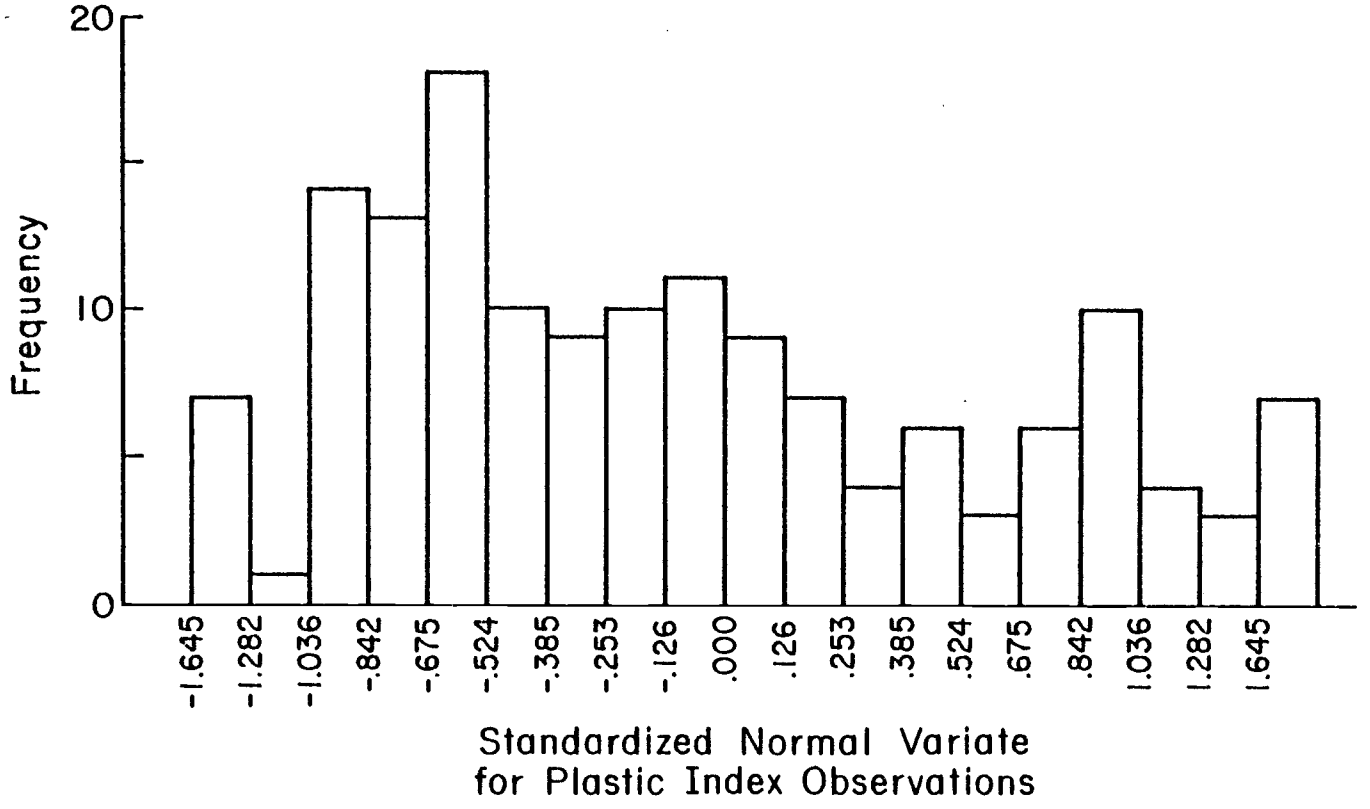

Figure 41. Frequency histogram of plastic index observations.

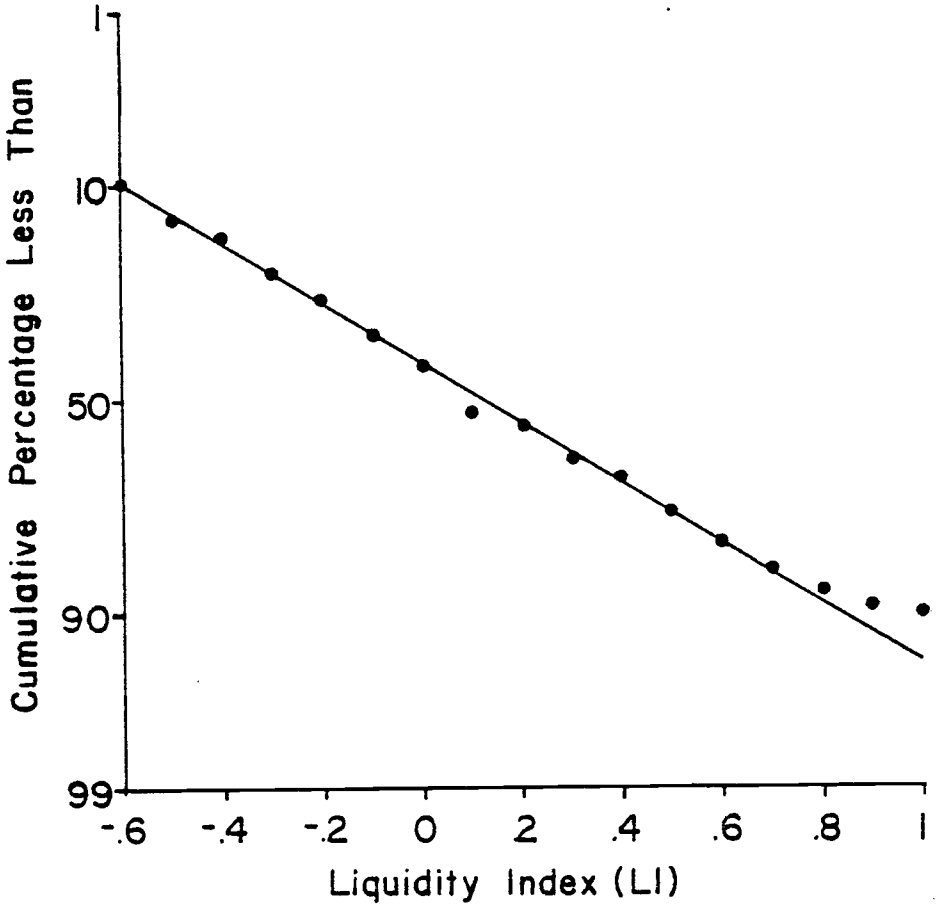

Figure 42. Cumulative frequency plot of liquidity index.

frequence plot of calculated liquidity indexes from the literature and laboratory study. This plot shows a remarkably constant normal distribution, considering results of the previous analysis of water content and Atterberg limit distributions. Figure 43 shows a frequency diagram of liquidity index values with a fitted normal distribution. The mean and standard deviation are 0.26 and 0.89 respectively.

Apparently, the low, medium and high groups indicated for water content and Atterberg limit observations combine in such a manner as to negate the effects of soil variabilities, when reported as liquidity index.

Drying affects on Atterberg limits were considered by analyzing percent change in Atterberg limits when dried from natural to oven dry conditions. Figures 44 and 45 show relationships between percent change in liquid limit and plastic limit versus natural water content.

Linear regression analysis on these samples indicate a strong logarithmic relationship between percent decrease in Atterberg limits upon drying, and natural water content. Regression coefficients of

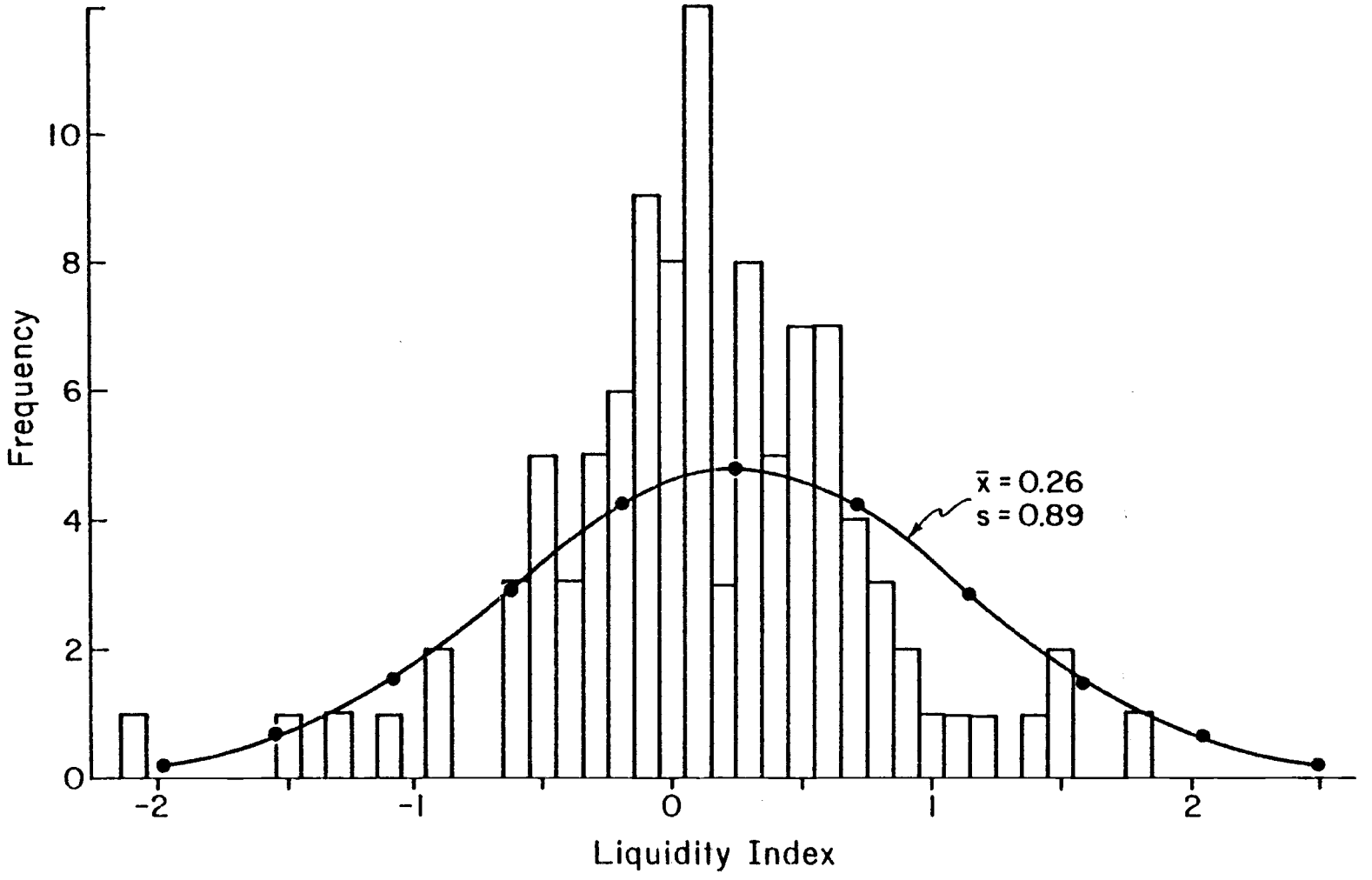

Figure 43. Frequency histogram of liquidity index observations with fitted normal distribution curve.

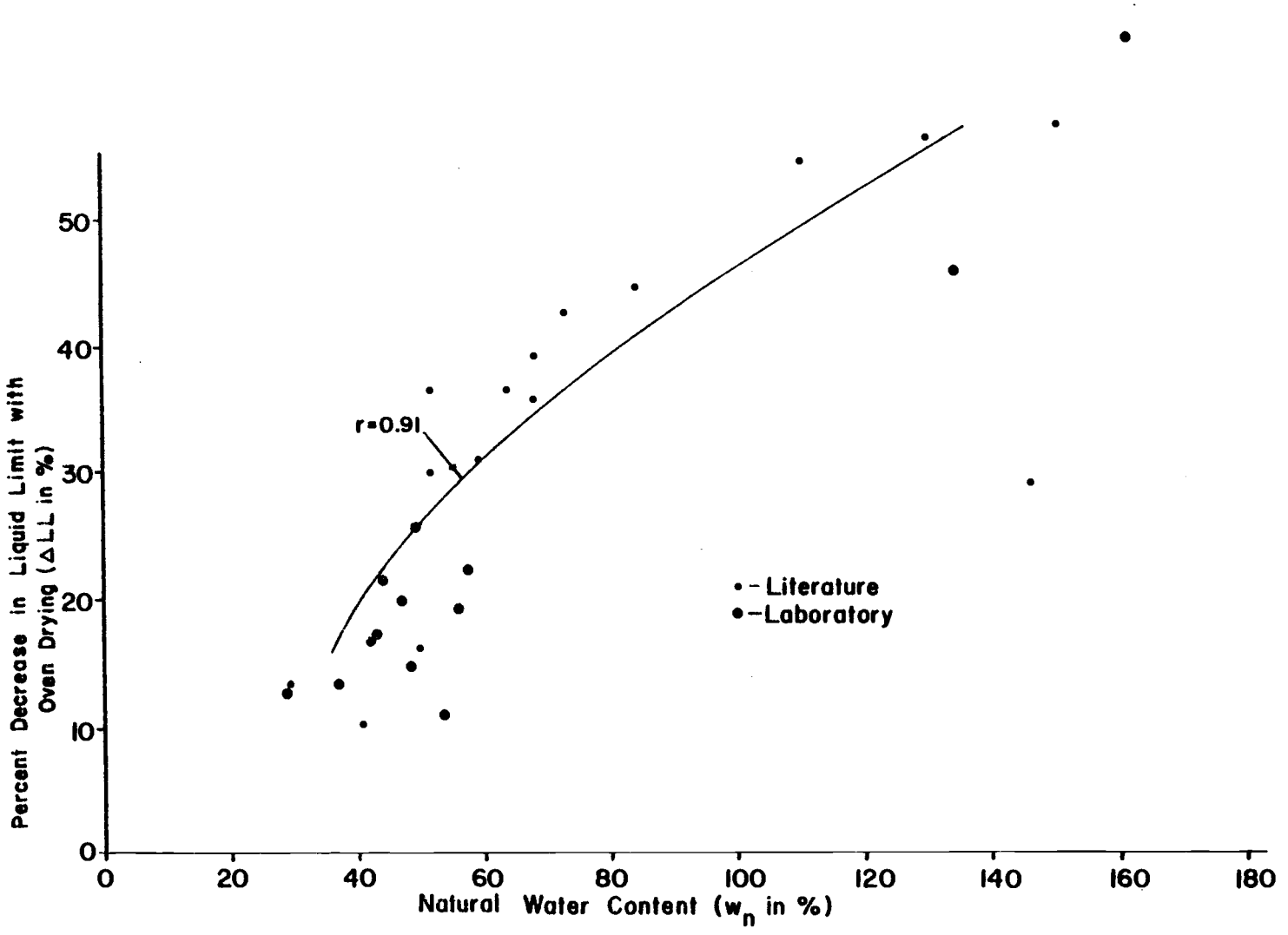

Figure 44. Percent decrease in liquid limit by oven drying vs. natural water content.

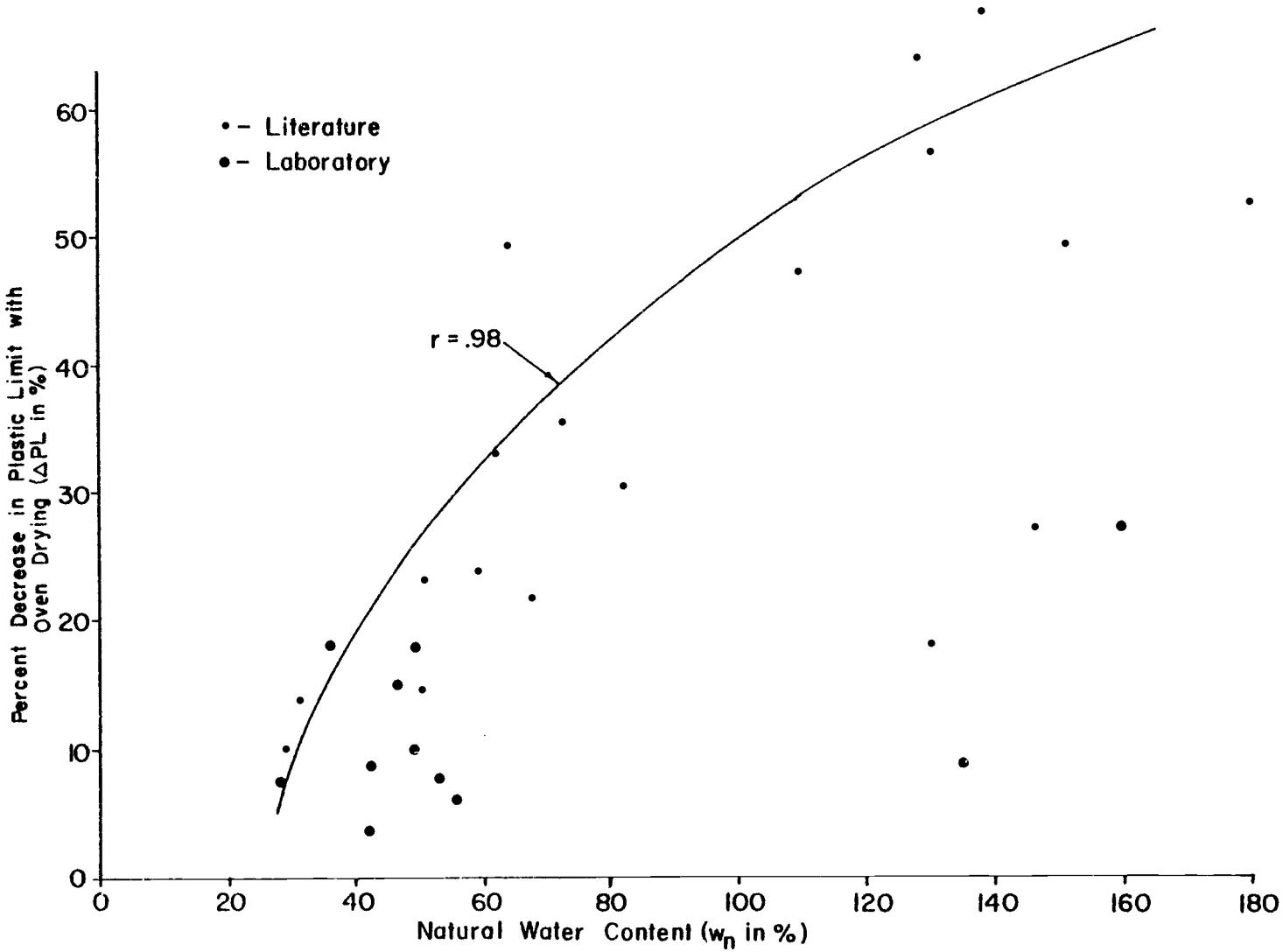

Figure 45. Percent decrease in plastic limit by oven drying vs. natural water content.

. 91 and . 98 are obtained for percent change in liquid limit and plastic limit respectively.

Two or three obviously "bad" points were eliminated during regression analysis. Difficulty in obtaining Atterberg limit results on dried sandy samples is thought to be the cause of these discrepant points.

The logarithmic relationship may be an accident of the parameter used, i. e., water contents cannot be negative, therefore points bunch up in the lower end of the water content scale. The logarithmic curves become nearly linear at natural water contents of about 60%. Thus there appears to be no theoretical or mathematical basis for a logarithmic relationship except the constraint that natural water contents must be greater than zero.

Moisture-Density

Figures 46 and 47 show percent change in moisture-density optimum values from natural to oven dry conditions vs. natural water content. Both plots show a reasonably good linear relationship, with regression coefficients of 0. 85 for percent increase in maximum dry density and 0. 91 for percent decrease in optimum water content.

Variability in percent change in optimum values increases with increasing water content. Variability is much larger for percent

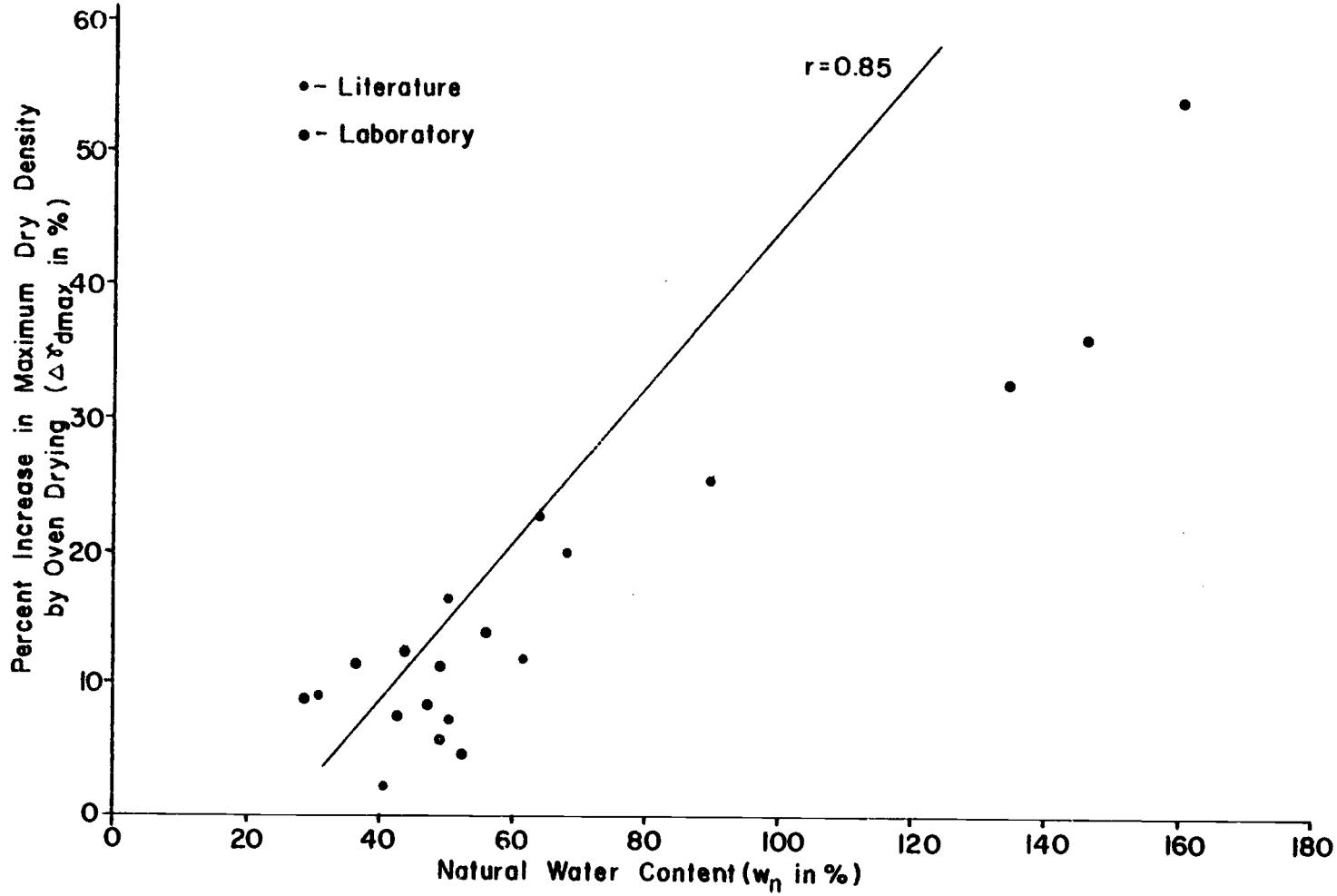

Figure 46. Percent change in maximum dry density with oven drying.

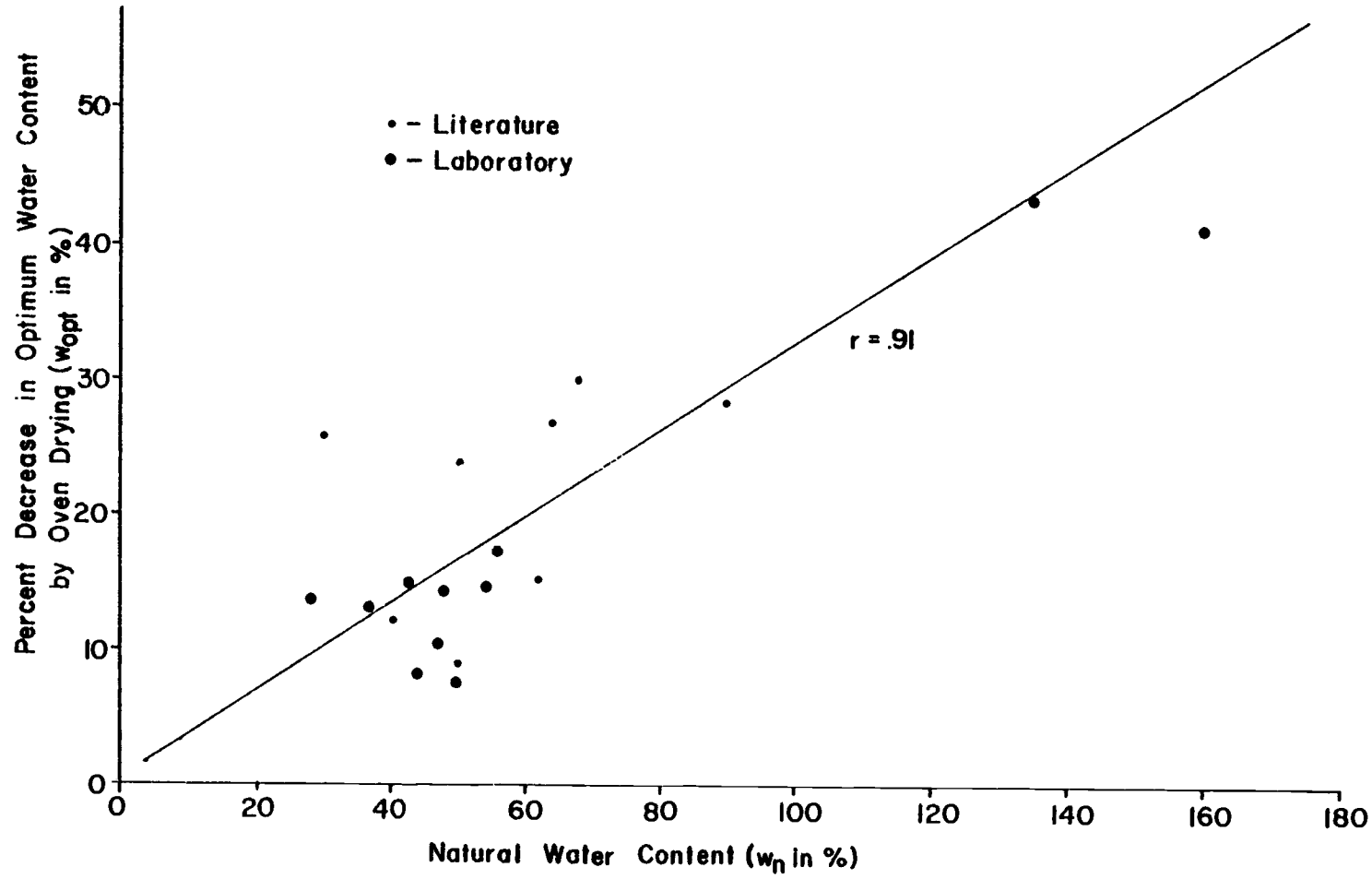

Figure 47. Percent change in optimum water content with oven drying.

change in maximum dry density at high natural water contents. Since these are from the same general area in the Oregon Cascades, small variability would be expected. Other reported samples are from all parts of the world, and higher variability could be expected.

Figure 48 shows a poor relationship between percent change in plastic limit with oven drying, and percent change in optimum water content with oven drying. Investigators have reported that an almost identical decrease in optimum water content and plastic limit takes place upon drying (Wesley, 1973). Results from Figure 48 suggest that this is not true for poorly crystalline soils derived from volcanic ash.

Wesley (1973) states that plastic limit and optimum water content are approximately equal. Figure 49 shows a plot of optimum water content versus plastic limit for natural and oven dried soils. Note that a strong linear tendency exists (regression coefficient approximately equal to 0. 85). At 20% optimum water content, the plastic limit is also approximately 20%. As optimum water content increases, the plastic limit gradually becomes larger than the optimum water content. At an optimum water content of 100%, plastic limits, on average, are about 140%.

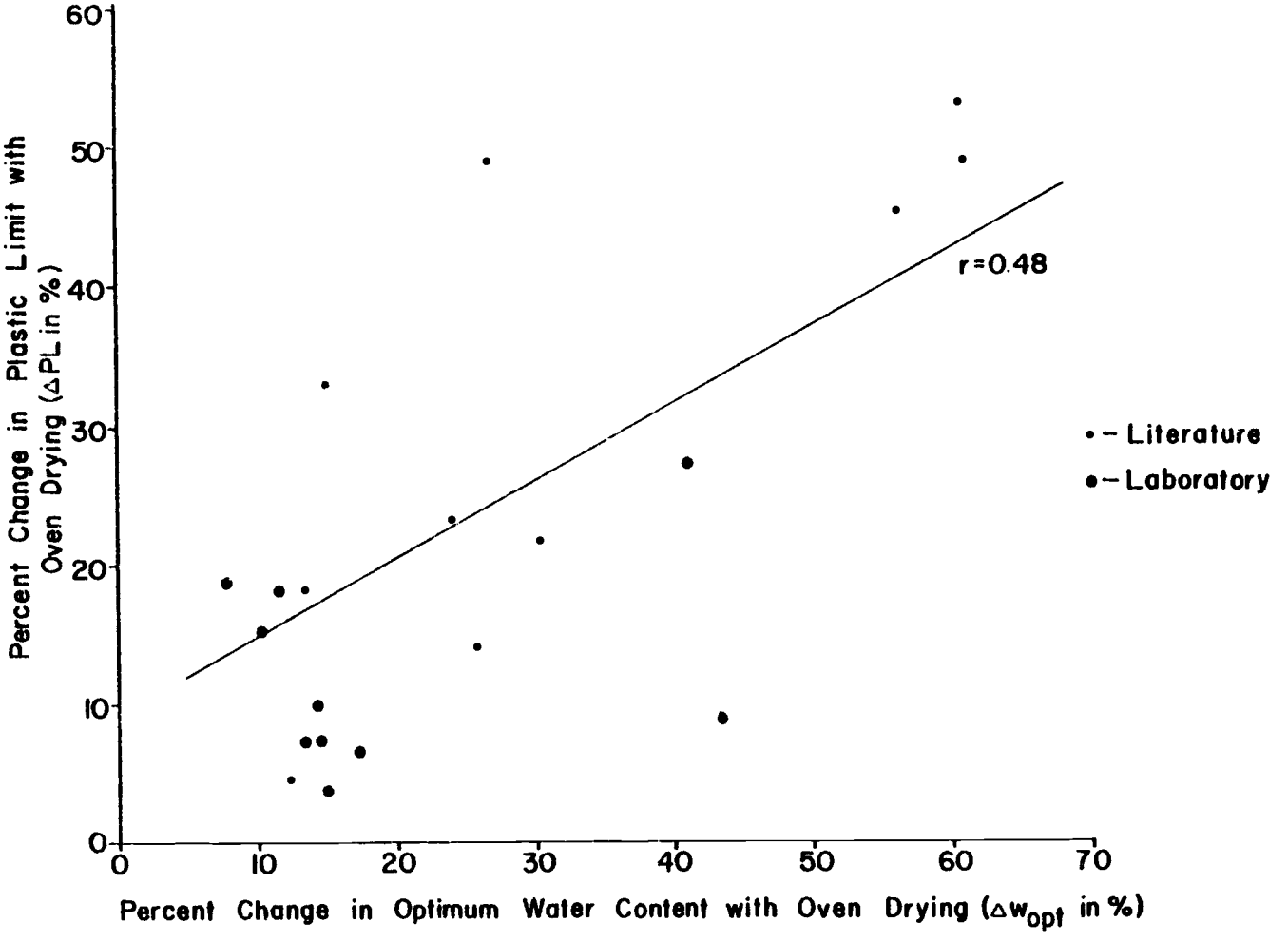

Figure 48. Percent change in plastic limit vs. percent change in optimum water content with oven drying.

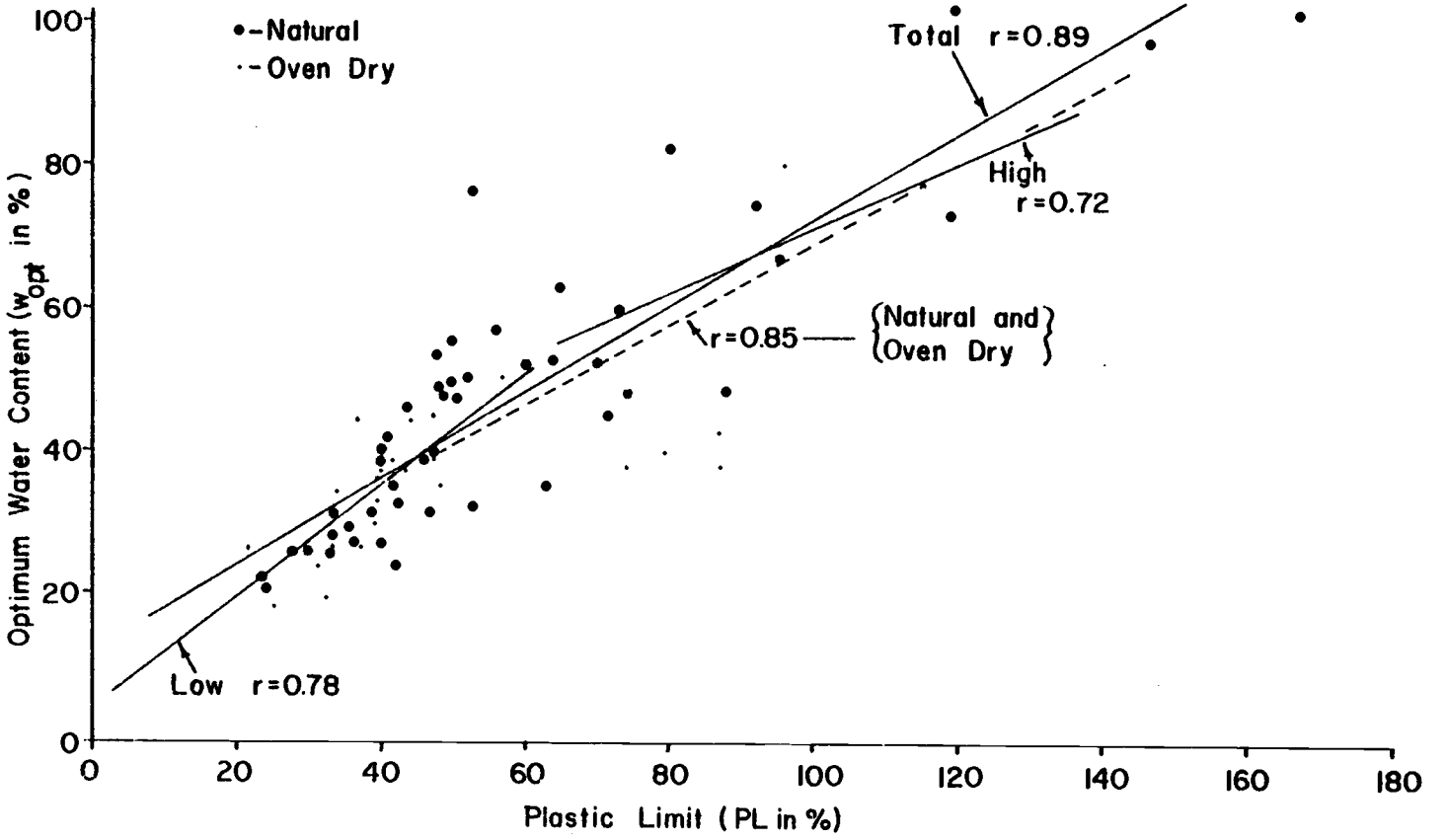

Figure 49. Optimum water content vs. natural water content.

Strength

Strength results are presented in Table 12, Appendix D for the laboratory study, and Appendix A for strength parameters reported in the literature. Strength parameters which present angle of internal friction (ϕ') and cohesion intercept (c') are effective stress parameters. Those which report only cohesion (c) with no accompanying angle of internal friction are undrained strength parameters. Some discussion of strength results is presented in Chapter III.

When considering shear strengths of poorly crystalline soils derived from volcanic ash, three major problems in interpretation of strength results are evident. These are:

1. Heterogeniety of soil samples.
2. Theoretical definition of failure.
3. Determination of the failure point during the shear process.

Pope and Anderson (1960) report that shear strength evaluation of residual soils derived from volcanic materials yields scattered shear test data. They state: "In many cases it is impossible to duplicate with reasonable agreement, test data obtained on specimens cut from a one-cubic-foot sample."

In this section, strength is discussed in terms of the effective stress parameters c' and ϕ'. The detailed lab procedure is given in Appendix C, and briefly outlined below.

1. Samples removed during sampling from site locations.
2. Samples transferred from shelby tube to triaxial cell in the laboratory.
3. Specimens saturated with backpressure under a constant confining stress of less than 5 psi (2.5 psi: average value).
4. Specimens consolidated to confining pressures of 5, 10, or 15 psi.
5. Samples sheared undrained under constant strain rate and confining pressures.

Mohr-Coulomb failure theory which has been widely accepted is used to interpret the test results.

Table 12 (Chapter III) presents three sets of effective stress strength parameters, each representing a different interpretation of the point of failure for each sample. These are:

1. Maximum deviator stress--The point of shear failure for this method was assumed to occur at the point of maximum deviator stress.
2. Maximum effective principle stress ratio--Failure is assumed to occur at the strain for which the effective principal stress ratio is a maximum.

3. Effective stress path envelope--An effective stress path failure envelope is developed which defines a maximum deviator stress for any given confining pressure.

For each of these methods of interpretation, a Mohr envelope can be developed which defines effective stress strength parameters.

Maximum deviator stress was determined from the maximum point on the deviator stress versus strain curve. Often, this point was difficult to identify due to the gentle curvature and indistinct peaking of some of the curves. Deviator stress versus strain cannot predict effective stress maximums without accompanying pore pressure data. For this reason, the deviator stress maximum may not identify the maximum effective stress behavior. All deviator stress versus strain curves are presented in Appendix D.

Principal effective stress ratio versus strain curves are shown for each site in Appendix D. Effective stress ratio versus strain show distinct peaking characteristics. The presence of distinct peaks make maximum point identification easy. For each curve, the strain at which principal effective stress ratio are a maximum, is considered to be the failure strain. Deviator stress and pore pressure corresponding to this failure strain are taken to be the failure values for purposes of determining the effective stress strength parameters. Investigators have reported that principal effective stress ratio maximums peak before actual failure occurs (Mitchell, 1976).

Effective stress path methods exhibit the path which the maximum shear stress has followed during the loading process. Several effective stress paths, determined at different confining pressures, will define a maximum shear stress failure envelope for a particular soil type. This envelope can then be mathematically transformed to a Mohr effective stress failure envelope by the method described in Chapter III. Effective stress path plots for Sites 1 11 are presented in Appendix D.

Regression coefficients determined from "best fit" Mohr envelopes for each of the three methods are on average higher for the maximum deviator stress and stress-path methods, and significantly lower for the maximum effective principle ratio approach.

For poorly crystalline volcanic ash soils, the stress-path method of defining a Mohr effective stress failure envelope seems superior to the other methods for the following reasons.

1. Deviator stress maximum values are difficult to determine for gently curving deviator stress versus strain curves.
2. Principal effective stress ratio maximums do not occur at failure thus, deviator stress and pore pressures determined by this method are not valid failure values.
3. Examination of the effective stress strength parameters presented in Table 12, and analysis of "best fit" regression coefficients show that results determined by the effective stress

path method are reasonably within expectations, and define more constant trends than the other methods.

Statistical analysis of effective stress strength parameters for a frictional-cohesive residual clayey silt has shown that the effective angle of internal friction is independent of void ratio and degree of saturation (Lumb, 1966). Lumb (1966) stated that when analyzing angles of internal friction, tan ϕ' is preferable to ϕ'. Distribution of ϕ' and c' for these soils were reported to be approximately normal.

Statistical t-tests on strength parameters from the literature and laboratory study indicate that the effective angle of internal friction divides into at least two distributions which are coincident with multi-normal water content and Atterberg limit distributions previously described. The same statistical test on effective cohesion intercept indicate that these measurements cannot be statistically separated by water content. The low water content group corresponds to a ϕ' averaging 37.7^{o} and the medium and high water content groups correspond to ϕ' averaging 18.2 degrees. Samples from the low and high water contents groups have the same average cohesion intercept of 0.57 kg/cm^2.

Development of Amorphous/Crystalline Constituent Percentage Correlations

Chapter IV presented several estimates of allophanic component percentages for the Oregon and Alaska soils. These estimates were based on various methods of analysis. Table 23 summarizes these estimated percentage values. Estimates of percentage by Transmission Electron Microscope (TEM) were accomplished by visually integrating the amounts of cloudy indistinct materials relative to the crystalline materials present. Estimates were made from the TEM photos presented in Chapter IV.

Examination of the percentages shown in Table 23 show that assignment of an absolute percentage of allophanic material to a specific soil sample is very approximate. A more logical extension of these detection methods would be to assign percentage ranges and rankings based on relative comparisons. Analysis of the percentages reported in Table 23 show that the relative measured percentage of allophanic constituents may be ranked as shown in the last column of Table 23. The number 1 corresponds to the highest relative allophanic percentage, and 12 the lowest.

Table 24 shows percent allophanic constituent rankings compared to similar rankings for engineering and index properties of the Oregon and Alaska samples. For example, the highest liquid

Table 23. Summary of allophanic constituent percentage.

Number	Site Name	Allophanic Constituent Percentage				
		Rehydration	Infrared Spectography	TEM* Visual Estimate	Rapid Field Test	Rank**
1a	Dome Creek	13.0	27	0-25	5 to 7	10
1b	Dome Creek	23.0	53	0-25	5 to 7	3
2	Dome Creek	18.2	54	25-50	>7	2
3	Buck Creek	8.8	45	25-50	5 to 7	6
4	Pyrimid Creek	9.2	30	0-25	<5	12
5	Batchellor Creek	13.2	38	0-25	5 to 7	8
6	Box Canyon Creek	16.6	38	25-50	<5	5
7	Quartzville Creek	12.0	31	25-50	5 to 7	6
8	Fritz Creek	10.6	16	0-25	5 to 7	11
9	Lookout Creek	10.8	34	0-25	5 to 7	9
10	Alaska	8.4	--	50-75	>7	4
11	Alaska	20.0	--	50-75	>7	1

* Transmission Electron Microscope

** Number one corresponds to highest allophanic constituent percentage.

Table 24. Ranking Comparisons.

Site Number	Site Name	Percent Allophanic Material	Natural Water Content	Liquid Limit	Plastic Limit	Void Ratio	Maximum Dry Density	Optimum Water Content	Effective angle of Friction
1	Done Creek	10*	11*	11*	12*	4*	5**	5*	10**
1b	Dome Creek	3	8	3	3	4	3	3	10
2	Dome Creek	2	3	5	10	4	4	4	10
3	Buck Creek	6	9	10	11	10	11	10	4
4	Pyrimid Creek	12	7	6	8	11	7	8	8
5	Batchellor Creek	8	10	4	5	9	7	9	2
6	Box Canyon Creek	5	5	8	4	8	9	7	7
7	Quartzville Creek	6	5	7	6	7	6	6	3
8	Fritz Creek	11	4	12	9	3	12	12	9
9	Lookout Creek	9	12	9	7	12	10	11	6
10	Alaska	4	2	2	2	2	2	2	1
11	Alaska	1	1	1	1	1	1	1	5
Average Rank Difference			2.42	2.08	2.42	2.67	2.17	1.92	3.67

* 1 corresponds to highest value

** 1 corresponds to lowest value

Table 24. Continued

Site Number	Site Name	Specific Gravity	Percent Fines	Insitu Dry Density	Percent Change with Oven Drying: Liquid Limit	Plastic Limit	Max. Dry Density	Opt. Water Content
1	Dome Creek	7**	12*	4**	10*	3*	5*	8*
1b	Dome Creek	12	5	4	4	5	3	11
2	Dome Creek	11	1	4	6	11	4	3
3	Buck Creek	10	3	11	8	12	10	4
4	Pyrimid Creek	6	7	10	5	4	9	9
5	Batchellor Creek	2	10	9	7	8	8	10
6	Box Canyon Creek	8	8	8	3	2	11	12
7	Quartzville Creek	9	2	7	9	6	6	6
8	Fritz Creek	5	9	3	12	10	12	5
9	Lookout Creek	2	4	12	11	9	7	7
10	Alaska	2	6	2	2	7	2	1
11	Alaska	1	11	1	1	1	1	2
Average Rank Difference		4.83	3.42	2.83	2.08	3.25	2.08	3.08

* 1 corresponds to highest value

** 1 corresponds to lowest value

limit was assigned the number 1 (Site 11, Alaska), the lowest number 12 (Site 8, Fritz Creek). These rankings were compared to the rankings for percent allophanic material (% ALO). Measure of agreement between rankings was accomplished by determining the average rank difference. This number is calculated by averaging the absolute values of rank differences between % ALO and the index or engineering property of interest. Lower numbers mean better agreement.

As evidenced by the average rank differences in Table 24, very general agreement exists between allophanic percentage and index-engineering property trends. This agreement however is not good enough to be used for any specific practical application except to describe general trends. Liquid limit and moisture density optimum values show the best agreement. Effective angle of internal friction, specific gravity, and percent fines show the least agreement.

Allophanic percentages for soils presented in the literature review are summarized in the description section of Appendix A. These allophanic constituent percentages were compared to reported index and engineering properties using linear regression analysis. The measure of agreement for this method is the correlation coefficient (r). The value of r indicates quality of agreement between data points and the linear regression "best fit" line. The number 1.0 is a perfect fit. Numbers between 1.0 and 0.0 show progressively less

Table 25. Summary of linear regression analysis for data from the literature study.

Percent Allophanic Constituents (ALO in %) vs.	Total w_n (low + high)		Low w_n (60%)		High w_n (60%)	
	Linear Regression Equation	r*	Linear Regression Equation	r	Linear Regression Equation	r
Natural Water Content (w_n in %)	% ALO** = .27 w_n + 6.39	0.64	% ALO = .35 w_n + 0.56	0.75	% ALO = .20 w_n + 16.34	0.41
Liquid Limit (LL in %)	% ALO = .29 LL + 0.22	0.65	% ALO = .11 LL + 9.63	0.33	% ALO = .25 LL + 8.71	0.48
Plastic Limit (PL in %)	% ALO = .45 PL - 0.76	0.69	% ALO = .16 PL + 9.71	0.35	% ALO = .41 PL + 5.19	0.53
Void Ratio (e_o)	% ALO = 16.2e_o - 14.0	0.72	% ALO = 3.2 e_o + 8.0	0.40	% ALO = 2.4 e_o - 40.2	0.78
Maximum Dry Density (γd_{max} in pcf)	% ALO = -.95 γd_{max} + 96.0	0.70	% ALO = -.28 γd_{max} + 36.7	0.66	% ALO = -1.02 γd_{max} + 104.6	0.62
Optimum Water Content (w_{opt} in %)	% ALO = .93 w_{opt} - 17.1	0.79	% ALO = .36 w_{opt} + 0.91	0.73	% ALO = .98 w_{opt} - 19.0	0.71
Specific Gravity (G_s)	% ALO = -35.4 G_s - 61.8	0.26	% ALO = -38.2 G_s + 113.4	0.60	% ALO = 107.4 G_s - 219.8	0.82
Percent Fines (%F)	% ALO = .46%F + 4.62	0.46	% ALO = -.1%F + 21.0	0.28	% ALO = .69%F + 2.22	0.66
Insitu Dry Density (γ_d in pcf)	% ALO = .27γ_d + 35.1	0.39	% ALO = -.21 γ_d + 28.2	0.49	% ALO = 0.12 γ_d + 30.9	0.10
Percent Change in Liquid Limit ($\triangle$LL in %)	% ALO = 0.54$\triangle$LL + 24.1	0.33	------		% ALO = .12 $\triangle$LL + 50.48	0.10
Percent Change in Plastic Limit ($\triangle$PL in %)	% ALO = .94 $\triangle$PL + 20.2	0.53	------		% ALO = .62 $\triangle$PL + 36.7	0.40

* r is correlation coefficient

** % ALO is Percent Allophanic Constituents

agreement as the number gets smaller. Table 25 summarizes the best fit line equations and their regression coefficients for the low and high natural water content groups. Comparisons reported in Table 25 were made with index and engineering properties which were amply reported in the literature. All regression lines were based on 10 or more points.

Table 25 shows that general agreement exists between allophanic percentage and most of the index and engineering properties analyzed. The regression coefficients however are so low that prediction of a particular engineering or index property based on allophanic percentage would be subject to large errors.

For the total sample, it appears that plastic limit, void ratio and moisture density optimum values have the highest correlation coefficients. Specific gravity, percent fines, insitu dry density and percent change in Atterberg limits upon drying exhibit the least desirable comparisons.

For the low natural water content group, very low correlation coefficients are evident except that natural water content and optimum water content exhibit correlation coefficients of 0.75 and 0.75 respectively. The same general trend is true for the high natural water content group except that void ratio and specific gravity are moderately high with correlation coefficients of 0.78 and 0.82 respectively. For those correlation coefficients ranging from about

0.7 to 0.8, rough approximations of engineering or index properties may be attempted, but further investigations should also be pursued.

Development of Engineering Correlations

It has long been shown that some engineering behaviors can be predicted by correlation with certain diagnostic index properties. Table 26 summarizes index properties and corresponding engineering properties often correlated in the engineering literature. In most cases, the measured index properties are mathematically combined so that fimiliar quantities such as plasticity index or void ratio are used for purposes of correlation.

Table 26. Index and engineering properties used for correlation.

Index Properties	Engineering Properties
Void ratio	
Grain size distribution	
Liquid limit	Shear strength
Plastic limit	Compressibility
Bulk density	Moisture-density
Moisture content	Permeability
Relative density	

Correlation of Index and Engineering Properties for Crystalline Soils

Correlations between engineering and soil index properties are usually based on physical laws which govern behavior of the soil media. For example; it can be shown that void ratio (e_o) could

be directly related to compressibility while grain size distribution could not. Void ratio is controlled by the same factors of grain and fabric properties which control compressibility. This, of course, is not true for indexes which measure grain size distribution.

Many correlations between index and engineering properties have restrictions which govern their use. Skempton's original equation relating liquid limit to compression index (Cc) was for remolded soils. Remolded C_c was then related to undisturbed C_c for normally consolidated sedimentary soils of low to moderate sensitivity, hence the equation $C_c = 0.009$ (LL-10) (Terzaghi and Peck, 1967).

Table 27 presents several typical correlations often attempted for crystalline soils. Also listed are restrictions which limit the use of these correlations. Many additional correlations besides those presented in Table 27 have been reported in the engineering literature.

Correlation relationships were only considered for parameters with sufficient data in Appendix A to produce a comparative correlation with poorly crystalline soils derived from volcanic ash. Many of the correlations feature undisturbed index properties versus undisturbed engineering properties. The relationship between

optimum water content and plasticity index is a comparison of two tests which require severe disturbance of the soil structure, and thus can logically be related. Effective angle of internal friction (ϕ') versus plasticity index (PI) and compression index (Cc) versus liquid limit (LL) attempts to relate of remolded index properties with undisturbed engineering properties.

For effective angle of internal friction (ϕ') vs. plastic index (PI), this can be justified by observing that plastic index is a measure of surface water holding properties of fine grained soils, and can be related to minerology of the soil clay grains. Angle of internal friction is also a measure of soil grain surface friction which can be related to fluid viscosity at the grain surface, and grain minerology related to surface roughness. This explanation is only valid for fine grained soils which corresponds to the restrictions placed on the relationship between ϕ' and PI.

Two relationships between Cc and LL are given in Table 27. It appears that the difference between the two can be related to the differences in remolded and undisturbed Cc for Brazilian Clay, and normally consolidated clays in general.

Development of engineering correlations for poorly crystalline soils derived from volcanic ash was accomplished by mathematically comparing relationships between index and engineering properties

Table 27. Summary of engineering correlations for crystalline soils.

Relationship	Equation	Restrictions	Reference
Effective angle of Internal Friction vs. Plastic Index (ϕ' vs. PI)	Plot on page 7-3-17 in reference	Valid only for fine grained soils.	Navfac, 1969
Effective angle of Internal Friction vs. Void Ratio (ϕ' vs. e_o)	Plot on page 7-3-17 in reference	Valid only for silts of low plasticity	Navfac, 1969
Natural water content vs. log Unconfined Compressive Strength (w_n vs. log q_u)	Plot on page 289 in reference	Valid only for reconstituted saturated kaolinite	Mitchell, 1976
Void Ratio vs. log Unconfined Compressive Strength (e_o vs. log q_u)	Plot on page 7-3-15 in reference	Valid for samples having common preconsolidation pressures. Approximately parallel to void ratio-pressure curve from consolidation tests.	Navfac, 1969

Table 27. Continued

Relationship	Equation	Restrictions	Reference
Compression Index vs. Liquid Limit (Cc vs. LL)	Cc = 0.009 (LL-10)	Undisturbed, normally consolidated clays of sensitivity less than 4	Terzaghi & Peck, 1967
Compression Index vs. Liquid Limit (Cc vs. LL)	Cc =.0046(LL-9)	Brazilian Clays	Bowles, 1979
Compression Index vs. Void Ratio (Cc vs. e_o)	$Cc = 0.75(e_o - 0.50)$	Soils with low plasticity	Bowles, 1979
Compression Index vs. Natural Water Content (C_c vs. w_n)	$Cc = .0054(2.6w_n - 35)$	None listed	Navfac, 1969
$Cc/(1+e_o)$ vs. Natural Water Content	Plot on page 321 in reference	None listed	Lambe & Whitman, 1969
Optimum Water Content vs. Plastic Index (w_{opt} vs. PI)	Plot on page 116 in reference	None listed	Schroeder, 1975

reported in the literature and laboratory studies. All mathematical relationships (equations) were determined by regression analysis using the least squares method.

Figure 50 shows the relationship between effective angle of internal friction (ϕ'), and plasticity index (PI). The regression line for the total sample fits the correlation reported by Bowles (1979), very closely. Regression analyses for low and high water content groups give poor to non-existant relationships.

The correlation between effective angle of internal friction (ϕ') and void ratio (e_o) is shown in Figure 51. The data values generally outline the desired relationships and definitive correlation is evident. This relationship seems to be the best of two alternatives for predicting the effective angle of internal friction from index properties. The regression relationship, however, does not agree well with reported correlations for crystalline soils. This is especially true for the high water content group.

The relationship between undrained shear strength (c) and natural water content (w_n) is presented in Figure 52. A well defined trend is outlined by the data values and the regression line agrees favorably with the data for the total sample. Values for the high water content group are sketchy and scattered while those in

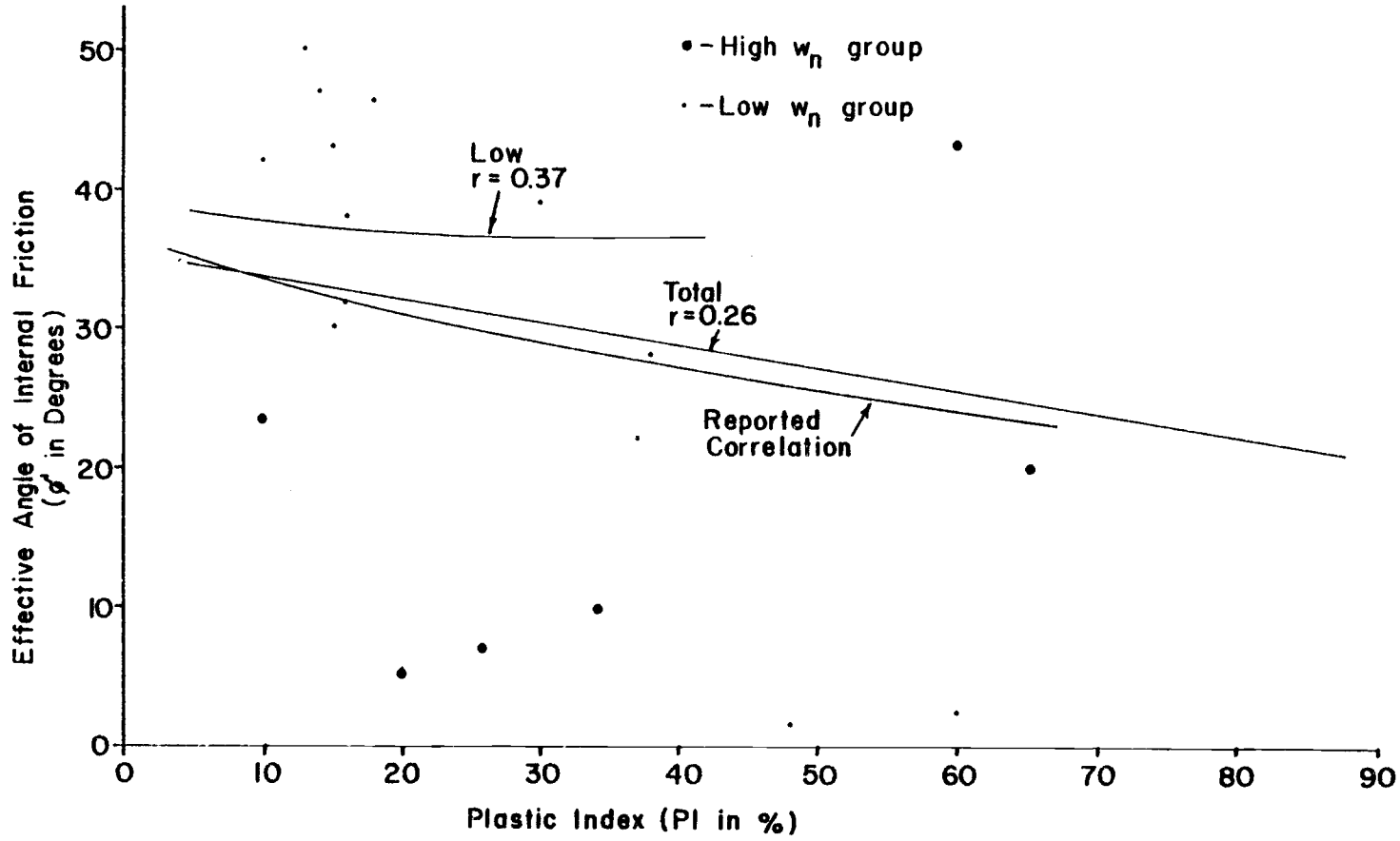

Figure 50. Effective angle of internal friction vs. plastic index (PI in %).

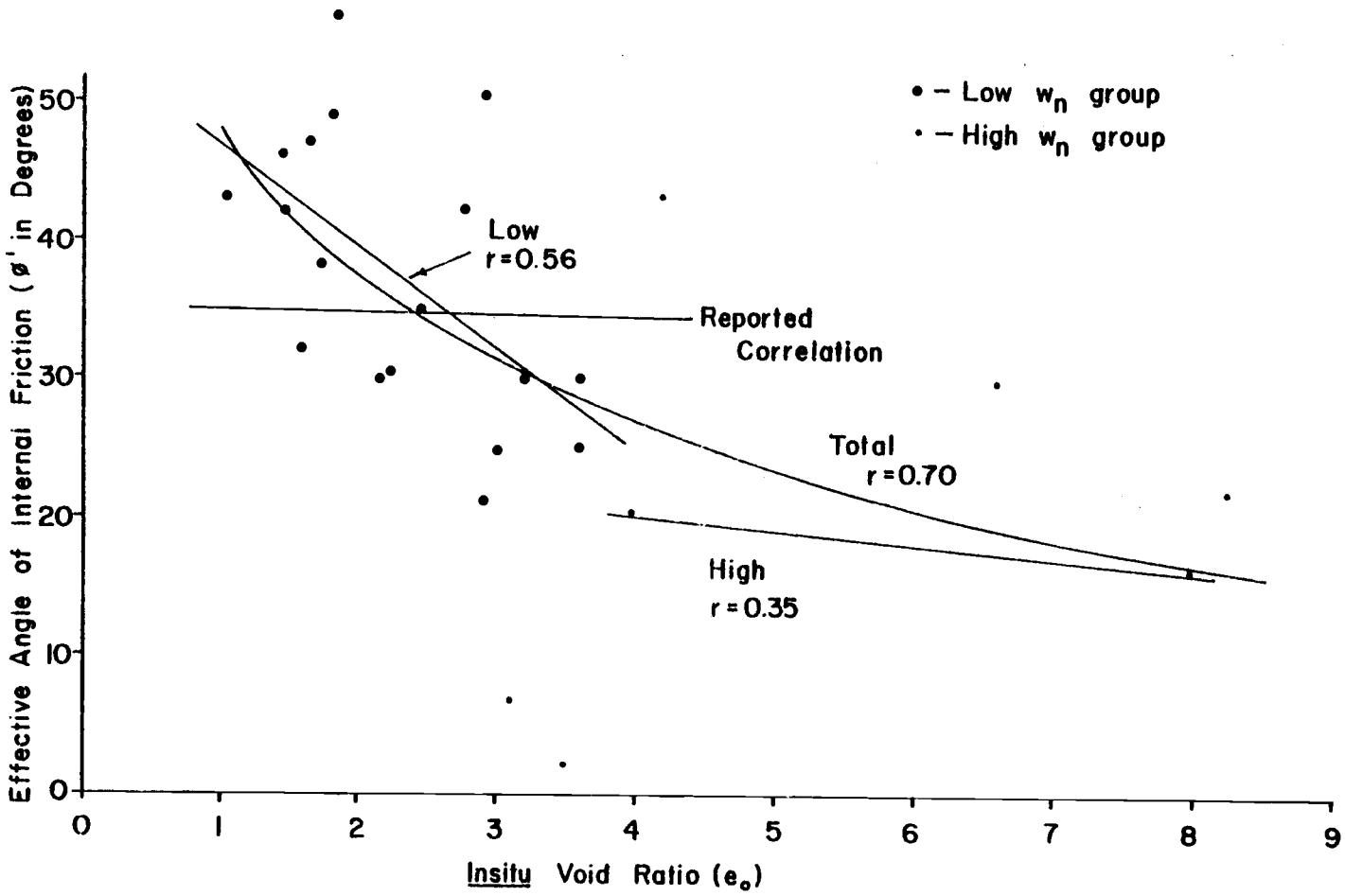

Figure 51. Effective angle of internal friction vs. void ratio.

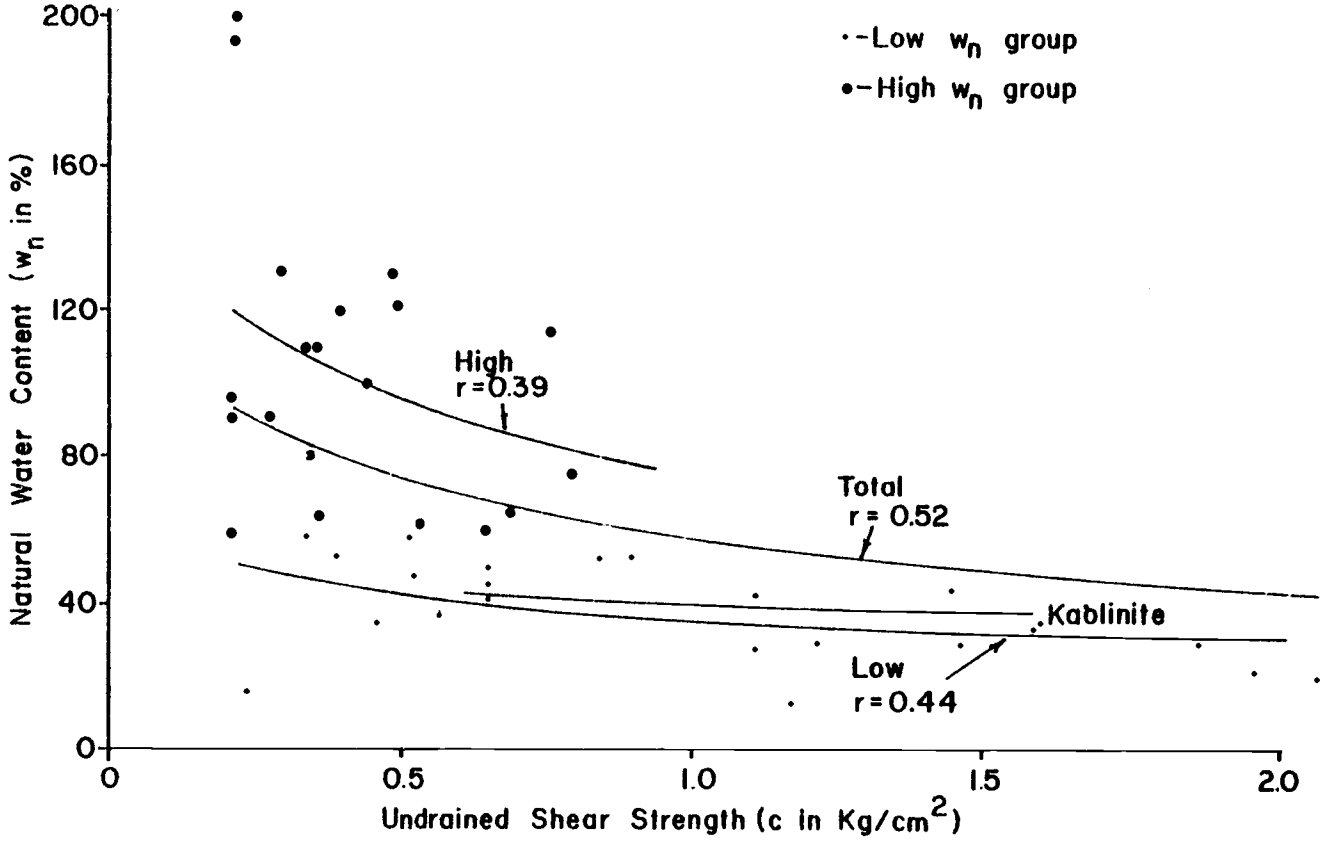

Figure 52. Undrained shear strength vs. natural water content.

the low natural water content group align themselves well over a small range in water content. This relationship is unique for different clay mineral types. The low water content group agrees well with the relationship for kaolinite reported by Mitchell (1976).

Figure 53 shows the relationship between undrained shear strength (c) and void ratio (e_o). As expected, undrained shear strength increases with decreasing void ratio. The high water content group, by itself, does not correlate. If the total sample is analyzed, the regression coefficient increases dramatically, and the visual relationship between e_o and c is reasonably good. Also the high water content group varies over a relatively small range of c, with the average at about 0.5 kg/cm^2. For crystalline silty materials this relationship is reported to be approximately parallel to the pressure-void ratio curve determined from consolidation tests (Navfac, 1969).

Relationships for compressibility versus index properties are shown in Figures 54 thru 57. Figure 54 shows that a relationship between compression index and liquid limit exists but large variability exists among the data values. The regression line agrees somewhat with the relationship reported by Terzaghi and Peck (1967),

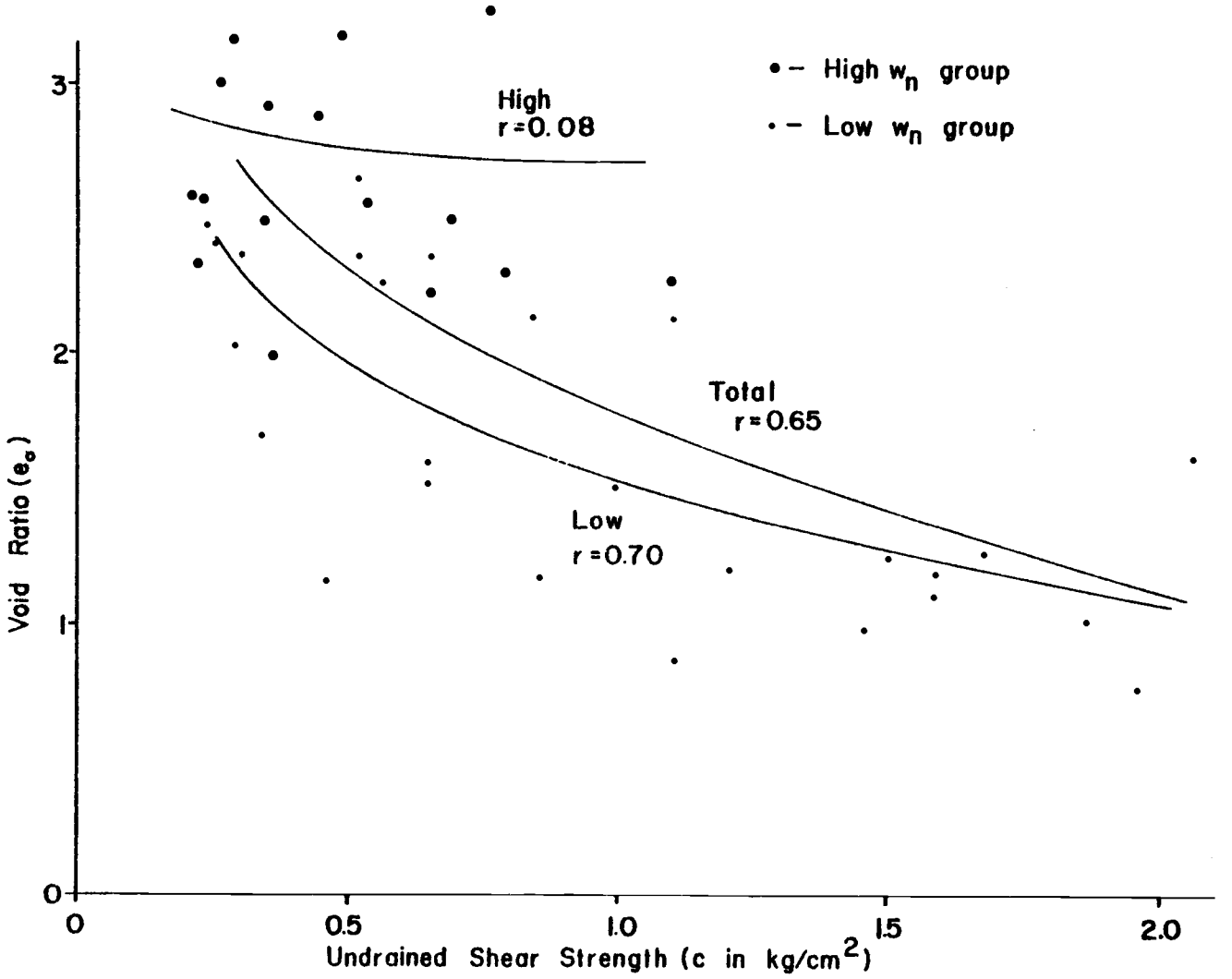

Figure 53. Undrained shear strength vs. void ratio.

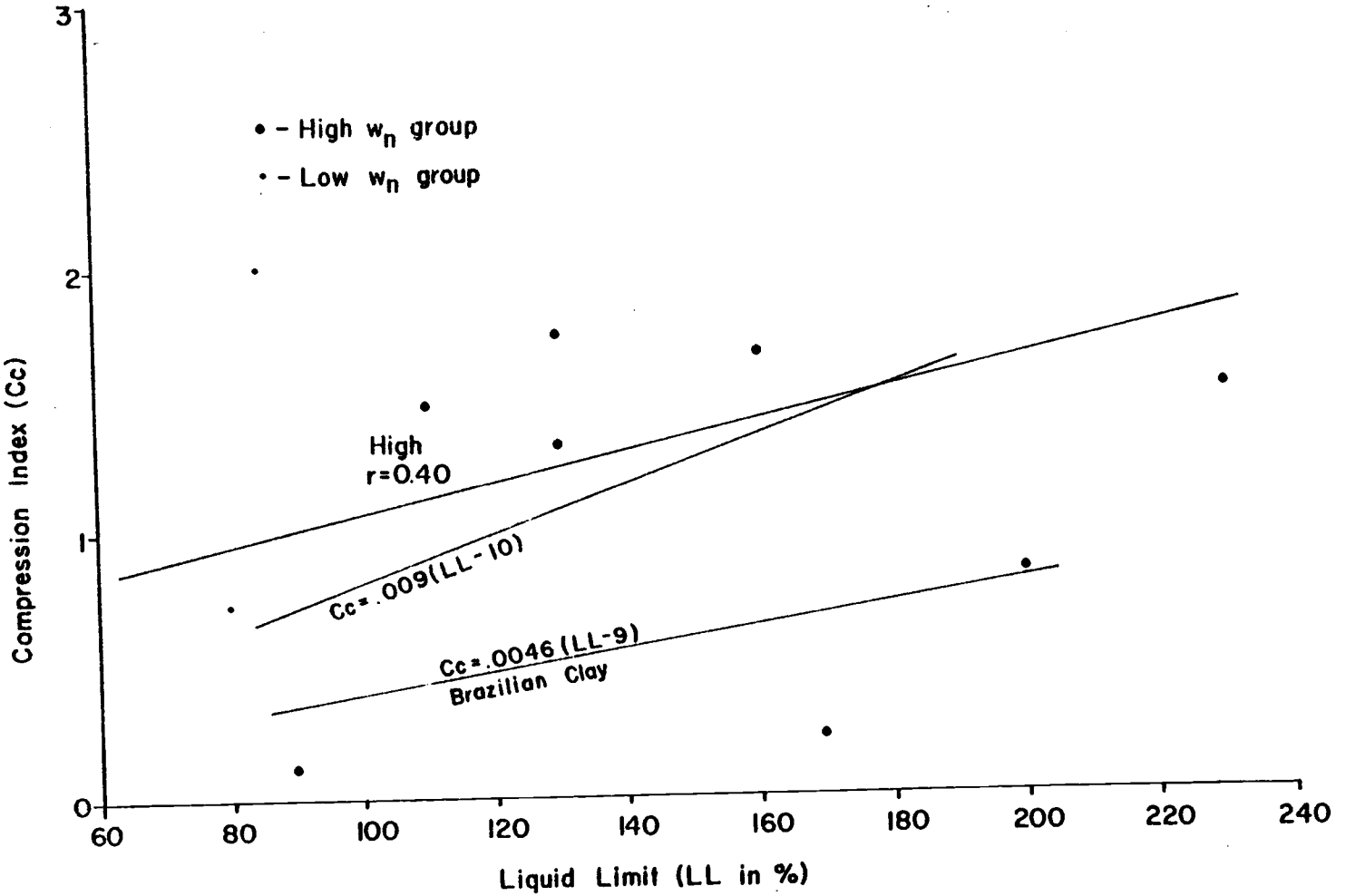

Figure 54. Compression index vs. liquid limit.

and is parallel to and offset above the relationship reported for Brazilian Clays by Bowles (1979).

Figure 55 shows the logarithmic relationship between compression index and void ratio. An excellent mathematical and visual correlation is evident. The regression curve also follows the trend of the reported relationship (Bowles, 1979), but predicts a considerably lower compression index.

Figures 56 and 57 show the relationship between compression index and natural water content. The compression index values in Figure 57 are transformed by dividing Cc by $1 + e_o$. Both regression lines are poorly defined by the data values, but general trends are evident. The regression lines do not agree well with reported relationships except for the low natural water content portion of the $Cc/1 + e_o$ line.

Figure 49 shows optimum water content versus plastic limit. A good visual relationship exists between these two variables. Good correlation is evident for the low w_n, high w_n, and total group. The regression line follows the accepted trend, for crystalline soils, of the optimum water content gradually decreasing with the plastic limit. The difference is proportional to the plastic limit.

Table 28 summarizes the results of these correlation attempts. The quality of correlation column in Table 28 combines point

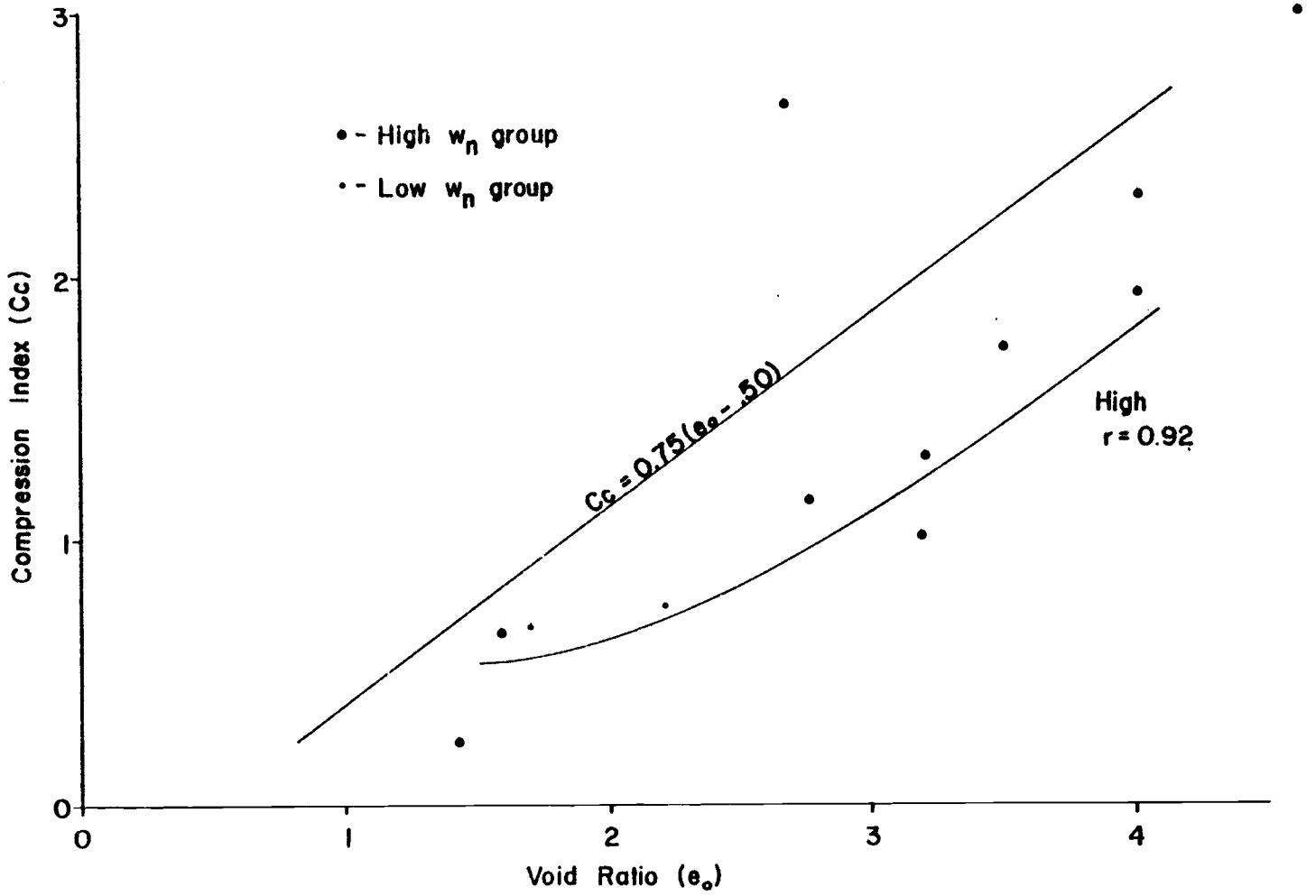

Figure 55. Compression index vs. void ratio.

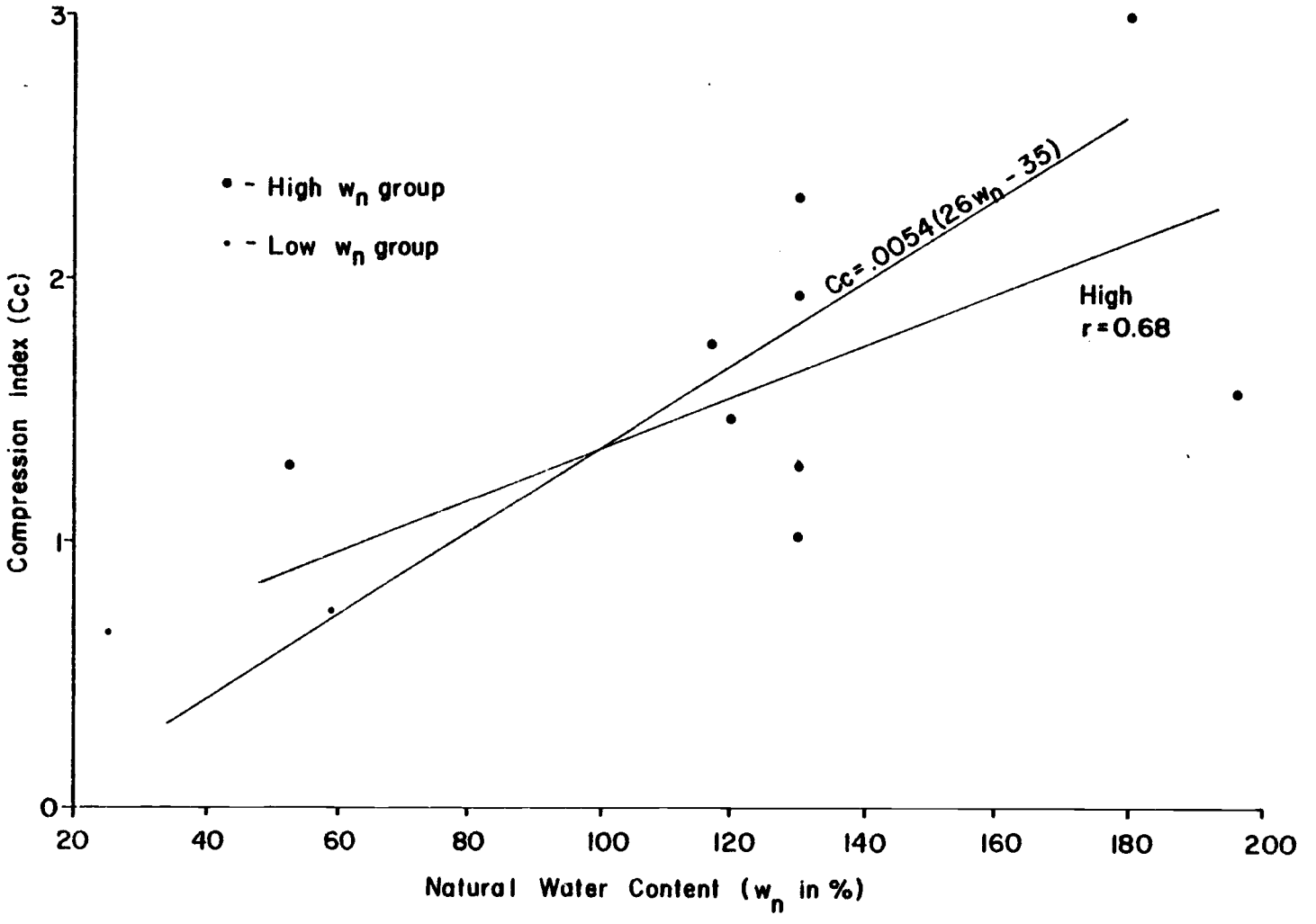

Figure 56. Compression index vs. natural water content.

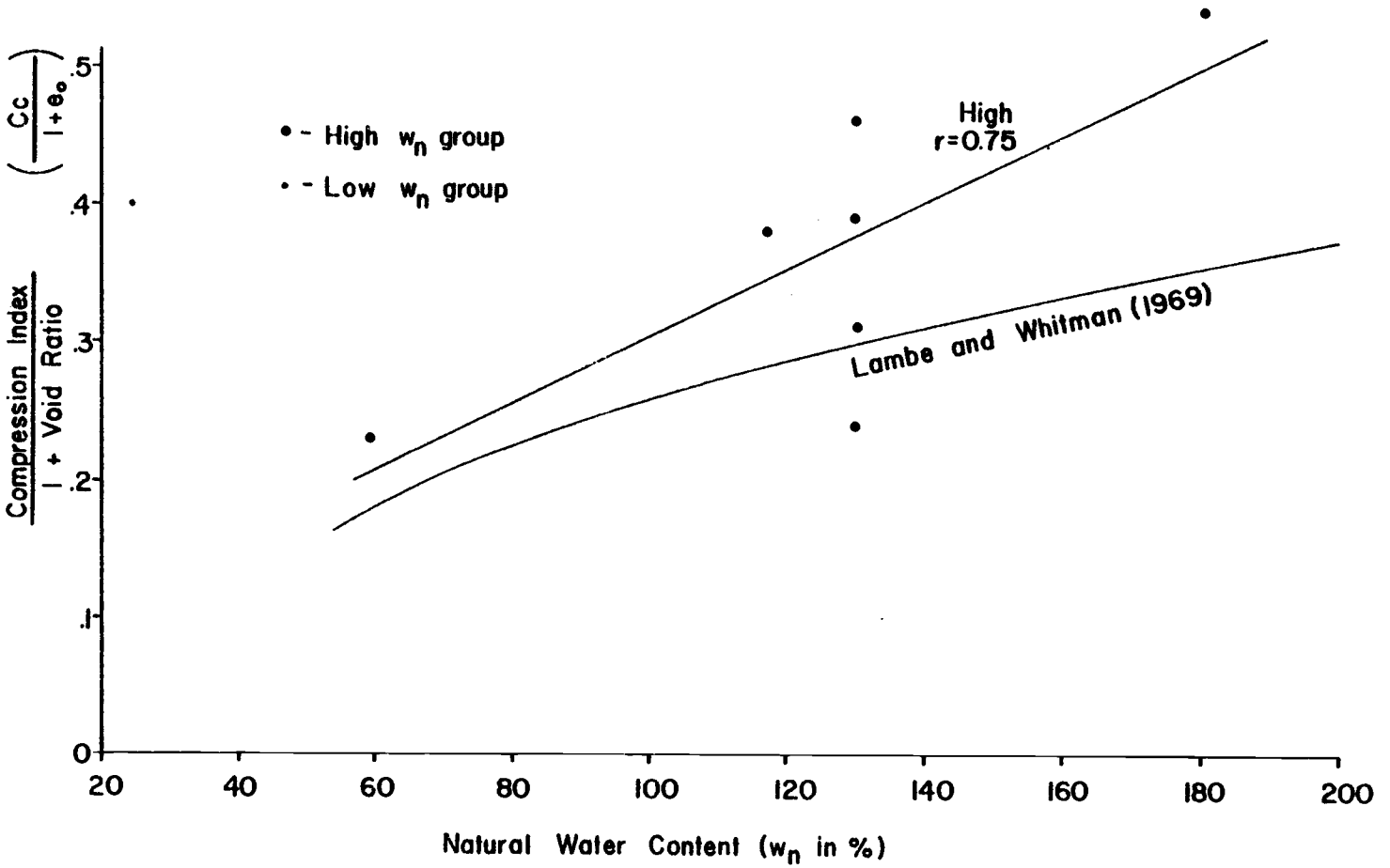

Figure 57. $Cc/1 + e_o$ vs. natural water content.

Table 28. Summary of engineering correlations.

Engineering Property	Index Property or Combination of Index Properties	Quality of Correlation	Equation of Regression line (regression coeff.)	Comparison with Crystalline Soil Correlation
Shear Strength				
Effective angle of internal friction (ϕ' in degrees)	Plastic Index (total samples) (PI in %)	poor	$\phi' = -.16\ (PI - 219)$ (0.26)	Excellent (Bowles, 1979)
	Plastic Index (low w_n group) (PI in %)	fair-poor	$\phi' = -0.79\ (\ln PI - 50)$ (0.37)	good-fair
	Plastic Index (high w_n group) (PI in %)	no correlation	---	poor
effective angle of internal friction (ϕ' in degrees)	Void Ratio (e_o) (total samples)	fair-good	$\phi' = -15(\ln e_o - 3.2)$ (0.70)	fair-poor (Navfae, 1969)
	Void Ratio (e_o) (low w_n group)	fair	$\phi' = -7.30\ (e_o - 7.4)$ (0.56)	fair
	Void Ratio (e_o) (high w_n group)	poor	$\phi' = -1.02\ (e_o - 23.8)$ (0.35)	fair
undrained shear strength (c in Kg/cm^2)	Natural Water Content (w_n in %) (total samples)	good	$w_n = -23.33\ (\ln c - 2.52)$ (0.52)	fair (with kaolinite) (Mitchell, 1976)
	Natural Water Content (w_n in %) (low w_n group)	good-excellent	$w_n = -9.58\ (\ln c - 3.78)$ (0.44)	good (with kaolinite)
	Natural Water Content (w_n in %) (high w_n group)	fair	$w_n = -30.42\ (\ln c - 2.46)$ (0.39)	poor (with kaolinite)

Table 28. Continued

Engineering Property	Index Property or Combination of Index Properties	Quality of Correlation	Equation of Regression line (regression coeff.)	Comparison with Crystalline Soil Correlation
Undrained Shear Strength (c in Kg/cm^2)	Void Ratio (e_o) (total samples)	good	$e_o = -0.78\ (\ln c - 2.26)$ (0.65)	---
	Void Ratio (e_o) (low w_n group)	fair	$e_o = -0.65\ (\ln c - 2.26)$ (0.70)	---
	Void Ratio (e_o) (high w_n group)	poor	$e_o = -.08\ (\ln c - 33.75)$ (.08)	---
Compressibility				
Compression Index (Cc)	Liquid Limit (LL in %) (high w_n group)	poor	$Cc = .0057\ (LL + 88.6)$ (0.40)	fair (Terzaghin & Peck, 1967) (Bowles, 1979)
Compression Index (Cc)	Void Ratio (e_o) (high w_n group)	good-excellent	$Cc = .5(\ln e_o + .48)$ (0.92)	fair-good (Bowles, 1979)
Compression Index (Cc)	Natural Water Content (w_n in %) (high w_n group)	fair-poor	$Cc = .0098(w_n + 39)$ (0.68)	fair-poor (Navfae, 1969)
$Cc/(1 + e_o)$	Natural Water Content (w_n in %) (high w_n group)	fair	$Cc = .0024\ (w_n + 26.6)$ (0.75)	fair-poor
Moisture Density				
Optimum Water Content (w_{opt} in %)	Plastic Limit (total samples) (PL in %)	good-excellent	$W_{opt} = 0.59\ (PL + 22.7)$ (0.89)	Excellent (Schroeder, 1975)
	Plastic Limit (low w_n group) (PL in %)	excellent	$w_{opt} = 0.77\ (PL + 5.7)$ (0.78)	Excellent
	Plastic Limit (high w_n group) (PL in %)	fair-good	$w_{opt} = 0.46\ (PL + 53.8)$ (0.72)	excellent

distribution, fit, and linearity into a series of one word descriptions ranging from poor to excellent, excellent meaning, even distribution of data points tightly grouped along the regression "best fit" line. Poor means poorly distributed scattered points which do not appear to be related to the regression line.

The comparison with crystalline soil correlation column rates correlation equations for volcanic ash soils, with respect to typical crystalline soil correlations. Excellent means the relationships are about the same. Poor indicates that the same general trends are present but that the relationships are significantly different.

From Table 28, values of index properties PI, e_o and w_n from the high water content group show poor correlation with strength parameter ϕ', and undrained shear strength c. Void ratio (e_o) and natural water content (w_n) show reasonably good correlation with c and ϕ'. Void ratio seems to produce very good visual and mathematical relationships with ϕ', c and Cc. Correlations of optimum water content versus plastic limit are good to excellent for the low, high, and total natural water content groups.

Analysis of Table 28 indicates the following for poorly crystalline soils derived from volcanic ash:

1. There is a poor to non-existant relationship between effective angle of internal friction and plasticity index. For this reason

plasticity index should not be used to predict effective angle of internal friction.

2. Void ratio can effectively be used to predict effective angle of internal friction if the equation for total sample is used. There are no restrictions on the use of this relationship if used for poorly crystalline volcanic materials.

3. Natural water content can be used to predict undrained shear strength if the equation for total sample is used. No restrictions apply if poorly crystalline soils derived from volcanic ash are being analyzed.

4. Void ratio can also be used to predict undrained shear strength. The equation for total sample provides a good approximation. Regression coefficients suggest that void ratio is slightly better than natural water content for predicting undrained shear strength. No restrictions apply to the use of this relationship except it must be applied to the use of poorly crystalline volcanic ash soils.

5. Liquid limit should not be used to predict compression index for these soils.

6. Void ratio provides an excellent measure of compression index for poorly crystalline volcanic ash soils of natural water contents greater than 60%.

7. Natural water content can also predict compression index for these soils but void ratio seems the superior predictor property.

8. Plastic limit provides an excellent approximation of optimum water content for total sample. This relationship applys only to poorly crystalline volcanic ash soils.

These observations indicate that values for effective angle of internal friction, undrained strength, and compression index can best be estimated if void ratio is used as the predictor property.

For comparisons with crystalline soils, Table 28 shows that only the correlation relationships between optimum water content (w_{opt}) and plastic limit (PL) are similar for crystalline and poorly crystalline soils. The other relationships indicate the same trends, but show considerable deviation from typical reported relationships for crystalline soils, as evidenced in Figures 50 thru 57. This kind of deviation appears greater for the high natural water content group. Possible reasons for this behavior will be discussed in Chapter VI.

The correlation properties of poorly crystalline soils derived from volcanic ash show reasonable agreement if undisturbed index properties are used to describe undisturbed engineering behaviors. This is not strictly true for crystalline soils. As shown in Table 27, several disturbed index properties have been successfully correlated

with undisturbed engineering properties. These correlation differences are probably due to fabric, mineralogy and structure differences between crystalline soils and poorly crystalline soils derived from volcanic ash. Chapter VI discusses fabric and possible relationships to engineering and correlation behavior.

Data results presented in Appendix A, and used for correlation, were determined by many different individuals, using different test methods, test apparatus, sampling methods, and sampling apparatus. Much of the variation observed in the correlation attempts was most likely due to sampling and testing uncertainties. Unfortunately, there is no reliable way of estimating this variability.

Other index or engineering properties such as overconsolidation ratio, sensitivity, ectera, are not reported in the literature in sufficient numbers to produce reasonable results if correlation is attempted. Further research is required if relationships of this kind are to be developed.

Summary

The following major points have been made for poorly crystalline soils derived from volcanic ash:

1. Natural water content and Atterberg limit observations appear to separate themselves into two or three groups of normal

distributions, each with separate means and variabilities.

2. These groups may be distinguished by specific physical characteristics such as color, mineral content, drying history, and silt-sand percentage.

3. The stress-path method of defining the Mohr failure envelope seems the best for these soils.

4. Effective angle of internal friction can be statistically separated by the low and high natural water content group. Low natural water contents (<60%) correspond to effective angles of internal friction averaging 37.7 degrees. Natural water contents greater than 60% correspond to Φ' averaging 18.2 degrees. Effective cohesion intercept shows no statistical relationship to the water content groups.

5. Allophanic material percentage can be related to the indicated index properties by the given equations as follows:

$\%ALO = .35\ (w_n + 1.60)$ $\quad (w_n < 60\%)$

$\%ALO = .45\ (PL - 1.69)$

$\%ALO = 16.2\ (e_o - 0.86)$

$\%ALO = -0.95\ (\gamma d_{max} - 101.5)$

$\%ALO = 0.93\ (w_{opt} - 18.4)$

$\%ALO = 107.4\ (G_s - 2.05)$ $\quad (w_n > 60\%)$

Where %ALO is allophanic material percentage.

6. Void ratio appears to be the best index property for predicting undisturbed engineering behaviors. The most reliable relationships as determined by linear regression are:

$$\phi' = -15\ (\ln e_o - 3.2) \qquad \phi' \text{ in degrees}$$

$$c = e^{-1.28(e_o - 1.77)} \qquad c \text{ in } kg/cm^2$$

$$Cc = 0.5\ (\ln e_o + 0.48)$$

Moisture density optimum water content and plastic limit are related by the equation:

$$w_{opt} = 0.59\ (PL + 22.7)$$

These results are valid only for poorly crystalline soils derived from volcanic ash.

7. Relationships between index properties and engineering properties for poorly crystalline soils derived from volcanic ash produce relationships which do not compare well with the same relationships for crystalline soils. Often they are in the same area and show the same general trends, but significant differences are apparent.

VI. RELATIONSHIPS BETWEEN ENGINEERING BEHAVIOR MINERALOGICAL, AND STRUCTURAL CHARACTERISTICS

This chapter discusses the form and function of amorphous components present in volcanic ash soils, and relates their structure and mineralogy to engineering behavior. Scanning electron microscope (SEM) micrographs from the laboratory study are used as a tool to relate the structure and occurrence of amorphous constituents to possible engineering behavior.

Structure, Arrangement and Fabric of Allophanic Materials

Introduction

The characterization of pore space along with the classification of particle arrangements bounding the pore space have been shown to be closely related to engineering behavior (Collins and McGown, 1974).

Three types of basic soil fabric elements have been described by Mitchell (1976) and Collins and McGown (1974). These are:

Elementary particle arrangements

Particle assemblages

Pore spaces

Mitchell (1976) reports that individual clay particle associations are rare and probably most representative of clay suspensions. More commonly, particles in typical soil deposits occur in variously connected particle systems. Elementary particles interact through individual sand silt and clay particle contacts. Particle assemblages are units of agglomerated elementary particles which may occur in regular or irregular shaped aggregations. Several types of pore spaces have been described by Collins and McGown (1974). These can occur between individual grain elements, between groups of elements, and between the particle assemblages themselves.

Observations have shown that the nature of these particle interactions can be very complex and that any number of soil fabric features can exist adjacent to one another in an undisturbed soil deposit. It has been shown, however, that most soils exhibit a set of dominant features which control engineering behavior (Collins and McGown, 1974).

Information about the fabrics of soils can be obtained from electron microscope observation. This information can assist in understanding the engineering behavior of soils (Tovey, 1973).

Fabric as it applies to engineering behavior was studied for the laboratory samples from Oregon and Alaska. These studies were conducted using micrographs from scanning electron microscopy and

to a limited extent, transmission electron microscopy. Sample preparation techniques and laboratory procedures were described in Chapter III, and Appendix E.

Micrographs from the transmission electron microscope (TEM) study are presented in Chapter IV. Results indicate that for Sites 1 to 9, the particles appear to be coated with amorphous gells. These amorphous gels are connected by fibrous webbed materials. Any distinct or partially distinct minerals appear to be surrounded by an amorphous matrix. Jones and Uehara (1973) reported similar coatings on mineral surfaces for several different soils. TEM results for Sites 10 and 11 suggest that the materials are mostly amorphous, the matrix consisting of confused mixtures of rounded, threadlike gelatinous masses of poorly crystalline constituents with obviously large void ratios.

Examinations of SEM micrographs from Sites 1 to 11 provide an examination of possible fabric elements. Much more sophisticated analytical techniques involving photogrammetric and stereoscopic examinations of electron micrographs have been described by Tovey and Wong (1973). These techniques provide quantitative measurements of particle alignments and degree of anisotropy which are useful for studies of shear failure mechanisms. These techniques are unnecessary for the intended scope of this paper.

Fabric Descriptions - By Site

Site 1a - Dome Creek Slide

Figures 58a and 58b show scanning electron microscope (SEM) micrographs of soil from Site 1a. The fabric structure is dominated by a heavy amorphous coating. Elementary particle arrangements are undistinguishable because of the heavy clothing of individual particles.

Amorphous coatings appear as indistinctly stacked face-to-face plates of varying thickness. The edges of the amorphous coatings are well developed and fairly distinct with some minor edge roughness.

It seems that the amorphous coating solidly links individually coated particles together to form interconnected regular and irregularly shaped particle assemblages ranging from 10 to 100 μm in diameter. Discernable individual coated particles range in size from 1 to 10 μm in size. Any particles less than 1 μm are obscured in the matrix coating.

Since the amorphous coating is so dominant, all aggregate and particle interactions appear to be through the amorphous coating at points of contact.

Pores between groups of elementary particles (intra-elemental), and pores within particle assemblages (intra-assemblage) appear to be blocked, closed or filled with amorphous coating material. Pores

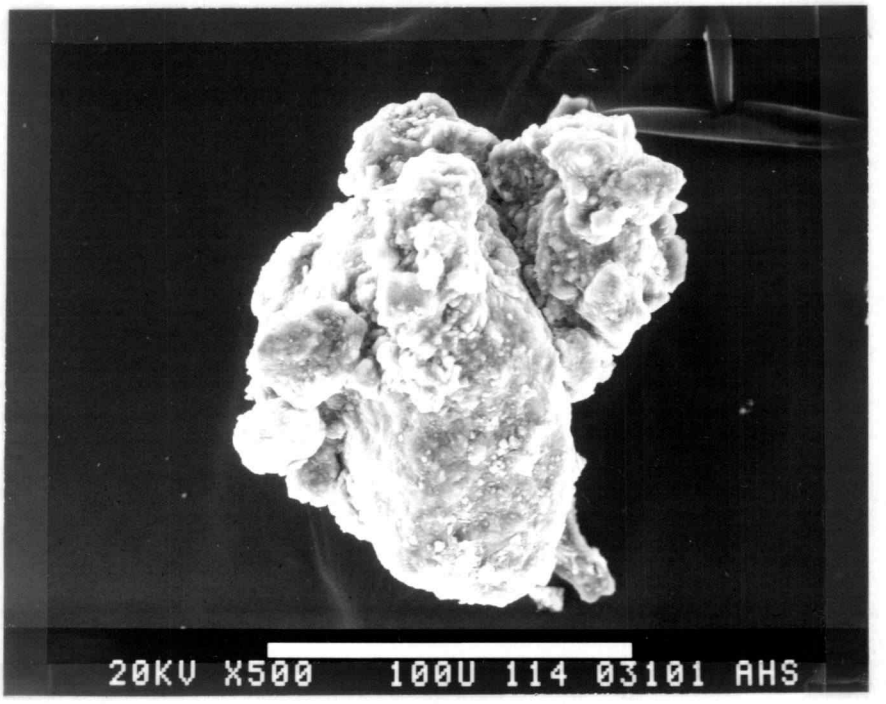

(a)

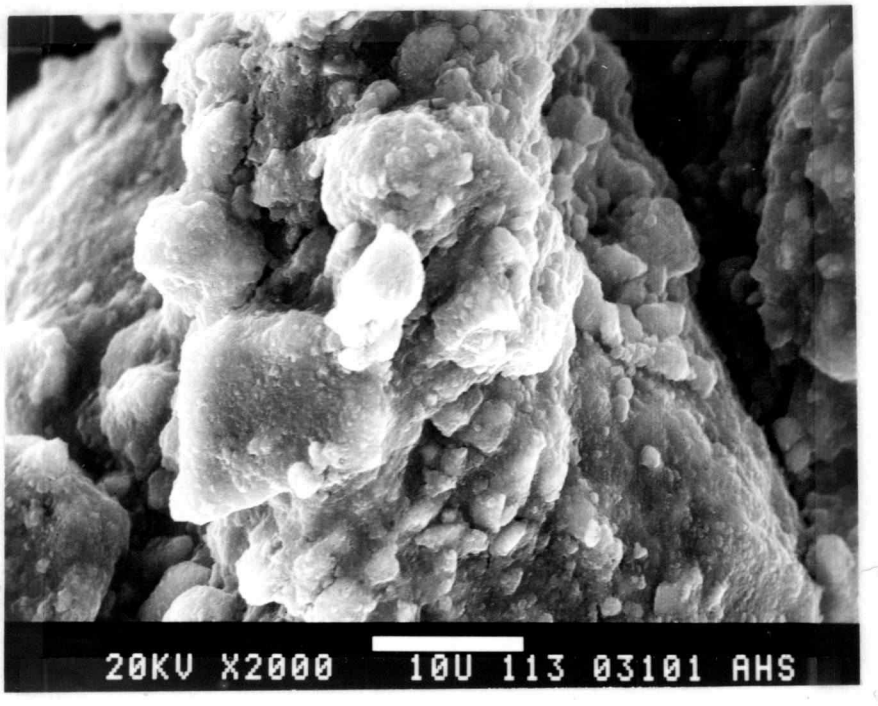

(b)

Figure 58 (a) SEM micrograph Site 1a (500x); (b) SEM micrograph Site 1a (2000x).

between particle assemblages (inter-assemblages) appear to be open to the grain surface. These pores have irregular shapes averaging about 1 mm in diameter.

Site 1b - Dome Creek Slide

Figures 59a and 59b show SEM micrographs of Site 1b. Figure 59a indicates that the basic fabric elements are made up of regularly shaped aggregations with rough surface texture. These are of various sizes averaging about 0.5 mm in diameter.

Figure 59b shows the individual silt sized particles to be lightly sheathed in an amorphous coating. Particles are very distinct and well formed. They appear to interact as groups of clustered particles with fairly uniform grain size.

The particle assemblages consist of aggregated small silt sized particles in an amorphous matrix. Connectors between the particle assemblages are chains of coated granular particles. The binder matrix appears to consist mainly of coated silt sized particles.

Some of the amorphous coatings again show a poorly developed platy structure with the plate edges being distinctly angular.

Intra-elemental pore spaces are blocked or filled by amorphous material. Intra-assemblage pore spaces are numerous and consist of many uniformly distributed approximately equal sized pores of 0.1 μm diameter. Inter-assemblage and trans-assemblage pores

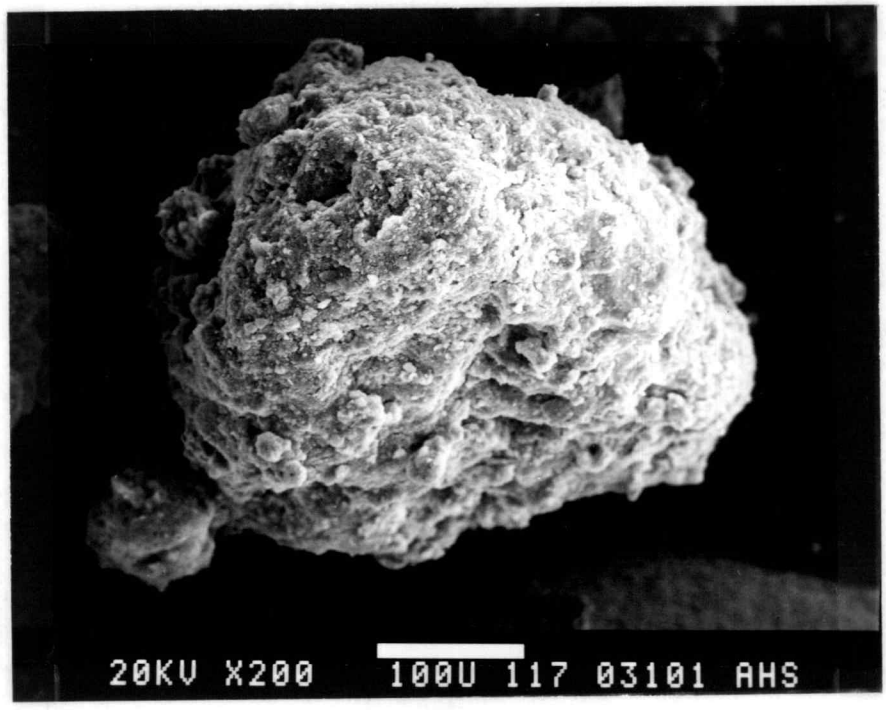

(a)

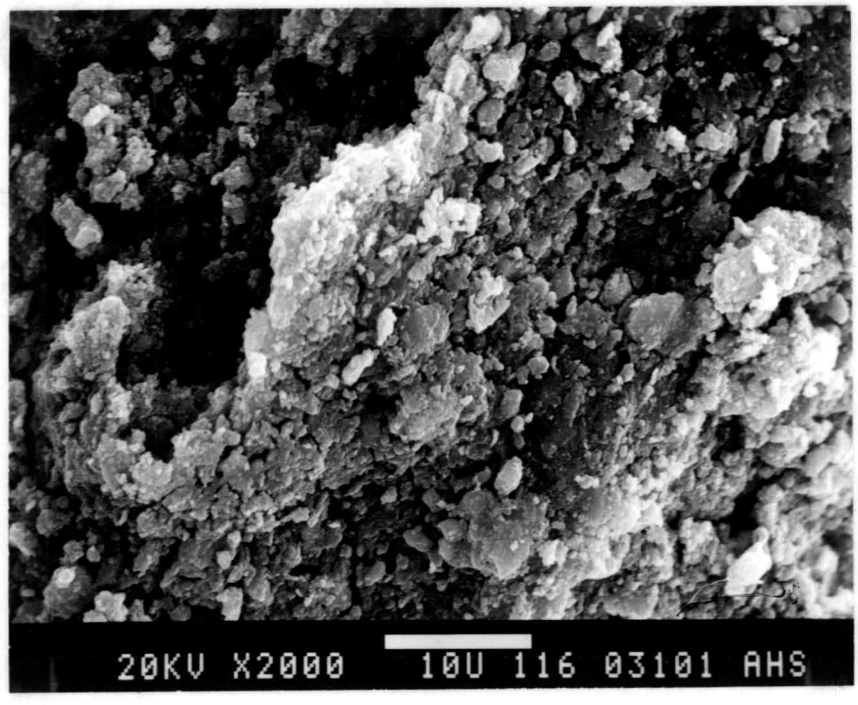

(b)

Figure 59 (a) SEM micrograph of Site 1b (200x); (b) SEM micrograph of Site 1b (2000x).

appear large, irregular, and seem to be independent of smaller pore spaces much like pumice vesicles.

Site 2 - Dome Creek Cutbank

Figures 60a and 60b present SEM micrographs of Site 2. Figure 60a shows that the soil fabric is dominated by amorphous coated grains with some platelike development.

Much like the soil in Figure 58, individual grains and particle assemblages appear to interact only through the amorphous coatings at contact points.

Particle aggregations are very irregular and occur over a wide range of sizes from 2 to 10 mm in diameter. In Figure 60b these aggregations have fairly smooth surfaces. These particles assemblages are connected by thickly bridged amorphous links which seem to continuously connect and coat each particle.

The intra-elemental and intra-assemblage pores are blocked or filled with amorphous coating materials. Inter-assemblage pores are variable in size and shape, the smallest pores being approximately 1 to 2 μm across.

Fabric Description - Site 3

Figures 61a and 61b are micrographs of Site 3. Figure 61a

(a)

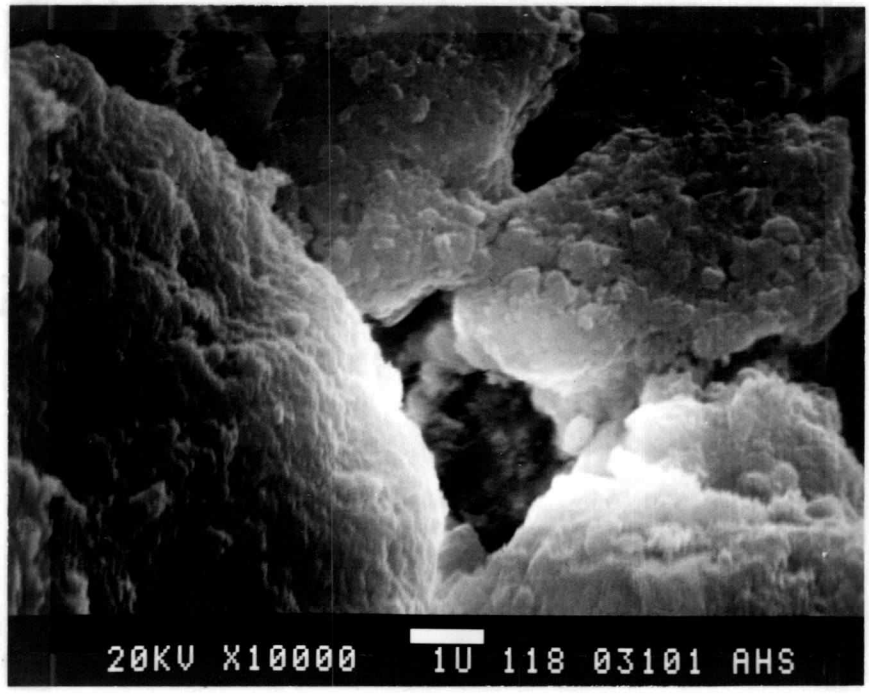

(b)

Figure 60 (a) SEM micrograph of Site 2 (2000x); (b) SEM micrograph of Site 2 (10000x).

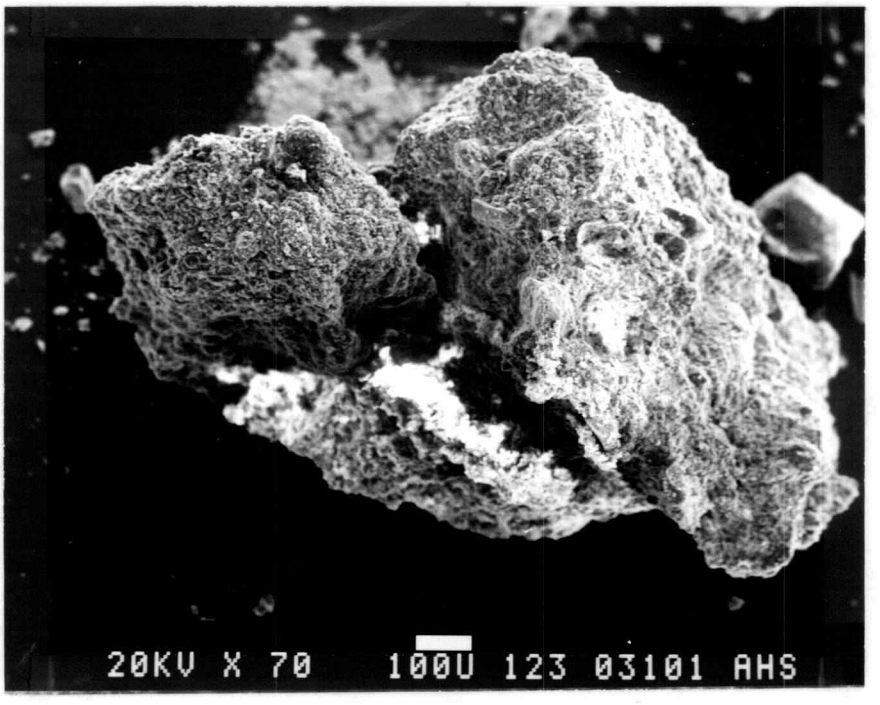

(a)

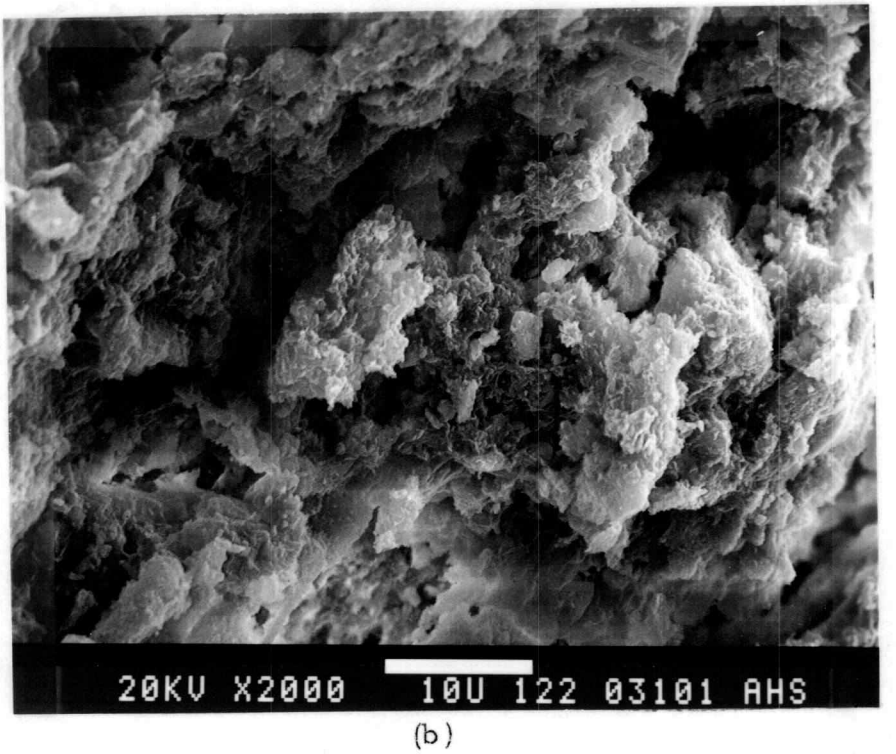

(b)

Figure 61 (a) SEM micrograph of Site 3 (70x); (b) SEM micrograph of Site 3 (2000x).

shows shape and size characteristics of the macro-grain aggregates studied. Surface morphology is much like that of pumice grains. At higher magnifications (Figure 61b), surface morphology has a flaky arrangement of poorly formed plate-like amorphous material. Plate edges are very irregular and angular.

Elementary particle arrangements are not discernable. Particle assemblages appear to consist of aggregated amorphous platy materials connected by interwoven flexible platy amorphous constituents of two dimensional order.

Intra-assemblage and inter-assemblage pores of vesicular nature dominate the overall fabric structure.

Site 4 - Pyrimid Creek Cutbank

Large particles for soils from Site 4 consist of rough textured pumice type grains about 0.5 mm in diameter. Macrograins are similar to those from Site 1b. Overall fabric arrangement is also similar to Site 1b soils.

Elementary, single, lightly colored silt-sized particles, and their arrangements, dominate the fabric shown in Figure 62a. These particles interact through thin connectors consisting of amorphous coating materials. Some particle aggregations are present.

Intra-elemental pore space is plugged by amorphous coatings by intra-and inter-assemblage pore space can be characterized much

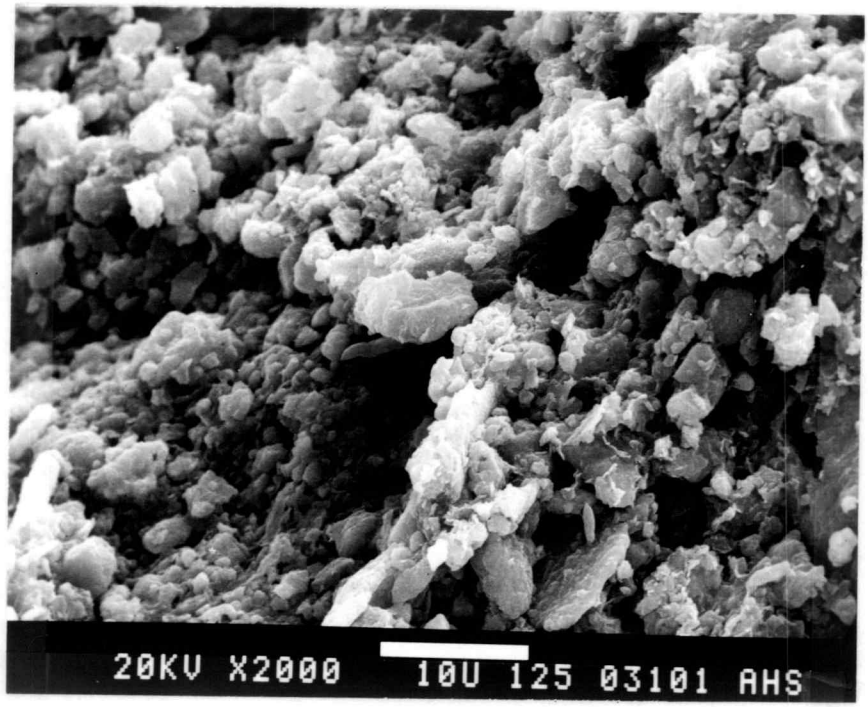

(a)

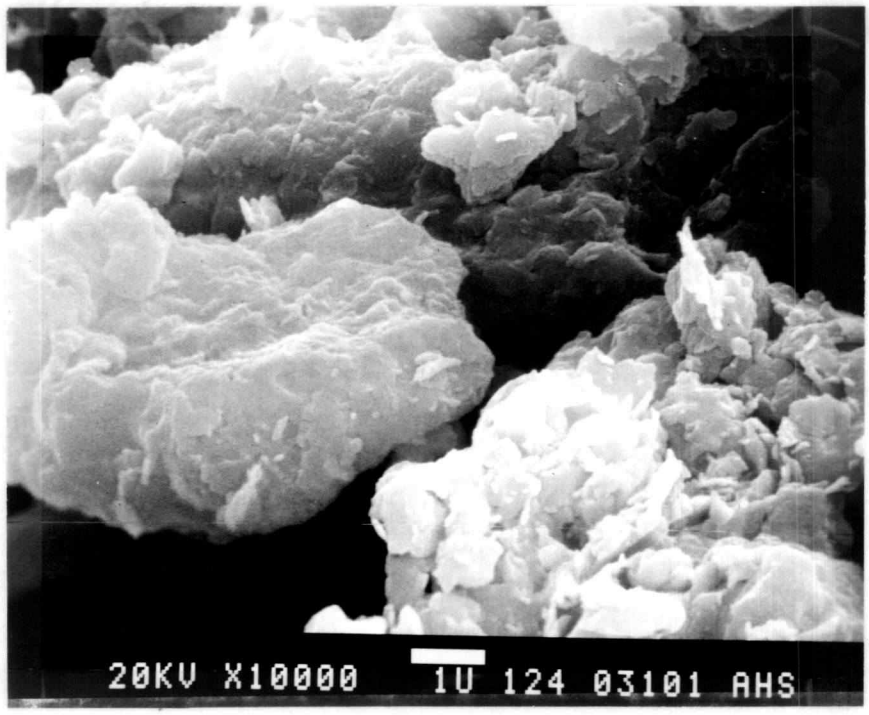

(b)

Figure 62 (a) SEM micrograph of Site 4 (2000x); (b) SEM micrograph of Site 4 (10000x).

like regular and irregular shaped pores occurring in granular soils.

Site 5 - Batchellor Creek Cutbank

Electron micrographs from Site 5 (Figures 63a and 63b) show fabric and grain coatings similar to those from Site 1a. Figure 63a presents a typical grain aggregate approximately 1 mm in diameter. Note the rough surface texture and presence of smaller regular shaped particle assemblages ranging from 10 to 100 μm across.

Higher magnification (Figure 63b) reveals the fabric structure to be dominated by amorphous coatings of sufficient thickness to obliterate individual grains. This amorphous coating serves as connector material between grains and particle assemblages, and also serves as the matrix material for the grains. The amorphous material appears to have plate-like face-to-face structure with distinct somewhat angular edges.

Pore spaces are predominantly inter-assemblage with the majority of pores ranging from 1 to 100 μm across, in vesicular fashion.

Site 6 - Box Canyon Creek

Figure 64a presents a typical pumice-like agglomeration from Site 6. Again, much like the sand-sized grains from other sites,

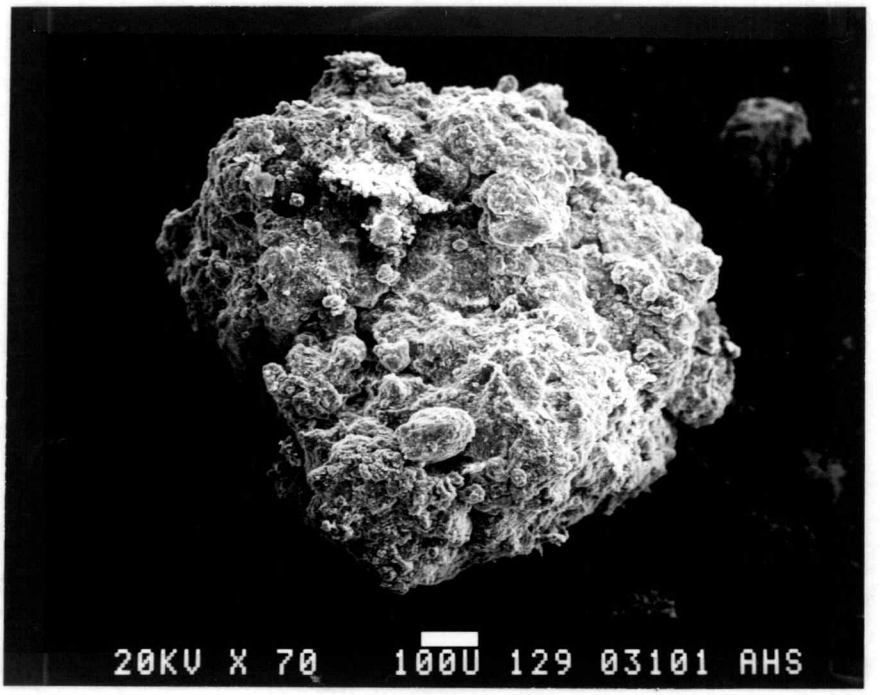

(a)

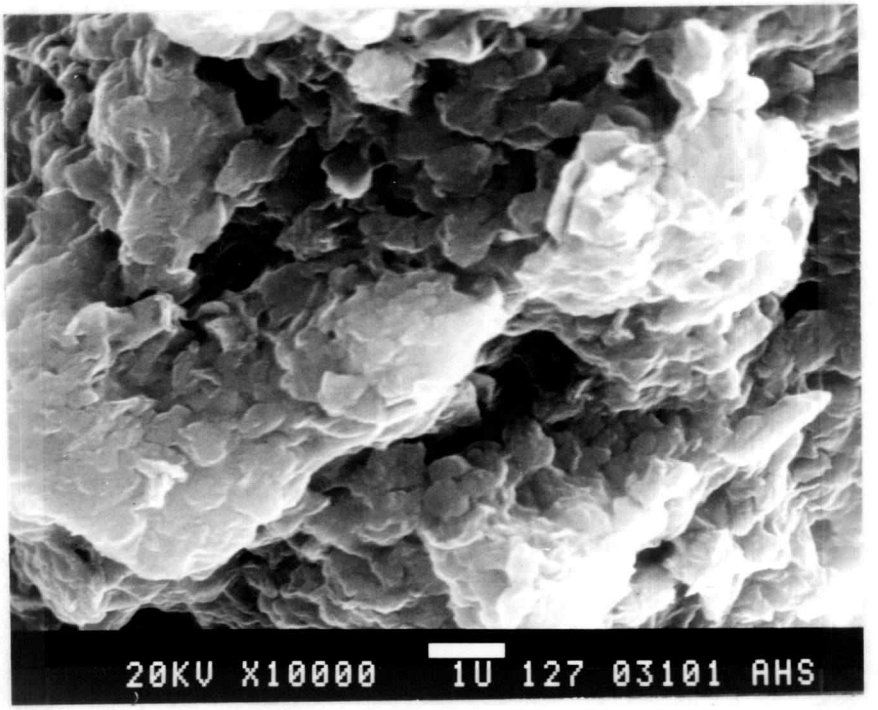

(b)

Figure 63 (a) SEM micrograph Site 5 (70x); (b) SEM micrograph Site 5 (2000x).

(a)

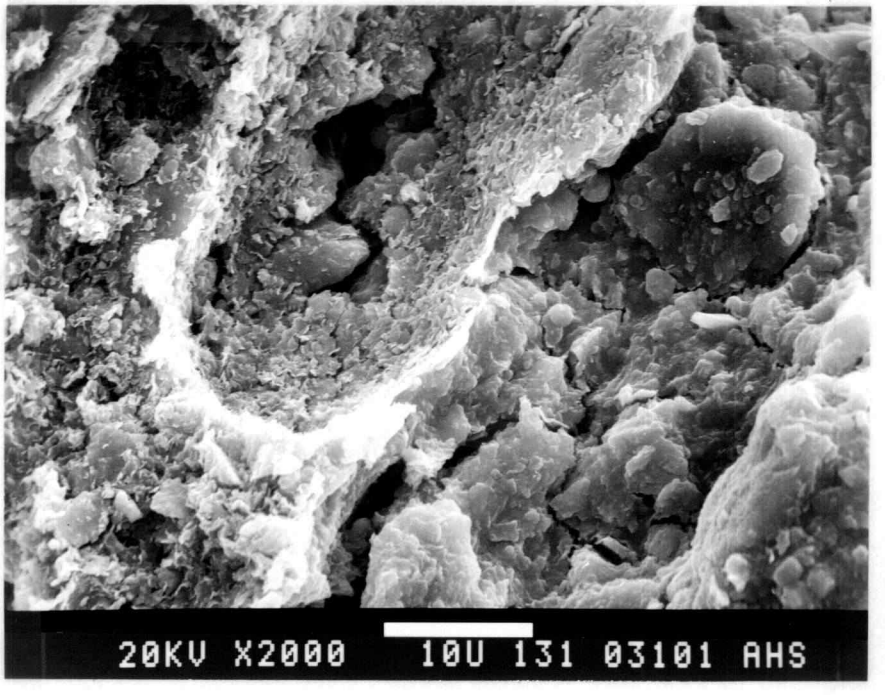

(b)

Figure 64 (a) SEM micrograph Site 6 (100x); (b) SEM micrograph Site 6 (2000x).

angular, rough surface texture is the dominant characteristic.

Figure 64b shows that the soil matrix is dominated by plate-like amorphous coatings which form grains, connecting materials, and particle agglomerations. Many of the grains appear to be separated by angular cracks or breaks.

The smaller pore spaces appear to be blocked or filled with amorphous materials. Large irregular pores greater than 5 μm are the largest pores with surface access.

Site 7 - Quartzville Creek Cutbank

Figures 65a and 65b are SEM micrographs from Site 7. The grain in Figure 65 is an approximate 1 mm size pumice-like aggregated grain, typical of these soils. Note the anomalous smooth area in the upper center of Figure 65a. This may be a slickned area formed from stress movements in the soil. The surface may represent the failure surface during shear in these soils.

Microfabric features (Figure 65b) indicates the predominence of plate-like amorphous coatings. Observe the folded amorphous "plate" in the center of Figure 65b. This material appears as amorphous gel with two dimensional order. The face is extremely smooth, and the platelet thickness is about .5 μm. The x and y dimensions are much greater than the z dimensions, like sliced cheese.

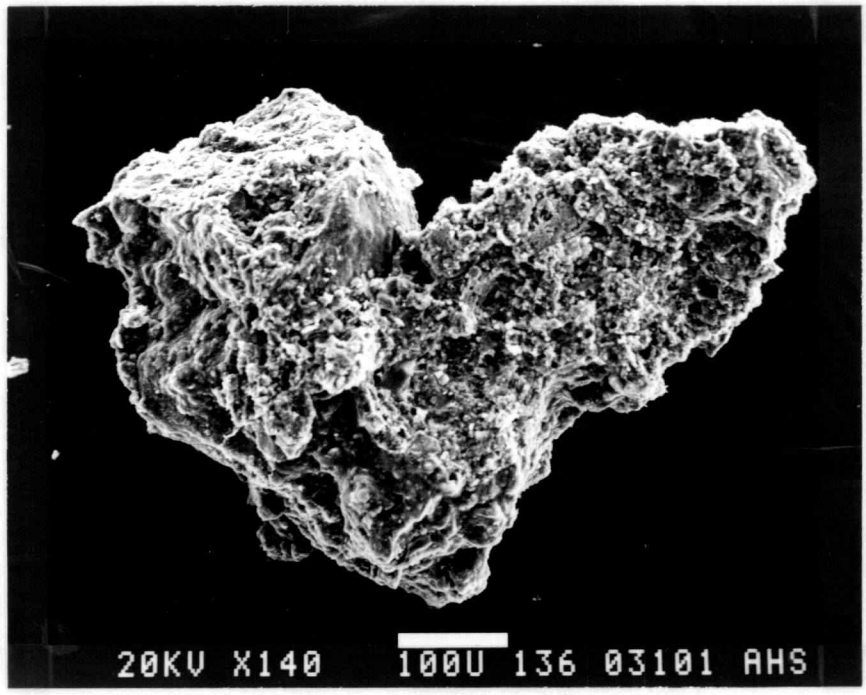

(a)

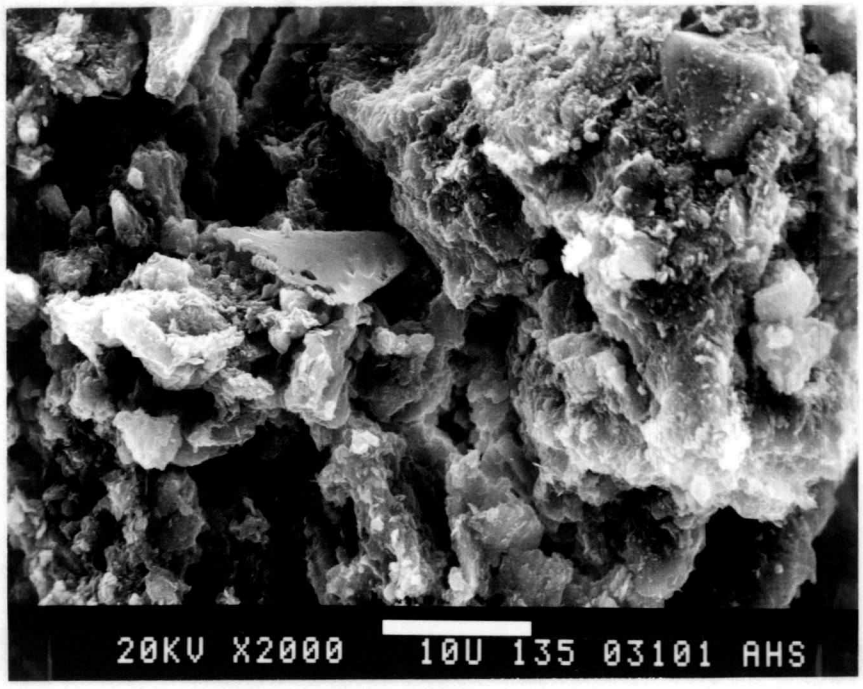

(b)

Figure 65 (a) SEM micrograph Site 7 (140x); (b) SEM micrograph Site 7 (2000x).

Pore space can be characterized as inter-assemblage pores ranging from 2 to 50 μm and vesicular in nature.

Site 8 - Fritz Creek Slump

Figure 66a is a micrograph of a pumice-like soil grain from Site 8. The surface is relatively smooth and the grain relatively well rounded. Clusters of face-to-face platy amorphous aggregates jut from the surface much as if the grain has undergone only superficial weathering to a depth of 7 to 10 μm.

Amorphous aggregates are irregularly shaped and approximately 5 to 10 μm across. These aggregates interact with the partially weathered grain and with adjacent grains of the soil matrix.

Pore space is limited to surface pores between the amorphous particle assemblages.

Site 9 - Lookout Creek Cutbank

Figures 67a and 67b are electron micrographs from Site 9. Figure 66a shows highly irregular pumice-like grains. The grain appears to be an aggregated mass of smaller irregular shaped aggregated particles.

Figure 67b reveals that elementary particles are masked by an amorphous coating. The coating has a poorly developed plate-like

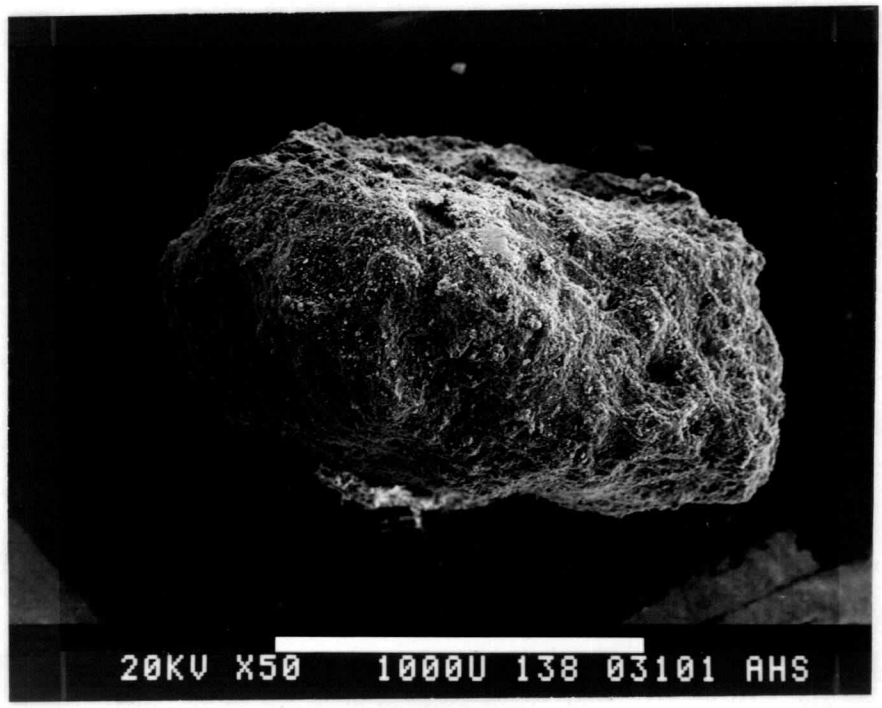

(a)

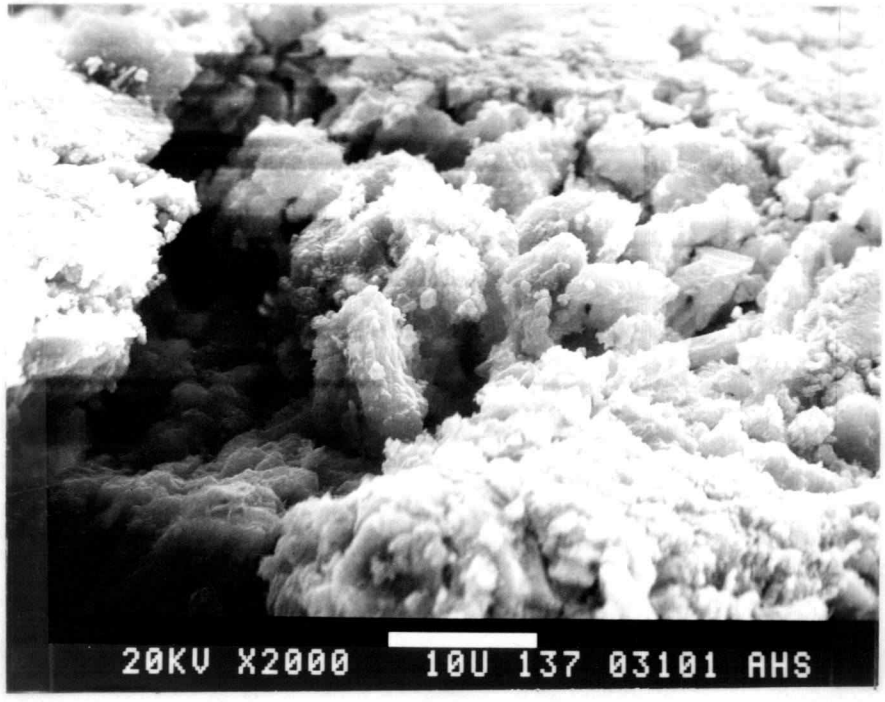

(b)

Figure 66. (a) SEM micrograph of Site 8 (50x); (b) SEM micrograph of Site 8 (2000x).

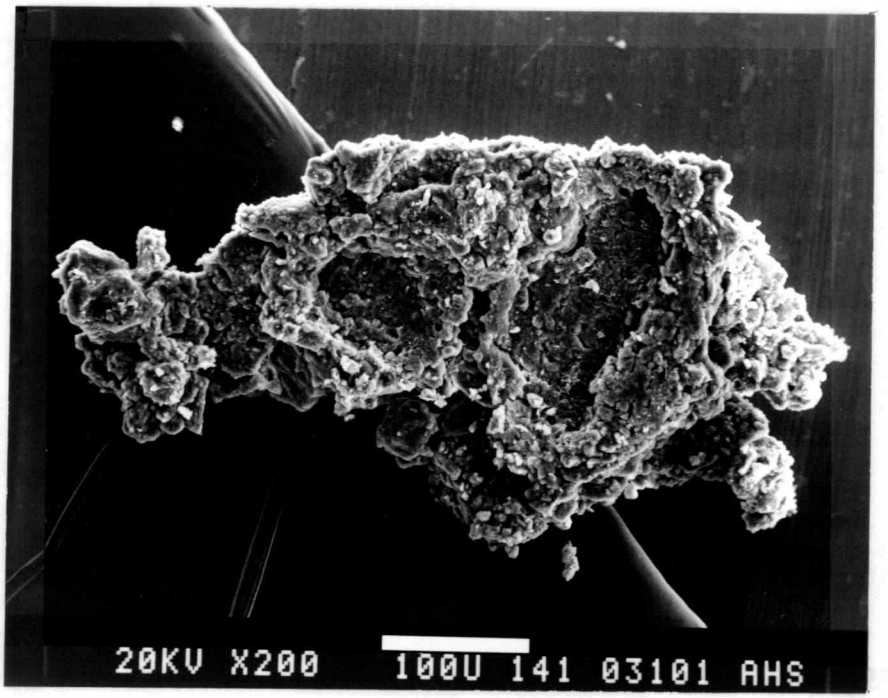

(a)

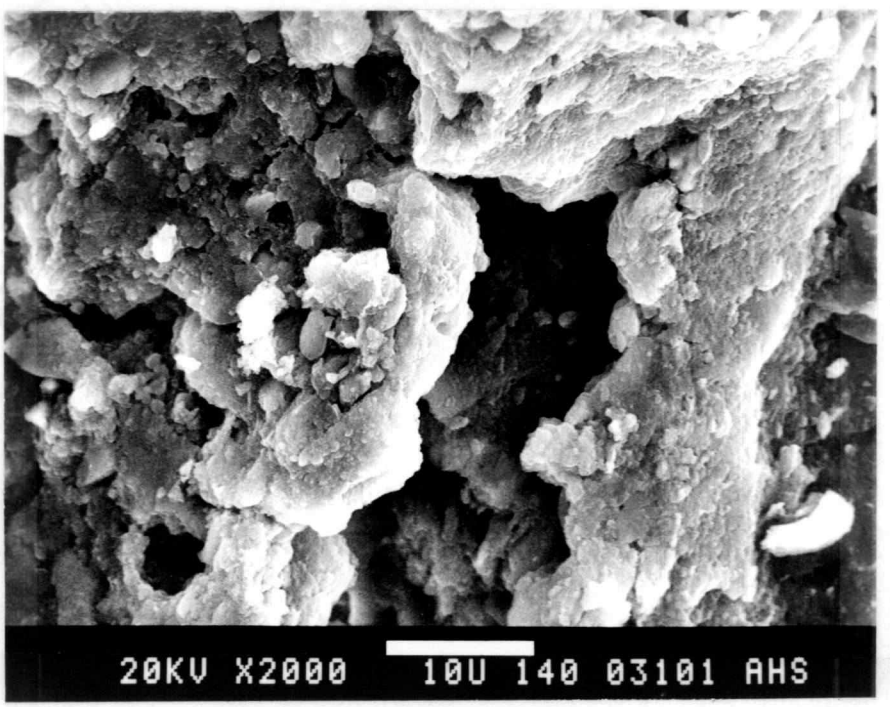

(b)

Figure 67. (a) SEM micrograph of Site 9 (200x); (b) SEM micrograph of Site 9 (2000x).

structure. The amorphous material serves as connecting material between particles and aggregates with a partially granular matrix.

Pore spaces in this material are intra- and inter-assemblage pores of variable sizes and shapes ranging from 1 to 100 μm across. The pores are vesicular in nature.

Site 10 - Alaska Shelikof

Figures 68a and 68b are SEM micrograph of Site 10 soils from Alaska. Figure 68a indicates that the grain resembles a very rough-textured pumice grain. Figure 68b shows that the soil grain consists of irregular shaped plate-like assemblages of amorphous gel with very angular edges.

Much of the aggregate interaction occurs along the particle assemblage boundaries through the thin flaky amorphous plates.

Much of the pore space occurs between the assemblages and the rough edged plates of individual aggregates. The pores are irregularly shaped and much small pore space is contained along the angular dissected boundaries of the larger pores. The smallest pores are much smaller than 1 μm diameter.

Site 11 - Alaska Sitka

Figure 69a presents a highly dissected grain of amorphous aggregate. The irregular surface made electron microscopic

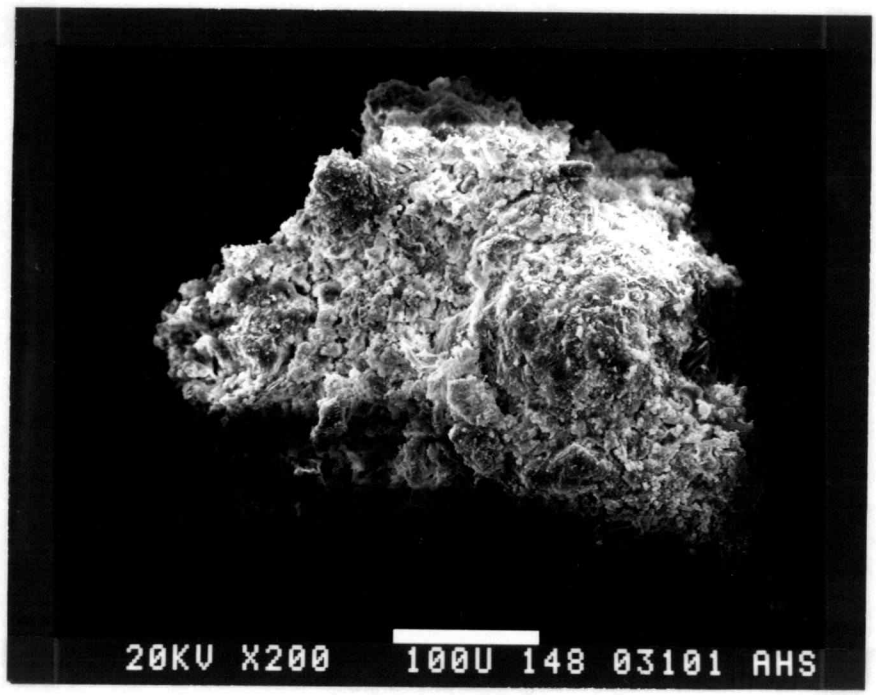

(a)

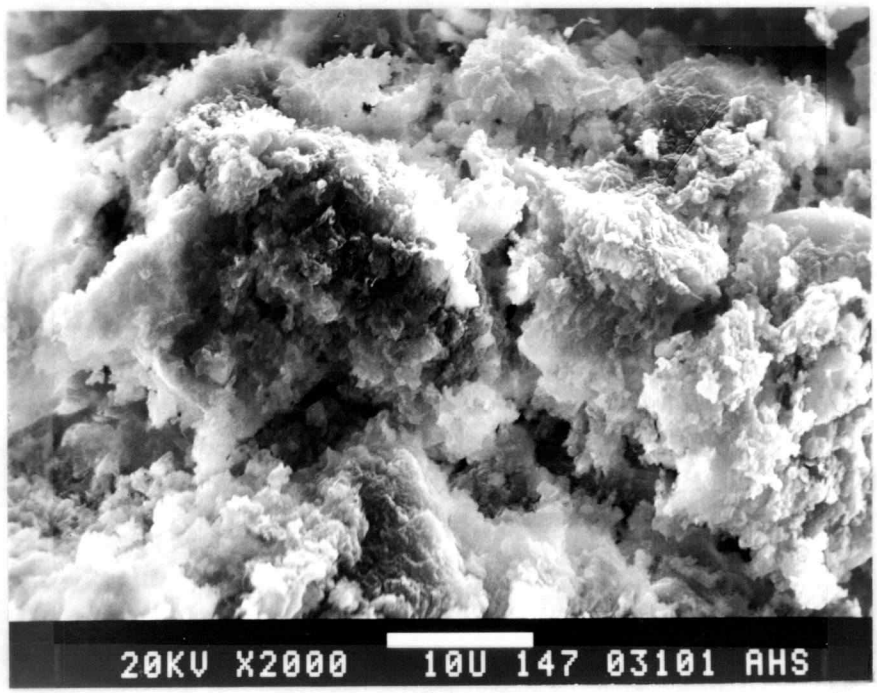

(b)

Figure 68. (a) SEM micrograph of Site 10 (200x); (b) SEM micrograph of Site 10 (2000x).

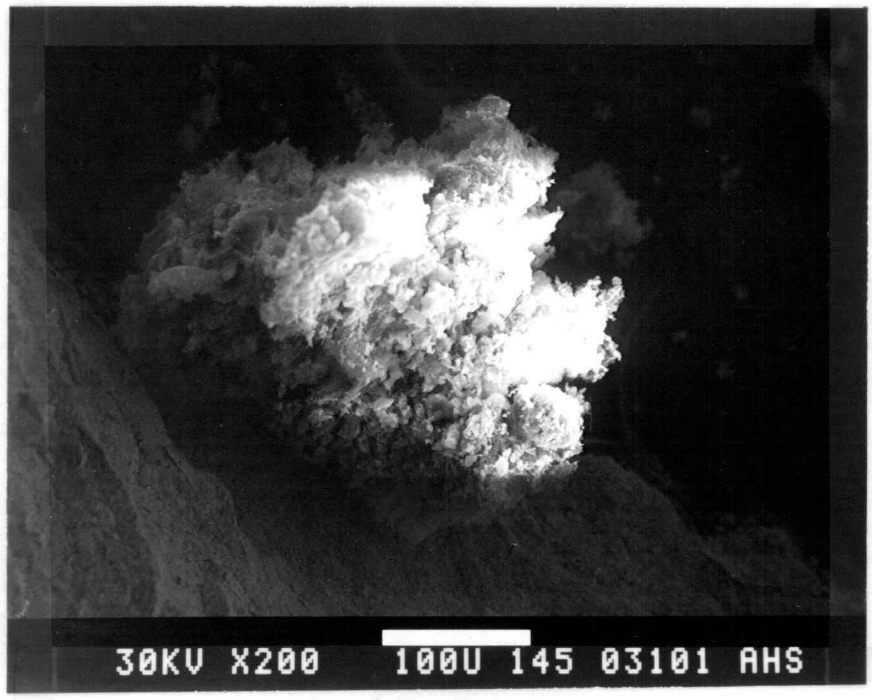

(a)

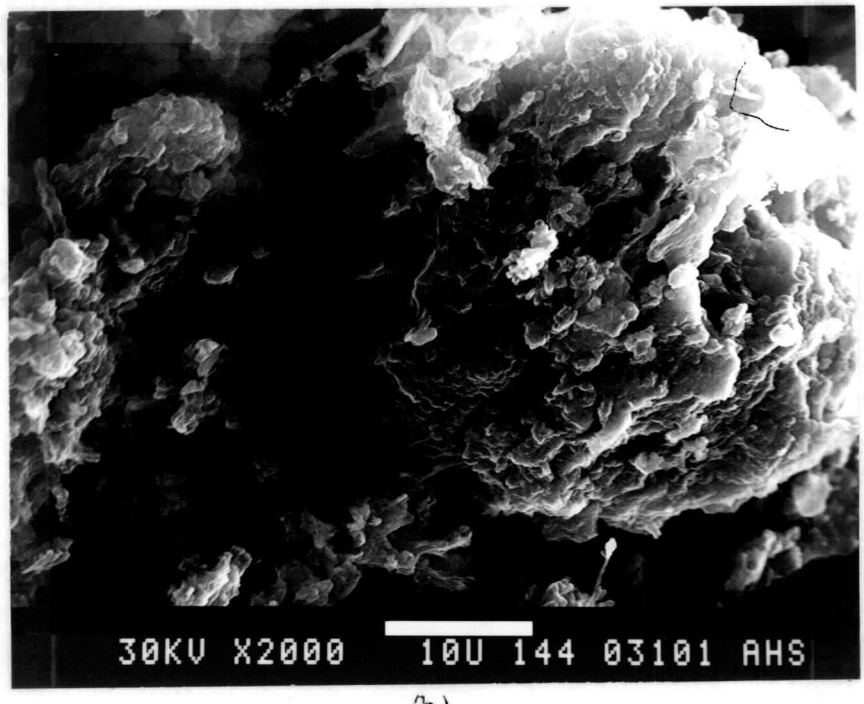

(b)

Figure 69. (a) SEM micrograph of Site 11 (200x); (b) SEM micrograph of Site 11 (2000x).

analysis difficult due to charge buildup on the particle surface.

Figure 69b shows the soil microfabric with platelike arrangements of amorphous materials. The plate edges are very irregular and contain many voids. The entire grain appears to be made up of amorphous materials with connectors of amorphous strands connecting particle assemblages of dissected face-to-face amorphous gels with two-dimensional shapes.

Pore spaces occur over a wide range of sizes and shapes. Many of the smaller pores occur in intra-assemblage positions, larger pores occur between the particle assemblages.

Fabric Summary and Discussion

As indicated by the descriptions of fabric for Sites 1 thru 11, the presence of abundant amorphous coatings dominate the microstructure of these soils. The majority of soil grains and particle assemblages are clothed in amorphous gel like materials of two-dimensional shape. Grain-to-grain contacts and connections are found to involve the interaction of these coatings.

In general, the soil grains appeared to be particle assemblages made up of smaller particle assemblages. Individual elementary soil grains are masked by amorphous coatings.

The amount and availability of pore space to grain surface interactions also seems to be controlled by the amount and occurrence

of amorphous coating materials. For Sites 1 to 9, pores between elementary particles and pores within particle assemblages are blocked, or filled with amorphous coating material. Only pore space between particle assemblages are open to grain surface interaction. For Sites 10 and 11, only pores between elementary particles are blocked; intra- and inter-assemblage pores are open to surface processes. Thus it appears that small pores in Site 1 to 9 samples are blocked but abundant larger pores exist. For Sites 10 and 11 smaller and more abundant pores are available for interaction.

There appears to be no evidence of obvious arrangement, or preferred orientation of soil particles in any of the micrographs from Sites 1 to 11. But, as pointed out by Tovey (1971), a complex analysis of many micrographs is required to establish positive anisotropic trends when they are not visually obvious.

Relationships of Mineralogy and Fabric to Engineering Behavior

This section combines the mineralogical, structural, correlation and engineering characterization data from the laboratory study thus far presented for sites 1 to 11. Schematic representations of fabric structure are developed for poorly crystalline soils derived from volcanic ash. Possible mechanisms for irreversable drying and other engineering behavior are discussed.

Development of Schematic Fabric Representations

Analysis of Figures 58 to 69, and accompanying discussions, show that several of the soils have similar microfabric and texture. Sites grouped together, based on obvious visual and descriptive similarities are listed and described as follows:

Sites 1a and 2 -- Similar in that they both exhibit a thick amorphous coating. At 10, 000x, individual coated grains appear relatively smooth.

Sites 1b, 4, and 8 -- Similar in granular brittle appearance at 2000x.

Sites 3, 7, 9 and 10 -- Similar in fluffy indistinct appearance of grains at 2000x, and rough cloudlike edges at 10, 000x.

Sites 5, 6 and 11 -- Similar in that rounded individual grains have transparent appearance at 2000x and 10, 000x. Much of the amorphous material appears in bulk rather than coating form.

For each set of sites so grouped, data from the electron microscope, mineralogical, and engineering studies are summarized and compared. Similarities, trends and differences are noted.

Table 29 presents grouped engineering and index properties taken from laboratory results presented in Chapter III. Observe that

Table 29. Diagnostic engineering and index properties.

	Water Content w_n (%)	Liquid Limit LL (%)	Plasticity Limit PL (%)	Plastic Index PI (%)	Optimum Density γd_{max} (pcf)	Optimum Moisture w_{opt} (%)	Percent Fines -200 (%)	Specific Gravity G_s (ratio)	Void Ratio e_o (ratio)	Internal Friction ϕ' (degrees)	Cohesion Intercept c (kg/cm^2)
Site 1a	36.5	47.8	50.6	N.P.	71.5	45.0	21.4	2.78	1.85	56.1	-0.12
Site 2	56.0	63.0	50.2	12.8	71.2	46.5	66.7	2.87	--	--	--
Site 1b	44.0	72.5	49.8	22.7	60.0	55.0	44.4	2.88	1.85	56.1	-0.12
Site 4	46.9	60.8	46.6	14.2	81.2	32.5	42.1	2.71	1.42	46.9	-0.09
Site 8	53.7	46.3	33.4	12.9	92.0	28.0	38.3	2.68	2.92	50.3	-0.11
Site 3	42.6	48.8	38.8	10.0	85.9	31.7	47.7	2.86	1.46	42.1	.01
Site 7	48.5	60.0	44.0	16.0	76.5	39.0	57.6	2.80	1.70	38.1	0.0
Site 9	28.2	50.3	35.3	15.0	85.5	29.5	45.3	2.67	1.05	43.3	0.01
Site 10	135.3	160.5	95.3	65.2	48.5	67.0	43.4	2.67	3.98	20.1	0.14
Site 5	42.3	69.0	52.7	16.3	81.2	32	28.7	2.86	1.55	32.1	0.08
Site 6	49.6	59.7	41.5	18.2	83.5	35.5	39.1	2.79	1.66	46.7	-0.10
Site 11	160.3	233.9	119.3	114.2	42.0	73	24.5	2.65	4.17	43.2	0.10

Table 30. Allophane constituent percentage determined from correlation equations presented in Table 25.

	Measured Percentage % ALO (%)	Water Content w_n (%)	Plastic Limit PL (%)	Void Ratio e_o (ratio)	Optimum Density γd_{max} (pcf)	Optimum Moisture w_{opt} (%)	Specific Gravity G_s (ratio)	Average by Correlation % ALO (%)
Site 1a	15-25	13.3	25.5	15.0	28.5	24.7	Not valid	21.0
Site 2	30-40	20.2	21.8	--	28.8	26.1	Not valid	24.2
Site 1b	25-35	16.0	21.6	16.0	39.4	34.0	Not valid	25.4
Site 4	15-25	17.0	20.2	9.1	19.3	13.1	Not valid	15.7
Site 8	10-20	19.4	14.3	33.4	9.0	8.9	Not valid	17.0
Site 3	25-35	15.5	16.7	9.7	14.8	12.4	Not valid	13.8
Site 7	20-30	17.5	19.0	13.6	23.7	19.2	Not valid	18.6
Site 9	15-25	10.4	15.1	1.0	15.2	10.3	Not valid	10.4
Site 10	40-50	Not valid	42.1	50.5	50.3	45.2	66.6	50.9
Site 5	20-30	15.4	23.0	11.2	19.3	12.6	Not valid	16.3
Site 6	20-30	17.9	17.9	13.0	17.1	15.9	Not valid	16.4
Site 11	50-60	Not valid	52.9	53.6	56.5	50.8	64.4	55.6

Table 31. Engineering properties by correlation.

	Shear Strength c (kg/cm^2)	Shear Strength c (kg/cm^2)	Internal Friction ϕ' (degrees)	Compression Index C_c	Optimum Moisture w_{opt} (%)
Site 1a	2.59[a] (0.97)[d]	0.90[b] (0.56)	38.8[b] (40.5)	Not valid	43.2[c] (43.4)
Site 2	1.12 (0.14)	--	--	-	43.0 (43.0)
Site 1b	1.87[a] (0.46)	0.90[b] (0.56)	38.8 (40.5)	Not valid	42.8[c] (42.7)
Site 4	1.65 (0.34)	1.60 (1.08)	42.7 (43.6)	Not valid	40.9 (40.3)
Site 8	1.23 (0.17)	0.23 (0.11)	31.9 (32.7)	Not valid	33.1 (30.1)
Site 3	1.99[a] (0.53)	1.49[b] (1.02)	42.3[b] (43.4)	Not valid	36.3[c] (34.3)
Site 7	1.54 (0.29)	1.09 (0.70)	40.0 (41.6)	Not valid	39.4 (58.3)
Site 9	3.70 (2.23)	2.50 (1.91)	47.3 (46.3)	Not valid	34.2 (31.6)
Site 10	0.04 (0.14)	0.06 (0)	27.3 (20 2)	(0.93)[b] (1.71)[a]	69.6 (68.6)
Site 5	2.02[a] (0.54)	1.33[b] (0.88)	41.4[b] (42.7)	Not valid	44.5[c] (45.0)
Site 6	1.47 (0.26)	1.2 (0.75)	40.4 (41.9)	Not valid	37.9 (36.3)
Site 11	0.01 (0.06)	0.05 (0)	26.6 (20.0)	(0.95)[b] (1.95)[a]	83.8 (79.6)

[a] From correlation with natural water content (w_n in %), equation in Table 28.

[b] From correlation with void ratio (e_o), equation in Table 28.

[c] From correlation with plastic limit (PL), equation in Table 28.

[d] Numbers in parenthesis refer to high ($w_n > 60\%$) or low ($w_n < 60\%$) natural water content group, whichever is appropriate for that site.

for soils within these fabric groups, considerable variation in engineering behavior is evident. Soils with similar fabric and textural appearance may exhibit either high or low natural water content group behaviors described in Chapter V.

Table 30 compares measured allophanic constituent percentages (% ALO) determined from laboratory samples in Chapter IV, with % ALO determined from correlation equations developed in Chapter V. Natural water content, plastic limit, void ratio, optimum density, optimum moisture, and specific gravity are used to approximate % ALO, the results of which are averaged in the last column of Table 30.

Table 31 presents engineering properties for Sites 1 to 11, as determined from correlation equations developed in Chapter V. Numbers without parenthesis are for total sample correlation equations in Table 28. Numbers with parenthesis are for the high-low natural water content correlations, also presented in Table 28.

Tables 32 and 33 summarize engineering and index properties for oven dried samples from each fabric group. The results in Tables 32 and 33 indicate that large differences exist within fabric groups. These differences are independent of drying history, and could be attributed to mineralogical differences.

From these data, schematic representations of the soil matrix, particles shapes, particles assemblages, and their relationships are constructed to model observed behaviors. These results are discussed and appropriate conclusions drawn.

Table 32. Engineering and index properties for oven dried soils.

	Liquid Limit LL (%)	Plasticity Limit PL (%)	Plastic Index PI (%)	Optimum Density $\gamma_{d_{max}}$ (pcf)	Optimum Moisture w_{opt} (%)
Site 1a	41.5	41.5	N. P.	79.8	39.0
Site 2	50.9	47.0	3.9	81.0	38.5
Site 1b	56.7	56.7	N. P.	67.5	50.0
Site 4	48.7	39.5	9.2	87.8	29.2
Site 8	41.3	31.0	10.3	96.5	24.0
Site 3	40.5	37.4	3.1	92.4	27.0
Site 7	51.2	39.7	11.5	85.0	33.5
Site 9	44.0	32.7	11.3	93.0	25.5
Site 10	86.8	86.8	N. P.	64.5	38.0
Site 5	57.2	48.2	9.0	74.5	35.0
Site 6	44.3	33.8	10.5	88.3	32.8
Site 11	84.0	86.7	N. P.	64.5	43.0

Table 33. Percent change in engineering and index properties with oven drying.

	Liquid Limit LL (%)	Plastic Limit PL (%)	Optimum Density $\gamma_{d_{max}}$ (pcf)	Optimum Moisture w_{opt} (%)
Site 1a	-13.2	-18.0	11.6	-13.3
Site 2	-19.2	- 6.4	13.8	-17.2
Site 1b	-21.8	13.9	12.5	- 9.1
Site 4	-19.9	-15.2	8.1	-10.2
Site 8	-10.8	- 7.2	4.9	-14.3
Site 3	-17.0	- 3.6	7.6	-14.8
Site 7	-14.7	- 9.8	11.1	-14.1
Site 9	-12.5	- 7.4	8.8	-13.6
Site 10	-45.9	- 8.9	33.0	-43.3
Site 5	-17.1	- 8.5	- 8.3	9.4
Site 6	-25.8	-18.6	5.7	- 7.6
Site 11	-64.0	-27.3	53.6	-41.1

Sites 1a and 2

The dominate feature for samples from these sites is the thick amorphorphous coatings which continuously clothe and connect soil grains and particle assemblages. Other significant fabric features are:

1. Continuous coating-linkage-coating-linkage sequence from grain to grain.
2. Particles less than 1 mm in diameter are engulfed and undistinguishable in the amorphous matrix.
3. Some indistinct face-to-face platelike development is evident.
4. Amorphous coatings have relatively smooth edges.
5. There are regular and irregular shaped particle assemblages ranging from 10 to 100 mm in diameter.
6. There exist thickley bridged amorphous linkages between particles.
7. Small pores are blocked by amorphous coating.

Minerology and transmission electron microscope studies (Chapter IV) indicate that for Site 1a, halloysite, imogolite, allophane, quartz and various feldspars are the major constituents. Visually the materials can be described as cloudy mottled amorphous materials, composed of rough edged 2 μm particles. These appear as agglomerates of smaller particles. Site 2 consists of halloysite, quartz and

feldspars with allophanic constituents very prominent. They appear as irregular distinct particles surrounded by clouds of indistinct materials of various shapes and minerology. Percent allophanic content analysis (Chapter V) indicates that Site 1a contains 15 to 25% amorphous material, and Site 2 has 30 to 40%.

Table 29 shows considerable variation in individual index properties between Sites 1a and 2. Moisture-density optimum values show good agreement.

These differences may be explained by variations in drying history and mineralogy. This result is expected for samples taken at different locations. The Site 1a samples were taken from south-facing slide scarp subject to drying from direct sun during the summer. Site 2 was located in a shaded roadcut. Some previous drying has probably also occurred at Site 2.

Figures 58 and 60 are scanning electron microscope micrographs of Sites 1a and 2. Site 2 appears to have a much larger percentage of fine materials than Site 1a. The percent fines column in Table 29 shows this to be true. Natural water content (w_n) and liquid limit (LL) are significantly larger for Site 2 than 1a. This can be explained by smaller grain size for Site 2 resulting in larger surface area. Warkentin (1972) and Gradwell and Birrell (1954) report that liquid limit is related to surface area and not clay content for allophanes.

Plastic limits are the same for both sites. This could mean that as the soil was dried below the natural water content to the plastic limit, the behavior of Site 2 soils approached that of Site 1a soils. This same phenomena can be observed for the moisture-density optimum values shown in Table 29, for both sites. Engineering properties of oven dried soils shown in Table 32 indicate that Site 2 soils have slightly larger liquid limits, plastic limits and plasticity index, but the differences are small, and the behavior is similar when dried.

Allophanic constituent percentage (% ALO) results in Table 30 show that the percentages for Site 2 are greater than Site 1a. Engineering and index property data in general support this observation. However, oven drying data show that the percent change in index and engineering properties are small. Much larger, more consistent variation would be expected for the indicated difference in % ALO. For these reasons, it appears that % ALO has small effect on engineering properties when the amorphous materials in the soil matrix occur as particle coatings.

These observations indicate that Soil 1a shown in Figure 58b may result if Soil 2 were allowed to air dry. In particular, the grains appear to coalesce, and pores close or are blocked with amorphous materials upon drying.

Figure 70 shows a schematic of a possible fabric structure.

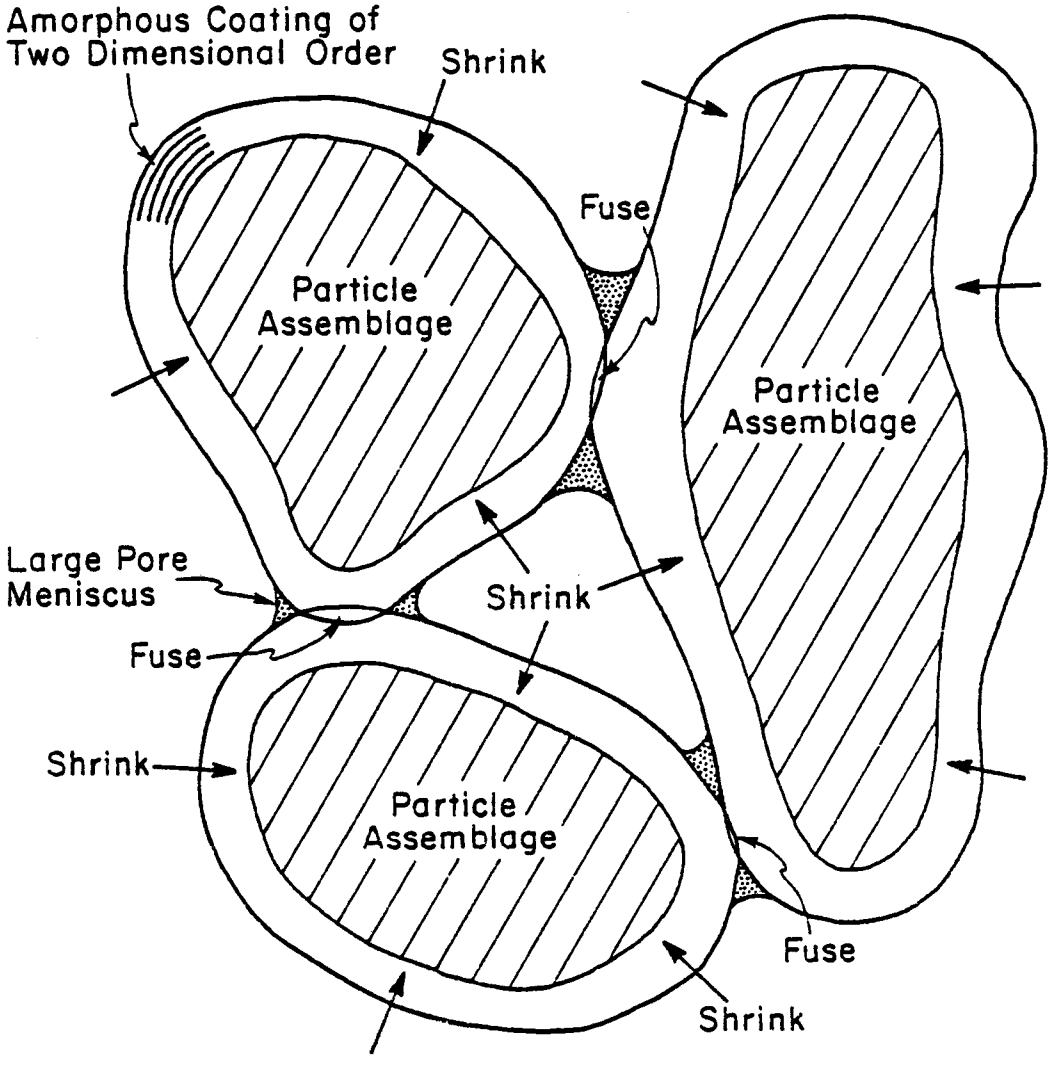

Figure 70. Schematic fabric structure for Sites 1a and 2.

The particle assemblages make up the soil skeleton. Transmission electron microscope micrographs show these assemblages to be agglomerations of irregular distinct and indistinct particles surrounded by clouds of indistinct materials of various shapes and compositions.

Strength results presented in Table 29 show an extremely high angle of internal friction of 56.1° for Site 1a. The reason for this high angle of internal friction may be related to the apparent drying and aggregation experienced by the exposed slide scarp. Correlations between index and engineering properties for Sites 1a and 2 are shown in Table 31. Only optimum moisture determined by correlation with plastic limit shows good agreement with measured values.

Sites 1b, 4 and 8

Soils in this group are dominated by granular appearance, and reasonably well developed platy structure of amorphous materials. Soil macro-grains are made up of rounded pumice like aggregations with rough surface texture. Particles from Site 8 appear to have undergone only surficial weathering of the macro-grain with the grain interior relatively unweathered.

Distinct and well-formed amorphous aggregates of various sizes interact through thin amorphous connectors. These aggregates appear

to be randomly arranged in a granular matrix. These soils have an abundance of medium to large vesicular pores with much inter- and intra-assemblage pore space.

Mineralogical characterization tests for Site 1b show that the soils consist of halloysite, quartz, feldspar and some iron oxides. Large amounts of allophane are evident. The soils appear as irregularly shaped solid particles, agglomerations of smaller particles arranged in circular type structures. Some amorphous gel -like coatings are evident.

Site 4 consists of halloysite, illite, allophane, imogolite, quartz and various feldspars. They appear as indistinct spheres, platelike grains and pieces of tubular halloysite held in an amorphous matrix.

Site 8 is made up of halloysite, illite and various amorphous materials which occur as clay sized particles surrounded by smaller agglomerates of distinct and indistinct particles. This mass is held together by webs of cloudy indistinct amorphous strands.

Table 29 and 32 show some variation in grouped index and engineering properties. Most of the variation can be adequately explained based on percentage of allophanic constituents present in each sample. Table 30 shows these percentages for Sites 1b, 4 and 8. As would be expected, the soil with the highest measured allophanic percentage (% ALO) shows the highest liquid limit, plastic limit,

plasticity index, optimum moisture content, and percent fines (Site 1b). Site 8 has the lowest % ALO and shows the lowest of these properties. Site 4 is intermediate for both % ALO and measured index properties.

Void ratio and natural water content do not follow this trend. Site 8, with the lowest allophane percentage, has much larger void ratio and natural water content than the other soils. Allophanic constituent percentage by correlation shown in Table 30 shows the same result. Percentages determined by void ratio, or natural water content are not consistent with measured results, or correlated percentages from different index properties. It appears that allophanic constituent percentage has some effect on engineering and index properties for allophanic soils of this form, but the engineering properties depend upon undisturbed structure to a greater extent.

This behavior could be explained if the soils are formed of aggregated weathered vesicular ash grains. For this case, void ratio and natural water content would be dependent on the initial undisturbed vesicular structure. Other disturbed index properties may depend on the amount of amorphous materials present.

Irreversible drying and aggregation upon drying could be explained as before, i.e., the amorphous grains undergo some change in structure upon drying due to large stresses generated in small pores contained within the amorphous matrix. In particular, water would be removed within and between the platelike amorphous

matrix.

Figure 71 represents a possible structure. Scanning electron micrography of Site 8 (Figure 66b) indicate surficial weathering of grain resulting in jumbled, dissected amorphous clusters of platy materials randomly oriented on the grain surface. These amorphous clusters may also be forming within the vesicles of the ash grain. Shrinkage of the amorphous platy clusters will proceed perpendicular to the plane of two dimensional shape.

Strength parameters shown in Table 29 show consistently high effective angles of internal friction. These are thought to result from the granular texture and surface roughness of individual grains like those shown in Figures 59a and 66a.

Table 31 shows engineering properties by correlation with index properties. Based on the preceeding arguments, those engineering properties correlated with void ratio would be suspect. Angle of internal friction by correlation do not agree with results by testing presented in Table 29. The shear strength results correlated from natural water content are much higher than those correlated from void ratio. The optimum moistures by correlation are significantly lower than the measured values from Table 29. Thus it appears that the correlations determined in Chapter V between engineering properties and index properties are not valid for soils which fit into this soil fabric group.

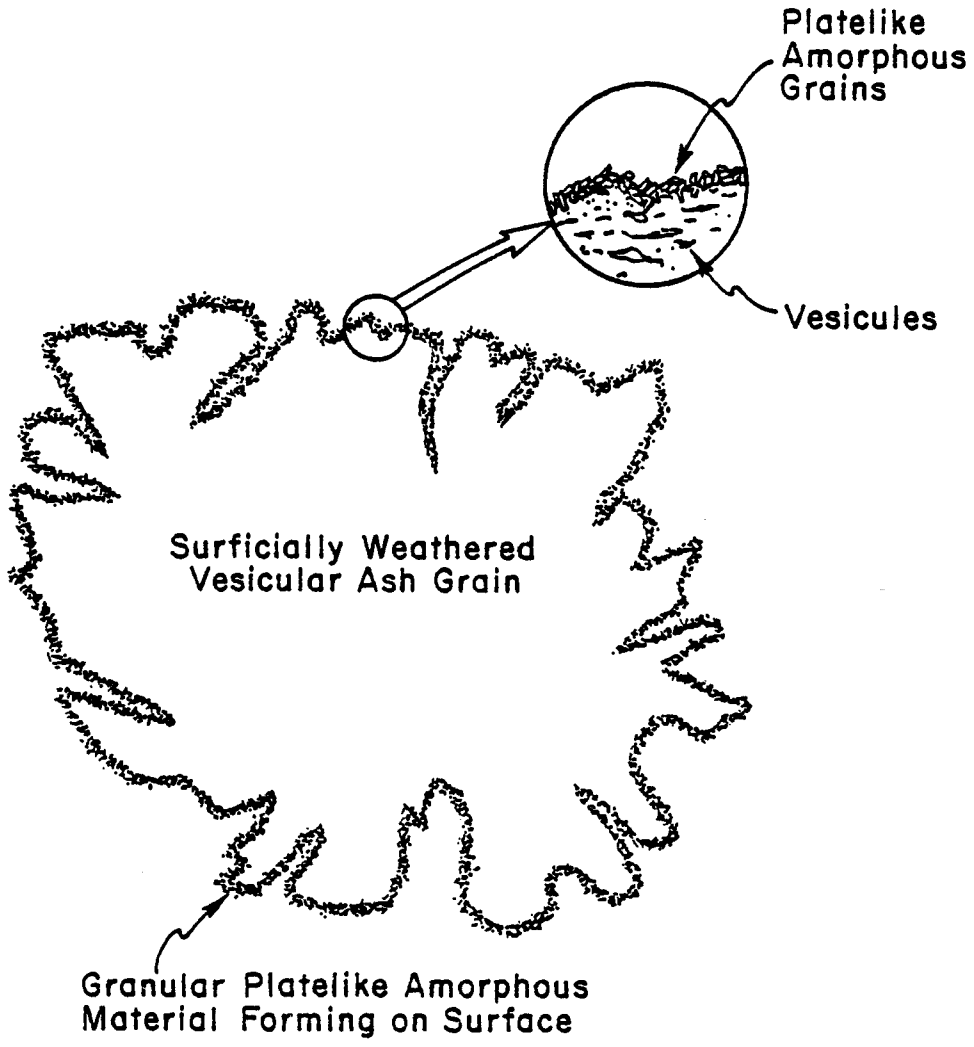

Figure 71. Possible schematic structure for Sites 1b, 4 and 8.

Sites 3, 7, 9 and 10

Dominant microfabric features for these sites include the fluffy indistinct appearance of grains at 2000x, and rough cloudlike edges at 10, 000x. The cloud-like fluffy appearance is an artifact of electron microscopy. When the surface being observed is highly dissected, charge does not drain well from the particle, and bright "hot spots" appear, reducing sharpness of detail, and overall clarity of the micrograph.

Soil macro-grains appear as irregular pumice-like particles. The surface morphology of the grains show an arrangement of poorly formed plate-like amorphous aggregates, the edges of which are highly dissected. The predominent platelike amorphous materials are much like stacked sliced cheese. Plate thickness is about 0. 5 μm.

Particle assemblages consist of aggregated amorphous platy materials connected by interwoven flexible appearing amorphous gels of two dimensional shape. Interaction between assemblages occur through the thin flake-like dissected plate edges at assemblage boundaries.

Pore space is characterized by intra- and inter-assemblage vesicular pores of variable size and shape ranging from 1 μm to

100 μm across. Much small pore space is contained along the angular dissected boundaries of the amorphous plates.

Characterization tests for Site 3 show that they consist primarily of kaolinite, halloysite, allophane, quartz, and various feldspars. Visually these appear as agglomerations of distinct particles with rough surfaces mixed with indistinct cloudy amorphous gel.

Site 7 contains primarily halloysite, illite, amorphous constituents, quartz and feldspars. Transmission electron micrographs show these as poorly formed halloysite tubes surrounded by a dense cloudy matrix of amorphous material.

Site 9 consists of halloysite, disordered kaolinite, feldspar and quartz. These appear as distinct and indistinct particles set in an amorphous matrix.

Characterization tests for Site 10 indicate the strong presence of allophanic constituents, quartz and feldspar which appear as indistinct particles connected by strand-like amorphous materials.

Engineering and index properties shown in Table 29 show remarkable consistency in variation of index properties. Site 10, Site 7, Site 3, and Site 9, in that order, reflect graduated degrees of allophanic character with Site 10 the highest, and Site 9 the lowest. Measurements for natural water content, liquid limit, plastic limit, void ratio, and optimum moisture decrease for Sites 10, 7, 3 and 9

respectively. Optimum density increases, as expected, in the same manner. Measured allophanic constituent percentages in Table 30, follow the same pattern.

The degree of allophanic character appears to be related to the degree of dissection of amorphous plate edges shown in Figures 61b, 65b, 67b, and 68b. Site 10 (Figure 68b) has the greatest amount of edge dissection which corresponds to high allophanic character. Site 9 (Figure 67b) shows the lowest amount of dissection which corresponds to low allophanic character exhibited by the index properties.

Grouped engineering and index properties for oven dried soils in Table 32, and percent change in properties with oven drying also have good agreement with indicated trends in allophanic percentage.

Engineering properties by correlation in Table 31 show very good agreement with angle of internal friction and optimum moisture estimated from index properties, using the correlation equations developed in Chapter V.

This evidence indicates that for allophane soils in this form, engineering and index properties are very dependent on the amounts of allophanic materials present in the soil system.

A general structure description for this soil type includes aggregated plates of amorphous gels with two-dimensional shape.

The entire soil grain is made up of various collections of these aggregations in somewhat random orientation. Other poorly formed minerals are in the process of formation within the amorphous matrix, or have been incorporated into the soil matrix during soil genesis. Figure 65b is an example of the described structure.

It is thought that these grains are heavily weathered ash particles which have experienced substantial internal and surficial weathering. The original materials have been completely transformed to a weathering product.

Shrinkage of the amorphous platy clusters occur perpendicular to the plane of two dimensional order. Due to random orientation of these clusters, volume change is minimal since soil skeleton support is taken along the longitudinal axis of the amorphous clusters.

Strength results presented in Table 29 show an increase in angle of internal friction with decrease in allophanic content. Soils from Site 10 have the highest cohesion intercept of 0.14 kg/cm^2, and also the highest degree of allophanic character. Scanning electron micrographs shown in Figures 61, 65, 67, and 68 indicate increasing angularity or surface roughness with increase in allophane content. The expected result would be an increase in angle of internal friction with increasing allophanic percentage, if particle interactions depend on friction along grain surfaces. The actual result suggests that shear

occurs either through the body of the amorphous platy clusters, or along the dissected particle edges so that the strength parameters depend on shear properties of the amorphous material, rather than interlock and grain surface friction.

Sites 5, 6 and 11

This set of grouped sites is characterized by the transparent appearance of rounded individual grains at 2000x and 10000x, as shown in Figures 63b, 64b and 69b.

Major particles occur as angular, rough surfaced sand size grains made up of smaller, regularly shaped particle assemblages. The micro-fabric is dominated by thick amorphous coatings and aggregates of poorly developed platelike face-to-face structure, with sufficient thickness to obliderate independent elementary particles. The amorphous coatings serve as connector and matrix material.

Pore space is predominantly inter-assemblage pores. The smaller pore spaces are blocked or filled with amorphous materials.

Mineral characterization test show that soils from Site 5 consist of halloysite, illite, allophane, imogolite, feldspar and quartz. These appear as indistinct halloysite tubes with scattered and variable clouds of amorphous materials.

Site 6 contains mostly halloysite, allophane, imogolite, quartz,

and some feldspars which visually show as small aggregated clay size particles connected by strands and films of amorphous materials.

Characterization analysis from Site 11 soils indicate the presence of amorphous allophanic materials, quartz and feldspars, which appear as agglomerations of distinct and indistinct particles under the transmission electron microscope.

Table 30 shows that Site 11 has an amorphous content of about 55%, Site 5 and Site 6 are about even, in the 20% range. Table 29 shows inconsistent variation in index properties for Sites 5 and 6. Natural water contents and void ratios are higher for Site 6 than Site 5, but liquid limit and other index properties are higher for Site 5 than Site 6. Oven dried index properties in Table 32 indicate that Site 5 shows consistently higher allophanic character than Site 6. The percent change in index properties with drying are larger for Site 6 than site 5.

Visual evidence presented in Figures 63a and 64b provides a reason for these observations. Figure 63a (Site 5) appears as an aggregated cluster of weathered constituents. Figure 64a appears to be a moderately weathered intact ash grain. It is then reasonable to assume that the undisturbed index properties, void ratio and natural water content, depend more upon the undisturbed intact structure of the weathered ash grain than on allophanic content. It follows that for

disturbed or aggregated severely weathered materials, amorphorus content may dominate, when predicting engineering behavior.

Materials from Site 5, 6 and 11 appear to consist of mixtures of the other fabric forms previously described. They consist of coated particles assemblages shown in Figure 70, intact weathered ash grains shown in Figure 71, and aggregated amorphous gels of two dimensional shape with highly dissected plate edges shown in Figure 65b.

Shrinkage upon drying occurs perpendicular to the plane of two dimensional shape. The soil skeleton would be supported by the particle assemblages, partially intact ash grains and amorphous aggregates.

Strength results in Table 29 show the highest angle of internal friction for Site 6 materials, and the lowest for Site 5 materials. It appears that if the soil matrix is dominated by intact ash grains, as in Site 6, strength parameters are controlled by grain surface friction and interlock. For Sites 5 and 11, strength parameters depend on the relative mixture of fabric types contained in the soil matrix. Lower angles of internal friction would be expected for aggregated platy amorphous gells, and intermediate for coated particle assemblages. High internal friction angles would be expected for intact, surficially weathered ash grains.

Summary and Discussion of Fabric Structures and Drying Behavior

Soil micro-fabrics from the Oregon and Alaska samples (Sites 1 thru 11) occur in three basic forms. These are:

1. Coated particle assemblages, shown schematically in Figure 70.
2. Surficially weathered intact ash grains, shown schematically in Figure 71.
3. Aggregates of amorphous plate-like gels, shown in Figure 65b.

Drying behaviors of the coated particle assemblages, in Figure 70 require that shrinkage take place in the amorphous coating and fusion of the coatings at grain contact points take place within the soil matrix. This result requires that the amorphous coatings undergo a drastic physical change upon drying. This may be related to the large water holding capacity of amorphous materials. Change is thought to be caused by the presence of very small pores within the amorphous matrix. These pores result in large capillary pressures throughout the amorphous structure. The evidence for two dimensional shape of the amorphous coatings suggest that small pores may occur between platelets, and drying pulls these plates together.

These reactions upon drying are consistent with observations that poorly crystalline volcanic ash soils aggregate upon drying

and that this drying is irreversable. Larger pores, upon drying would have relatively large capillary menisci which pull the grains together increasing pressures at contact points. The stresses at these contact points increase as drying proceeds. Amorphous coating material fuse at the contact points. This fusion process is described by Hirashima (1948) who reported that drying of Hawaiian allophane soils caused them to cement themselves enough to resemble volcanic tuffs.

As drying continues, the small pores in the amorphous matrix begin to exert stresses. These much larger pressures shrink the coating and pull the soil skeleton together. These forces are not enough to significantly change the overall soil volume due to the buttressing effect of the soil skeleton.

The fusion process at grain contact points requires that the amorphous coatings be soft and pliable when the soil has not been dried. This condition is easy to imagine since water in unsaturated systems occurs as films along grain surfaces. Thus, the water occupies the same space around each grain as the amorphous coating. For this reason, water collects in the amorphous coating layer and the layer must have very high water content in relation to other portions of the grain assemblage.

Shrinkage of the amorphous layer perpendicular to the coated grain boundary requires that the two dimensional order of the amorphous coating be oriented parallel to the grain boundary. The amorphous coating may arrange itself in this manner as a consequence of the water film which tends to flow along grain boundaries in unsaturated well-drained systems. The coating could be deposited along the grain surface as a result of leachate from ash overburden moving down through the soil profile.

The mechanism and structure shown in Figure 70 explains several engineering behaviors unique to poorly crystalline soils derived from volcanic ash. These are:

1. Large increase in permeability upon drying reported by Maeda, et al. (1977). This is due to closing of small pores and opening of large pores as the amorphous coating dries and shrinks.
2. Aggregation of grains with drying reported by Wesley (1973), Martini and Palencia (1975), and many others.
3. Lack of large volume changes upon drying.
4. Continuous irreversable changes with drying with the amount of change depends upon the amount of water removed from the structure.

Drying behaviors of surficially weathered ash grains, shown in Figure 71, would proceed in much the same manner as for amorphous materials within the grain matrix. The residual open structure of the ash grain would be subject to collapse. Therefore, larger changes in undisturbed engineering properties, such as strength, would be expected with drying.

Drying of the plate-like amorphous aggregates shown in Figure 65b is controlled by the presence of small pores between the platelets, and pores along the highly dissected amorphous aggregate edges exposed to surface drying and wetting action. Much like the coated materials, large pore menisci form between the macro-aggregates which, upon drying, pull the structure together, fusing the soft amorphous materials at points of contact. As drying proceeds, capillary pressures in the small pores of the amorphous matrix pull the amorphous plates together. Upon further drying, hydrogen bonding between the plates is lost, and much stronger primary bonds between the amorphous plates replace the weaker hydrogen bonds. This mechanism could explain irreversible drying. Water, if reintroduced into the system has no method of forcing the bonded amorphous plates apart, and therefore, does not re-enter the soil system.

Irreversable drying depends on particle movement resulting from

pore water tensions developed from capillary menisci. For soil fabric, smaller pores create larger capillary stresses (Mitchell, 1976). For materials with high crystal order, clay plates or grains move together upon drying, but severe structural change does not take place because the soil crystals are competent. For soils with poorly crystalline amorphous materials, an even distribution of small voids is present throughout the amorphous matrix. These small pores develop large capillary stresses capable of severely deforming the matrix of strands, gels, randomly connected particles, and amorphous plates. Rupture or plastic flow deformations of the structure can never be regained.

Summary and Discussion of Fabric Structures and Engineering Behavior

It has been shown that engineering behaviors of poorly crystalline soils derived from volcanic ash are controlled by allophanic constituent percentage, soil fabric, and drying history.

Soil fabric dominates engineering behaviors in immature soils where parent material behavior is more prominent than weathering product behavior. Allophanic constituent percentage dominates where amorphous weathering products are more prevalent than relic ash-grain structures.

Drying history can negate the effects of residual ash grain structure and amorphous constituent percentage simply because drying

breaks down the relic structure (except in very young unweathered ash) and severely alters amorphous materials.

The major difference in engineering behavior between crystalline soils, and poorly crystalline volcanic ash soils, is the presence of saturated amorphous materials with unusually porous structures. Previous discussion has shown that amorphous materials within the soil matrix may be saturated while the soil, in total, may be only partially saturated. These amorphous materials whether they occur as outside coatings, weathering constituents in ash grain vesicules, or amorphous aggregates, are subject to large changes in structure when dried.

Atterberg Limits

Visual evidence from electron microscope studies indicates that allophane soils act like clay size aggregates with surface charge dependent upon the pH of porewater solutions.

Warkentin (1972) reports that liquid limit (LL) is related to the surface area to volume ratio (SA/V), and not amorphous clay content for allophane. Surface areas are dependent on fabric type and a high SA/V would be expected for amorphous aggregates with dissected edges, lower for intact ash grains, and lowest for coated materials. Table 29 shows that, in general, liquid limits follow this trend.

Atterberg limits for allophane soils plot in the low portion of the MH range (USCS classification), due to small difference between liquid

limits and plastic limits. Low plasticity with high liquid limits result from high SA/V ratios, and the inability of amorphous aggregates to adsorb water into their grain structures. For crystalline soils, as the SA/V ratio increases so does ability to adsorb water into interstitial clay layers. Thus for crystalline soils, and amorphous aggregates with comparable SA/V ratios, more water is needed to reach the liquid limit than for amorphous aggregates with high SA/V ratios. This difference decreases as SA/V ratios decrease.

Warkentin (1972) and others state that liquid limit measurements on dried soils do not indicate properties in the natural state. Observation of drying changes of Atterberg limits, when plotted on the plasticity chart, indicate that liquid limit decreases more than plastic limit. This is probably due to collapse of the diffuse double layer upon drying.

Drying has several irreversible effects on soil grains which are reflected in Atterberg limit changes. These are:

1. Removal of internal water between amorphous plates of two dimensional shape, resulting in replacement of hydrogen bonds with stronger bonds.
2. Collapse of the diffuse double layer. The layer will not regain original configuration due to changes in ion concentration.
3. Reduction of SA/V ratio due to aggregation of soil grains.

If these soils are dried for the purpose of Atterberg limits

tests, drastic irreversible changes in structure and grain surface behavior take place such that the resulting Atterberg limits may have no relationship to insitu soil behavior.

Moisture-Density

It has been shown by many investigators (See Chapter II) that large errors may be introduced into moisture-density test results if poorly crystalline volcanic ash soils are dried before performing compaction tests.

Barden and Sides (1970) show by electron microscope examination of compacted soils that at low compaction moisture contents, low dry densities are caused by the presence of large air filled macropores. As compaction moisture increases, macropores are reduced in size, and the dry density rises until most of air pores become filled with soil. Further increase in compaction moisture content causes the dry density to fall as pore water layers increase in thickness.

For soils which exhibit large irreversible changes with drying, soil structure changes such that air filled macropores decrease in size. Therefore starting dry densities are higher and optimum water contents lower for samples dried prior to testing.

Matyas (1969) reported that maximum dry density increased approximately 2 pcf and optimum water content did not change when soil was re-used during compaction testing. The increase in optimum density was attributed to a breakdown in clay aggregations during re-compaction.

Test conditions for these soils must approximate field conditions. Terzaghi and Peck (1967) state that for soils with high natural contents which show irreversible drying, no amount of compactive effort can be applied to reach 90 to 95% of air dried standard proctor optimum density. They suggest that the fill should be designed based on strengths that can be achieved by compacting wet soils.

Undisturbed Index Properties

Poorly crystalline soils derived from volcanic ash are usually described as residual soils. Residual soils, by definition, take on the structure and some properties of their parent materials. For this reason undisturbed structure and fabric of residual soils may be the single most important soil property describing engineering behavior.

Residual soils have never been remolded, therefore, void ratio, and to some extent, natural water content, may be used to predict structure, where other index properties may not. As reported in Chapter V, void ratio is by far the most effective index property for correlation with undisturbed engineering behaviors. Natural water contents are not as effective because they are subject to variations not controlled by soil structure.

Void ratio and natural water content can be related to soil fabric. Expected results are that void ratios and natural water contents be highest for amorphous aggregates with dissected edges. Void ratios and natural water contents should be intermediate but still

high for intact ash grains, and lowest for coated particle assemblages. These observations are supported by results reported in Table 29. Soil fabrics dominated by amorphous aggregates have average void ratios and natural water contents of 2.47 and 83.0% respectively. Those soils consisting predominantly of intact ash grains average 1.96 and 48.5%. Fabrics consisting of coated particles have average void ratios and natural water contents of 1.70 and 44.9% respectively.

Strength

Table 34 compares allophanic constituent percentage, fabric type, and smallest pore space type with several strength behaviors. These are; peaking behavior of the deviator stress versus strain curves, degree of overconsolidation determined from the A pore pressure parameters, and the effective angles of internal friction.

The degree of overconsolidation for each site was determined from the A pore pressure parameters for small strains, and at failure. A pore pressure parameters calculated from strength test data were compared with average values for A given by Lambe and Whitman (1969). Lambe and Whitman (1969) assign a degree of consolidation description to average values for A for small strains, and failure conditions.

Table 34. Fabric and strength behavior.

	Measured Allophanic Percentage (% ALO)	Dominant fabric type	Smallest pore space	Peaking of deviator stress vs. strain curve	Degree of overconsolidation (from A-pore pressure parameter)	Internal Friction ϕ' (degrees)
Site 1a	15-25	Coated	Inter-assemblage[a]	Distinct	Heavily overconsolidated	56.1
Site 2	30-40	Coated	Inter-assemblage	---	---	---
Site 1b	25-35	Ash grain	Intra-assemblage[b]	Distinct	Heavily overconsolidated	56.1
Site 4	15-25	Ash grain	Intra-assemblage	Distinct	Lightly overconsolidated	46.9
Site 8	10-20	Ash grain	Inter-assemblage	Indistinct	Heavily overconsolidated	50.3
Site 3	25-35	Amorphous aggregate	Intra-assemblage	Distinct	Heavily overconsolidated	42.1
Site 7	20-30	Amorphous aggregate	Inter-assemblage	Distinct	Lightly overconsolidated	38.1
Site 9	15-25	Amorphous aggregate	Intra-assemblage	Distinct	Lightly overconsolidated	43.3
Site 10	40-50	Amorphous aggregate	Intra-assemblage	Distinct	Normally consolidated	20.1
Site 5	20-30	Coated-mix	Inter-assemblage	Indistinct	Normally consolidated	32.1
Site 6	20-30	Ash grain-mix	Intra-assemblage	Indistinct	Normally consolidated	46.7
Site 11	50-60	Amorphous aggregate-mix	Intra-assemblage	Indistinct	Normally consolidated	43.2

[a] Inter-assemblage -- larger pores between particle assemblages. [b] Intra-assemblage -- smaller pores within particle assemblages.

c A pore pressure parameter at failure, $\sigma_3 = 10$ psi.

A_{σ}-pore pressure parameters for small strains, and A at failure for undrained triaxial tests performed on samples from Sites 1 to 11 indicate that Sites 5, 6, 10 and 11 are normally consolidated. Sites 4, 7 and 9 are lightly overconsolidated, and Sites 1, 3 and 8 are heavily overconsolidated.

There exists no geologic evidence that overburdened pressures have been exerted at those sites which exhibit overconsolidated behavior. Hill, et al. (1975), and others report the same phenomenon for allophane soils from Japan, New Zealand, and other areas of weathered volcanic ash deposits. Wallace (1973) suggests that this apparent overconsolidated behavior may be due to cemented bonds between particles. Consolidation due to drying capillary pressures may also explain this behavior.

Table 34 suggests that apparent overconsolidation pressures may be related to fabric type. Those soils in the coated and ash grain groups appear to be heavily overconsolidated, possibly due to a combination of previous drying and cementation. The soils in the amorphous aggregate group appear to be lightly overconsolidated, probably resulting from light cementation between grains. Those in the mixed group are normally consolidated, and have not undergone drying, but may have been slightly disturbed during the course of soil formation. The presence of mixed soil fabric types suggests that some sort of

mixing action may have occurred at these sites due to creep, tree throw, organic activity, etc.

Since none of the deviator stress versus strain curves for Sites 1 to 11 exhibit peaking behavior, curve shapes are described as distinct or indistinct. Distinct implies that an easily definable failure point is apparent. Indistinct means that the curves were rounded and a definitive failure point was difficult to find. All deviator stress versus strain curves for each site are contained in Appendix D.

Due to the effective stress principle, undrained strength increases with decreasing water content for any given confining stress (Mitchell, 1976). For samples from Sites 1 to 11, possible peaking of deviator stress versus strain curves due to water tensile cohesive forces, was eliminated during backpressure saturation. Thus, only cementation, friction behavior and pore pressure response are reflected in undrained stress-strain behavior.

Strength data for the Oregon and Alaska samples indicate that cementing is not strong, as evidenced by the conspicuous absence of peaks in deviator stress vs. strain curves. Scanning electron microscope analysis shows that amorphous materials control interactions at grain contact points but stress-strain behavior indicates non-cementing materials. This suggests that the allophanic connecting materials between grains must be relatively soft in the natural state.

Barden (1972) reports that for residual halloysite soils drying causes the particles to aggregate into silt clusters imparting high shear strengths and the characteristics of granular soils. Barden (1972) also states that clays often resemble granular materials, and aggregated clusters of clay often resemble sand grains. Therefore there is no essential difference in mechanical behaviors, especially at low stresses where grain crushing is not a factor.

Drying and aggregation behavior could explain the large range of shear strength values, and angles of internal friction reported in the literature (See Appendix A). Depending on fabric type, drying history, and allophanic constituent percentage, allophane soils in some cases may behave as granular particles, and in others, behave as clays.

Appendix D shows deviator stress vs. strain curves for Sites 1 to 11. Two types of curve shapes are noted in Table 34. Those with distinct slope breaks are described by Paulos (1971) as typical constant volume stress-strain curves for dilative soils composed mostly of platey grains. He describes the distinct slope break as the point at which a loss in strength occurs when particles in the failure zone become distinctly oriented. Those curves with indistinct slope shapes correspond to contractive soils consisting mostly of platey grains. No peak or distinct slope break point is noted because the

effect of grain orientation at large strains is small. Void ratios are high enough that the grains are not very close together.

Analysis of Table 34 shows no apparent relationships between stress-strain curve shape, degree of consolidation, and effective angle of internal friction except that the normally consolidated soils appear to generate stress-strain curves with indistinct peaks, and the heavily overconsolidated soils appear to correspond to the highest effective angles of internal friction.

VII. RECOMMENDATIONS FOR ENGINEERING IDENTIFICATION OF ALLOPHANE SOILS

The purpose of this chapter is to formulate a guide with which geotechnical engineers can recognize and identify soil deposits which might have the special properties of allophane soils. Allophane soil identification is simple, and requires very little extra effort beyond testing normally performed during routine site exploration. These simple procedures may, however, save much time if allophanic character is recognized immediately, and further testing programs are designed accordingly.

Identification of allophane soils proceeds in several steps, as follows:

Step 1 Geologic and climactic associations--The presence of volcanic ash parent materials under conditions of moderate to high rainfall must be established in the area of interest.

Step 2 At-site evaluation--For a particular soil deposit, allophanic character would be suspected if a non-sticky, ash-like soil, were present on a well-drained site.

Step 3 Routine laboratory testing--Strong allophanic character is suspected if soils tend to aggregate upon drying, have natural water contents of 40% or greater, and Atterberg

limits falling in the MH range of the soil plasticity chart. Further testing should be conducted if these indicators are positive.

Step 4 Specific laboratory tests for allophanic character--Conduct Atterberg limit tests to determine changes with drying. Also check pH reactions when saturated with NaF. These tests, in combination give good indications of presence and amount of allophanic materials.

Step 5 Further identification--If steps 1 to 4 strongly indicate the presence of allophanic character, and further identification is desired, the detection techniques described in Chapter IV provide morepositive identification.

For geologic associations described in Step 1, volcanic ash soils occur in several well-defined areas of the world. Their occurrence in the United States is limited to the Pacific Northwest, Alaska, and Hawaii (See Map, Figure 2). The occurrence of poorly crystalline soils derived from volcanic ash is synonymous with geologically recent volcanic activity, and although ash may be carried great distances by air, present knowledge suggests that significant amounts required to form allophane soils may only occur in areas close to the source. Refer to the background section in Chapter II for more detailed information on geologic occurrence and formation.

For Step 2, the probable presence of ash-derived soil should be established at the particular site of interest. All soil deposits in areas of volcanic activity are not necessarily derived from volcanic ash. The site should be elevated and well drained. Allophane soils when rubbed between the fingers should have a greasy, slick feel, with attendant release of water when disturbed. If the soil is sticky and highly plastic, the deposit most likely does not contain significant amounts of allophanic constituents. Again refer to the background section in Chapter II for more detailed descriptions of allophane soil occurrence and behavior.

For routine laboratory testing outlined in Step 3, allophane soils may have high water contents, but not necessarily extremely high. If the natural water content is 40% or greater, and other observations indicate allophane soils, check Atterberg limit results.

Atterberg limits for allophane soils plot in the MH range of the soil plasticity chart, usually far below the A-line. For this step, special considerations regarding the drying of soils before Atterberg limits testing are not a concern. Dried or undried, the results will plot in the MH range if significant allophane is present. The one point method of liquid limit determination, however, is not recommended if the presence of allophane soil is suspected (Maeda, et al., 1977).

For Step 4, conduct natural, air dry, and oven dry Atterberg

limits tests on succesively dried soil samples. The detailed test procedures outlined in Appendix C should be followed. Allophanic constituent percentage may be approximated from position on the plasticity chart using the percent allophane curve shown in Figure 19b.

The NaF saturation method introduced in Step 4, was adopted from laboratory procedures outlined by Fieldes and Perrott (1966). This method requires that a small portion of soil be placed on phenolphthalein paper and treated with saturated NaF solution. The color reaction of the paper indicates the amount of allophanic activity exhibited by the soil. This procedure is described in Appendix E. A positive reaction provides good proof that allophanic materials are present. A negative reaction does not necessarily indicate that allophane soils are not present. Allophanic constituents may be chemically locked into the soil structure, unable to react with NaF.

For further identification (Step 5), infrared spectroscopy, X-ray diffraction, and electron microscope techniques have been documented and are available for sophisticated characterization of allophanic materials. Test procedures for each of these laboratory detection methods are presented in Chapter IV, and outlined in detail, in Appendix E.

VIII. SUMMARY AND CONCLUSIONS

Allophane soils have unique engineering properties which depend, to varying degrees, on the amount of drying they have experienced. These soils consist of constituents which frequently are the weathering products of geologically young volcanic ash deposits, and thus, most often occur in areas of recent volcanic activity.

General Engineering Properties

The background section in Chapter II provides a synopsis of literature review results gathered from a variety of reports describing poorly crystalline volcanic ash soils from many parts of the world. Geotechnical data from this review are presented in Appendix A.

Figures 12 thru 19 summarize the results of the data presented in Appendix A. In general, the following observations were made.

1. Natural water contents range from 8 to 313%.
2. Most Atterberg limits data plot well below the A-line in the MH (Unified Soil Classification System) range of the Casagrande plasticity chart.
3. Liquid limits range from 23 to 350% for natural conditions, 26 to 125% for air dry, and 40 to 111% for oven dry conditions.

4. Soil Atterberg limits and natural water contents seem to arrange themselves along contours on the plasticity chart as shown in Figures 13, 14 and 15.

5. Soils with relatively low natural water contents plot closer to the A-line than those with high natural water contents.

The presence and amounts of allophanic materials may be inferred from positions of Atterberg limits on the plasticity chart. This approach was first suggestedfor air dry soils by Warkentin (1972). Analysis of soil data presented in Appendix A indicates this may be true for most allophane soils (wet or dry). Figures 19a and 19b show that allophanic percentage corresponds to combinations of angles on the plasticity chart measured from horizontal, and distance from the A-line.

Disturbed and undisturbed soil specimens from ten sites in Oregon and two sites in Alaska were studied. Engineering classification and strength tests were run on samples from each site. Tables 9, 10, 11, 12 and 13 summarize these data. The following general results were observed from this testing:

1. The Oregon sites (Sites 1 to 9) have much lower natural water content and Atterberg limit values than those from Alaska (Sites 10 and 11). Natural moisture contents average 40 to 50% and 150% for the Oregon and Alaska samples, respectively.

2. Grain size analyses indicate that samples from Sites 10 and 11 show a marked decrease in plus #40 sieve material, and a marked increase in plus 200 material upon drying. The minus #200 sieve fraction decreased for Site 10 and increased for Site 11.

3. Moisture-density maximum dry unit weights ($\gamma_{d\ max}$) range from 42 to 92 lb/ft^3. Optimum water content (w_{opt}) range from 28 to 73%. $\gamma_{d\ max}$ increases with drying and w_{opt} decreases with drying.

4. Specific gravity varies among sites ranging from 2.65 to 2.88.

5. Insitu dry densities ranged from 0.43 to 1.44 g/cm^3.

6. Degrees of saturation for strength samples range from 54 to 100% with the average at about 80%.

7. Strength parameters summarized in Table 12 show that angles of internal friction range from 18.7 to 56.1 degrees. Apparent cohesion intercept values are small, and sometimes negative.

8. For poorly crystalline volcanic ash soils, the effective stress-path method of defining Mohr effective stress failure envelopes was found to be superior to other conventional methods of strength interpretation.

These observations indicate that large variability exists in index and engineering properties of these soils.

Soil Mineralogy and Structure

Chapter IV describes the mineralogical and structural properties of poorly crystalline volcanic ash soils reported in the literature review, and tested in the laboratory. Appendix A presents a mineralogical description for each soil reported in the literature review.

Table 14 summarizes these data by geographic area. Generally the soils are described as fine to clay-like coarse soils with sandy appearance. They are variously described as red or yellow-brown thixotropic soils which contain allophane and other amorphous constituents. Associated minerals are halloysites at various stages of hydration, some kaolinite with gibbsite, vermiculite, and iron oxides sometimes present.

Determinative tests for soil minerology, structure, and particle shape were conducted on the samples from Oregon and Alaska. Results of these tests are presented in Table 15 for infrared spectroscopy, and Table 17 for X-ray diffraction. Figures 25 thru 39 show transmission electron microscope results.

Results of infrared spectroscopy indicate that halloysite in various forms, large amounts of varying amorphous materials, and quartz are predominant constituents of the Oregon and Alaska samples. X-ray diffraction suggests that feldspars may also be major constituents.

Electron micrographs of the Oregon and Alaska soils suggest that halloysite, allophane, and imogolite are forming simultaneously in clouds of amorphous materials. The presence of significant amounts of poorly formed, indistinct soil grains, along with large amounts of cloudy amorphous gels supports the observation that the soils have undergone little soil development, and indicate that the soils are in the early stages of formation.

Statistical Analyses

Statistical analysis on natural water content and Atterberg limits data from the laboratory and literature study suggest that these quantities are each from more than one group. Table 35 summarizes the average values for each of the grouped Atterberg limit and natural water content data.

Table 35. Average values for natural water content and Atterberg limit observations.

	Low Group (w_n < 60%)	High Group (w_n > 60%)	Very High Group (w_n > 180%)
Mean Natural Water Content (w_n in %)	38	111	200
Mean Liquid Limit (LL in %)	63	115	180
Mean Plastic Index (PI in %)	14	33	64

Effective angle of internal friction can be statistically separated by the low and high natural water content groups. Low natural water contents ($w_n < 60\%$) correspond to effective angles of internal friction averaging 37.7 degrees. Natural water contents greater than 60% correspond to effective angles of internal friction averaging 18.2 degrees. Effective cohesion intercept shows no relationship to the water content groups.

The groups can be distinguished by specific physical characteristics such as color, mineral content, drying history, and silt and sand percentage.

Allophane Constituent Percentage

Allophanic component percentage estimates for Oregon and Alaska samples are summarized in Table 23. These estimates are based on various methods of analysis for soil mineralogy introduced and discussed in Chapter IV. Examination of the allophanic percentages in Table 23, show that assignment of an absolute percentage to a specific soil sample is practically meaningless. A more logical extension of these detection methods is to assign percentage ranges and rankings based on relative comparisons among soils of interest. Rankings of Oregon and Alaska samples, Table 24, show that very general

agreement exists between allophane percentage and trends describing index and engineering behavior. Liquid limit and moisture-density optimum values have the best agreement. Effective angle of internal friction, specific gravity, and percent fines do not show good agreement.

Regression analysis equations between allophanic percentage and index properties reported in the literature, are summarized in Table 25. The equations are divided into low, high and total (low plus high) natural water content groupings described previously. For the low and high natural water content groups, low correlation coefficients are evident. The total sample group gives reasonably high correlation coefficients.

For the total sample group, plastic limit, void ratio, maximum dry density, and optimum water content provide the best relationships between allophane percentage and index properties. Specific gravity, percent fines, insitu dry density, and percent change in Atterberg limits with drying give poor relationships.

Allophanic material percentage (% ALO) can, with reasonable reliability, be related to the indicated index properties by the equations:

$$\% \text{ ALO} = 0.35 (w_n + 1.60) \qquad (w_n < 60\%)$$

$$\% \text{ ALO} = 0.45 (\text{PL} - 1.69)$$

$$\% \text{ ALO} = 16.2 (e_o - 0.86)$$

$$\% \text{ ALO} = -0.95 (\gamma_{d\ max} - 101.5)$$

$$\% \text{ ALO} = 0.93 (w_{opt} - 18.4)$$

$$\% \text{ ALO} = 107.4 (G_s - 2.05) \qquad (w_n > 60\%)$$

Engineering Correlations

Development of engineering correlations for poorly crystalline soils derived from volcanic ash was accomplished by mathematically comparing relationships between index and engineering properties reported in the literature and laboratory studies. All mathematical relationships (equations) were determined by regression analysis using the least squares method. The relationships investigated were limited to those for which sufficient data were available from Appendix A and the laboratory study.

Table 28 summarizes the results of these correlation attempts by indicating correlation equations, quality of correlation, and comparison of crystalline soil behavior to poorly crystalline volcanic ash soil behavior. From Table 28, values of plastic index, void ratio, and natural water content from the high water content group show poor correlation with the strength parameters. Void ratio (e_o) and natural water content (w_n) show reasonably good correlation with c and ϕ'.

Void ratio seems to produce very good visual and mathematical relationships with ϕ', c and Cc. Correlations of optimum water content versus plastic limit are good to excellent for the low, high, and total natural water content groups.

Further analysis of Table 28 indicates the following for poorly crystalline soils derived from volcanic ash:

1. There is a poor to non-existant relationship between effective angle of internal friction and plastic index. For this reason plastic index should not be used to predict effective angle of internal friction.
2. Void ratio can effectively be used to predict effective angle of internal friction if the equation for total sample is used. There are no restrictions on the use of this relationship if used for poorly crystalline volcanic materials.
3. Natural water content can be used to predict undrained shear strength if the equation for total sample is used. No restrictions apply if poorly crystalline soils derived from volcanic ash are being analyzed.
4. Void ratio can also be used to predict undrained shear strength. The equation for total sample provides a good approximation. Regression coefficients suggest that void ratio is slightly better than natural water content for predicting undrained shear strength.

5. Liquid limit should not be used to predict compression index for these soils.
6. Void ratio provides an excellent measure of compression index for poorly crystalline volcanic ash soils of natural water contents greater than 60%.
7. Natural water content can also predict compression index for these soils but void ratio is the superior predictor property.
8. Plastic limit provides an excellent approximation of optimum water content for total sample. This relationship applys only to poorly crystalline volcanic ash soils.

These observations indicate that values for effective angle of internal friction, undrained strength, and compression index can best be estimated if void ratio is used as the predictor property.

Correlations between index properties and engineering properties for poorly crystalline soils derived from volcanic ash produce relationships which do not compare well with the same relationships for crystalline soils. Often they are in the same area and show the same general trends, but significant differences are apparent.

Data values used for correlation were determined by many different individuals, using different test methods, test apparatus, sampling methods and sampling apparatus. Much observed variation is most likely due to these sampling and testing differences.

Despite these uncertainties, correlation properties of poorly crystalline soils derived from volcanic ash show reasonable agreement, if undisturbed index properties are used to describe undisturbed engineering behavior.

Fabric

Soil fabric as it applies to engineering behavior was studied for Oregon and Alaska samples. The studies were conducted using standard scanning electron microscope techniques on undisturbed materials, and transmission electron microscopy on slurried samples.

Transmission electron microscope results presented in Chapter IV indicate that the soils are dominated by the presence of various amorphous masses of materials. Well formed, to poorly formed and indistinct particles appear to be surrounded by the amorphous matrix.

Scanning electron microscope results also indicate the presence of abundant amorphous materials. The soil grains appear as particle assemblages. Small pores for the Oregon samples are blocked or filled with amorphous materials, but abundant large pores are evident. For the Alaska samples, smaller and more abundant pores are evident.

The Oregon and Alaska samples were grouped based on

similarities of fabric. These groupings are as follows:

Sites 1a and 2 -- Similar in that they both exhibit a thick amorphous coating. At 10, 000x, individual coated grains appear relatively smooth.

Sites 1b, 4 and 8 -- Similar in granular brittle appearance at 2000x.

Sites 3, 7, 9 and 10 -- Similar in fluffy indistinct appearance of grains at 2000x, and rough cloudlike edges at 10, 000x.

Sites 5, 6 and 11 -- Similar in that rounded individual grains have transparent appearance at 2000x and 10, 000x. Much of the amorphous material appears in bulk rather than coating form.

Tables 29 to 33, present data comparisons for each fabric grouping. From these comparisons, schematic fabric representations were developed to represent each fabric group.

For Sites 1a and 2, Figure 70 shows these soils to be primarily particle assemblages coated with amorphous materials. Analysis of mineralogical and engineering data indicate the following for this type fabric structure:

1. Percent allophane has a small affect on engineering properties when the amorphous materials in the soil matrix occur as coatings.

2. Upon drying, the grains appear to coalesce and pores close or are blocked with amorphous materials.

Figure 71 shows a schematic representation of soil fabric from Sites 1b, 4 and 8. These soils have undergone intense surficial weathering, and moderate internal weathering so that individual particles appear as nearly intact ash grains. Analysis of electron micrographs, and engineering behavior show:

1. Allophane constituent percentage has some effect on engineering and index properties, but the engineering behavior depends more on undisturbed structure.
2. Strength parameters in Table 29 show consistently high effective angles of internal friction, thought to result from the granular texture and surface roughness of individual grains.
3. Due to the large dependence of engineering properties on intact ash grain structure, the correlations developed in Chapter V are not valid for soils which fit into this fabric group.

Figure 65b shows the dominant fabric features for the fabric type exhibited by Sites 3, 7, 9 and 10. Surface morphology appears as an arrangement of poorly formed amorphous aggregates composed of face-to-face plate-like allophanic constituents of two-dimensional shape. The plates have highly dissected edges and appear much like stacked sliced cheese.

Variation in index and engineering properties is reflected in a similar variation in amorphous content. The degree of allophanic character is also related to degree of dissection of amorphous plate edges. Thus, for this fabric form, engineering and index properties are very dependent on the amount of allophanic materials present.

For Sites 5, 6 and 11, soils appear as mixtures of the fabric forms previously described and shown in Figures 65b, 70 and 71. Analysis indicates that engineering behavior is dictated by the dominant soil fabric features exhibited for each particular soil.

Lower angles of internal friction would be expected for soils dominated by amorphous aggregates, intermediate for coated particles, and high internal friction angles for soil fabric mixtures dominated by intact ash grains.

In general, engineering behavior of poorly crystalline soils derived from volcanic ash is controlled by soil fabric type, drying history, and allophanic percentage. Soil fabric dominates engineering behavior in immature soils where parent material behavior is more prominent than weathering product behavior. Allophanic percentage dominates where amorphous weathering products are more prevalent than relic ash grain structures. Drying history can dominate both effects due to severe alteration of materials upon drying.

The major difference in engineering behavior between crystalline soils and poorly crystalline soils derived from volcanic ash is the presence of saturated amorphous materials within the soil matrix. These materials have been shown to have an unusual distribution of small pores within their structure, that are very sensitive to handling and drying.

Drying

Drying behavior of amorphous materials in any fabric form seems to be controlled by the presence of well-distributed small pores within the amorphous gel matrix. It has been postulated that these amorphous materials in their natural state are relatively soft and pliable and upon drying they harden, coalesce, and become brittle. Further large pore macro-aggregates, when dried, pull the structure together, fusing the soft amorphous materials at points of contact. As drying proceeds, capillary pressures in the small pores of the amorphous matrix pull the amorphous plates together. Upon further drying, hydrogen bonding between the plates is lost, and much stronger bonds between the amorphous plates replace the weaker hydrogen bonds. This process is illustrated in Figure 70.

Wells and Furkert (1972) have shown that water in undisturbed allophane is held in hydrogen bonded clusters. Drying removes

these clusters, and the amorphous plates move together. This mechanism could explain irreversible drying. Water, if reintroduced into the system has no method of forcing the bonded amorphous plates apart, and therefore, does not re-enter the soil system.

Irreversible drying depends on particle movement resulting from pore water tensions developed from capillary stresses (Mitchell, 1976). For materials with high crystal order, clay plates or grains move together upon drying, but severe structural change does not take place because the soil crystals are competent. For soils with poorly crystalline amorphous materials, an even distribution of small voids is present throughout the amorphous matrix. These small pores lead to the development of large capillary stresses capable of severely deforming the matrix of strands, gels, randomly connected particles, and amorphous plates. Rupture or plastic flow deformations of the structure can never be regained.

Observations and analysis of poorly crystalline volcanic ash soil behavior indicate that properties which may deviate from crystalline soil behavior can be explained using basic accepted soil mechanics principles. Deviant behavior is caused by unusual structural and mineralogical combinations, being acted upon by forces inherent in air-water-soil environments.

Recommendations for Further Research

All information gathered during the investigation is presented in the text or appendices for the convenience of any person willing to further expand the analysis presented in this thesis.

Additional information is needed to develop engineering correlations more fully. Correlation results from the literature review study are scattered due to sampling, testing, and reporting variables. Relationships between engineering and index properties might be further refined if uniformly sampled specimens from Hawaii, Alaska, the Pacific Northwest, Japan, New Zealand, and Indonesia were tested in a systematic manner using uniform test procedures and apparatus. This approach would provide reliable test results from a wide variety of samples. Statistical relationships and variabilities may be determined from the results. With this uniform testing program, general design recommendations for these soils may be attempted. This may involve the development of a separate classification system for volcanic ash soils based on their response to drying.

Slope stability problems which appear to be associated with the occurrence of poorly crystalline materials, should also be further investigated. The question to be addressed here is; Do amorphous minerals form in sites prone to landslide activity, or do the presence of amorphous minerals contribute to slope instability?

Strength and other engineering behaviors partially depend on interaction at points of contact between grains. Since the grains are coated, or are entirely made up of amorphous materials, selective investigations of amorphous materials which control behavior at points of contact would be instructive. Strength determination, and determinations of specific changes with drying of artificially prepared or extracted amorphous materials may give clues to how these materials behave under loading or drying stresses.

Changes in fabric with various degrees of drying could be investigated using electron microscopy. This type of investigation would involve sophisticated photographic techniques for quantitative determination of pore and grain changes. Investigation of changes in pore size distribution with drying may also yield useful results.

Further investigation of amorphous material morphology is needed. Soil science investigators have concentrated on the micromorphology of individual expressions of mineralogy, such as small tubes and spheres. The relationship between these small structures, and macrofabric coatings and amorphous aggregations is not obvious. Clay mineralogists could further the understanding of engineering behavior if they would expand investigations to include macrofabric studies. In particular, the assemblage relationships among amorphous spheres, imogolite tubes, amorphous gels, and other constituents would be of interest.

Further investigation of the fabric types described in Chapter VI could also help explain engineering behavior and possibly the extreme heterogeniety exhibited by most allophane soils. Investigations of possible associations between fabric types, and how they might grade from one to another in the weathering sequence would be of importance in describing engineering behavior based on soil fabric.

REFERENCES

Andrews, C. B., 1936. "The Relation Between Chemical Composition and Physical Characteristics of Some Hawaiian Soils," Proceedings, First International Conference on Soil Mechanics and Foundation Engineering, Vol. 1, p. 30.

Barden, L., 1972. "The Relation of Soil Structure to the Engineering Geology of Clay Soil," Quaternary Journal of Engineering Geology, Vol. 5, pp. 85-102.

Barden, L., Sides, G. R., 1970. "Engineering Behavior and Structure of Compacted Clay," Journal of the Geotechnical Engineering Division, American Society of Civil Engineers, Vol. 96, SM4, pp. 1171-1200.

Barrett, E. V., 1948. "Stabilization with Cutback Asphalt of 42 Kilometers of the Natural Surface Soil of the Perija Highway in Venezuala," Proceedings, Second International Conference on Soil Mechanics and Foundation Engineering, held in Rotterdam, Netherlands, Vol. 5, pp. 251-256.

Birrell, K. S., 1952. "Some Physical Properties of New Zealand Volcanic Ash Soils," First Australia-New Zealand Conference on Soil Mechanics and Foundation Engineering, pp. 30-34.

Birrell, K. S., 1964. "Some Properties of Volcanic Ash Soils," FAO/UNESCO Meeting on the Classification and Correlation of Soils from Volcanic Ash, Food and Agricultural Organization World Resources Report No. 14, Rome, Italy, p. 74.

Birrell, K. S., 1966. "Determination of Clay Contents in Soils Containing Allophane," New Zealand Journal of Agricultural Research, Vol. 9, No. 3, pp. 554-564.

Bohn, H. L., McNeal, B. L., O'Connor, G. A., 1979. Soil Chemistry, John Wiley and Sons, New York, pp. 141-144.

Bowles, J. E., 1979. Physical and Geotechnical Properties of Soils, McGraw-Hill, New York, p. 309.

Chan, C. K., 1975. "Low-Friction Seal System," Journal of the Geotechnical Engineering Division, American Society of Civil Engineers, Vol. 101, No. GT9, pp. 991-994.

Collins, K., McGown, A., 1974. "The Form and Function of Microfabric Features in a Variety of Natural Soils," Geotechnique, Vol. 24, No. 2, pp. 223-254.

Cradwick, P. D. G., et al., 1972. "Imogolite, A Hydrated Aluminum Silicate of Tubular Structure," Nature (London), Vol. 240, pp. 187-189.

da Costa Nues, A. J., Vargas, M., 1953. "Computed Bearing Capacity of Piles in Residual Soil Compared with Laboratory and Load Tests," Proceedings, Third International Conference on Soil Mechanics and Foundation Engineering, held in Zurich, Switzerland, Vol. 2, pp. 75-79.

Dingus, D. D. D., 1973. "The Nature and Properties of Amorphous Colloids Formed from Mazama Ash," thesis presented to Oregon State University, Corvallis, Oregon, in partial fulfillment of the requirements for the degree of Doctor of Philosophy.

Dixon, H. H., 1963. "A Review of Test Results on Halloysitic Soils and their Performance in the Field," Proceedings, Third Regional Conference for Africa on Soil Mechanics and Foundation Engineering, held in Salisbury, South Rhodesia, Vol. 1, pp. 183-185.

Dixon, J. B., 1977. Kaolinite and Serpentine Group Minerals, Chapter II in Minerals in Soil Environments, Richard C. Dinauer, Ed., Soil Science Society of America, Madison, Wisconsin, pp. 357-398.

Dixon, W. J., Massey, F. J., 1969. Introduction to Statistical Analysis, McGraw-Hill, Inc., New York, 638 p.

Dudal, R., 1964. "Correlation of Soils Derived from Volcanic Ash," presented at the 1964, FAO/UNESCO meeting on the Classification and Correlation of Soils from Volcanic Ash, held in Tokyo, Japan, Food and Agricultural Organization World Resources Report No. 14, Rome, Italy, 164.

Endo, M., Hashiba, T., Ouchi, T., 1970. "An Observation of Ultimate Bearing Capacity of Silty Clay," Soils and Foundations, Vol. X, No. 1, pp. 15-24.

Fieldes, M., Perrott, K. W., 1966. "Rapid Field and Laboratory Test for Allophane. The Nature of Allophane in Soils. Part 3," New Zealand Journal of Science, Vol. 9, No. 3, pp. 623-629.

Fieldes, M., Furkert, R. J., Wells, N., 1972. "Rapid Determination of Constituents of Whole Soils using Infra-red Absorption," New Zealand Journal of Science, Vol. 15, pp. 615-627.

Fieldes, M., Claridge, G. G. C., 1975. Soil Components, Springer-Verlag, New York, pp. 352-392.

Flach, K. W., 1964. "Genesis and Morphology of Ash Derived Soils in the United States of America," presented at the 1964 FAO/UNESCO meeting on the Classification and Correlation of Soils from Volcanic Ash, held in Tokyo, Japan, Food and Agricultural Organization World Resources Report No. 14, Rome, Italy.

Foss, I., 1973. "Red Soil from Kenya as a Foundation Material," Proceedings, Eighth International Conference on Soil Mechanics and Foundation Engineering, Held in Moscow, USSR, Vol. 2.2, pp. 73-80.

Gidigasu, M. D., 1976. Laterite Soil Engineering - Pedogenisis and Engineering Principles, Elsevier Scientific Publishing Co., New York, pp. XI-XIV.

Gradwell, M., Birrell, K. S., 1954. "Physical Properties of Certain Volcanic Clays," New Zealand Journal of Science and Technology, Vol. 13, No. 36, pp. 108-122.

Grim, R. E., 1968. Clay Minerology, 2nd ed., McGraw-Hill, New York.

Hannon, R. W., 1972. "An Investigation of the Engineering Properties of Kruzof Island Pumice Soil," unpublished report secured from J. R. Bell. Oregon State University, Department of Civil Engineering.

Henmi, T., Wada, K., 1976. "Morphology and Composition of Allophane," American Minerologist, Vol. 61, pp. 379-390.

Hill, D., Stamatopoulos, A., Kotzias, D., 1975. Discussion of "Some Basic Engineering Properties of Halloysite and Allophane Clays in Java, Indonesia," by L. D. Wesley, Geotechnique (London), Vol. XXIII, No. 4, Vol. XXV, No. 2, pp. 417-423.

Hirashima, K. B., 1948. "Highway Experience with Thixotropic Volcanic Clay," Proceedings, Highway Research Board, Vol. 28, pp. 481-496.

Hirashima, K. S., 1951. "Highway Construction Problems Involving Plastic Volcanic Ash," Proceedings, Highway Research Board, Bulletin No. 44, pp. 1-10.

Hoshino, K., 1953. "Site Exploration for Founding a Building by Sinking Method of a Large-Scale Caisson," Proceedings, Third International Conference on Soil Mechanics and Foundation Engineering, Vol. 1, pp. 384-389.

Iamura, K., 1969. "The Chemical Bonding of Atoms in Allophane, the 'Structural Formula' of Allophane," Proceedings, 1969 International Clay Conference, Held in Tokyo, Japan, Vol. 1, pp. 161-172.

Jones, R. C., Uehara, G., 1973. "Amorphous Coatings on Mineral Surfaces," Proceedings, Soil Science Society of America, Vol. 37, pp. 792-798.

Lai, S. H., Swindale, L. D., 1969. "Chemical Properties of Allophane from Hawaiian and Japanese Soils," Proceedings, Soil Science Society of America, Vol. 33, pp. 804-808.

Lambe, T. W., Whitman, R. V., 1969. Soil Mechanics, John Wiley and Sons, Inc., New York, 553 p.

Lohnes, R. A., Handy, R. L., 1968. "Shear Strength of Some Hawaiian Latosols," Proceedings, Annual Symposium on Engineering Geology and Soil Engineering, 6th, pp. 64-79.

Lumb, P., 1966. "Variability of Natural Soils," Canadian Geotechnical Journal, Vol. 3, No. 2, pp. 74-97.

Maeda, T., Warkentin, B. P., 1975. "Void Changes in Allophane Soils Determining Water Retention and Transmission," Proceedings, Soil Science Society of America, Vol. 39, pp. 398-403.

Maeda, T., Takenaka, H., Warkentin, B. P., 1977. "Physical Properties of Allophane Soils," Advances in Agronomy, Vol. 29, pp. 229-264.

Martini, J. A., Palencia, J. A., 1975. "Soils Derived from Volcanic Ash in Central America," Soil Science, Vol. 120, No. 4, pp. 278-287.

Matsuo, S., 1957. "A Study of the Effect of Cation Exchange on the Stability of Slopes," Proceedings, Fourth International Conference on Soil Mechanics and Foundation Engineering, Vol. 2, pp. 330-333.

Matuo, J., et al., 1953. "Field Test and Observation on the Soft Soil in the Coast of the Ariake Sea," Proceedings, Third International Conference on Soil Mechanics and Foundation Engineering, Vol. 1, pp. 436-439.

Matyas, E. L., 1969. "Some Engineering Properties of Sasuma Clay," Proceedings, Seventh International Conference on Soil Mechanics and Foundation Engineering, Specialty Session on Engineering Properties of Latteritic Soils, held in Mexico.

McNabb, D. H., 1979. "Correlation of Soil Plasticity with Amorphous Clay Constituents," Soil Science Society of America Journal, Vol. 43, No. 2, pp. 613-616.

Mesri, G., 1975. "Composition and Compressibility of Typical Samples of Mexico City Clay," Geotechnique, Vol. 25, No. 3, pp. 527-554.

Mitchell, J. K., 1976. Fundamentals of Soil Behavior, John Wiley and Sons, Inc., New York, 422p.

Mogami, T., Kishida, H., 1961 . "Some Piling Problems," Proceedings, Fifth International Conference on Soil Mechanics and Foundation Engineering, Vol. 2, pp. 111-115.

Naval Facilities Engineering Command (NAVFAC), 1969. Design Manual - Civil Engineering, Naval Facilities Engineering Command Publications Transmittal No. NAVFAC DM-5. Naval Publications and Forms Center, Philadelphia, PA.

Newill, N., 1961. "A Laboratory Investigation of Two Red Clays from Kenya," Geotechnique, Vol. XI, No. 4, pp. 302-318.

New Zealand Soil Bureau Staff, 1968. "Soils of New Zealand, Part 3," New Zealand Soil Bureau Bulletin, Jean Luke Ed., No. 26(3), pp. 52-77.

Nielsen, N., et al., 1977. "The Honomu, Hawaii Earthquake Report of Inspection," National Research Council, National Academy of Sciences, Washington, D. C.

Nixon, I. K., Skipp, B. O., 1957. "Airfield Construction on Overseas Soils. Part 5: Laterite, and Part 6: Tropical Red Clays," Proceedings, Institution of Civil Engineers, Vol. 8, pp. 211-292.

Northey, R. D., 1956. "Rapid Consolidation Tests for Routine Investigations," Proceedings, Second Australia-New Zealand Conference on Soil Mechanics and Foundation Engineering, held in Christchurch, New Zealand, Vol. 1, pp. 20-22.

Northey, R. D., 1966. "Correlation of Engineering and Pedalogical Soil Classification in New Zealand," New Zealand Journal of Science, Vol. 9, No. 4, pp. 809-832.

Pope, R. J., Anderson, M. W., 1960. "Strength Properties of Clays Derived from Volcanic Rocks," Proceedings, ASCE Research Conference on Shear Strength of Cohesive Soils, held at Boulder, Colorado, pp. 315-340.

Poulos, S. J., 1971. The Stress-Strain Curves of Soils, Geotechnical Engineers, Inc., Winchester, Massachusetts, 116 p.

Salas, J. A. J., 1963. "Note on a Halloysitic Red Clay from Fernando Poo Island," Proceedings, Third Regional Conference for Africa on Soil Mechanics and Foundation Engineering, Vol. 1, pp. 85-88.

Schalscha, E. B., et al., 1965. "Effect of Drying on Volcanic Ash Soil in Chile," Proceedings, Soil Science Society of America, Vol. 29, No. 4, pp. 481-482.

Schroeder, W. L., 1975. Soils in Construction, John Wiley and Sons, Inc., New York, p. 116.

Takeshita, H., 1957. "The Stability of Gravel Roads in Volcanic Ash--soil Retions," Proceedings, Fourth International Conference on Soil Mechanics and Foundation Engineering, held in London, England, Vol. 2, pp. 174-177.

Taskey, R. D., 1978. "Relationship of Clay Minerology to Landscape Stability in Western Oregon," thesis presented to Oregon State University, Corvallis, Oregon, in partial fulfillment of the requirements for the degree of Doctor of Philosophy.

Taylor, D. K., 1967. "Notes on Observations of Building Settlements," Proceedings, Fifth Australia-New Zealand Conference on Soil Mechanics and Foundation Engineering, held in Auckland, New Zealand.

Terzaghi, K., 1958. "Design and Performance of the Sasamua Dam," Proceedings, Institution of Civil Engineers, Vol. 9, pp. 369-393.

Terzaghi, K., Peck, R. B., 1967. Soil Mechanics in Engineering Practice, John Wiley and Sons, Inc., New York, 729 p.

Tokashiki, Y., Wada, K., 1975. "Weathering Implications of the Minerology of Clay Fractions of Ando Soiis, Kyushu," Geoderma, Vol. 14, pp. 47-62.

Tovey, N. K., 1971. Discussion of paper by Barden and Sides, "Engineering Behavior and Structure of Compacted Clays," Journal of the Geotechnical Engineering Division, American Society of Civil Engineers, Vol. 97, SM4, pp. 694-700.

Tovey, N. K., 1973. "Some Applications of Electron Microscopy to Soil Engineering, in Soil Microscopy, Proceedings, Fourth International Working-Meeting on Soil Micromorphology, G. K. Rutherford, Ed., held in Kingston, Ontario, Canada, pp. 119-142.

Tovey, N. K., Wong, K. Y., 1973. "Some Aspects of Quantitative Measurements from Electron Micrographs of Soil Structure," in Soil Microscopy, Proceedings, Fourth International Working-Meeting on Soil Micromorphology, G. K. Rutherford, Ed., held in Kingston, Ontario, Canada, pp. 207-222.

Udagawa, S., Nakada, T., Nakahira, M., 1969. "Molecular Structure of Allophane as Revealed by its Thermal Transformation," Proceedings, 1969 International Clay Conference, held in Tokyo, Japan, Vol. 1, pp. 151-159.

Uriel, S., Serrano, A. A., 1973. "Geotechnical Properties of Two Collapsible Volcanic Soils of Low Bulk Density at the Site of Two Dams in the Canary Islands (Spain)," Proceedings, Eighth International Conference on Soil Mechanics and Foundation Engineering, held in Moscow, USSR., Vol. 2.2, pp. 257-264.

Wada, K., Harward, M. E., 1974. "Amorphous Clay Constituents of Soils," Advances in Agronomy, Vol. 26, pp. 211-260.

Wada, S., Wada, K., 1977. "Density and Structure of Allophane," Clay Minerals, Vol. 12, pp. 289-298.

Wallace, K. B., 1973. "Structural Behavior of Residual Soils of the Continually Wet Highlands of Papua, New Guinea," Geotechnique, Vol. XXIII, No. 2, pp. 203-218.

Warkentin, B. P., 1972. "Use of the Liquid Limit in Characterizing Clay Soils," Canadian Journal of Soil Science, Vol. 52, No. 3, pp. 457-464.

Warkentin, B. P., 1974. "Physical Properties Related to Clay Minerals in Soils of the Carribbean," Tropical Agriculture (Trinidad), Vol. 51, No. 2, pp. 279-287.

Warkentin, B. P., Maeda, T., 1974. "Physical Properties of Allophane Soils from the West Indies and Japan," Proceedings, Soil Science Society of America, Vol. 38, pp. 372-377.

Warkentin, B. P., Maeda, T., 1981. "Physical and Mechanical Characteristics of Andosols," Oregon Agricultural Experiment Station, Publication No. 5516, Oregon State University, 33 p.

Wells, N., Furkert, R. J., 1972. "Bonding of Water to Allophane," Soil Science, Vol. 113, No. 2, pp. 110-115.

Wesley, L. D., 1973. "Some Basic Engineering Properties of Halloysite and Allophane Clays in Java, Indonesia," Geotechnique, Vol. XXIII, No. 4, pp. 471-494.

Wesley, L. D., 1974. Discussion of "Structural Behavior of Residual Soils of the Continually Wet Highlands of Paqua, New Guinea," by K. B. Wallace, Geotechnique, Vol. XXIII, No. 2, Geotechnique, Vol. XXIV, No. 1, pp. 101-106.

Williams, F. H. D., O'Reilly, M. P. 1963. "A Field Study of Conditions Under Roads in Kenya," Proceedings, Third Regional Conference for Africa on Soil Mechanics and Foundation Engineering, held in Salisbury, South Rhodesia, Vol. 1, p. 55.

Willis, E. A., 1946. "A Discussion of a Study of Lateritic Soils," Proceedings, Highway Research Board, Vol. 26, pp. 589-594.

Wooltorton, F. L. D., 1960. "Design Correlations for Kenya Red and Red-Brown Soils," Proceedings, Highway Research Board, Vol. 30, pp. 683-694.

Wright, A. C. S., 1964. "The 'Andosols' or 'Humic Allophane' Soils of South America," presented at the 1964, FAO/UNESCO Meeting on the Classification and Correlation of Soils from Volcanic Ash, held in Tokyo, Japan, Food and Agricultural Organization World Resources Report No. 14, Rome, Italy.

Yamazaki, F., Sudo, S., 1965. "Engineering Behavior of Soils, Mainly Kanto Loam," Transactions, Engineering Society, Japan, No. 14, pp. 1-10 (Japanese).

Yong, R. N., Warkentin, B. P., 1975. Soil Properties and Behavior, Elsevier Publishing Co., Amsterdam, pp. 449.

Yoshinga, N., Aomine, S., 1962. "Imogolite in some Ando Soils," Soil Science and Plant Nutrition, Vol. 8, pp. 22-29.

Zalazar, L. M., 1948. "Soil Stabilization in Argentine Highways," Proceedings, Second International Conference on Soil Mechanics and Foundation Engineering, held in Rotterdam, Netherlands, p. 294.

APPENDICES

APPENDIX A

Tabular Summary of Data

from Literature Review

Directions for Use of Table

Each soil from a particular local area has been assigned a soil number. The small letter designations on some soil numbers represent the same local soil type, but signify that this soil is reported by more than one investigator. The small letters may also represent different depths in the same soil profile. For example: Soils 1(a), 1(b) and 1(c) are from the same soil but are reported separately by three different authors. Soils 41(a) and 41(b) are at different depths in the same soil profile. Each soil number corresponds to a soil description with the same number. All of the soil descriptions are grouped together and placed after the table (pages 297 to 316 in Appendix A). Each soil description starts with a soil name followed by the location of the particular reported soil deposit. Most are followed by a general description of the soil and parent materials. All soil names, locations, and descriptions are listed as they were reported in the literature.

Each set of soil data has a reference key number at the end of each row. Using this key number from the table, a corresponding reference can be found in the reference key list located on page 317 in this appendix. For example, reference key number 34 corresponds to Wallace (1973). The citation for Wallace (1973) can then be found in the list of references.

Some of the soil data have footnotes (superscript numbers) beside them. A list of footnotes is included on page 296, at the end of the table.

	Grain Size			Index Properties				Insitu Conditions				Moisture Density		Strength		Consolidation		
1	2	3	4	5	6	7	8	9	10	11	12	13	14	15	16	17	18	19
Soil Number	Percent Sand (%)	Percent Silt (%)	Percent Clay (%)	Liquid Limit (LL in %)	Plastic Limit (PL in %)	Plastic Index (PI in %)	Activity	Natural Water Content (Wn in %)	Insitu Unit Weight (γ_d in pcf)	Void Ratio (e)	Specific Gravity (G_s)	Optimum Water Content (W opt in %)	Maximum Dry Density (γ_d max in pcf)	Angle of Internal Friction (ϕ' in degrees)	Cohesion Intercept or Shear Strength+ (c'/c in psf)	Compression Index (Cc)	Over-Consolidation Ratio (OCR)	Reference Key Number
1(a)	12	6	82	76	40	36		29			2.80							1
ad*				74	40	34												
od*			68	66	36	30												
1(b)			83	78	40	38	.46	32[1]	73.7					28	220			2
ad														38	560			
1(c)												34.8	82.0					3
ad												34	83.2					
od												33.5	82.5					
2(a)											2.37	50	59**					4
2(b)											2.47	50	56**					4
3(a)	8	25	67	62	42	20	0.36	30				33						5
3(b)	5	42	53	62	40	22	0.29					39						5
4			78	64	46	18	0.23	40.7	68.7			39	66.8	36[2]	40[2]			2
5			84	70	42	28	0.32	25.0[1]	64.9	1.7		24	62.4	29[2]	52[2]	0.68	3.5	2
6			90	68	40	28	0.30	26.0	58.1			27.0	65.6	28[2]	240[2]			2
7(a)			70-100	84[5]	49[5]	35[5]						50		34[2]	600[2]	0.5		3

* ad = air dry od = oven dry ** British Standard Compaction + undrained shear strength (c) if Ø' not given

Soil	Sand	Silt	Clay	LL	PL	PI	Act.	Wn	γ_d	e_o	G_s	W_{opt}	γ_d max	ϕ'	c'/c	Cc	OCR	Key
1	2	3	4	5	6	7	8	9	10	11	12	13	14	15	16	17	18	19
7(b)			20-50	88	59	29						49	70					6
7(c)			70	52	33	19		32			2.66							7
7(d)	8	13	79	102	70	32		62			2.94	53	68					1
ad				78	62	16						48	74					
od			47	65	47	18						45	76					
7(e)			51	107	73	34	.51	64			2.90	60	62	29.9^2	560^2			8
ad												51	69	31^2	1440^2			
od				65	37	28						44	76					
8(a)			25	85	50	35						49	69					6
8(b)	17	32	51	85	48	37					2.96	49	69	22.3	980^2	2		9
												32$	91$	27.5$	$5200^{2}$$			
8(c)																		3
9(a)	49	34	17	116	92	24		82										10
ad				82	77	5												
od				64	64	NP												
9(b)	40	26	33					95										10
9(c)	43	38	19	160	136	24		138										10
ad				70	70	NP												
od				44	44	NP												

$ Modified AASHTO

Soil	Sand	Silt	Clay	LL	PL	PI	Act.	Wn	γ_d	e_o	G_s	W_{opt}	γ_{dmax}	ϕ'	c'/c	Cc	OCR	Key
1	2	3	4	5	6	7	8	9	10	11	12	13	14	15	16	17	18	19
9(d)	59	23	18	90	76	14		73										10
a d				70	63	7												
od				52	49	3												
9(e)	46	32	22	120	104	16		110										10
ad				89	81	8												
od				55	55	NP												
9(f)			36	150	134	16												11
ad				44	44	NP												
10			66	110	64	46						53	67					6
11(a)			16	31	20	11												11
ad				26	13	8												
11(b)	64	18	18															10
12	27.9	48.5	23.6@						62.4									12
	35.2	39.7	25.1															
13	39.4	44.5	16.0@						62.4									12
	46.2	42.6	11.2															
14	47.0	39.8	13.2@						62.4									12
	49.2	34.5	16.3															
15	33.6	40.6	25.8@						62.4									12
	38.2	38.4	23.3															
16(a)								312.8	20.6									13

@ A and B horizons respectively

Soil	Sand	Silt	Clay	LL	PL	PI	Act.	Wn	γ_d	e_o	G_s	W_{opt}	γ_d^{max}	ϕ'	c'/c	Cc	OCR	Key
1	2	3	4	5	6	7	8	9	10	11	12	13	14	15	16	17	18	19
16(b)								114.1	33.7									13
17(a)	22	18	60	48	38	10		78						23.5	100			14
17(b)	13	32	55	58	48	10		85						23.5	100			14
17(c)	13	25	62	48	34	14		89						23.5	100			14
18(a)			80					139[4,5]	38.1[5]			100	38					15
ad			15									84	49					
18(b)				179	87	92		113			3.1							15
18(c)				136	103	33		120			2.8							15
18(d)				219	148	71		204			2.9							15
18(e)				245	135	110		248			2.9							15
18(f)	30	34	36								2.80	100	38					16
ad	86	11	3								2.84	38	77					
18(g)	34	10	56															16
ad	42	17	41															
18(h)								171	29					4.0	1100			16
18(i)								149	31					10.8	1200			16
18(j)								135	34					7.4	2000			16
18(k)								100	39					22.8	2400			16
18(l)								77	42					29.7	2200			16
18(m)								13	73					49.0	800			16
18(n)			90	110				200[5]	25.3						300-600			17

Soil	Sand	Silt	Clay	LL	PL	PI	Act.	Wn	γ_d	e_o	G_s	W_{opt}	$\gamma_{d\,max}$	ϕ'	c'/c	Cc	OCR	Key
1	2	3	4	5	6	7	8	9	10	11	12	13	14	15	16	17	18	19
19(a)	2	6	92	53	27	26		24										14
19(b)	0	6	94	65	53	12		28										14
19(c)	0	3	97	68	41	27		27										14
19(d)	1	6	93	61	43	18		27										14
20(a)	50.8	48.8	0.4					21.9	44.3									13
20(b)	38.2	56.7	5.1					43.7	41.2									13
21(a)	8	28	64	156	132	22		146			2.76	86	36					18
ad	35	48	17								2.71	90	44					
od	48	43	9	111	96	15					2.55	80	49					
21(b)	7	21	72	184	146	38		151			2.75	97	35					18
ad	86	12	2								2.73	69	54					
od	83	13	4	79	74	5					2.56	38	70					
21(c)	6	22	72	213	167	46		180		4.6	2.58	101	34	40	340	3.0	4.9	18, 19
ad	74	20	6								2.65	67	55					
od	76	20	4	86	79	7					2.57	40	70					
21(d)			93	176	106	70		157.4										
22(a)	7	28	65	165	119	46		128			2.80	102	37	40^2	340^2			18, 19
ad	68	22	10	60	53	7					2.78	54	60					
od	85	10	5	44	43	1					2.54	38	74					

Soil	Sand	Silt	Clay	LL	PL	PI	Act.	Wn	γ_d	e_o	G_s	W_{opt}	$\gamma_{d}max$	ϕ'	c'/c	Cc	OCR	Key
1	2	3	4	5	6	7	8	9	10	11	12	13	14	15	16	17	18	19
22(b)	5	19	76	95	65	30		68			2.88	63	60	40^2	340^2			18, 19
ad	7	28	65	74	58	16					2.84	52	68					
od	12	28	60	61	51	10					2.74	44	72					
22(c)			6.33	115	59	56						48	72					6
22(d)				117	55	62		97										3
				112	60	52												
				98	67	31												
				69	47	22												
				64	54	10												
				57	36	21												
				52	36	16												
				52	34	18												
				42	31	11												
23(a)	5	23	72	76	36	40	0.6	31			2.78	27	82					18
ad	6	21	73	71	36	35					2.78	26	84					
od	7	23	70	59	33	26					2.74	20	89					
23(b)	3	21	76	94	52	42	0.6	51			2.76	50	67					18
ad	2	13	85	85	51	34					2.76	47	71					
od	2	16	82	60	40	20					2.73	38	78					
23(c)	3	15	82	100	43	57		50			2.75	46	73					18
ad	2	13	85	100	43	57					2.73	43	74					
od	2	15	83	84	44	40					2.73	42	78					

Soil	Sand	Silt	Clay	LL	PL	PI	Act.	Wn	γ_d	e_o	G_s	W_{opt}	$\gamma_{d\,max}$	ϕ'	c'/c	Cc	OCR	Key
1	2	3	4	5	6	7	8	9	10	11	12	13	14	15	16	17	18	19
23(d)	3	17	80	80	40	40		41			2.77	41	79					18
ad	4	11	85	77	39	38					2.77	37	81					
od	3	14	83	72	39	33					2.79	36	81					
23(e)				100	46	54		42			2.85							7
				100	60	40					2.72							
24(a)		38[5]	32[5]	80[5]	41[5]	39[5]		59[5]	53.8	2.22	2.62[5]	42	78	30.5	2000[5]	.74	5.83	21
25(a)	26	51	19	111	81	30		250										10, 22
ad				103	81	22												
od				100	83	17												
26(a)	24	64	12															23
26(b)	27	70	3							2.67						2.65	6.6	
26(c)	32	65	3															
26(d)	3.5	71	25.5															
27	16	41	43	60	42	18		51										10, 22
ad				50	38	12												
od				42	36	6												
28[α]				155	94	61		110[5]							700[5]			24
				114	59	55									1200[5]			
29(a)	85	6	9					106										10

[α] Seasonal variations reported

Soil	Sand	Silt	Clay	LL	PL	PI	Act.	Wn	γ_d	e_o	G_s	W_{opt}	γ_{dmax}	ϕ'	c'/c	Cc	OCR	Key
1	2	3	4	5	6	7	8	9	10	11	12	13	14	15	16	17	18	19
29(b)				51[5]	31[5]	20[5]		61						5.2	160			25
30	48	24	28	71	63	8		59										10
ad				60	55	5												
od				49	48	1												
31				75[5]	41[5]	34[5]												25
32(a)	12	30	58	180	90	90		120	33.7	3.92	2.83				800		2-5	26
				136	81	55												
				130	88	42												
				120	54	66												
				115	48	67												
				105	55	50												
32(b)				160	120	40		120	28.1		2.65[++]							27
ad				120	111	9												
32(c)				184	123	61		140	28.1		2.65[++]							27
ad				97	81	16												
32(d)				110	80	30		100	36.4		2.65[++]							27
ad				103	96	7												
32(e)				110	80	30		98	41.3		2.65[++]							27
ad				98	79	19												

[++]Assumed value

Soil	Sand	Silt	Clay	LL	PL	PI	Act.	Wn	γ_d	e_o	G_s	W_{opt}	γ_d^{max}	ϕ'	c'/c	Cc	OCR	Key
1	2	3	4	5	6	7	8	9	10	11	12	13	14	15	16	17	18	19
32(f)				120	74	46		100	41		2.65[++]							27
ad				110	90	20												
32(g)				110	88	22		120	37		2.65[++]							27
ad				100	90	10												
33(a)	10	60	30	79	45	34		90-120			2.65			10	1000			28
				52	29	23												
33(b)				70	44	26		115	40.6	3.1	2.65			6.9	520			29
				55	40	15												
				51	33	18												
				48	39	9												
33(c)				99				90.6	47.8	2.58					440			30
33(d)												103	43					31
ad												86	48					
od												74	54					
34				115				110	42.8	2.92					720			30
35				51[5]	22[5]	29[5]												25
36(a)	74-91	9	26	43-50	43-50	0		30-42	67.4-82.7		2.87			35	500			32
36(b)	38-66	34	62	NP	NP	NP		8-24	43.6-58.3		2.44-2.63			42	3000			32
37	10	15	75	80[5]	46[5]	34[5]		50[1]			3.02	87[#]	35[#]					33

[++] Assumed value # Modified AASHTO

Soil	Sand	Silt	Clay	LL	PL	PI	Act.	Wn	γ_d	e_o	G_s	W_{opt}	$\gamma_d max$	ϕ'	c'/c	Cc	OCR	Key
1	2	3	4	5	6	7	8	9	10	11	12	13	14	15	16	17	18	19
38(a)	30	43	27	160	75	85		130	35-55	3.17-4.00					980$^{\alpha\alpha}$	1.01-2.3	13	34
od	79	18	3															
38(b)	7	27	66	136	82	54		130	35-55	3.17-4.00					600$^{\alpha\alpha}$	1.31-1.93	13	34
od	35	45	20															
39(a)			64	231	136	95	1.48	196[4,5]							440	1.53	50	35
39(b)			63	207	131	76	1.2	200										36
od				85	78	7												
40(a)[6]	42	39	19	69	43	26	1.37	41	65.5	1.51	2.64				1340[8]			37
ad												34	79		5060[2,8]			
40(b)[7]	36	42	22	48	30	18	0.82	33.9	78.8	1.10	2.64				3230[8]			37
ad												26	91		8440[2,8]			
41(a)[6]	52	32	16	87	49	38	2.4	43.5	46.2	2.37	2.49	48	70		1060[8]			37
															2950[2,8]			
41(b)[7]	44	34	22	53	33	20	0.91	29.5	74.9	1.2	2.65	26	91		2500[8]			37
															6680[2,8]			
42(a)[6]	65	26	9	79	59	20	2.22	37.4	46.2	2.28	2.43				1160[8]			37
42(b)[7]	67	21	12	79	53	26	2.17	43.2	51.8	2.13	2.61				2280[8]			37
42(c)			53	110	62	48	0.91	120[5]						1.5	840	1.49	13	35

$\alpha\alpha$ Torvane

Soil	Sand	Silt	Clay	LL	PL	PI	Act.	Wn	γ_d	e_o	G_s	W_{opt}	γ_d^{max}	ϕ'	c'/c	Cc	OCR	Key
1	2	3	4	5	6	7	8	9	10	11	12	13	14	15	16	17	18	19
43(a)[6]	39	33	22	49	29	20	0.91	28.6	81.7	1.03	2.67	29	87		3830[8] 3020[2,8]			37
43(b)[7]	39	34	27	53	27	26	0.96	29.0	88.6	0.87	2.67	26	92		2280[8] 2530[2,8]			37
43(c)			27	50	29	21	0.78	30.0				26	91					38
44	77	16	3	80	80	0		64.5	48.7	1.99	2.32				740[8]			37
45(a)[6]	32	34	34	94	60	34	1.0	51.7	53.0	2.14	2.68	52	65		1720[8] 4220[2,8]			37
45(b)[7]	9	34	57	93	47	46	0.81	43.9	64.9	1.60	2.69	40	76		1340[8] 3510[2,8]			37
46(a)			57	350	167	183	1.8	280										36
ad				108														
46(b)				119	54	65	1.1											36
47(a)[6]	53	30	17	25	20	5	.29	12.5	87.8	0.86	2.62				2390[8] 5980[2,8]			37
47(b)[7]	26	46	28	40	23	17	.61	20.2	94.0	0.76	2.66				4010[8]			37
47(c)			25	36	21	15	.60	20				21	101					38
48(a)[6]	83	14	3	63	63	NP	0	53	54.2	2.04	2.66	34	76		770[8] 5620[2,8]			37
48(b)[7]	92	4	4			NP	0	15.3	46.1	2.48	2.59	20	96		490[8]			37

Soil	Sand	Silt	Clay	LL	PL	PI	Act.	Wn	γ_d	e_o	G_s	W_{opt}	$\gamma_d max$	ϕ'	c'/c	Cc	OCR	Key
1	2	3	4	5	6	7	8	9	10	11	12	13	14	15	16	17	18	19
49(a)[6]	67	23	10	126	88	38	3.8	81.9	43.0	2.48	2.4	49.2	50.5		700[8]			37
															4290[2,8]			
49(b)[7]	51	24	17	152	92	60	3.7	91.8	37.4	3.0	2.4	74.2	73.5		560-1120[4]			37
															5200[2,8]			
50(a)[6]	47	27	26	173	95	78	2.96	115	31.2	3.26	2.12				1550[8]			37
ad												77	47.5		6300[2,8]			
50(b)[7]	58	21	21	166	80	86	4.1	121	28.6	3.78	2.19	82	44.5		1020[8]			37
															3200[2,8]			
50(c)				186	92	94		130										38
ad				98	82	16												
od				81	75	6												
51(a)[6]	33	39	24	92	55	39	1.5	60	54.8	2.57	2.63				420[8]			37
51(b)[7]	50	31	19	53	35	18	.75	20		1.61	2.63				4230[8]			37
51(c)			26				1.5	60				45	68					38
52(a)[6]	61	25	12	129	87	42	3.5	96	43	2.32	2.40				460[8]			37
52(b)[6]	50	36	13	38	23	15	1.15	35.3	74.8	1.16	2.59	22	96		950[8]			37
															6330[2,8]			
52(c)[7]									43.0	2.36	2.30				630[8]			37
53(a)[6]				117	73	44		51	46.1	2.36	2.49				1340[8]			37
53(b)[6]				120	61	59		65	44.9	2.5	2.49				1410[8]			37

Soil	Sand	Silt	Clay	LL	PL	PI	Act.	Wn	γ_d	e_o	G_s	W_{opt}	$\gamma_d$max	ϕ'	c'/c	Cc	OCR	Key
1	2	3	4	5	6	7	8	9	10	11	12	13	14	15	16	17	18	19
53(c)[7]										2.25	2.49							37
54(a)[6]	63	26	9	124	85	39	4.3	100	35.5	2.89	2.21				910[8]			37
54(b)[6]	70	24	3	66	66	NP		58.6	53.0	1.70	2.37				700[8]			37
54(c)[7]	80	8	1	58	58	NP		40	64.8	1.28	2.4				3410[8]			37
55(a)[6]	75	20	5	86	56	30	6.0	58.9	38.6	2.65	2.11	57	57		1060[8] 5480[2,8]			37
55(b)[6]	78	15	7	90	50	40	5.7	60.8	40.0	2.55	2.46				1090[8]			37
55(c)[7]				80	48	32		60.2	47.3	2.22		54	62		1340[8]			37
56(a)[6]	39	43	18	57	33	24	1.34	33.5	75.4	1.17	2.63	31	86.4		3240[8] 4080[2,8]			37
56(b)[7]	37	41	22	50	30	20	0.91	28.7	84.7	0.98	2.7				3000[8]			37
57(a)[6]	69	22	5	118	115	3	0.6	83.0	41.1	2.27	2.17				2460[8]			37
57(b)[6]	80	17	3	114	53	61	1.7	84.2	41.1	2.29	2.18	76	47.6		1620[8] 3520[2,8]			37
57(c)[7]				75	53	22		51.2				42	66.7		1830[8] 7730[2,8]			37
58(a)			40	130	70	60	1.48	117		3.5				2.3	880-1400	1.73	2.2/.12	35
58(b)	29	37	34				1.18			2.75						1.14	75.0	39
59(a)				90-170	40-110	50-60										0.11-0.23	72.0	40

Soil	Sand	Silt	Clay	LL	PL	PI	Act.	Wn	γ_d	e_o	G_s	W_{opt}	$\gamma_d max$	ϕ'	c'/c	Cc	OCR	Key
1	2	3	4	5	6	7	8	9	10	11	12	13	14	15	16	17	18	19
59(b)				47	34	13				1.41-1.60						0.24-0.65	0.96-1.40	40
60(a)				107	71	36						45	69					6
ad												30	90					
60(b)				107	75	32												3
61	7.4[5]		92.6[5]	34[5]	24[5]	10[5]						21	94					41
62	8.1[5]		91.9[5]	48[5]	29[5]	19[5]												41
63	3.5[5]		96.5[5]	65[5]	40[5]	25[5]												41
64(a)				65[5]	50[5]	15[5]		30	47.9					30	200			42
(b)								30	52.3					30	0			
(c)								30	69.7					30	200			
(d)								45	54.7					25	400			
(e)								42	59.8					25	200			
(f)								40	60.6					21	200			
65(a)[6]	36	48	16					109										43
ad	47	42	11															
od	51	43	6															
65(b)[7]	27	29	44					87										43
ad	52	29	19															
od	58	31	11															

Soil	Sand	Silt	Clay	LL	PL	PI	Act.	Wn	γ_d	e_o	G_s	W_{opt}	$\gamma_{d\,max}$	ϕ'	c'/c	Cc	OCR	Key
1	2	3	4	5	6	7	8	9	10	11	12	13	14	15	16	17	18	19
66(a)[6]	42	40	18					78										43
ad	52	41	7															
od	48	49	5															
66(b)[7]	36	52	12					100										43
ad	42	51	7															
od	43	54	3															
67(a)[6]	36	48	16					101										43
ad	34	53	13															
od	44	48	8															
67(b)[7]	28	65	7					120										43
ad	47	48	5															
od	43	52	5															
68	61.3	25.6	10.6	23[5]	13[5]	10[5]												44
69			15	200	140	60					2.47			43	1080	.083		45
70			6	101	75	26						48	64					6
71				55	40	15		56.7										46
ad				46	39	7												
72				81	51	30		70.4										46
ad				65	53	12												
73				80	45	35		49.6										46
ad				59	45	14												

Soil	Sand	Silt	Clay	LL	PL	PI	Act.	Wn	γ_d	e_o	G_s	W_{opt}	$\gamma_{d\,max}$	ϕ'	c'/c	Cc	OCR	Key
1	2	3	4	5	6	7	8	9	10	11	12	13	14	15	16	17	18	19
74(a)[6]	12.1	55.2	32.7						46.2									13
74(b)[7]	17.6	65.6	16.0						58.7									13
75(a)[6]	59.4	31.2	9.4															13
75(b)[7]	63.0	29.4	7.6															13

FOOTNOTES

1 Average value with depth

2 Values for compacted soils

3 Typical values

4 Highly variable

5 Average value(s)

6 Depth 0-2 feet

7 Depth 2-4 feet

8 Strength measured with proctor needle

Soil Descriptions

Soil Number

1 Kabete Soil

Kabete District of Nairobi, Africa

Description:

This coarse grained appearing red clay is usually found between 1200 and 2500 meters above sea level in areas of good drainage. The clays are residual soils formed by weathering and leaching of the parent rock which is mainly of volcanic origin. Soil depth is estimated at 15-20 meters, age at 180,000-60 million years. (Newill, 1961; Foss, 1973).

2 Ash and pumice

Kenya, Africa

3 Metahalloysite

Kenya, Africa

Description:

Metahalloysite and hydrated halloysite are the main constituents, however, "in agricultural circles, it is thought that these may be present in the red or brown Kenyan soils, varieties of high swelling amorphous material resembling allophane". (Wooltorton, 1960).

Soil Number

4 Red Soil

Nairobi School; Kenya, Africa

Description: See Kabete Soil (soil number 1).

5 Red Soil

Nyeri Police; Kenya, Africa

Description: See Kabete Soil (soil number 1).

6 Red Soil

Nyeri Hospital; Kenya, Africa

Description: See Kabete Soil (soil number 1).

7 Sasumua Clay

Sasumua Dam; Kenya, Africa

Description:

This coarse grained appearing-dark reddish brown clay is found at approximately 8,100 feet above sea level approximately 50 miles south of the equator. The clay turns a yellowish red when oven dried. The clay consists of the products of tropical weathering of rocks of volcanic origin. The weathered volcanic soil was found to range erratically in depth from zero to more than 50 feet in thickness.

Soil Number

7 (con't) "About 60-70% of a sample of Sasumua clay appears to be halloysite, which occurs here in the form of tubes or more commonly as troughs. Some crystals are partially or wholly unrolled. Seen end on these crystals appear as rings or horeshoes; some of the tubes or troughs are extremely small in size." (Wooltorton, 1960) F. L. D. Wooltorton (Gidigasu, 1976) has reported that the Sasumua clay also contains allophane.

8 Dehydrated Halloysite

Silvan Dam, Australia

Description:

Soil is described as a fine textured silty clay high in percent free iron oxides. It is reported to contain 90% red weathered basalt and 10% yellow weathered alacite. Mineralogically it contains 85% dehydrated halloysite and 9% free iron oxide. F. L. D. Wooltorton (Gidigasu, 1976) suggests that allophane might be present and in association with hydrated halloysite.

Soil Number

9 Boetica Allophane content = 27%

Dominica, West Indies

Description: Allophane (Warkentin and Maeda, 1974)

10 Hydrated Halloysite

Grand Etang Dam; Granada, West Indies

Description:

Soil described as residual soil founded on weathered volcanic ash. Is said to contain 55% hydrated halloysite, 28% dehydrated halloysite and 17% Goethite. Allophane may be associated with the Hydrated halloysite (Dixon, 1963).

11 Montreal Allophane content = 15%

St. Vincent, West Indies

Description: Allophane (Warkentin and Maeda, 1974)

12 Andosol Allophanc content = 21%

Costa Rica

Description:

Soils are thixotropic when wet, they have a smeary feel and release water when compressed. They have formed from gray andesite volcanic ash and pumice. "The high content of amorphorus and organic fractions

Soil Number

12 (cont.) causes such dynamic wetting and drying process that aggregates are constantly disrupted, reducing their stability. This is responsible for the weak structure under field conditions." (Martini and Palencia, 1975).

13 Andosol Allophane content = 17%

El Salvador

Description: See Costa Rica (soil number 12).

14 Andosol Allophane content = 45%

Guatemala

Description: See Costa Rica (soil number 12).

15 Andosol

Nicaragua

Description: See Costa Rica (soil number 12).

16 Hilo Silty Clay Loam

Island of Hawaii, United States

Description:

Soils described as dark reddish-brown clay weathered from basic volcanic ash (Flach, 1964).

17 Paaloa - Silty Clay

Oahu, Hawaii; United States

Soil Number

17 (cont.) Description:

Soil is described as a silty clay (humic latosol) occurring at high elevations. It is located on a series of weathered pliocene olivine basalt flows. The soil was found to vary from zero to 5 or 6 feet in thickness (Lohnes and Handy, 1968).

18 Pepeeko Soil

Papaikou - Pepeeko section of the Hawaii belt road on the island of Hawaii; United States

Description:

"In the natural state, this soil posesses the stable properties of a solid although the moisture contents are in excess of the plastic limit and many times in excess of the liquid limit. When remolded, these soils become plastic or even semi-liquid but are thixotropic. Upon drying the material turns granular." The soil is formed by the weathering of volcanic ash under heavy rainfall (> 200 in per year). The ash cover is approximately 30 inches thick (Hirashima, 1948).

Soil Number

19 Wahiawa

Oahu, Hawaii; United States

Description: See Paaloa (soil number 17).

20 Waimea very fine sandy loam

Island of Hawaii, United States

Description:

Soils described as dark brown, sandy loam derived from basic volcanic ash (Flach, 1964).

21 Andosol Allophane content 95-100%

Java, Indonesia

Description:

These yellowish brown soils are found at high altitudes; greater than 1000 meters. They are formed from volcanic parent materials under conditions of tropical weathering. The soil depth ranges up to 50 meters. The deeper soil deposits being formed from a series of ash showers. Investigators have found halloysite and allophane in the andosals tested. This particular soil consists primarily of allophane (95-100%) (Wesley, 1973).

Soil Number

22 Andosol Allophane content = 76%

Tjipanoendjang; Java, Indonesia

Description: See Andosol (soil number 21).

23 Red Latosol

Java, Indonesia

Description:

The latosols are reddish in color and are found at the lower altitudes; up to 1000 meters. They are formed from volcanic parent materials under conditions of tropical weathering. Soil depth is commonly up to 10 meter especially in flat regions. These soils contain predominantly halloysite, some kaolinite and some allophane (Wesley, 1973).

24 Latosol

Semangha Bay; Sumatra, Indonesia

Description:

This soil is similar to the red latosol--Java, Indonesia. It has a brown-yellow or green-blue color with grey brown mottles. The soil is a product of insitu weathering of tuff-buccia and andesite. The thickness of the residual material is erratic, varying from as little as

Soil Number		
24 (cont.)	3 meters to as much as 40 meters, within short distances. The ground surface is only a few meters above sea level. The same type of soil was found up to 700 meters off-shore, to a maximum water depth of 40 meter (Hill, et al., 1975).	
25	Venae Chitose; Hokkaïdo, Japan	Allophane content = 47%
26	Silty loam Coast of Ariake Sea, Japan	
27	Nezaki Hokodate; Hokkaido, Japan	Allophane content = 15%
28	MH - Volcanic Ash Soil Iwate District - Northeastern Japan	
29	Murasakino Kitakami; Tonhoko, Japan	Allophane content = 40%
30	Memuro Memuro; Hokkaido, Japan	Allophane content = 23%
31	Osaka Bay Silt Osaka Bay, Japan	
32	Kanto Loam	

Soil Number

33 Tokyo, Kanto District

Description:

Soil is a brown or yellowish brown clay less than 10 meters in thickness. It consists of aggregations .02 to .06 mm in size. X-ray studies have shown that the Kanto loam is composed mainly of amorphous allophane. The lower layer also has some hydrated halloysite evident.

34 Yakohama Soil

Yokohama, Japan

35 Yoshidayama Soil

Yoshidayama, Japan

36 Volcanic Soils

Canary Islands

Description:

The soil is described as being of volcanic origin. The clay fraction consists of poorly crystalized minerals and a great proportion of amorphous materials are abundant (Urel and Serrano, 1973).

Soil Number

37 Halloysite Red Clay

Landing strip; Fernando Poo Island

Description:

Soil described as red clay possessing properties akin to the Kenya red clay. Consists of tubular crystals of halloysite, badly shaped kaolinite crystals, and "clouds" of ferric and aluminum oxides (Salas, 1963).

38 Kandite Minerals

South Highland districts; Papua, New Guinea

Description:

Soils are described as firm, moist yellow-brown or olive brown fissured silty or sandy clay. They are composed of hydrated halloysite and allophane with moderate amounts of gibbsite and vermiculite. The soils are located on 'volcanics' (Wallace, 1973).

39 Water Sorted Ash Allophane content = 64%

Whenuapi Airfield, New Zealand

Description:

Described as sedimentary allophane (Birrell and Fields, 1952).

Soil Number

40 Belmont Silt Loam Allophane content = 12%

Belmont Army Reserve, New Zealand

Description:

Dark yellow brown silt loam derived from greywacke (New Zealand Soil Bureau).

41 Dannevirke Silt Loam Allophane content = 16%

Hamua, New Zealand

Description:

Yellowish brown friable silt loam derived from greywacke and volcanic ash.

42 Egmont Allophane content = 31%

New Plymouth Hospital, New Zealand

Description:

Silt loam derived from Egmont Andesitic ash shower.

43 Judgeford Silt Loam Allophane content = 10%

Judgeford, New Zealand

Description:

Dark yellow brown silt loam derived from moderately weathered loess from greywacke and volcanic ash.

Soil Number

44 Kaingaroa Loamy Sand

Kaingaroa Forest, New Zealand

Description:

Dark brown firm loamy sand derived from rhyolitic (Taupo) pumice erupted 1700 years ago.

45 Kiripaka Clay Loam

Pakaraka; North Auckland, New Zealand

Description:

Dark brown friable clay loam derived from weathered basalt scoria and ash.

46 Mairoa

Ngapinga Rd.; Mairoa, New Zealand

Description:

Soil described as a yellow-brown clay formed from andesitic and rhyolite ash. It contains allophane, gibbsite and a small amount of iron oxides. "Allophane has been found to be the principle mineral in the clay fractions of soils derived from andesitic and rhyolitic volcanic ash showers in New Zealand" (Birrell and Fields, 1952).

Soil Number

47 Matipiro Silt Loam Allophane content = 6%

Hatuma, New Zealand

Description:

Yellowish brown to pale yellow friable silt loam derived from moderately weathered Pleistocene silts.

48 Ngauruhoe Sand Allophane content = 10%

Mangatoetoenvi Station, New Zealand

Description:

Dark brown sand with lenses of black and of white sand. Soil derived from accumulating andesitic Ngauruhoe ashes on rhyolitic taupo pumice.

49 Papakauri Clay Loam Allophane content = 46%

Kamo, New Zealand

Description:

Red silt loam; friable and mellow. Soil derived from moderately weathered olivine basalt scoria on cone approximately 10, 000 years old.

50 Patua Allophane content = 30%

Carrington Road, New Zealand

Description:

Yellowish brown slightly gritty silt loam derived from andesitic ash.

Soil Number

51 Puketeraki Silt Loam Allophane content = 10%

Porters Pass, New Zealand

Description:

Yellowish brown friable silt loam derived from weathered greywacke loess.

52 Rotomahana Allophane content = 12%

Waimawgu Rel., New Zealand

Description:

Grey-brown friable sandy loam derived from Rotomahana mud, hydrothermically altered rhyolitic ejecta from Lake Rotamahana, erupted 1886.

53 Stratford Allophane content = 13%

Waipuku Station, New Zealand

Description:

Dark yellow-brown gritty silt loam derived from andesitic ash.

54 Taupo Allophane content = 17%

Wharepaina, New Zealand

Description:

Yellow-brown gritty sandy loam derived from rhyolitic Taupo Pumice erupted 1,700 years ago.

Soil Number

55 Tirau Allophane content = 24%

Tirau, New Zealand

Description:

Yellow-brown friable sandy loam derived from Tirau ash. The topsoil includes thin contributions of Taupo and Kaharoa ashes.

56 Waikini Allophane content = 18%

Morton Mains, New Zealand

Description:

Yellowish brown friable silt loam derived from tuffaceous greywacke and schist.

57 Waitcti Silt Loam Allophane content = 10%

Mamaku Plateau, New Zealand

Description:

Yellowish brown friable loamy sand derived from rhyolitic ash.

58 Westown Soil Allophane content = 5%

Westown; New Plymouth, New Zealand

Description:

Described as a brownish-yellow extrasensitive clay derived from andesitic ash. It consists mostly of halloysite with approximately 5% allophane and a small amount of

Soil Number

58 (cont.) iron oxides.

About 300 feet from this sample was a dark brown, brittle, sensitive, very stiff clay from andesitic ash. This sample had halloysite and allophane in equal proportions (Gradwell and Birrell, 1954).

59 Middlemore Soil

Middlemore Hospital, New Zealand

60 Hydrated Halloysite

Lumont, Philippines

Description:

Derived from weathered tuffs and andesite lavas (Dixon, 1963).

61 Podzol

Route 8; Cordoba State Line, Argentina

62 Podzolic

Route 18, Pasa La Laguna, Argentina

63 Podzol

Route 127, Villa Federal

64 Decomposed Basalt

Brazil

Soil Number

64 (cont.) Description:

Consists of a superficial porous layer of clayey or sandy clayey soil underlain by a base stratum of decomposed basalt or sandstone (da Costa Nues and Vargas, 1953).

65 Trumao

Frutillar, Chile

Description:

"These soils, which are of volcanic origin, are generally considered to be similar to volcanic ash soils in other parts of the world because of their high moisture holding capacity and high permeability" (Schalscha, et al., 1965).

66 Trumao

Puerto Octay, Chile

Description: See soil number 65.

67 Trumao

Santa Barbara, Chile

Description: See soil number 65.

68 Perija Soil

Perija Highway, Venezuala

Soil Number

69 Kruzof Island Pumice Soil Allophane content = 50%

Alaska, United States

Description:

Each sample appears to be weathered and contains a significant amount of fine, clay-like material. Some samples have a sandy appearance. Soil was probably deposited as an airfall pumice (ash) (Hannon, 1972).

70 Trail Bridge

Trail Bridge Dam Site; Oregon, United States

Description:

Allophane and hydrated halloysite residual soil (Dixon, 1963).

71 Cool Camp Allophane content = 26%

Western Oregon, United States

Description:

Described as being derived from basaltic colluvium overlying greenish breccia. The soil contains amorphous constituents, smectite-chloritic intergrades and halloysite (McNabb, 1977).

72 Middle Santiam Allophane content = 36%

Western Oregon, United States

Soil Number

72 (cont.) Description:

Described as being derived from red breccia and containing amorphous constituents, halloysite and smectite-chloritic intergrades (McNabb, 1977).

73 Neskowin Silt Loam Allophane content = 19%

Western Oregon, United States

Description:

Described as being derived from Colluvium from weathered basalt and containing morphous constituents, smectite-chloritic intergrades and possibly kaolin (McNabb, 1977).

74 Quillayute Silt Loam

Tillamook County; Oregon, United States

Description:

Black (moist) silt loam derived from alluvium influenced by volcanic ash (Flach, 1964).

75 Windy Sandy Loam

Amador County; California, United States

Description:

Dark grayish brown sandy loam derived from andesitic tuff breccia (Flach, 1964).

Reference Key List

Key Number	Reference
1	Newill, 1961
2	Foss, 1973
3	Terzaghi, 1958
4	Williams, 1963
5	Wooltorton, 1960
6	Dixon, 1963
7	Nixon and Skipp, 1957
8	Matyas, 1969
9	Glynn, 1952
10	Warkentin and Maeda, 1974
11	Warkentin, 1974
12	Martini and Palencia, 1975
13	Flach, 1964
14	Lohnes and Handy, 1968
15	Hirashima, 1948
16	Willis, 1946
17	Nielsen, et al., 1977
18	Wesley, 1973
19	Wesley, 1974
20	Iamura, 1969
21	Hill, et al., 1975
22	Warkentin, 1972
23	Matuo et al., 1953
24	Takeshita, 1957
25	Matsuo, 1957
26	Koizumi and Ito, 1963
27	Yamazaki and Sudo, 1965

Key Number	Reference
28	Hoshino, 1953
29	Endo, et al., 1970
30	Mogami and Kishida, 1961
31	Maeda, et al., 1977
32	Uriel and Serrano, 1973
33	Salas, 1963
34	Wallace, 1973
35	Gradwell and Birrell, 1954
36	Birrell, 1952
37	New Zealand Bureau, 1968
38	Northey, 1966
39	Northey, 1956
40	Taylor, 1967
41	Zalazar, 1948
42	da Costa Nues and Vargas, 1953
43	Schalscha, 1965
44	Barrett, 1948
45	Hannan, 1972
46	McNabb, 1977

APPENDIX B

Field Site Descriptions

Field Site Description

Site Name: Dome Creek Slide Site No.: 1

Elevation: 3025 feet Aspect: South Slope Shape: Concave

Geologic Formation/Parent Materials: Little Butte (Tlt); weathered basalt nodules and light tan volcanic ash.

General Site Description: Headwall of 70, 000 yd^3 landslide. Average talus slope 30^o; average hillslope angle 30^o. Site near headwaters of Dome Creek, topography steepens considerably approximately 1/2 mile west up to dome rock. Hillslopes covered with volcanic ash soils to depths of 30 feet or more. Basalt rock/chip float in most soils.

Soil Sample log:

Sample Number	Depth, from Surface (ft.)	Soil Description
2	3	Moist brown-red friable silt; some basalt nodules.
3-SH*	3-5	Medium brown silt with variable basalt rock chips.
4-SH	5-7	Medium brown silt with variable basalt rock chips. Slightly more rocky.
1	15	Light tan very friable silt.

* SH = Shelby Tube

Field Site Description

Site Name: Dome Creek Cutbank Site No.: 2

Elevation: 3100 feet Aspect: North Slope Shape: Ridge top

Geologic Formation/Parent Materials: Little Butte (Tlt); volcanic ash.

General Site Description: 1/2 mile south of Dome Creek slide on 5 foot shaded roadcut. Slope approximately 28°.

Soil Sample log:

Sample Number	Depth, from Surface (ft.)	Soil Description
1	5-6'	red-brown clayey silt.

Field Site Description

Site Name: Buck Creek Site No.: 3

Elevation: 3280 ft. Aspect: North Slope Shape: Concave

Geologic Formation/Parent Materials: Little Butte (Tlt); volcanic ash matrix supporting basalt cobbles and boulders.

General Site Description: Five foot high roadcut on south shaded portion of road. Soils were moist from recent rains and consist of red brown friable silt with rock, basalt cobble float. Site located on gently sloped hills with large basalt boulders evident. Site slope approximately 25°. Soil depth 3-4 feet. Many roots in upper 2 feet of soil column.

Soil Sample log:

Sample Number	Depth, from Surface (ft.)	Soil Description
1	2-4	Moist red-brown friable silt.
2-SH	3.5-4.5	Moist red-brown friable silt soil becomes rockier, drier and lighter with depth.
3	4.5-5	Light red-brown medium-stiff silt with angular gravel and cobble float.
4-SH	5-7	Moist red-brown silt with basalt cobble float.
5	7	Moist red-brown silt with basalt cobble float.

Field Site Description

Site Name: Pyrimid Creek Cutbank Site No.: 4

Elevation: 3200 ft. Aspect: NW Slope Shape: Convex

Geologic Formation/Parent Materials: Little Butte (Tlt); volcanic ash and decomposed ignimbrite of varying colors. Basalt or andesite bedrock.

General Site Description: Approximate 20 ft. cutbank on edge of steep stream cut. Materials consist of very moist, grey-brown clayey silt at least 10 to 15 feet deep. Average hillslope angle approximately 35 to 40°. Surrounding area characterized by large slump features in forested and clearcut areas. Fresh slumping evident in clearcuts, along stream and road fills and cutbanks.

Soil Sample log:

Sample Number	Depth, from Surface (ft.)	Soil Description
1	3-5	Moist grey brown clayey silt.
2-SH	3-5	Moist grey brown clayey silt.
3-SH	3-5	Moist grey brown clayey silt.

Field Site Description

Site Name: Batchellor Creek Cutbank Site No.: 5

Elevation: 3280 ft. Aspect: North Slope Shape: Concave

Geologic Formation/Parent Materials: Sardine (Tsa); deep well drained ash, weathered basalt bedrock.

General Site Description: Twelve ft. cutband consisting of moist brown friable silt with basalt cobble float. Soil depth approximately 12 feet. Area surrounded by many slumps in roadcuts and clearcuts. Average slope approximately 20°.

Soil Sample log:

Sample Number	Depth, from Surface (ft.)	Soil Description
1	3-4	Yellow brown silt-stiffens with depth.
2-SH	2-4	Yellow brown silt-stiffens with depth.
3-SH	2-4	Moist yellow-brown silt some 1/4 inch sands-stiffens with depth.

Field Site Description

Site Name: Box Canyon Creek Slump Site No.: 6

Elevation: 3600 ft. Aspect: NW Slope Shape: Concave

Geologic Formation/Parent Materials: Sardine (Tsa); volcanic tuffs and ash.

General Site Description: Headwall of small slump in 15 foot road cut. Materials consist of yellow-brown greasy clayey silt with much gravel float. Area surrounded by large older slumps occurring in isolated areas, not a general feature of landscape.

Soil Sample log:

Sample Number	Depth, from Surface (ft.)	Soil Description
1	1.5	Dark brown clayey silt.
2-SH	0.5-1.5	Dark brown clayey silt.
3-SH	1.5-3.5	Yellow-tan slightly plastic clayey silt with variable coloring and stiffness.

Field Site Description

Site Name: Quartzville Creek Cutbank Site No.: 7

Elevation: 2280 ft. Aspect: SE Slope Shape: Concave

Geologic Formation/Parent Materials: Sardine (Tsa); deep volcanic ash with basalt basement rock.

General Site Description: Samples taken near top of 20 foot cutbank. Soils consist of moist medium light brown moist clayey silt with occasional cobbles. Surrounding area is stable basalt with large areas characterized by deep rotational sliding in clearcut and forested areas. Average slope is 25-30°.

Soil Sample log:

Sample Number	Depth, from Surface (ft.)	Soil Description
1	4-6	Moist light brown clayey silt.
2-SH	4-6	Moist light brown clayey silt.
3-SH	3-5	Moist light brown clayey silt.

Field Site Description

Site Name: Fritz Creek Slump Site No.: 8

Elevation: 4200 ft. Aspect: NE Slope Shape: Concave

Geologic Formation/Parent Materials: High Cascade Volcanics (Qtv); Volcanic ash with gravel and cobbles, dacitic bedrock.

General Site Description: Sample taken in headwall scarp of small roadcut failure. Soil is moist friable yellow brown gravelly sandy silt with scattering of cobbles. Surrounding area is very slumpy indicative of continuing small rotational movements, or areas of creep. Average slope approximately 30^{o}.

Soil Sample log:

Sample Number	Depth, from Surface (ft.)	Soil Description
1	1-3	Moist yellow brown gravelly sandy friable silt, inhomogeneous with some cobbles.
2-SH	1-3	Moist yellow brown gravelly sandy friable silt, inhomogeneous with some cobbles.
3-SH	1-3	Moist yellow brown gravelly sandy friable silt, inhomobeneous with some cobbles.

Field Site Description

Site Name: Lookout Creek Cutbank Site No.: 9

Elevation: 3150 ft. Aspect: East Slope Shape: Concave

Geologic Formation/Parent Materials: Sardine (Tsa); volcanic ash and breccia with basalt bedrock.

General Site Description: Twenty ft. cutbank near ridgetop. Material consists of dark brown mottled inhomogeneous silt with some basalt cobbles and boulders. Surrounding area is forested stable slopes. Average slope 20-25°.

Soil Sample log:

Sample Number	Depth, from Surface (ft.)	Soil Description
1	7-8	Brown tan friable sandy silt.
2-SH	7-9	Brown tan friable sandy silt.
3-SH	9-11	Moist dark brown sandy silt with cobbles.
4	10-11	Moist dark brown sandy silt with cobbles.

Field Site Description

Site Name: Alaska-4 Shelikof Site No.: 10

Elevation: 900 ft. Aspect: NE Slope Shape: Convex

Geologic Formation/Parent Materials: Glacial till substratum; weathered volcanic ash.

General Site Description: Gently sloping hills. Site is on edge of stream V-notch.

Soil Sample log:

Sample Number	Depth from Surface (ft.)	Soil Description
1	1-4	Orange brown and grey medium plastic sandy-silty clay
2	1-4	Orange brown and grey medium plastic sandy-silty clay
3-SH	1-4	Orange brown and grey medium plastic sandy-silty clay
4-SH	1-4	Orange brown and grey medium plastic sandy-silty clay
5-SH	1-4	Orange brown and grey medium plastic sandy-silty clay
6	2	Orange brown and grey medium plastic sandy-silty clay

Field Site Description

Site Name: Alaska-5 Sitka Site No.: 11

Elevation: 650 ft. Aspect: NE Slope Shape: Convex

Geologic Formation/Parent Materials: Twenty-forty inch deep volcanic ash underlain by glacial till.

General Site Description: Gently sloping hills. Site is on a stream V-notch.

Soil Sample log:

Sample Number	Depth, from Surface (ft.)	Soil Description
1	1-2	Orange brown sandy-silty clay
2	1-2	Orange brown sandy-silty clay
3-SH	1-4	Orange brown sandy-silty clay
4-SH	1-4	Orange brown sandy-silty clay
5-SH	1-4	Orange brown sandy-silty clay
6	2	Orange brown sandy-silty clay

APPENDIX C

Sampling and Engineering

Laboratory Procedures

APPENDIX C

Sampling Procedures

Undisturbed Sampling

After the general area location was identified, suitable specific sampling sites were chosen in roadcuts or slump headwalls based on the following criteria.

1. The site must be representative of typical surficial materials in the area.
2. The site soils must be deep enough to obtain suitable length samples.
3. Soils must have minimum amounts of roots and cobbles. Large rocks or roots preclude insertion of thin wall tube.
4. Site must appear to be shaded a considerable portion of the day.
5. Soils must not have been previously disturbed.

Figure C1 shows a typical sample site from Pyrimid Creek.

Undisturbed sampling procedure was as follows: assemble the frame over desired sampling site and connect the thin walled tube to the loading head. Place open end of tube on ground in straight line with push rod so that lateral forces are not imposed on the sample during sampling. Figure C2 shows the frame and shelby tube set up

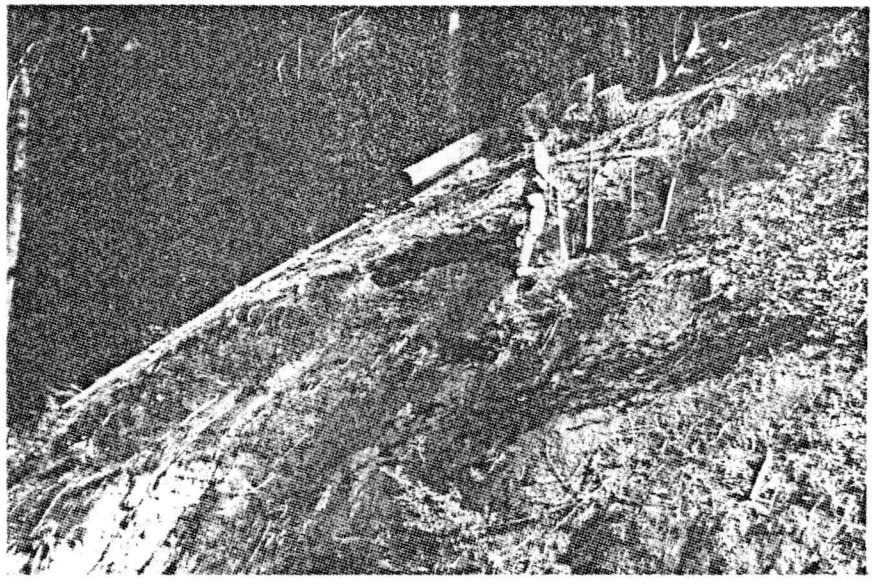

Figure C1. Typical sampling site.

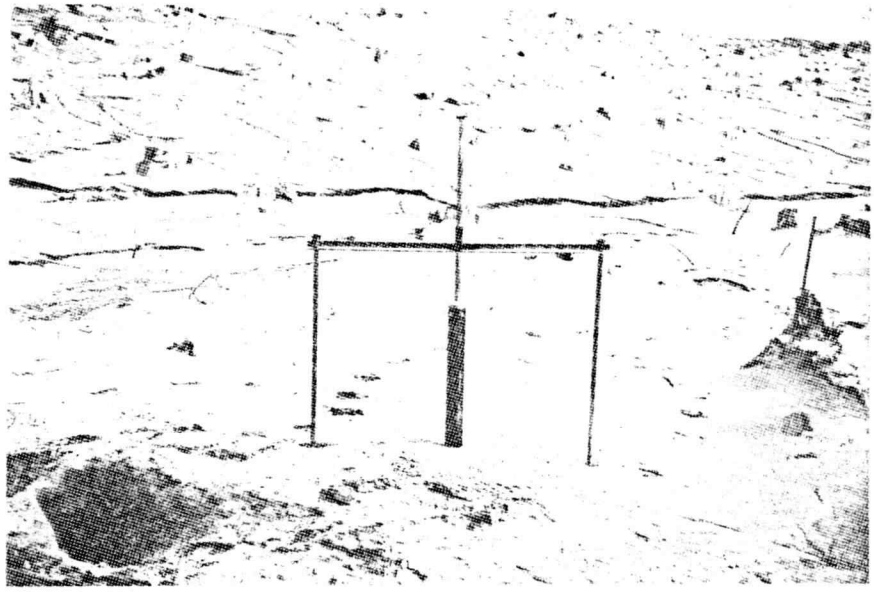

Figure C2. Sample frame and shelby tube.

and ready to push. The support frame prevents lateral movements and allows smooth, steady vertical movement of the shelby tube during the pushing and trimming sequence.

To fill tube, excavate around the tube leaving an approximate 6 to 12 inch diameter pedestal of undisturbed material, 3 or 4 inches high. For most soils, the tube can easily be pushed 3 or 4 inches. Construct another pedestal below the first and push the tube. Repeat this sequence until a desired length of sample has been inserted into the tube. For stiff soils, the pedestal can be trimmed to slightly larger than tube diameter. The tube can easily be pushed over this trimmed soil plug. If small rocks or roots are encountered, the tube can be gently tapped past the obstruction. Figure C3 shows pedestal excavation with the tube nearly full.

Field and laboratory observations indicate that reasonably good undisturbed samples were obtained in soft to medium stiff soils of low to high cohesion, if large rocks or roots were not encountered. If rock was soft, generally the tube cut through. If hard rock was encountered, the rock or cobble was often pushed out of the path of the tube cutting edge, destroying the undisturbed structure of the sample. If large obstructions were encountered during sampling, the frame was moved laterally, and the site re-sampled.

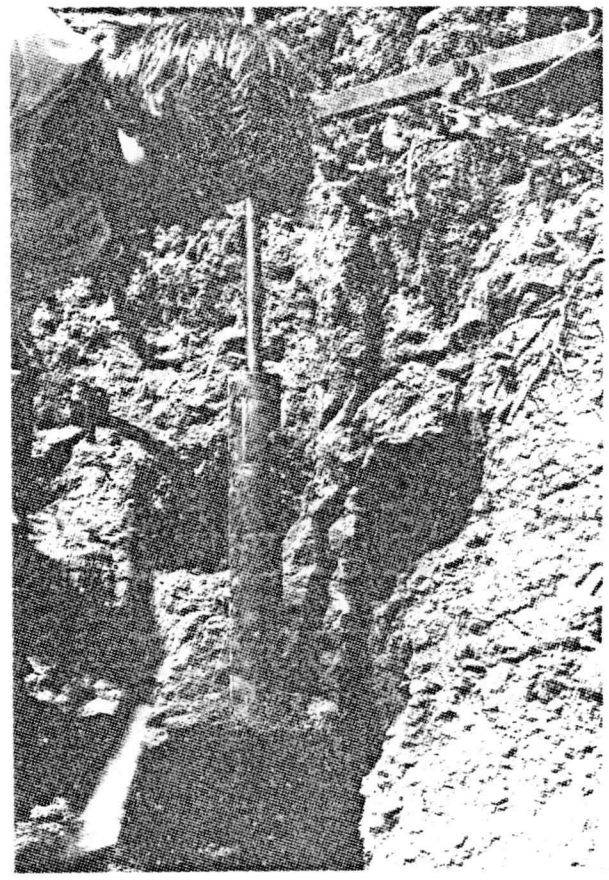

Figure C3. Undisturbed sampling technique.

Disturbed Sampling

For each site, 1 or 2, plastic lined canvas bags were filled with 20 to 40 pounds of material excavated from around the tube during undisturbed sampling. Jars were also filled with this material.

Sample Storage

All samples were stored in a cool, humid-room until needed for testing.

Laboratory Engineering Testing Procedures

Moisture Contents

All moisture contents were determined by ASTM Designation: D2216. The samples were dried to equilibrium for 24 hours at a constant oven temperature of 110°C.

Actual moisture contents were determined on whole soil samples taken from the jars, bags, and shelby tubes. Jar sample moisture contents were determined immediately upon arrival in the laboratory. Shelby tube natural moisture contents were determined for each sample extruded for strength testing. Bag sample natural moisture contents were determined during grain size analysis. Drying of some of the bag samples may have occurred between sample storage and

water content determination due to splitting of bags, etc.

Natural moisture contents from the jar samples represent an approximate 2 foot cross-section of soil through which the shelby tubes were pushed. Natural moisture contents from the shelby tube strength samples represent a more localized value; representative over the 7-10 inch length of each extruded soil sample.

Atterberg Limits

Atterberg limits were performed on samples from each site for natural moisture, air dry, and oven dry conditions.

For the natural moisture condition, several steps were required for sample preparation. These were:

1. A representative mass of soil at the natural moisture content was allowed to soak overnight in distilled water.
2. The soaked soil was then wet sieved through a number 40 U. S. Standard mesh screen by repeated stirring, spraying and soaking, until all minus #40 material had passed through the screen.
3. The water and minus number 40 soil suspension were then poured into a plaster of paris bowl coated with filter paper. Water was air evaporated from the suspension in the bowl until a thick slurry formed. The bowl and filter paper allowed even evaporation of water from the suspension

without forming a drying crust around the edges.

4. The filter paper containing the slurry was removed from the bowl and wrapped around the slurry. The slurry was air dried to a water content slightly above the liquid limit. The sample was then ready for liquid limit and plastic limit determinations.

The liquid limit for the natural moisture condition on the minus #40 material was determined according to ASTM designation D423 except that the three blow count determinations for plotting of the flow were successively dried to the desired water content rather than wet. The plastic limit for this case was determined according to ASTM procedure D424. The plastic index was determined by subtracting the plastic limit from the liquid limit.

For the air dried case, the liquid and plastic limits were determined exactly as outlined in ASTM designations D423 and D424 respectively.

For the oven dry case, sample preparation is the same as that for the air dry case except the minus number 40 material was oven dried at 110^{o}C for 24 hours, and allowed to cool to room temperature. Liquid and plastic limits were then determined as before.

Specific Gravity

Specific gravity for each sample was determined by the method prescribed by ASTM Designation: D854. All samples were air dried

then, approximately 50 grams of lightly crushed total sample were poured into the calibrated pyenometer. De-aired distilled water was used as the displacement fluid. Air was removed by slight heating and vacuum. Floating organic matter, if present, was removed by dipping a paper towel into the pycnometer.

At least two and sometimes three tests were conducted on each sample. Tests were run until variation in test results were minimal. The final specific gravity values were taken as the average of tests run, excluding obvious bad values. Most of the samples tested yielded consistent and reasonable results.

Grain Size

A partial grain size fractionation was determined for each sample site, on whole soil at the natural water content. This fractionation was performed in several steps as follows:

1. A representative mass of soil at the natural moisture content was allowed to soak overnight in distilled water. The weight and water content of this mass was measured, and total dry sample weight calculated.
2. The soaked soil was then wet sieved through a number 40 mesh screen by repeated stirring, spraying and soaking, until all minus #40 material had passed through the screen.

3. The water and minus number 40 soil suspension were poured into a plaster of paris bowl coated with filter paper. Water was air evaporated from the suspension in the bowl until a thick slurry formed.
4. The plus 40 material was dried and weighed. Percent retained on the #40 sieve was calculated by dividing dry weight of plus #40 material by the total dry sample weight.
5. The suspension slurry was split into two samples. The sieve analysis portion of the minus 40 suspension slurry was weighed, and water contents taken. Dry weight was determined for this part. The other part was used for Atterberg limits determination.
6. The sieve analysis suspension was wet sieved through the number 200 sieve by repeated stirring, spraying and soaking until all of the minus 200 material had passed through the screen.
7. The plus 200 material was dried and weighed. Percent retained on the number 200 sieve was calculated by dividing by the dry weight of the suspension sample, and multiplying this result by the decimal percentage passing the number 40 screen. Percent passing the #200 is simply the remaining percentage of total sample not accounted for on the number

40 or number 200 screens.

8. In this way, percent retained on the number 40, percent retained on the number 200, and percent passing the number 200 sieves were determined for each sample.

Observations during lab testing indicate that minimal amounts of material were larger than 1/4 inch size. Particles this size or larger were usually easily crushed. Since most of the larger grains appear to be aggregates of mush smaller particles, it is thought that drying, grinding, and mechanical shaking of materials would yield significantly different results than those obtained by wet sieving. Further it has been found that the amount of drying and the time of grinding and shaking have very large influences on grain size distribution results (Wesley, 1973; Martini and Palencia, 1975).

Moisture Density

Moisture density relationships for each sample of interest were determined for conditions at natural moisture, air dry, and oven dry.

For natural moisture tests, Proctor points were run for samples dried from natural conditions, and if appropriate, wet up from natural conditions. Maximum dry densities were determined for points 4 to 6 percentage points apart, for both cases. Samples were prepared by hand breaking moist soil peds to sizes less than 1/4 inch in diameter. After soil preparation, the moisture density curves were run according

to ASTM designation D698 except that the soil was dried between points rather than wet.

For air dry conditions, the soils were wet, from the limit of drying for the natural case. From this minimum water content, maximum dry densities, and optimum water contents were determined according to ASTM designation D698. The soil was from the same batch as that used for natural moisture content conditions.

For the oven dry case, a different batch of soil was oven dried for 24 hours at 110°C. The soil was then passed thru a number 4 U. S. standard sieve. Points describing the relationship between moisture content and density were then determined according to ASTM D698.

Insitu Density

Insitu density was determined for undisturbed samples by measuring the volume and weight of undisturbed shear strength samples extruded and cut from the shelby tubes. Water contents were determined, and dry densities calculated using $\gamma_d = \frac{\gamma}{1+w}$; where γ_d = dry density, γ = wet density, and w = water content of the extruded sample.

Strength

Stress-strain and pore pressure behavior was investigated by developing a Mohr envelope of effective stresses for undisturbed

samples from each site. Three or four consolidated undrained triaxial test samples saturated with backpressure, were failed at low confining pressures. Pore pressure changes were recorded during failure. Conventional triaxial testing procedures were followed throughout the testing sequence.

Equipment

Equipment used for strength testing consisted of three major component systems. These were the pressure system, the triaxial cell and the recording system.

Two pressure systems were required as shown in Figure C4. Confining pressures were provided by regulated compressed air pressure, tapped into the top of the cell. Backpressure was provided with a mercury pot system. The mercury pots were connected into one of two pore pressure taps at the base of the sample. The mercury pots apply pressure to the inside of the sample when raised above the sample base, the pressure being equal to the unit weight of mercury times the height of mercury above sample. These two pressure systems, capable of maximum pressures of about 60 psi, allow regulation of both the confining pressure and internal pore pressure such that the effective confining pressures (confining pressure - pore pressure) applied to the sample could be adjusted to about $\pm$ 05 psi.

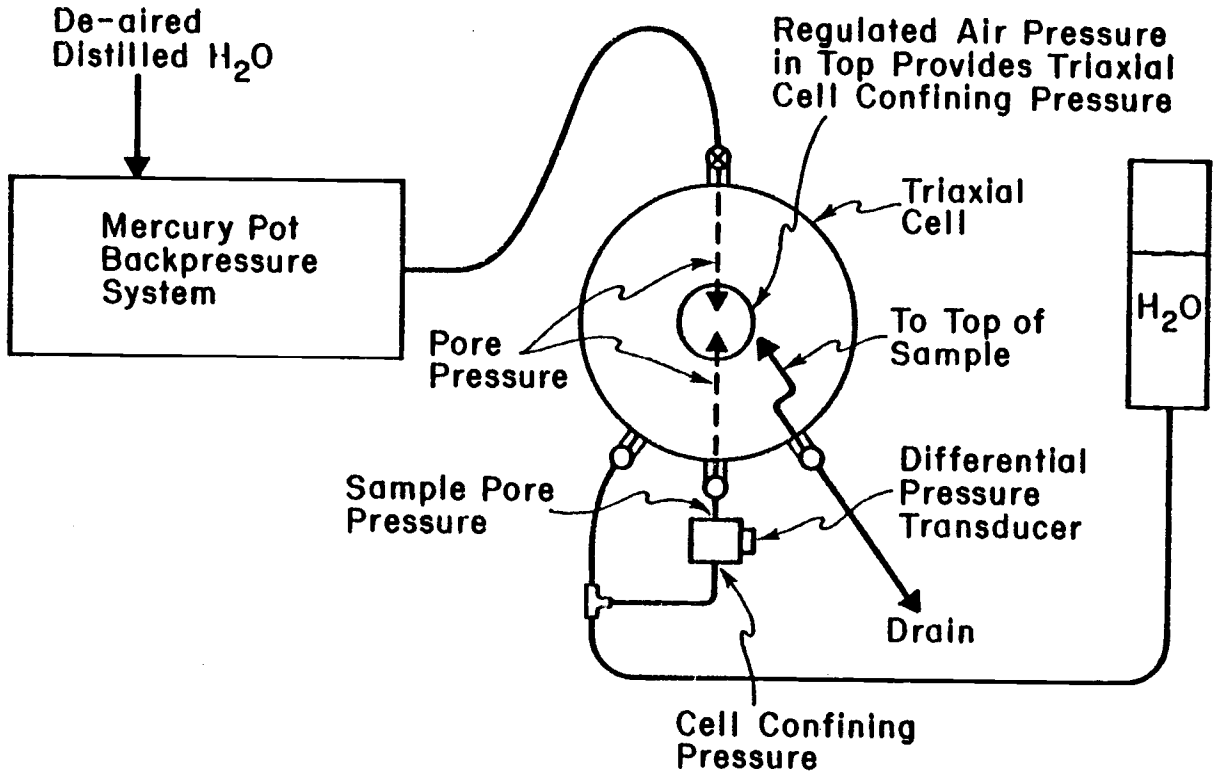

Figure C4. Schematic of triaxial cell and pressure system.

The cell, shown schematically in Figure C4 and pictorally in Figure C5, is capable of accommodating samples 2.8 inches in diameter and 7 inches high. Figure C4 shows that the top of the samples were connected to an external drain. This top drain allowed flow of water through the sample, from bottom to top, for purposes of de-airing. A special low friction seal system, developed and reported by Chan (1975) was adapted for use on this cell. Figure C6 shows that this low friction system allows the axial loading rod to move with negligible friction, eliminating the need for a correction for resistance in the rod. Figure C6 also shows that the air pressure, introduced into the low friction system housing, transmits the cell confining pressure to the sample across an air, cell water interface.

The recording system consists of several components which measure water pressures, axial stresses and axial strains. All of these measuring devices were connected to a Validyne Model MC1 signal conditioner which output stress-strain readings to an x-y recorder and pore pressure readings to a didgitized LED display. This system is shown in Figure C7.

Water pressures were measured with the Validyne Model DP 215 differential pressure transducer shown in Figure C8.

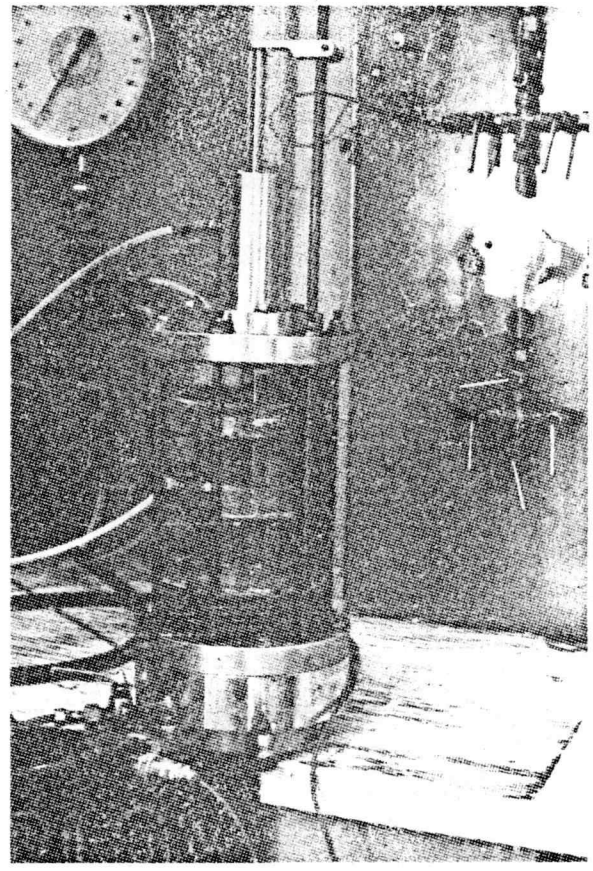

Figure C5. Triaxial cell.

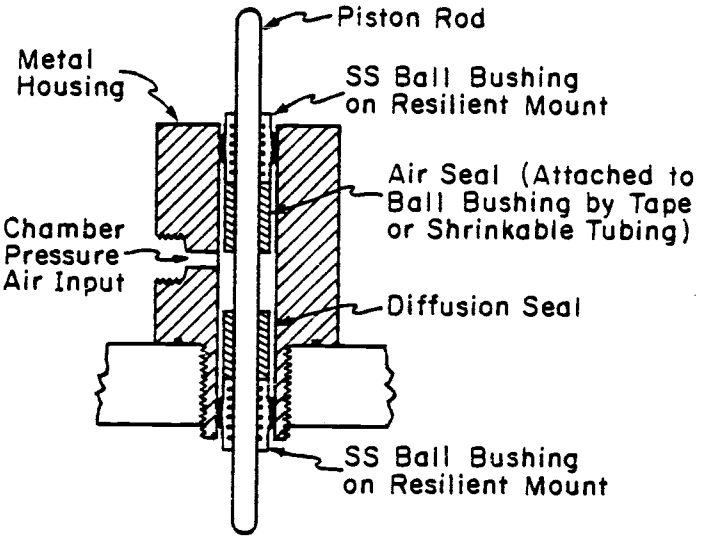

Figure C6. Low friction seal system (Chan, 1975).

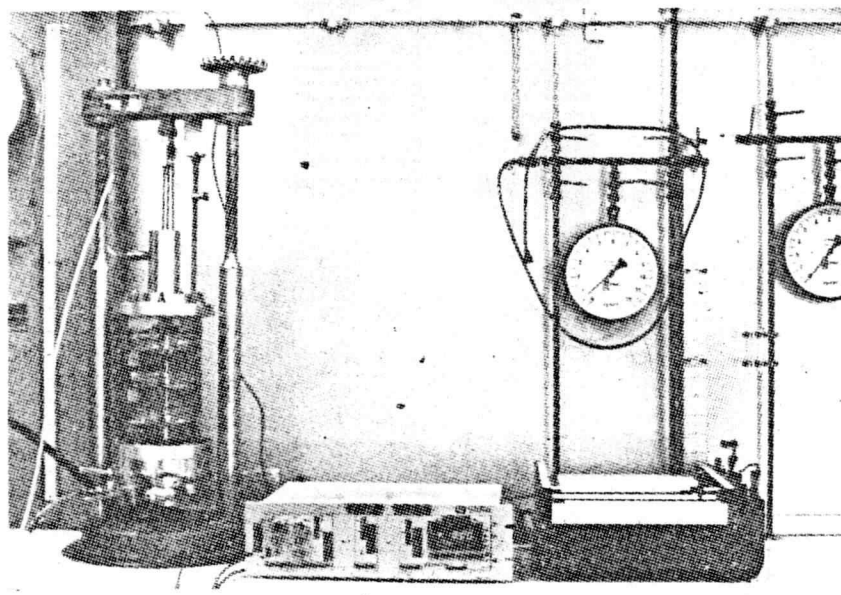

Figure C7. Load frame, triaxial cell and recording system.

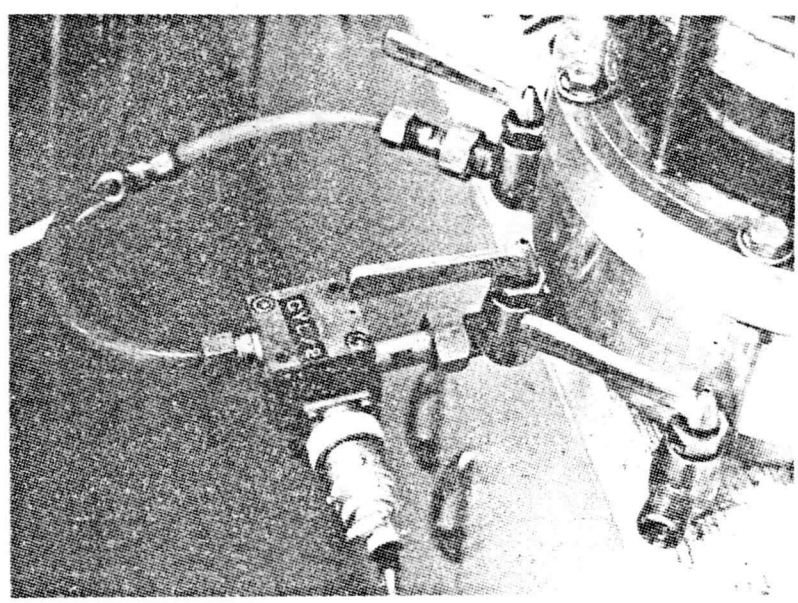

Figure C8. Differential pressure transducer.

This pressure transducer was electrically connected to a Validyne CD 18 Carrier Demod unit in the signal conditioner. The differential pressure transducer measured the difference between the outside confining pressure and the sample pore pressure. With this device, small effective confining pressures (less than 1 psi) can be imposed on the sample. During failure, the change in pore pressure was measured as the difference between the differential pressure readings during failure, and the initial confining pressure. Output from the differential pressure transducer into the signal conditioner was calibrated to readout on the LED display in units of psi to hundredths. A positive reading indicated that cell pressures were larger than pore pressures. A negative reading indicated the opposite was true.

Axial forces were measured with an Interface 250 load cell electrically connected to a Validyne SG 71 Strain Gage Amplifier in the signal conditioner system. The load cell was bolted to the top of the load frame. Axial loads were transmitted to the sample through the load cell, which connected with the load rod. Axial compressive force was then output in pounds through the calibrated signal conditioner, LED output device.

Axial strains were measured with a linear variable differential transformer (LVDT) type GCA 121-1000 made by Shaevitz Engineering. The LVDT was electrically connected to a Validyne CD 148 Carrier Demod unit plugged into the signal conditioner system. This particular

LVDT was capable of a 2 inch displacement. The LVDT was mounted on the load frame so that relative movements between the axial load rod and the triaxial cell were measured. In this way, the vertical deflection of the top of the sample was determined. Distances were calibrated to read in inches on the LED display.

During failure, stresses and strains input into the signal conditioner were again output to a Houston Instrument Omnigraphic 2000 x-y Recorder. The x-y recorder was calibrated to produce a force-deflection curve from which stress and strain could be determined. Pore pressure changes were recorded by hand along the curve at appropriate intervals, from the LED display.

Sample Preparation and Test Procedure

The determination of stress-strain-pore pressure behavior for each sample tested required the performance of three major tasks. These were:

1. Preparation of the undisturbed samples for testing. This requires the transfer of fragile samples from the shelby tubes to the triaxial cell without sample disturbance.
2. Saturation of samples by flow through of water and incremented backpressure sequences.
3. Axial loading and failure of samples.

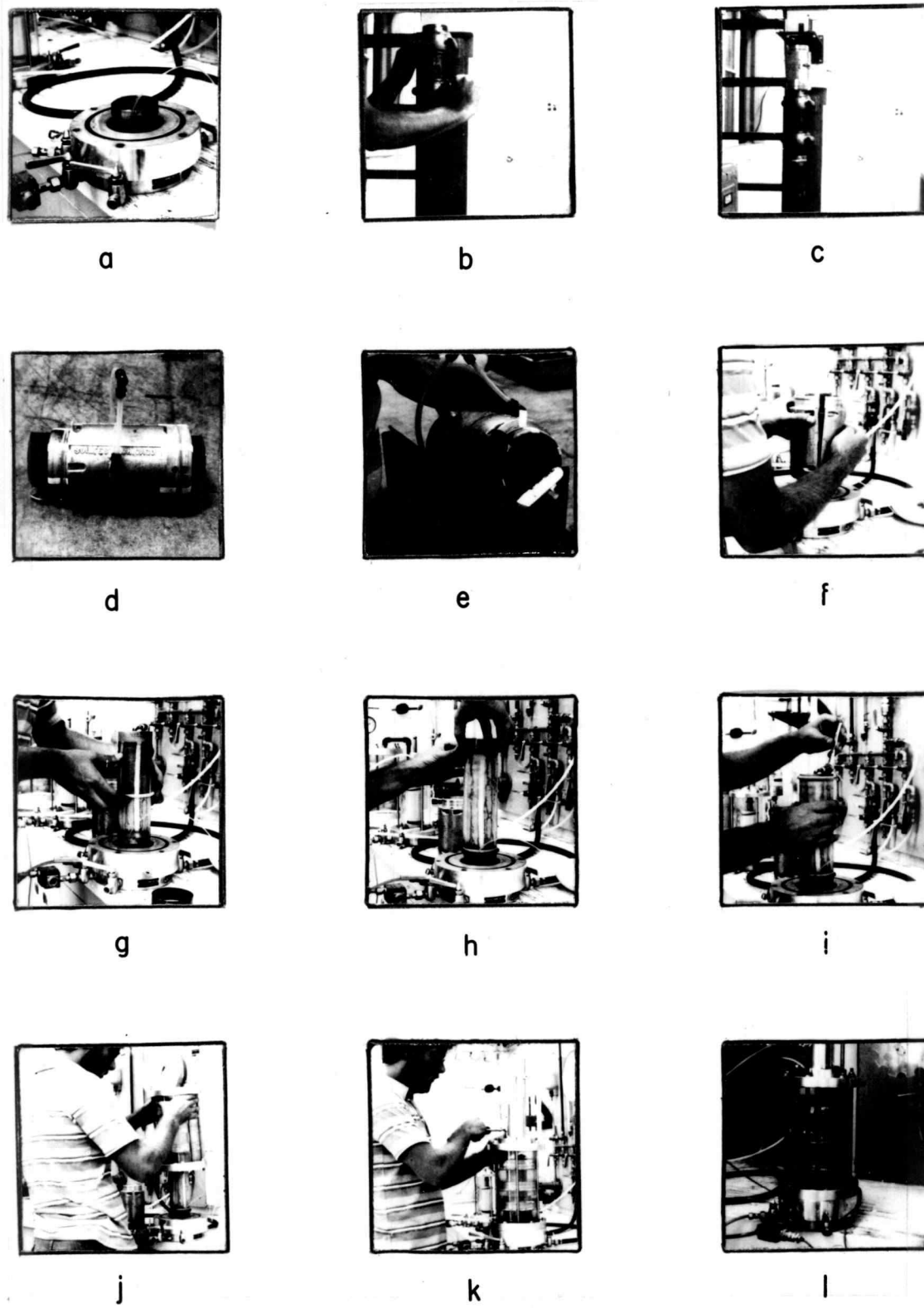

Figure C9. Sample preparation sequence.

Sample preparation proceeded in several steps as shown in Figure C9; Steps a through i. Each step in Figure C9 is described as follows:

step a - The cell base is readied for assembly. All parts, valves and tubes are saturated.

step b - The shelby tube containing the sample is being fit into the extrusion device.

step c - A sample is extruded into the vacuum mold. The mold, slightly larger than the sample accommodates a .012 inch thick rubber membrane, several filter paper drain strips, and allows easy extrusion of undisturbed soil cylinders into the mold. The membrane is stretched inside the mold, drainage strips are then placed and held in place with rubber bands. A vacuum applied to the mold holds the membrane and drainage strips tightly, in the form of the mold.

step d - Sample in the vacuum mold has been cut from remaining sample in the tube.

step e - Sample ends are trimmed so they are smooth and level. Trimmings from both ends are used to determine the water content of the sample. The trimmed sample is weighed.

step f - The sample is centered on the base with porous stones top and bottom. Membrane ends are rolled up, and the split mold is removed.

step g - A second rubber membrane is rolled up along the sample. This extra protection guards against leaking between the cell and sample interior.

step h - The top cap is placed above the top porous stone, and O-rings are snapped into place top and bottom.

step i - External drainage tap is connected to the top-cap.

step j - The cell wall is then lowered over the sample and bolted into place.

step k - The frictionless seal system containing the air tap and axial local rod assembly is bolted into place.

step l - The cell is filled with de-aired water, a slight confining pressure is applied, and de-aired distilled water is allowed to flow through the sample, porous stones, and drain assembly such that trapped air is forced into the top-cap and out the external drain.

After de-aired distilled water was allowed to flow through the sample for several hours (usually overnight), the samples were further saturated by a simple backpressuring procedure which involved incremental increases in confining and pore pressures. The incremental backpressure sequence was as follows:

1. Initial confining pressure and differential pressure transducer readings were recorded. The transducer reading (Pd_o) is equal to cell confining pressure (σ_3) minus pore pressure (u).
2. Pore pressure taps were closed and σ_3 was raised by the amount $\Delta\sigma_3$. As σ_3 increased, u increased by the amount Δu. Care was taken not to raise the effective confining pressure (Pd') above the confining pressure to be used for subsequent test failure. The change in confining pressure ($\Delta\sigma_3$) and the final differential pressure transducer reading (Pd') were noted. The change in porepressure (Δu) and Skempton's B pore pressure parameter were calculated from these measured values, and Pd_o as follows:

$$B = \frac{\Delta u}{\Delta \sigma_3} \qquad \text{and} \qquad Pd_o = \sigma_3 - u$$

$$Pd' = (\sigma_3 + \Delta\sigma_3) - (u + \Delta u)$$

$$Pd' - Pd_o = \Delta\sigma_3 - \Delta u$$

$$\Delta u = \Delta\sigma_3 - Pd' + Pd_o$$

$$B = \frac{\Delta\sigma_3 - Pd' + Pd_o}{\Delta\sigma_3}$$

3. A pressure equal to the new porewater pressure ($u + \Delta u$) was applied to the inside of the sample. This internal pressure was then raised so that Pd_o was small (usually about 1 psi). The sample was then allowed to equilibrate for several hours under the new pressures. In this way, the internal pore water pressure can be incrementally increased without increasing effective stresses on the sample. Increasing pressures force pore-air into solution thus, saturating the sample.
4. After a time (usually 2 to 3 hours), Steps 1 to 3 were repeated. All samples were incrementally back pressured until B approached 1. This usually occurred at pore water pressures of about 50 to 60 psi.
5. When high B pore pressure parameters were achieved, the samples were consolidated by increasing σ_3, and leaving u constant and open to the mercury pot system. In this way, the desired confining pressure was achieved, and excess pore water pressure could dissipate into the mercury back pressure system. The samples were allowed to consolidate overnight (about 12 hours) before testing.

Sample failure was conducted in a conventional manner. Undisturbed samples from each site were axially failed at confining pressures of 5, 10 and 15 psi. All samples were failed under undrained conditions at a constant strain rate of .61 percent per minute. It can

be shown by conventional methods that this strain rate is slow enough to allow equilibration of pore pressure for these particular soils. Load frame and gear box configurations limited the strain rate to this value. Failure of each sample proceeded as follows:

1. The consolidated sample was placed in the load frame. The load cell, and LVDT were initialized, and the x-y plotter set to zero.
2. The backpressure tap was closed at the same time axial loading began. Differential pore pressure tranducer readings were recorded directly on the load-deflection plot at frequent intervals. Figure C10a shows the cell in the load frame during loading. Figure C10b shows the load-deflection curve with pore pressure measurements being plotted. All samples were loaded to about 20% strain.
3. The triaxial cells were dismantled and the samples removed. A sketch of each failed sample was made. Figure C11 shows a typical failed sample.

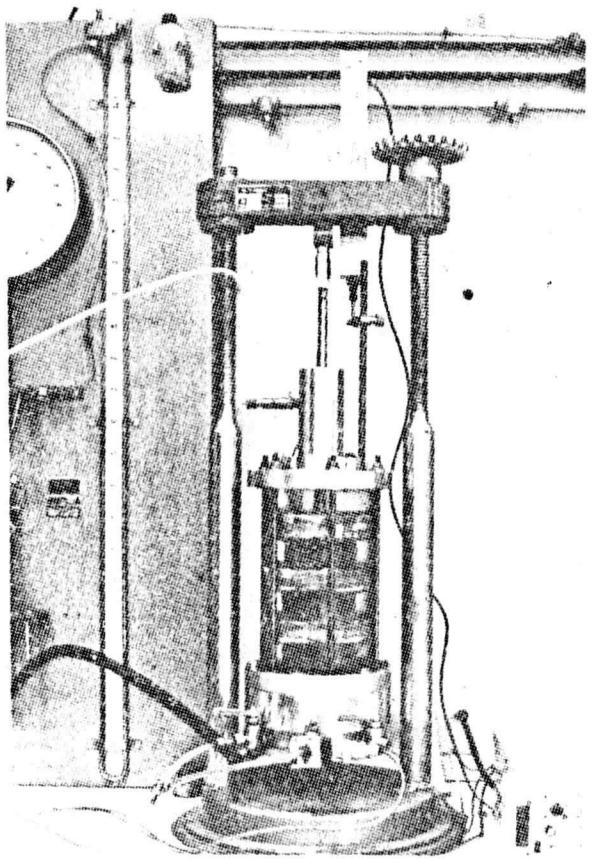

(a)

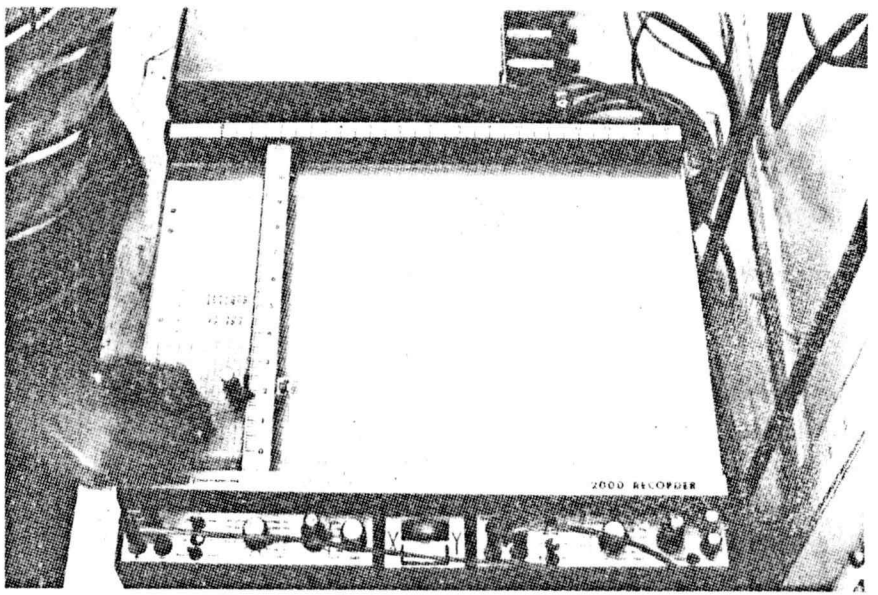

(b)

Figure C10. (a) Cell in loading frame during loading; (b) x-y plotter.

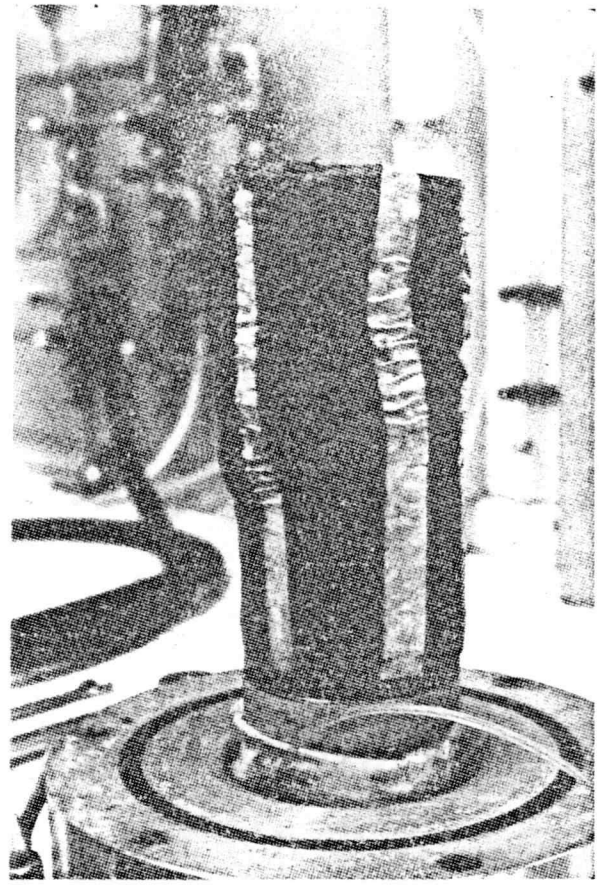

Figure C11. Typical failed sample.

APPENDIX D

Engineering Laboratory Test Results

Summary of Strength Data

APPENDIX D

Strength Results

Introduction

Appendix D presents detailed data determined from strength testing for each site including a summary of insitu values and a summary of effective stress strength parameters.

Plots in Appendix D for each site include:

Deviator Stress vs Strain

Pore Water Pressure vs strain

Major Principal Stress Ratio vs Strain

One Half Deviator Stress vs Average Principal Stress

Mohr Effective Stress Envelope - Maximum Stress - Strain Case

Mohr Effective Stress Envelope - Maximum Stress Ratio Case

Each set of summaries and plots are grouped together by site, and arranged according to site number.

Strength testing summary of sample and test data

Site 1 - Dome Creek

Effective Consolidation Pressure ($\sigma_3 - U_o$ in Kg/cm^2)	0.35	0.70	1.41
Natural Moisture Content (W_n in %)	37.5	42.6	38.7
Insitu Wet Unit Weight (γ in g/cm^3)	1.35	1.44	1.29
Insitu Dry Unit Weight (γ_d in g/cm^3)	0.98	1.01	0.93
Insitu Degree Saturation (S in %)	56.9	66.2	54.1
Cell Pressure during Test (σ_3 in Kg/cm^2)	3.71	4.38	3.82
Initial Pore Pressure (U_o in Kg/cm^2)	3.36	3.68	2.41
B-Pore Pressure Parameter during Test (Ratio)	0.99	0.99	0.99

Strength testing summary of effective stress strength parameters

Site 1 - Dome Creek

For Mohr Envelope Derived from Stress-Strain Maximum Values				
Effective Consolidation Pressure ($\sigma_3 - U_o$ in Kg/cm^2)		0.35	0.70	1.41
Deviator Stress at Failure ($\Delta\sigma_1$ in Kg/cm^2)		0.40	2.95	0.88
Pore Pressure at Failure (ΔU in Kg/cm^2)		0.24	0.15	1.05
Axial Strain at Failure (ϵ in %)		2.0	2.8	1.7
A-Pore Pressure Parameter at Failure (Ratio)		0.60	0.05	1.19
Effective Angle of Internal Friction (ϕ' in Degrees)	$\phi' =$	49.7		
Effective Cohesion Intercept (C' in Kg/cm^2)	$C' =$	-0.14		
Correlation Coefficient (r - dimensionless)	$r =$	.9947		
For Mohr Envelope Derived from Stress Ratio Maximum Values				
Effective Consolidation Pressure ($\sigma_3 - U_o$ in Kg/cm^2)		0.35	0.70	1.41
Deviator Stress at Failure ($\Delta\sigma_1$ in Kg/cm^2)		0.39	2.40	0.78
Pore Pressure at Failure (ΔU in Kg/cm^2)		0.27	0.40	1.17
Axial Strain at Failure (ϵ in %)		5.0	1.6	7.0
A-Pore Pressure Parameter at Failure (Ratio)		0.69	0.17	1.50
Effective Angle of Internal Friction (ϕ' in Degrees)	$\phi' =$	57.3		
Effective Cohesion Intercept (C' in Kg/cm^2)	$C' =$	-0.15		
Correlation Coefficient (r-dimensionless)	$r =$	.9949		
For Mohr Envelope Derived from Effective Stress Path Plot				
Effective Angle of Internal Friction (ϕ' in Degrees)	$\phi' =$	56.1		
Effective Cohesion Intercept (C' in Kg/cm^2)	$C' =$	-0.12		
Correlation Coefficient (r-dimensionless)	$r =$	.9953		

DOME CREEK SITE 1
UNDISTURBED TRIAX W/ BACKPRESSURE
DEVIATOR STRESS VS STRAIN

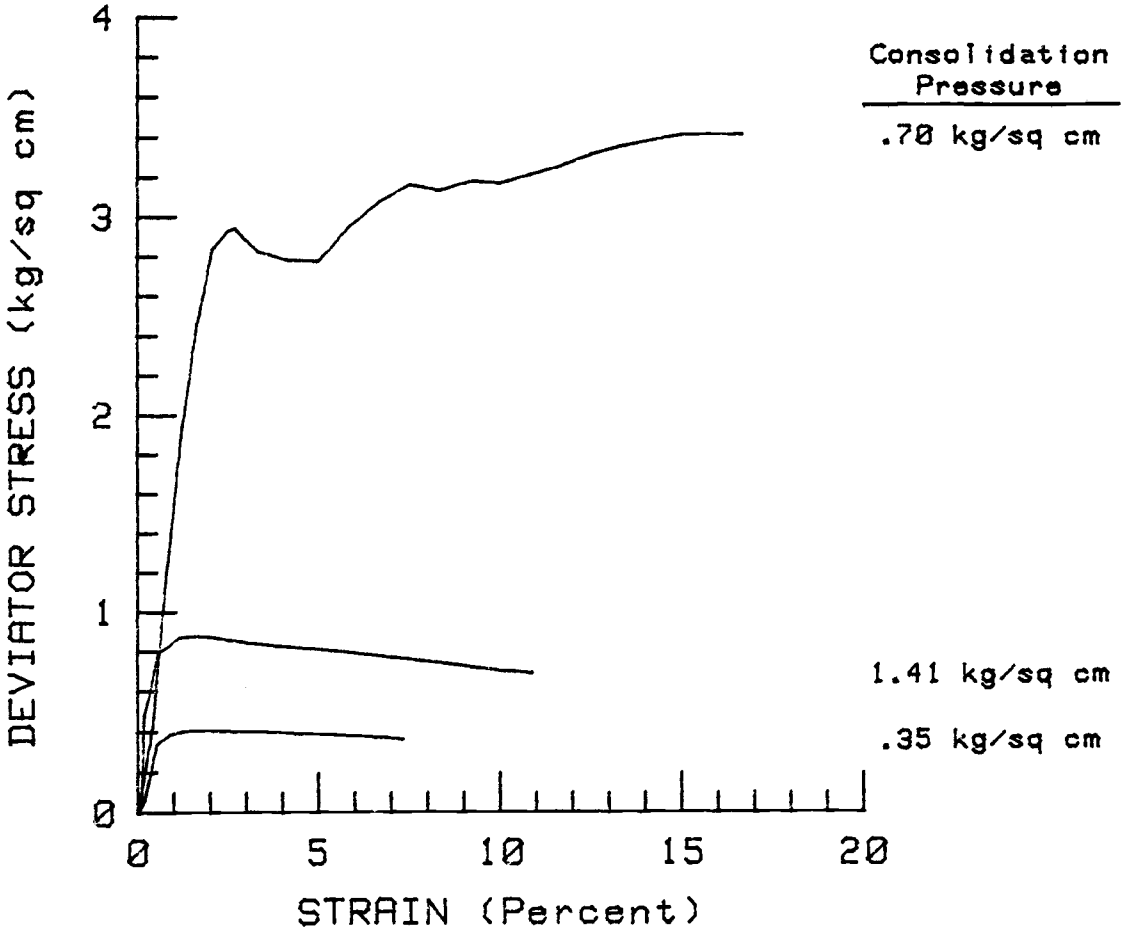

DOME CREEK SITE 1
UNDISTURBED TRIAX W/ BACKPRESSURE
PORE WATER PRESSURE VS STRAIN

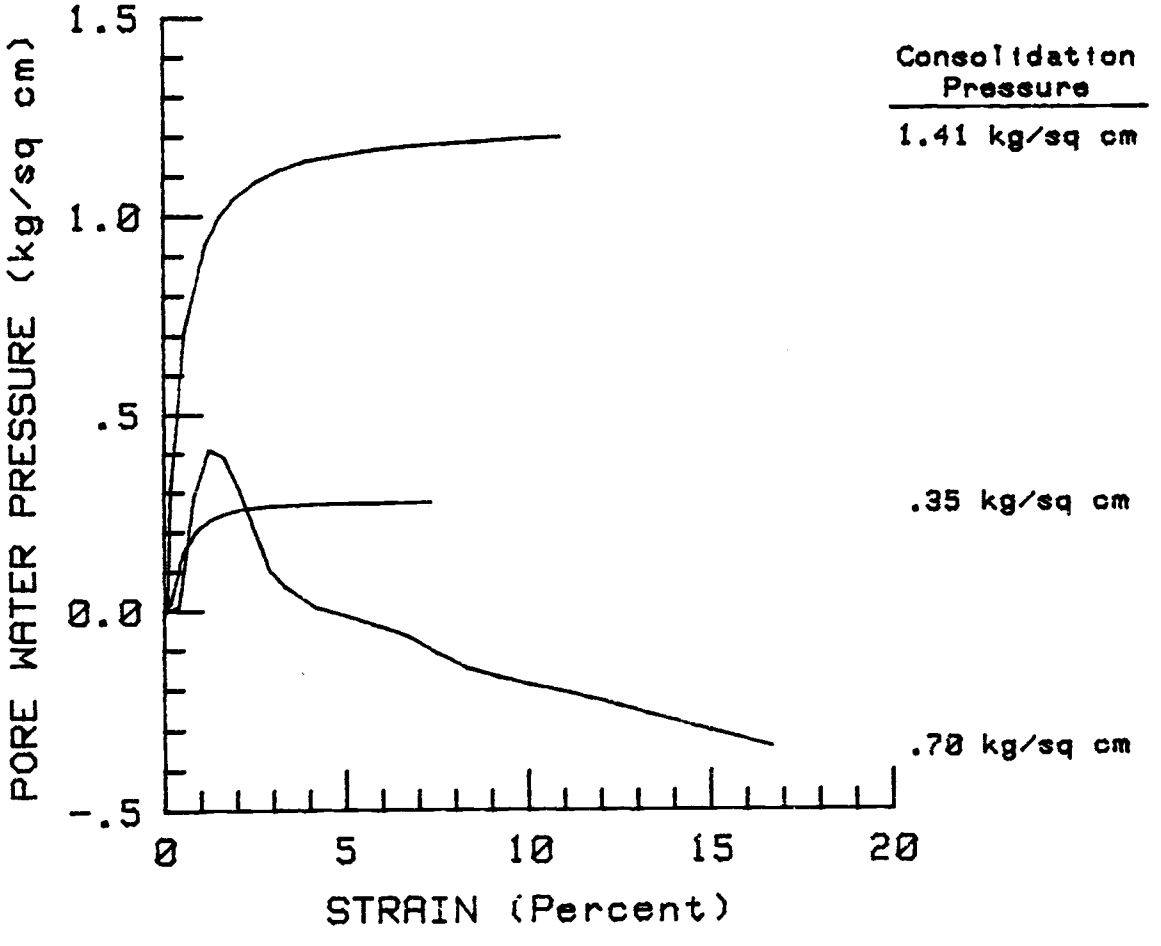

DOME CREEK SITE 1
UNDISTURBED TRIAX W/ BACKPRESSURE
MAJOR PRINCIPAL STRESS RATIO VS STRAIN

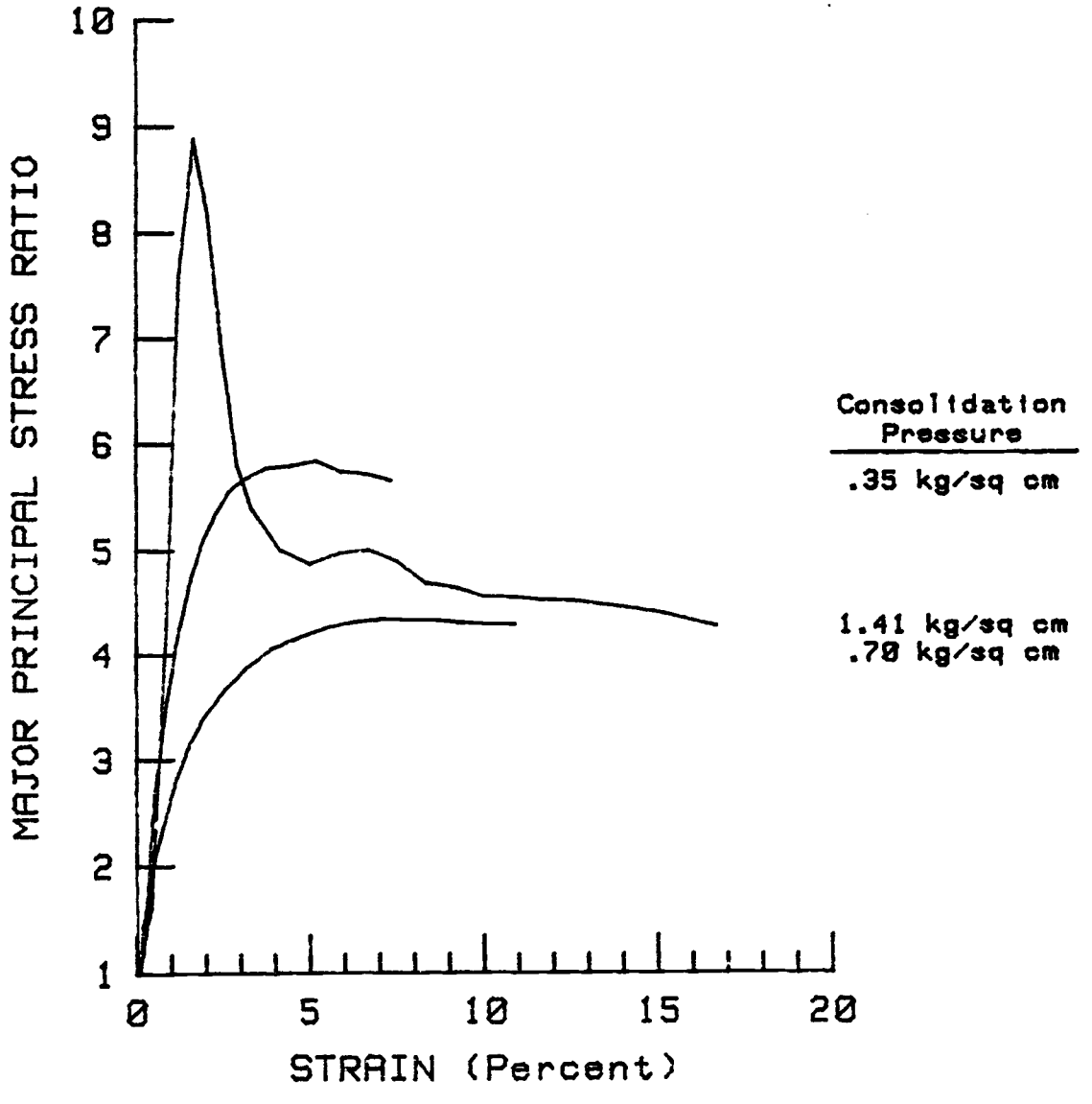

DOME CREEK SITE 1
UNDISTURBED TRIAX. W/ BACKPRESSURE
EFFECTIVE STRESS PATH PLOT

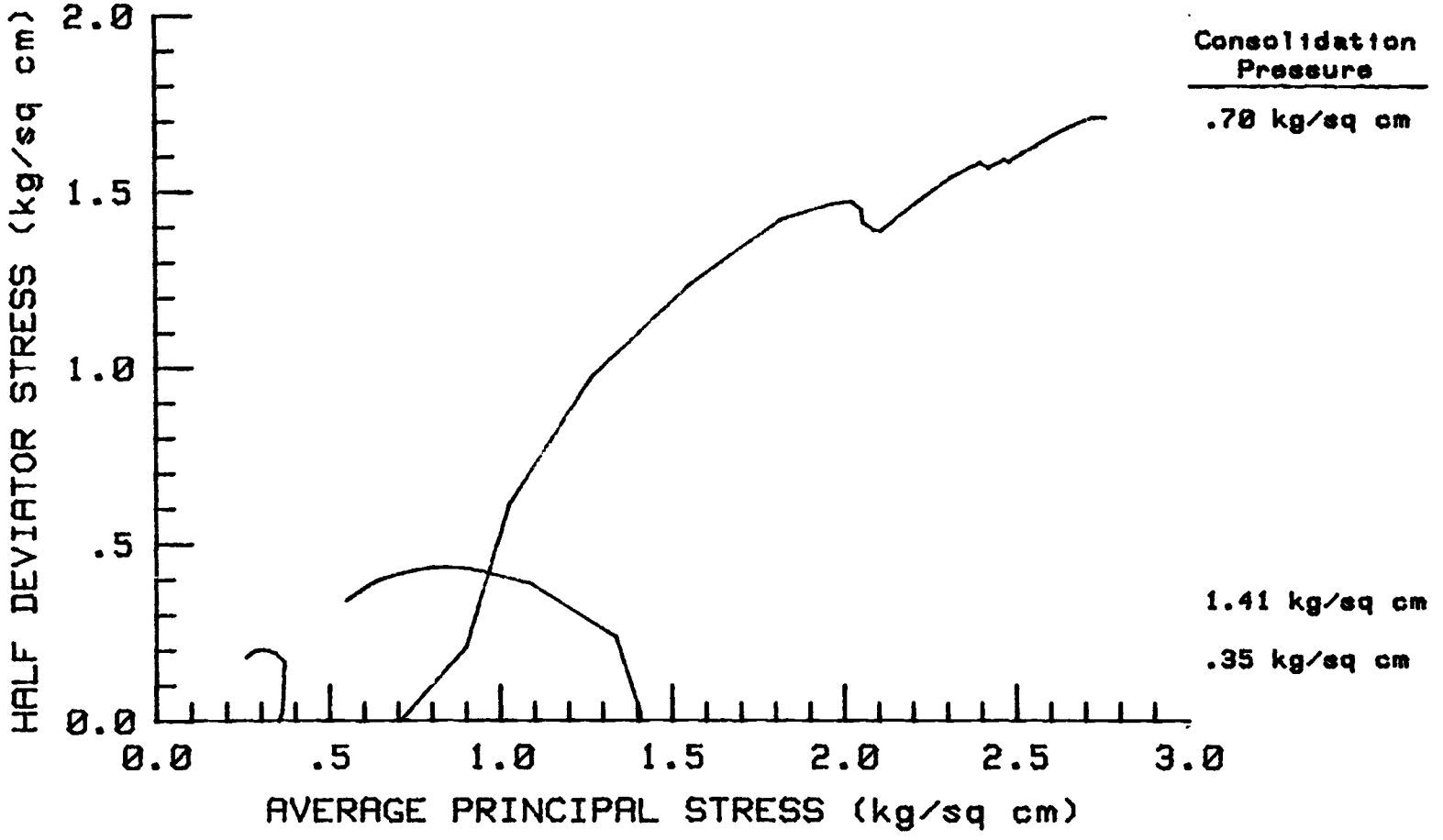

DOME CREEK SITE 1
UNDISTURBED TRIAX. W/ BACKPRESSURE--SS
EFFECTIVE STRESS ENVELOPE

ANGLE OF INTERNAL FRICTION = 49.8 Degrees
COHESION INTERCEPT =-.14 kg/sq cm

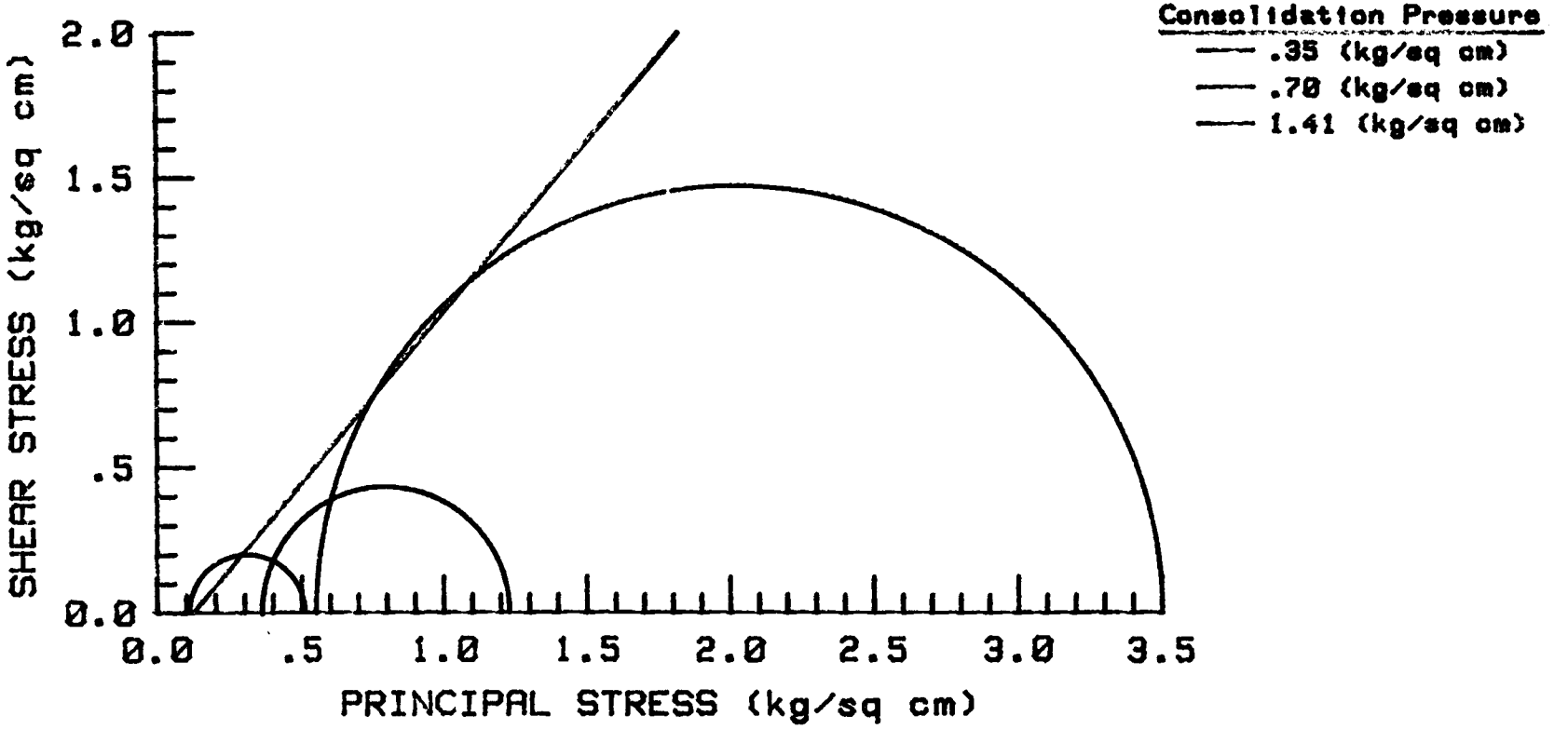

DOME CREEK SITE 1
UNDISTURBED TRIAX. W/ BACKPRESSURE--SR
EFFECTIVE STRESS ENVELOPE

ANGLE OF INTERNAL FRICTION = 57.6 Degrees
COHESION INTERCEPT =-.16 kg/sq cm

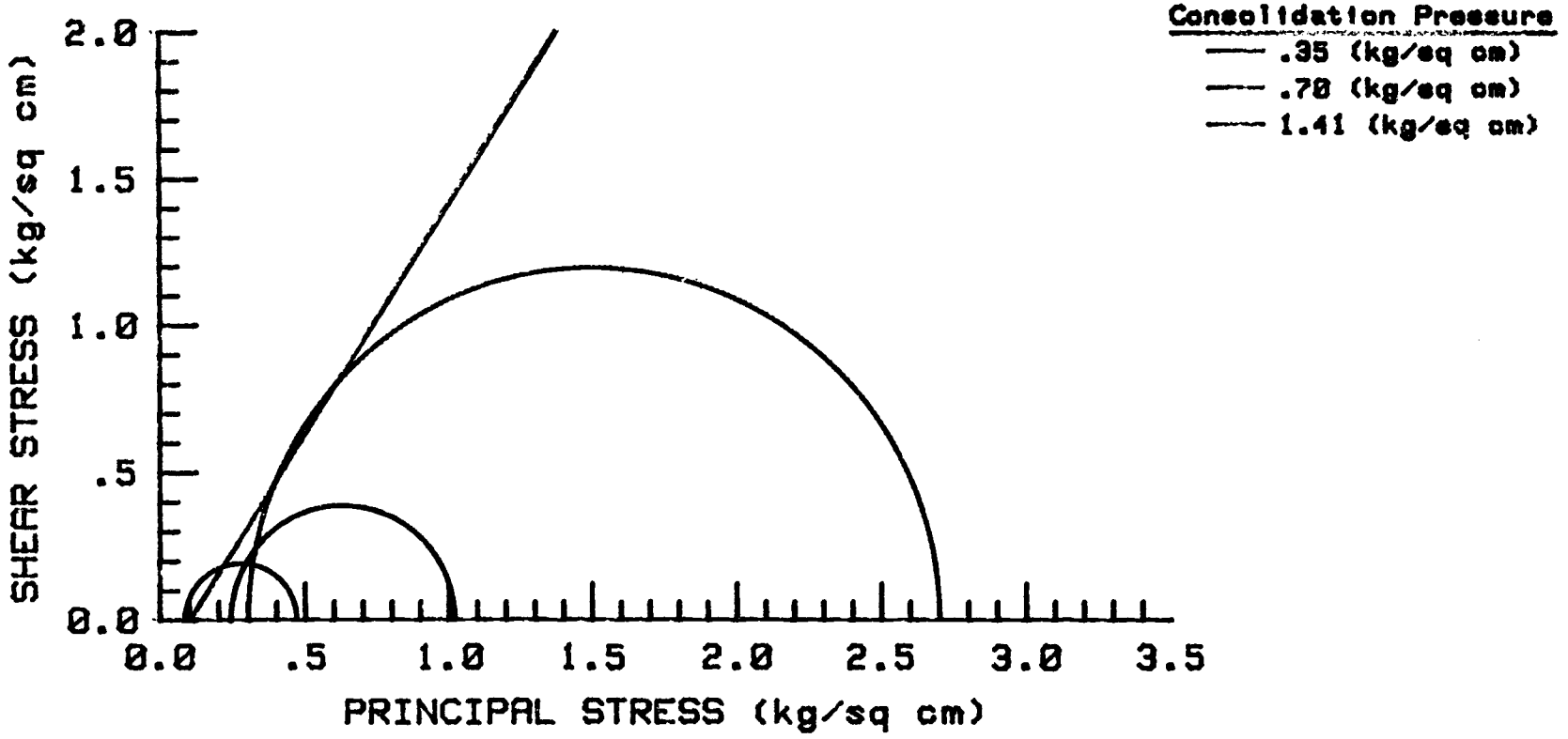

Strength testing summary of sample and test data

Site 3 - Buck Creek

Effective Consolidation Pressure ($\sigma_3 - U_o$ in Kg/cm^2)	0.35	0.70	1.41
Natural Moisture Content (W_n in %)	39.8	39.6	28.4
Insitu Wet Unit Weight (γ in g/cm^3)	1.57	1.66	1.52
Insitu Dry Unit Weight (γ_d in g/cm^3)	1.12	1.19	1.18
Insitu Degree Saturation (S in %)	73.6	80.6	57.4
Cell Pressure during Test (σ_3 in Kg/cm^2)	2.96	3.74	3.64
Initial Pore Pressure (U_o in Kg/cm^2)	2.61	3.04	2.59
B-Pore Pressure Parameter during Test (Ratio)	0.90	0.95	0.97

Strength testing summary of effective stress strength parameters

Site 3 - Buck Creek

For Mohr Envelope Derived from Stress-Strain Maximum Values

Effective Consolidation Pressure ($\sigma_3 - U_o$ in Kg/cm^2)		0.35	0.70	1.05
Deviator Stress at Failure ($\Delta\sigma_1$ in Kg/cm^2)		0.34	2.28	1.52
Pore Pressure at Failure (ΔU in Kg/cm^2)		0.26	-0.08	0.58
Axial Strain at Failure (ϵ in %)		6.0	7.0	1.8
A-Pore Pressure Parameter at Failure (Ratio)		0.76	-0.04	0.38
Effective Angle of Internal Friction (ϕ' in Degrees)	$\phi' =$	35.9		
Effective Cohesion Intercept (C' in Kg/cm^2)	$C' =$	0.03		
Correlation Coefficient (r - dimensionless)	$r =$	.9996		

For Mohr Envelope Derived from Stress Ratio Maximum Values

Effective Consolidation Pressure ($\sigma_3 - U_o$ in Kg/cm^2)		0.35	0.70	1.05
Deviator Stress at Failure ($\Delta\sigma_1$ in Kg/cm^2)		0.31	2.15	1.45
Pore Pressure at Failure (ΔU in Kg/cm^2)		0.28	0.19	0.84
Axial Strain at Failure (ϵ in %)		3.2	1.6	8.6
A-Pore Pressure Parameter at Failure (Ratio)		0.90	0.09	0.58
Effective Angle of Internal Friction (ϕ' in Degrees)	$\phi' =$	42.7		
Effective Cohesion Intercept (C' in Kg/cm^2)	$C' =$	0.04		
Correlation Coefficient (r-dimensionless)	$r =$	.9938		

For Mohr Envelope Derived from Effective Stress Path Plot

Effective Angle of Internal Friction (ϕ' in Degrees)	$\phi' =$	42.1
Effective Cohesion Intercept (C' in Kg/cm^2)	$C' =$	0.01
Correlation Coefficient (r-dimensionless)	$r =$	.9924

BUCK CREEK SITE 3
UNDISTURBED TRIAX. W/ BACKPRESSURE
DEVIATOR STRESS VS STRAIN

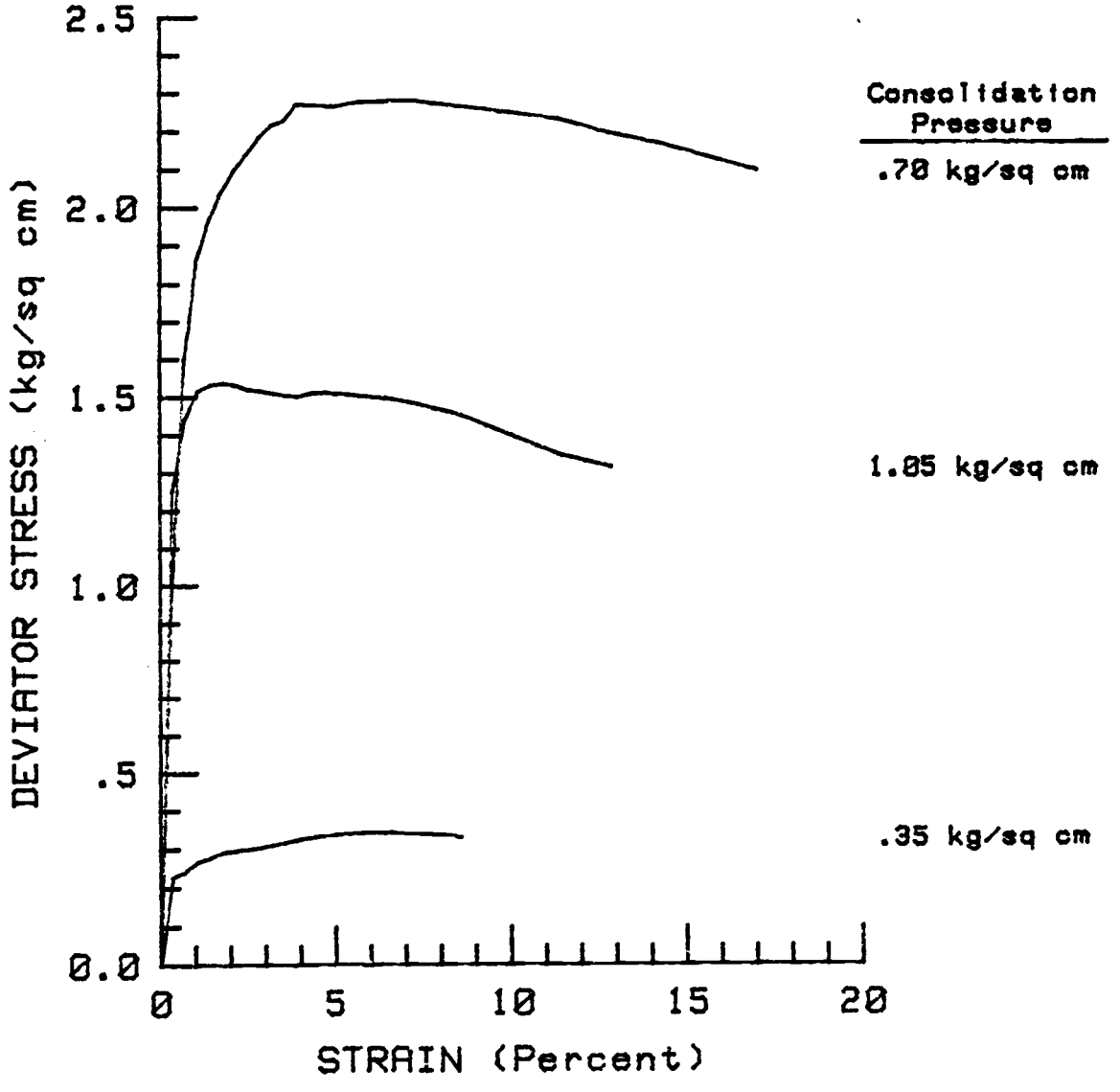

BUCK CREEK SITE 3
UNDISTURBED TRIAX. W/ BACKPRESSURE
PORE WATER PRESSURE VS STRAIN

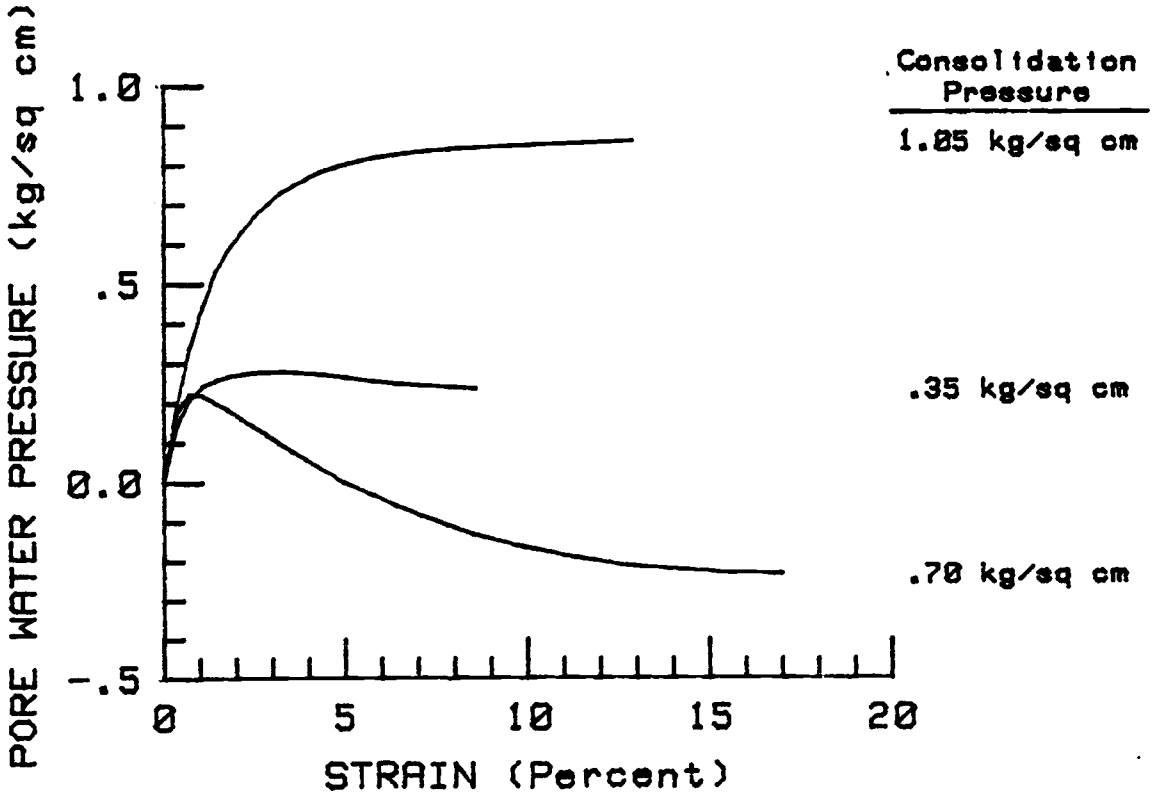

BUCK CREEK SITE 3
UNDISTURBED TRIAX. W/ BACKPRESSURE
MAJOR PRINCIPAL STRESS RATIO VS STRAIN

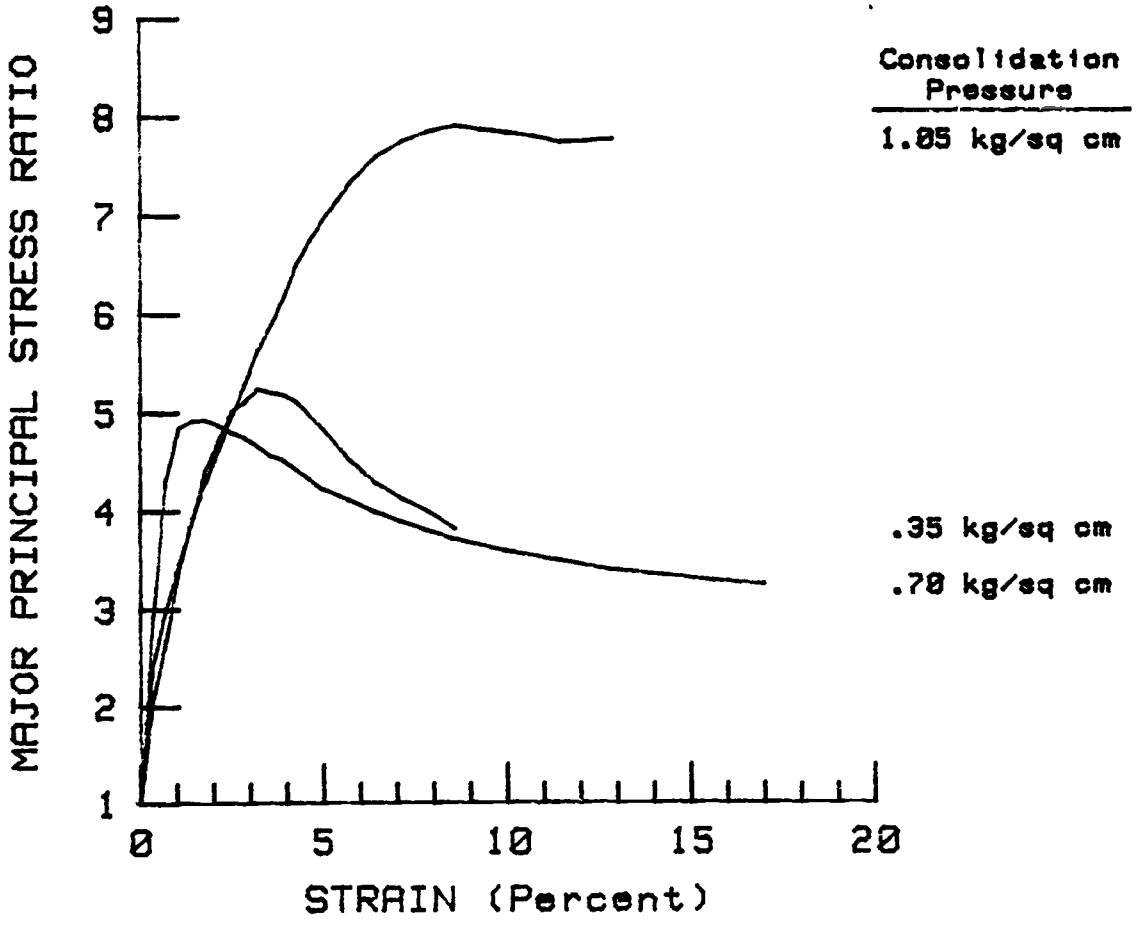

BUCK CREEK SITE 3
UNDISTURBED TRIAX. W/ BACKPRESSURE
EFFECTIVE STRESS PATH PLOT

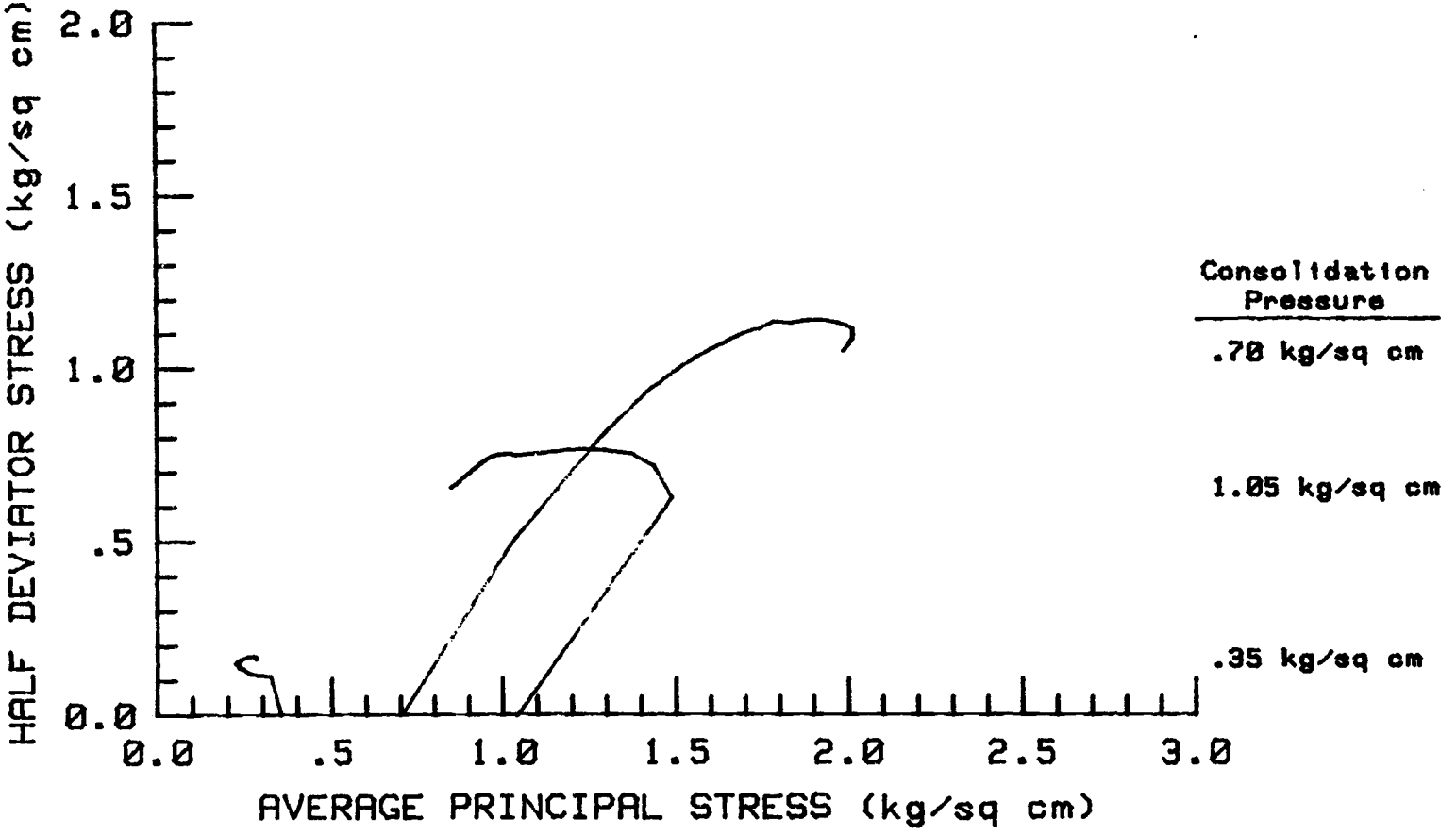

BUCK CREEK SITE 3
UNDISTURBED TRIAX. W/ BACKPRESSURE--SS
EFFECTIVE STRESS ENVELOPE

ANGLE OF INTERNAL FRICTION = 36.0 Degrees
COHESION INTERCEPT = .02 kg/sq cm

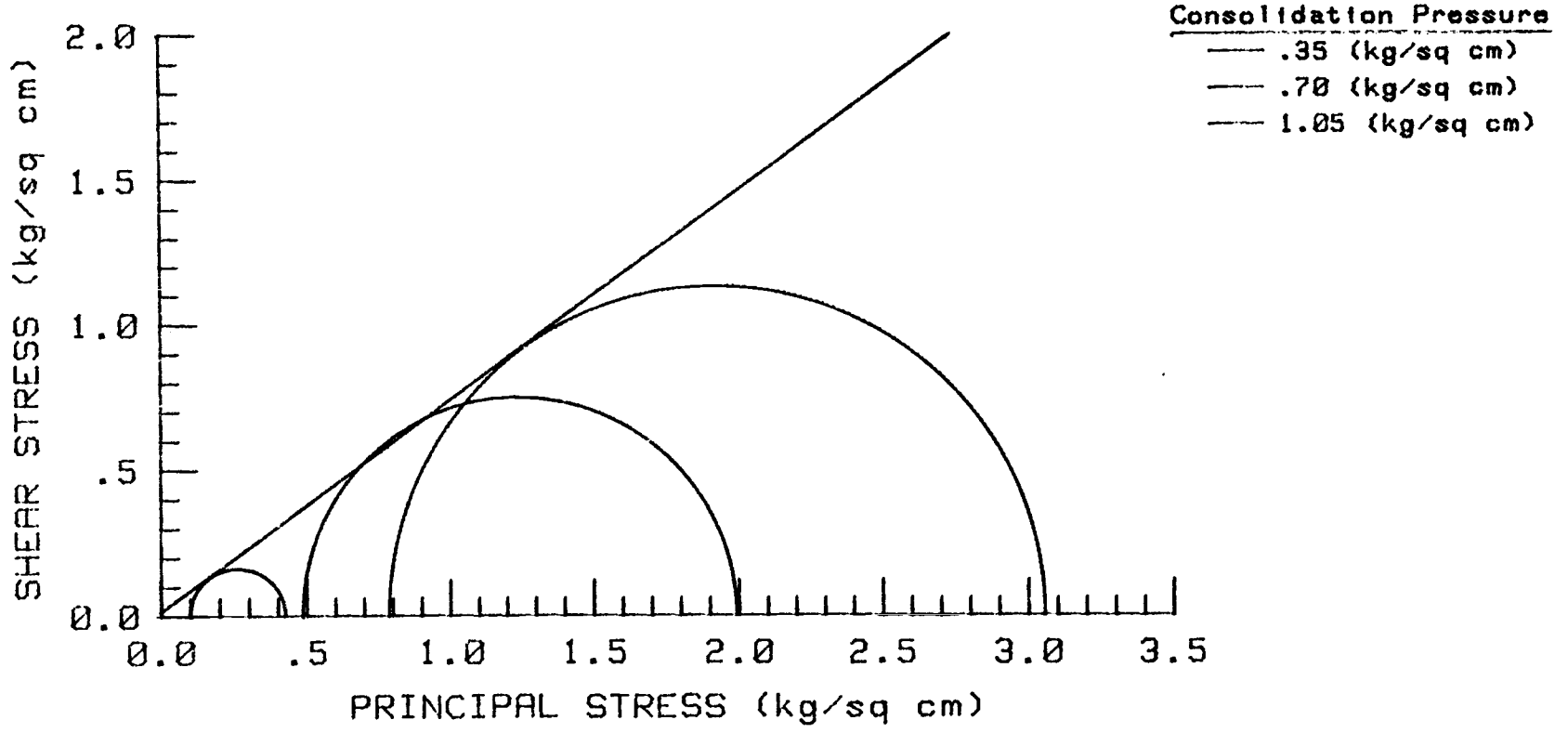

BUCK CREEK SITE 3
UNDISTURBED TRIAX. W/ BACKPRESSURE--SR
EFFECTIVE STRESS ENVELOPE

ANGLE OF INTERNAL FRICTION = 43.2 Degrees
COHESION INTERCEPT = .03 kg/sq cm

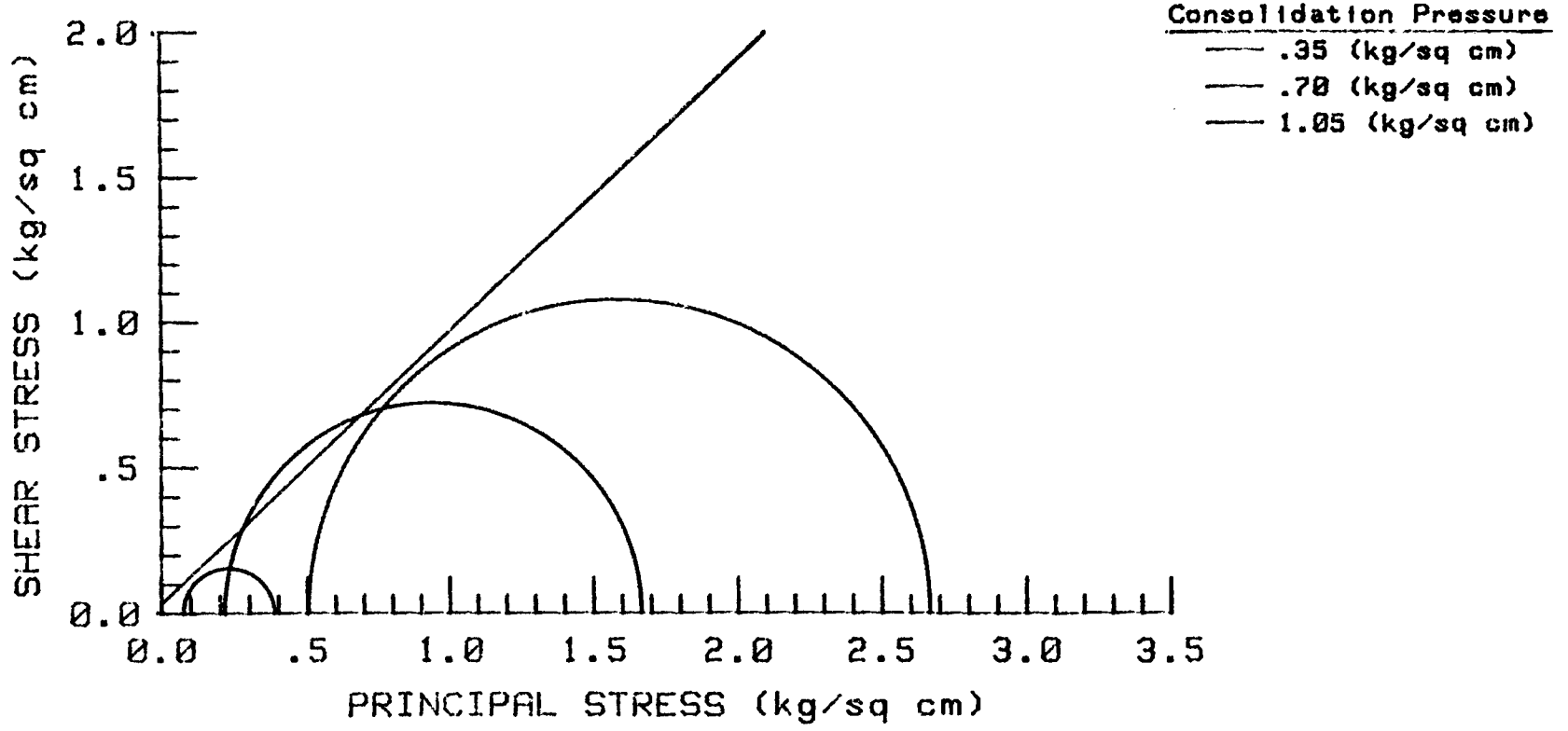

Strength testing summary of sample and test data

Site 4 - Pyrimid Creek

Effective Consolidation Pressure ($\sigma_3 - U_o$ in Kg/cm^2)	0.35	0.70	1.41
Natural Moisture Content (W_n in %)	48.0	45.5	51.0
Insitu Wet Unit Weight (γ in g/cm^3)	1.58	1.75	1.43
Insitu Dry Unit Weight (γ_d in g/cm^3)	1.07	1.20	0.95
Insitu Degree Saturation (S in %)	84.6	98.4	74.2
Cell Pressure during Test (σ_3 in Kg/cm^2)	3.61	2.88	3.54
Initial Pore Pressure (U_o in Kg/cm^2)	3.26	2.18	2.49
B-Pore Pressure Parameter during Test (Ratio)	0.96	1.00	0.99

Strength testing summary of effective stress strength parameters

Site 4 - Pyrimid Creek

For Mohr Envelope Derived from Stress-Strain Maximum Values

Effective Consolidation Pressure ($\sigma_3 - U_o$ in Kg/cm^2)		0.35	0.70	1.05
Deviator Stress at Failure ($\Delta\sigma_1$ in Kg/cm^2)		0.46	2.34	0.76
Pore Pressure at Failure (ΔU in Kg/cm^2)		0.19	0.0	0.7
Axial Strain at Failure (ϵ in %)		1.5	8.0	2.0
A-Pore Pressure Parameter at Failure (Ratio)		0.41	0	0.92
Effective Angle of Internal Friction (ϕ' in Degrees)	$\phi' =$	42.3		
Effective Cohesion Intercept (C' in Kg/cm^2)	$C' =$	-0.07		
Correlation Coefficient (r - dimensionless)	$r =$	.9920		

For Mohr Envelope Derived from Stress Ratio Maximum Values

Effective Consolidation Pressure ($\sigma_3 - U_o$ in Kg/cm^2)		0.35	0.70	1.05
Deviator Stress at Failure ($\Delta\sigma_1$ in Kg/cm^2)		0.45	1.71	0.68
Pore Pressure at Failure (ΔU in Kg/cm^2)		0.22	0.6	0.82
Axial Strain at Failure (ϵ in %)		7.0	2.5	6.5
A-Pore Pressure Parameter at Failure (Ratio)		0.49	0.35	1.20
Effective Angle of Internal Friction (ϕ' in Degrees)	$\phi' =$	52.5		
Effective Cohesion Intercept (C' in Kg/cm^2)	$C' =$	-0.08		
Correlation Coefficient (r-dimensionless)	$r =$	.9575		

For Mohr Envelope Derived from Effective Stress Path Plot

Effective Angle of Internal Friction (ϕ' in Degrees)	$\phi' =$	46.9
Effective Cohesion Intercept (C' in Kg/cm^2)	$C' =$	-0.09
Correlation Coefficient (r-dimensionless)	$r =$	.9976

PYRIMID CREEK SITE 4
UNDISTURBED TRIAX. W/ BACKPRESSURE
DEVIATOR STRESS VS STRAIN

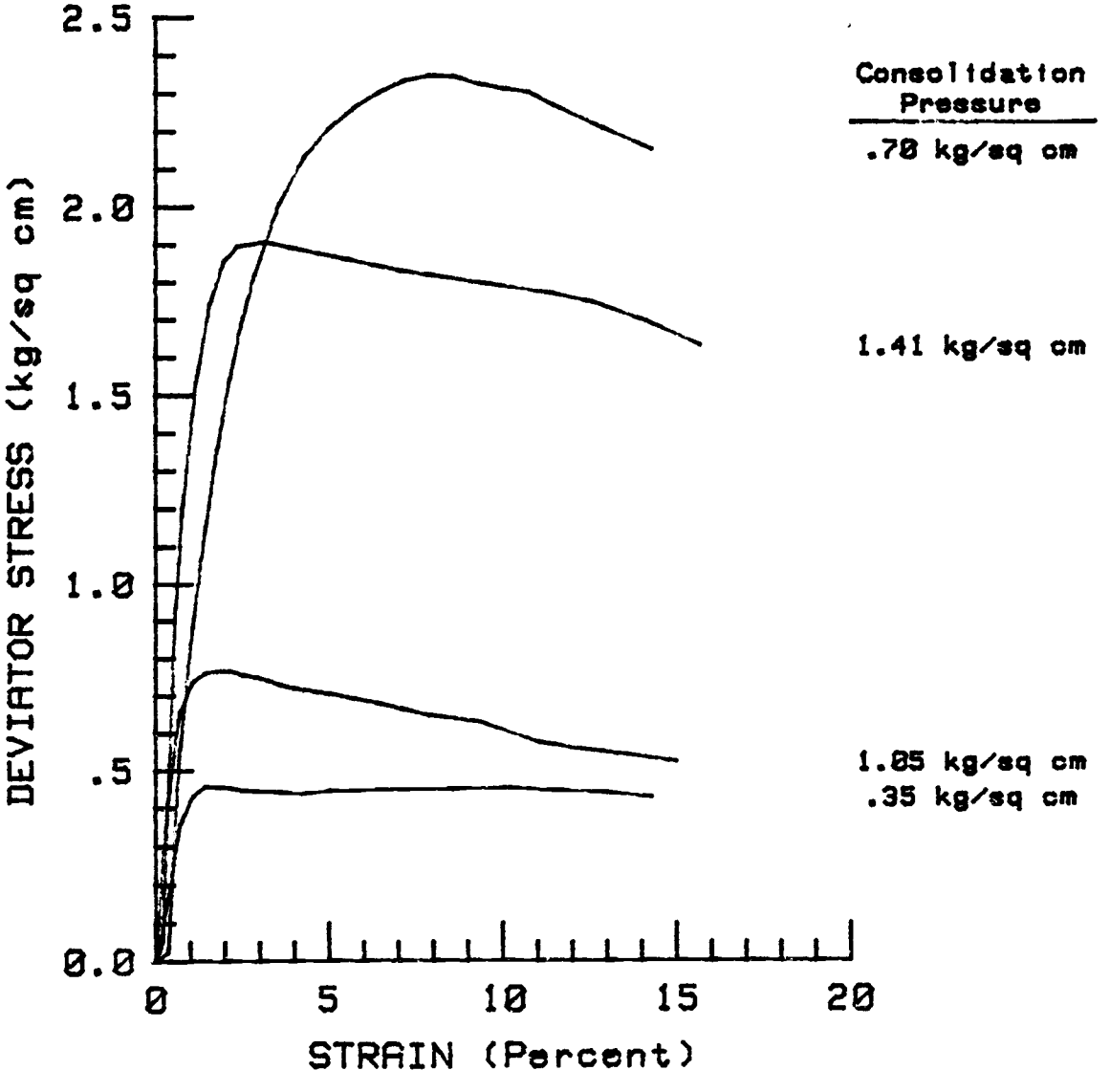

PYRIMID CREEK SITE 4
UNDISTURBED TRIAX. W/ BACKPRESSURE
PORE WATER PRESSURE VS STRAIN

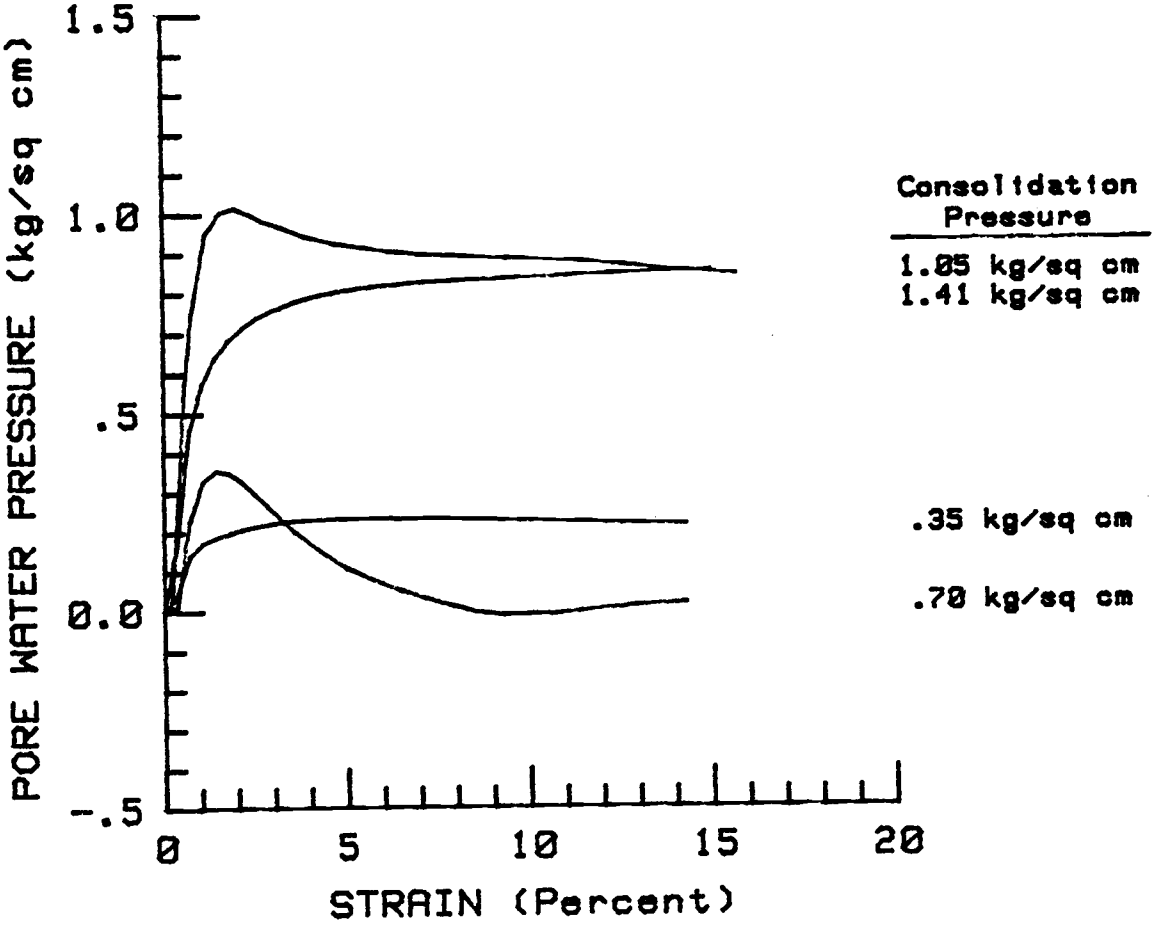

PYRIMID CREEK SITE 4
UNDISTURBED TRIAX. W/ BACKPRESSURE
MAJOR PRINCIPAL STRESS RATIO VS STRAIN

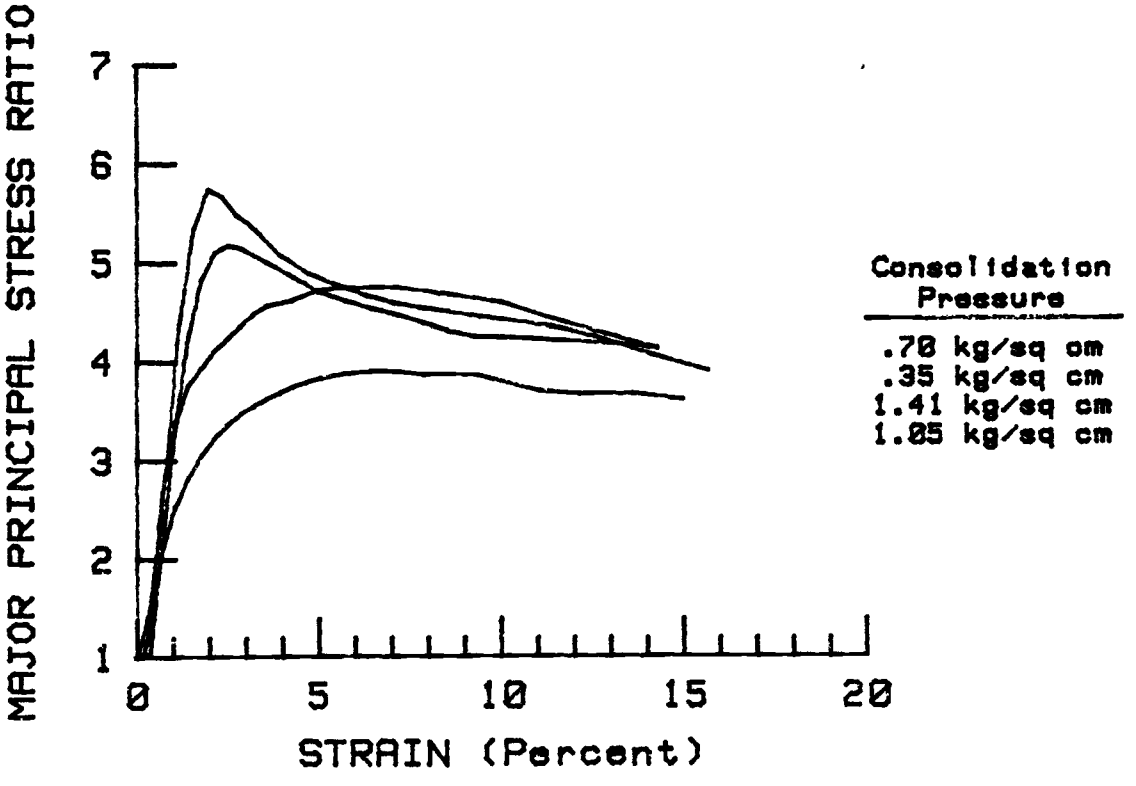

PYRIMID CREEK SITE 4
UNDISTURBED TRIAX. W/ BACKPRESSURE
EFFECTIVE STRESS PATH PLOT

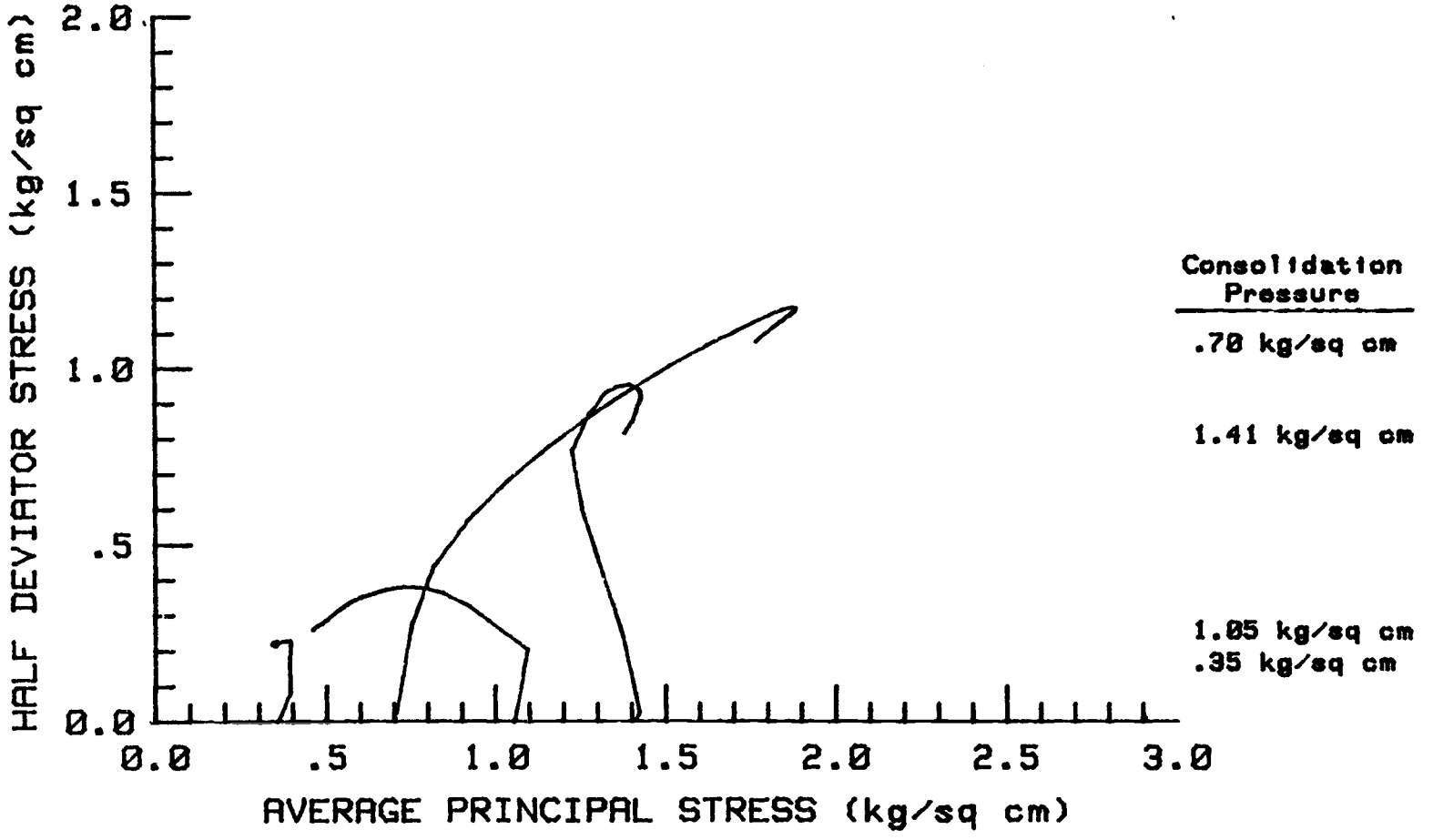

PYRIMID CREEK SITE 4
UNDISTURBED TRIAX. W/ BACKPRESSURE--SS
EFFECTIVE STRESS ENVELOPE

ANGLE OF INTERNAL FRICTION = 42.3 Degrees
COHESION INTERCEPT =-.08 kg/sq cm

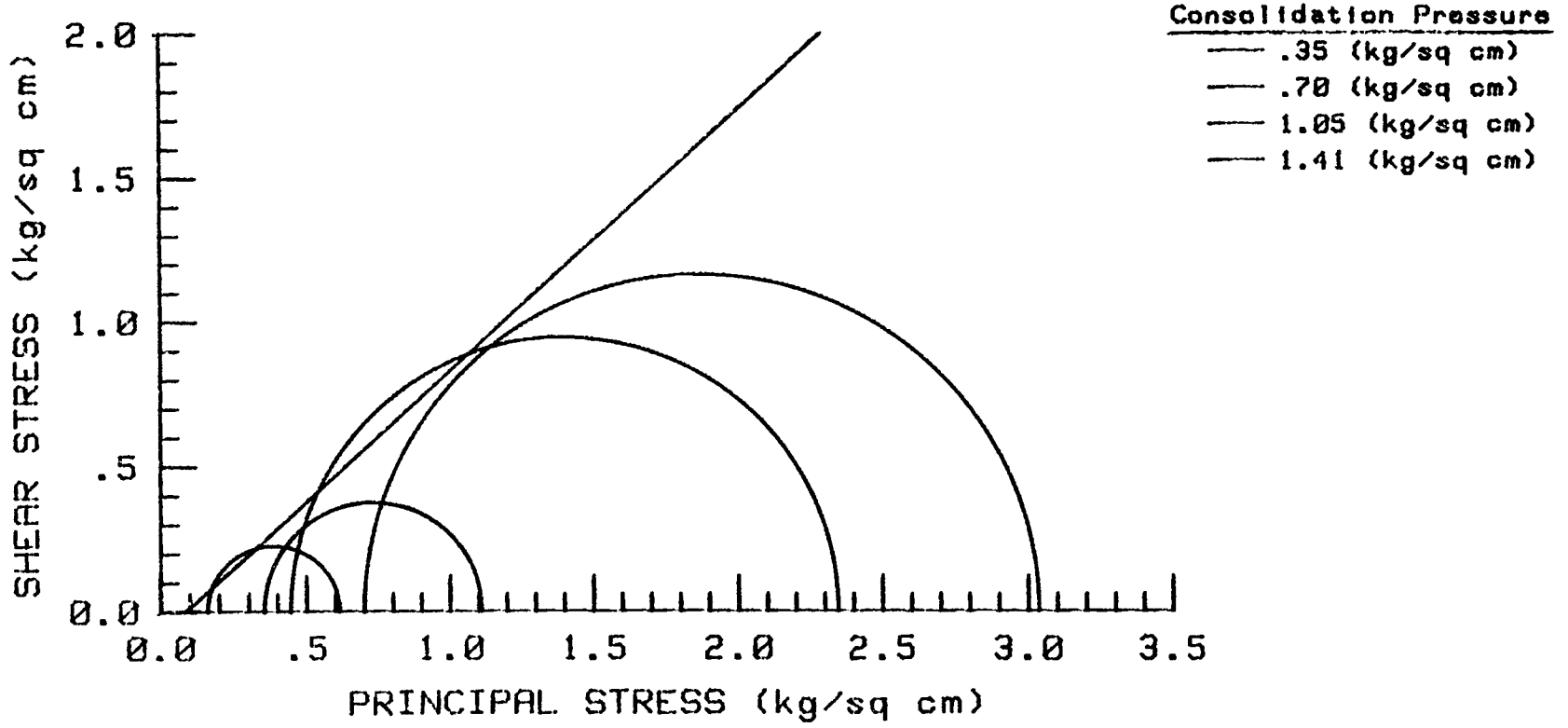

PYRIMID CREEK SITE 4
UNDISTURBED TRIAX. W/ BACKPRESSURE
EFFECTIVE STRESS ENVELOPE

ANGLE OF INTERNAL FRICTION = 52.4 Degrees
COHESION INTERCEPT =-.08 kg/sq cm

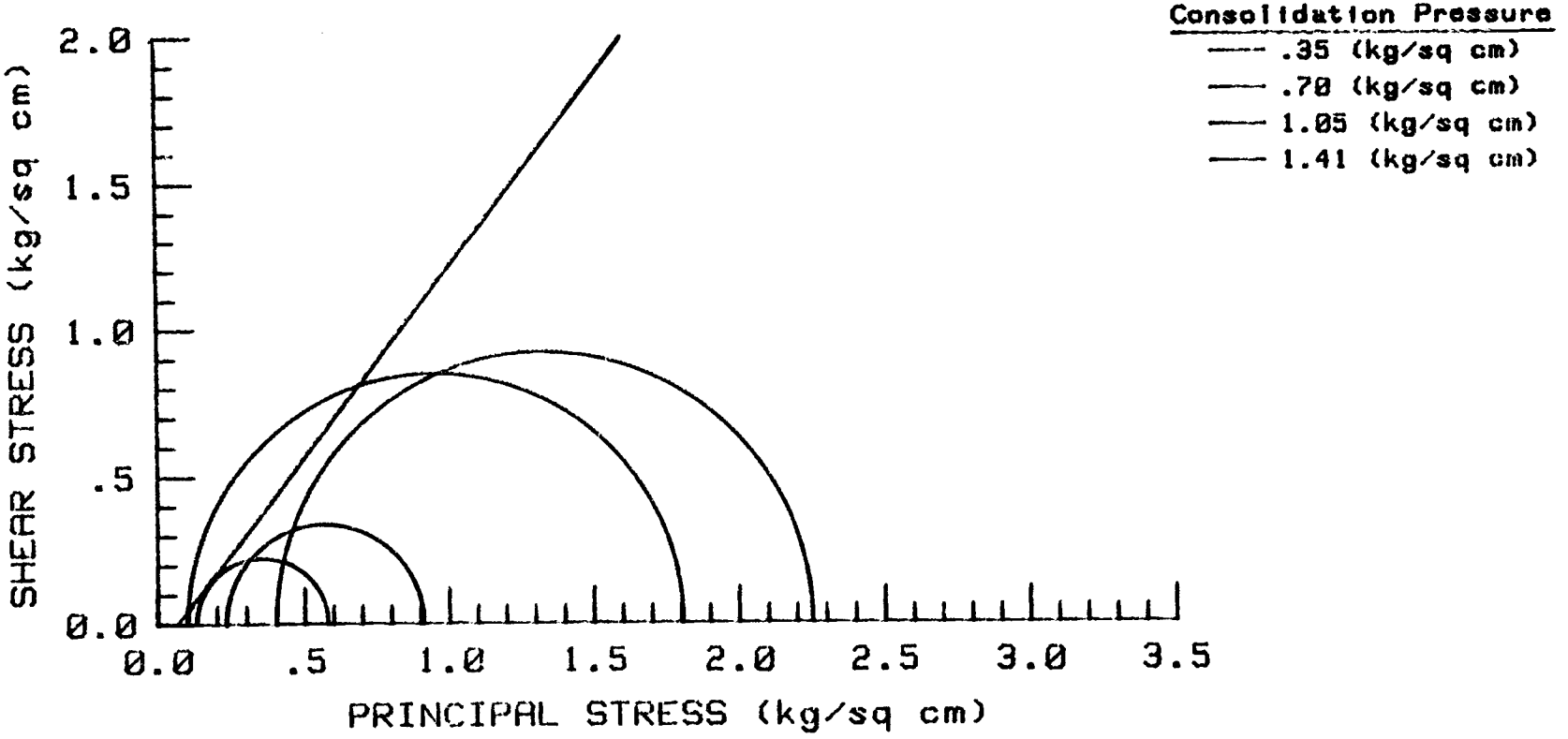

Strength testing summary of sample and test data

Site 5 - Batchellor Creek

Effective Consolidation Pressure ($\sigma_3 - U_o$ in Kg/cm^2)	0.35	0.70	1.41
Natural Moisture Content (W_n in %)	46.6	48.8	40.6
Insitu Wet Unit Weight (γ in g/cm^3)	1.55	1.52	1.50
Insitu Dry Unit Weight (γ_d in g/cm^3)	1.06	1.02	1.07
Insitu Degree Saturation (S in %)	81.6	80.7	72.1
Cell Pressure during Test (σ_3 in Kg/cm^2)	3.76	2.11	3.52
Initial Pore Pressure (U_o in Kg/cm^2)	3.41	1.41	2.47
B-Pore Pressure Parameter during Test (Ratio)	0.95	0.97	0.95

Strength testing summary of effective stress strength parameters

Site 5 - Batchellor Creek

For Mohr Envelope Derived from Stress-Strain Maximum Values

Effective Consolidation Pressure ($\sigma_3 - U_o$ in Kg/cm^2)		0.35	0.70	1.05
Deviator Stress at Failure ($\Delta\sigma_1$ in Kg/cm^2)		0.76	0.70	1.12
Pore Pressure at Failure (ΔU in Kg/cm^2)		0.18	0.48	0.65
Axial Strain at Failure (ϵ in %)		3.0	3.0	3.0
A-Pore Pressure Parameter at Failure (Ratio)		0.24	0.68	0.58
Effective Angle of Internal Friction (ϕ' in Degrees)	$\phi' =$	28.9		
Effective Cohesion Intercept (C' in Kg/cm^2)	$C' =$	0.11		
Correlation Coefficient (r - dimensionless)	$r =$	.9846		

For Mohr Envelope Derived from Stress Ratio Maximum Values

Effective Consolidation Pressure ($\sigma_3 - U_o$ in Kg/cm^2)		0.35	0.70	1.05
Deviator Stress at Failure ($\Delta\sigma_1$ in Kg/cm^2)		0.76	0.70	1.14
Pore Pressure at Failure (ΔU in Kg/cm^2)		0.18	0.48	0.66
Axial Strain at Failure (ϵ in %)		3.0	4.0	4.0
A-Pore Pressure Parameter at Failure (Ratio)				
Effective Angle of Internal Friction (ϕ' in Degrees)	$\phi' =$	28.9		
Effective Cohesion Intercept (C' in Kg/cm^2)	$C' =$	0.11		
Correlation Coefficient (r-dimensionless)	$r =$	.9846		

For Mohr Envelope Derived from Effective Stress Path Plot

Effective Angle of Internal Friction (ϕ' in Degrees)	$\phi' =$	32.1
Effective Cohesion Intercept (C' in Kg/cm^2)	$C' =$	0.08
Correlation Coefficient (r-dimensionless)	$r =$	.9844

BATCHELLOR CREEK SITE 5
UNDISTURBED TRIAX. W/ BACKPRESSURE
DEVIATOR STRESS VS STRAIN

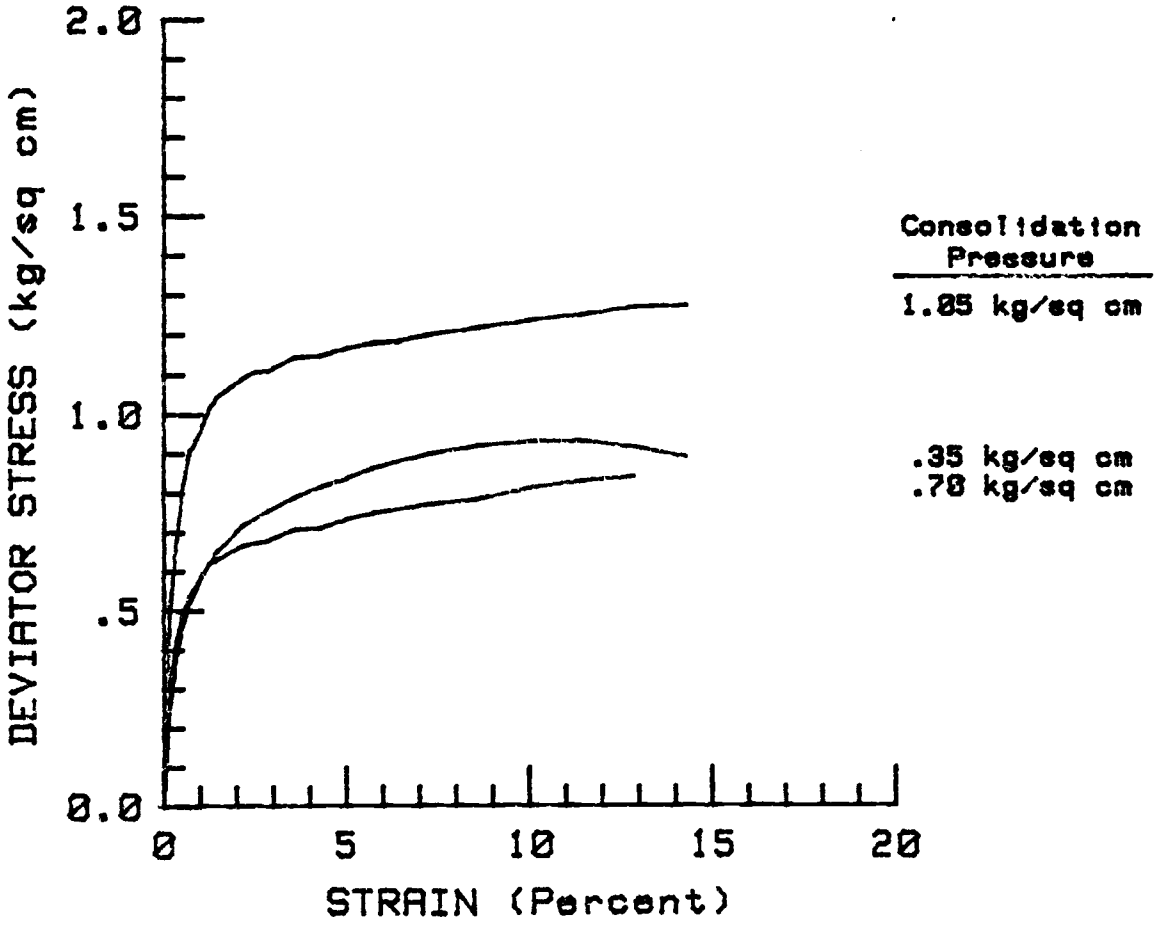

BATCHELLOR CREEK SITE 5
UNDISTURBED TRIAX. W/ BACKPRESSURE
PORE WATER PRESSURE VS STRAIN

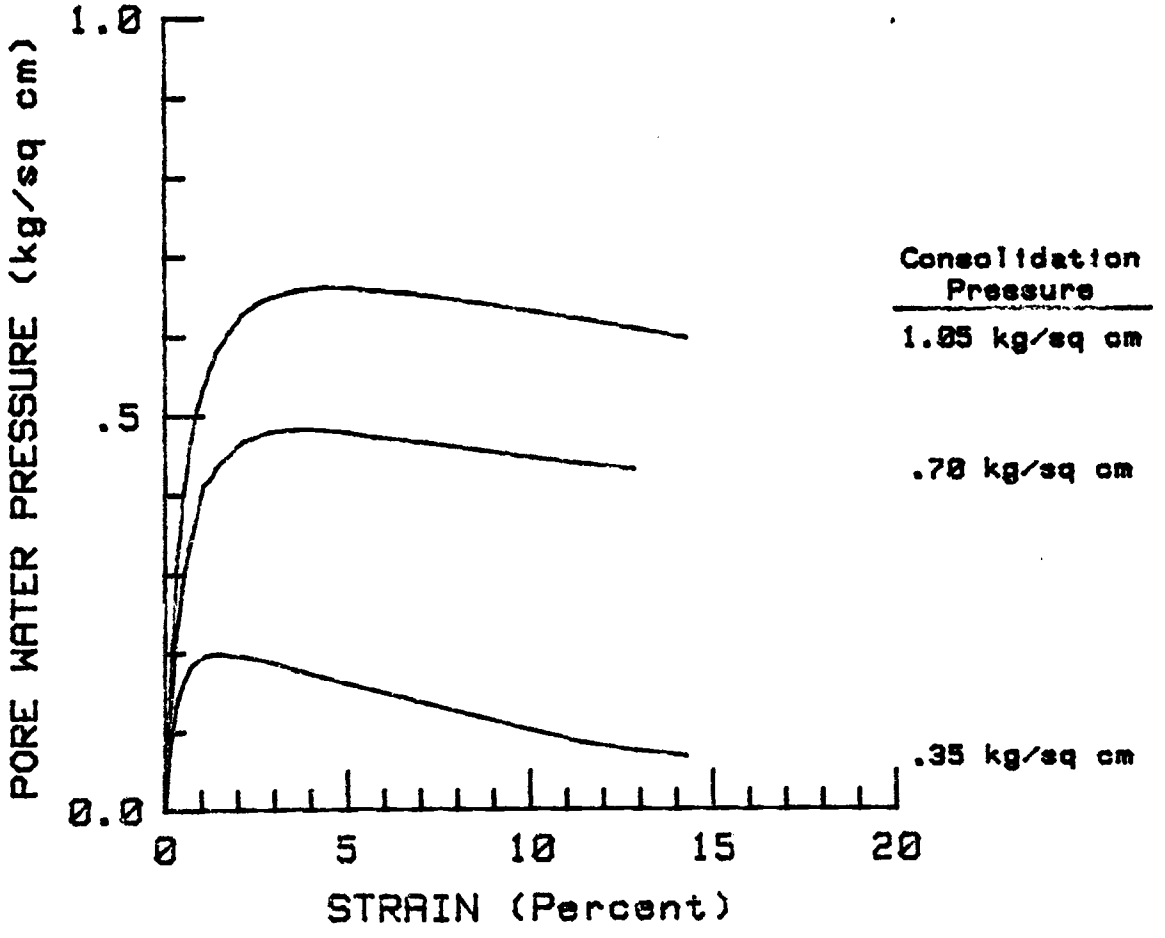

BATCHELLOR CREEK SITE 5
UNDISTURBED TRIAX. W/ BACKPRESSURE
MAJOR PRINCIPAL STRESS RATIO VS STRAIN

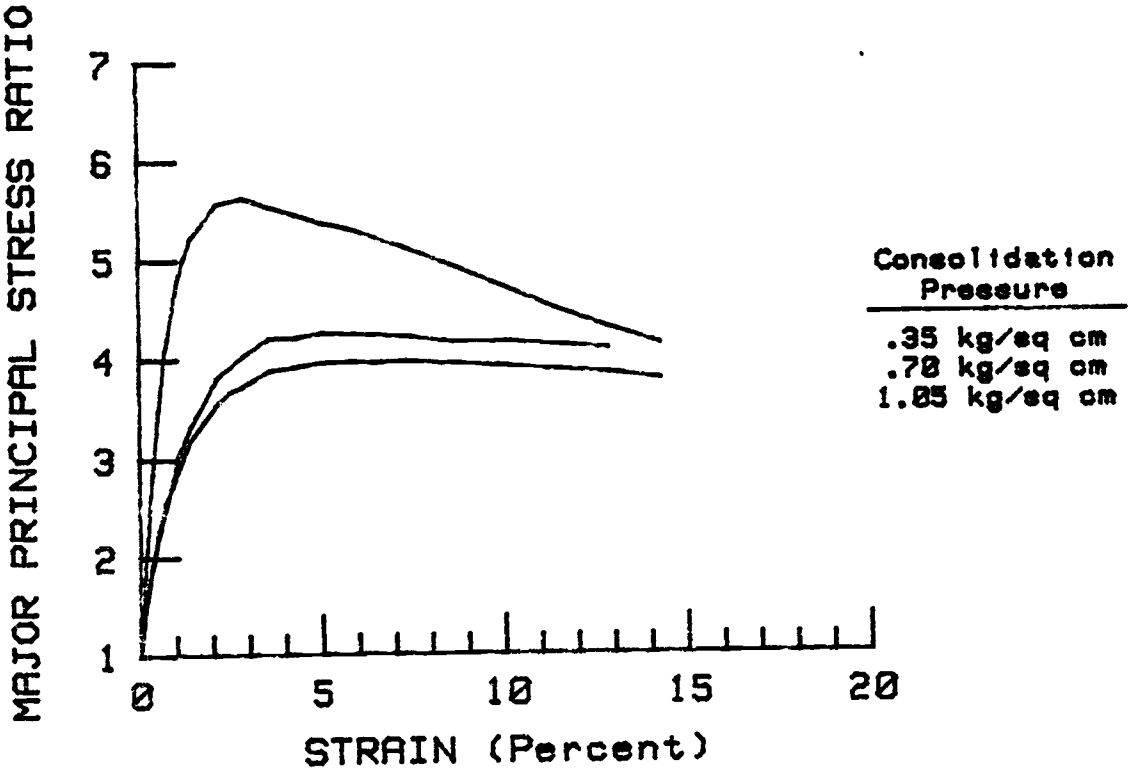

p. 390 missing from original. Author unavailable to supply.

ALASKA SITE 10
UNDISTURBED TRIAX. W/ BACKPRESSURE--SS
EFFECTIVE STRESS ENVELOPE

ANGLE OF INTERNAL FRICTION = 18.7 Degrees
COHESION INTERCEPT = .15 kg/sq cm

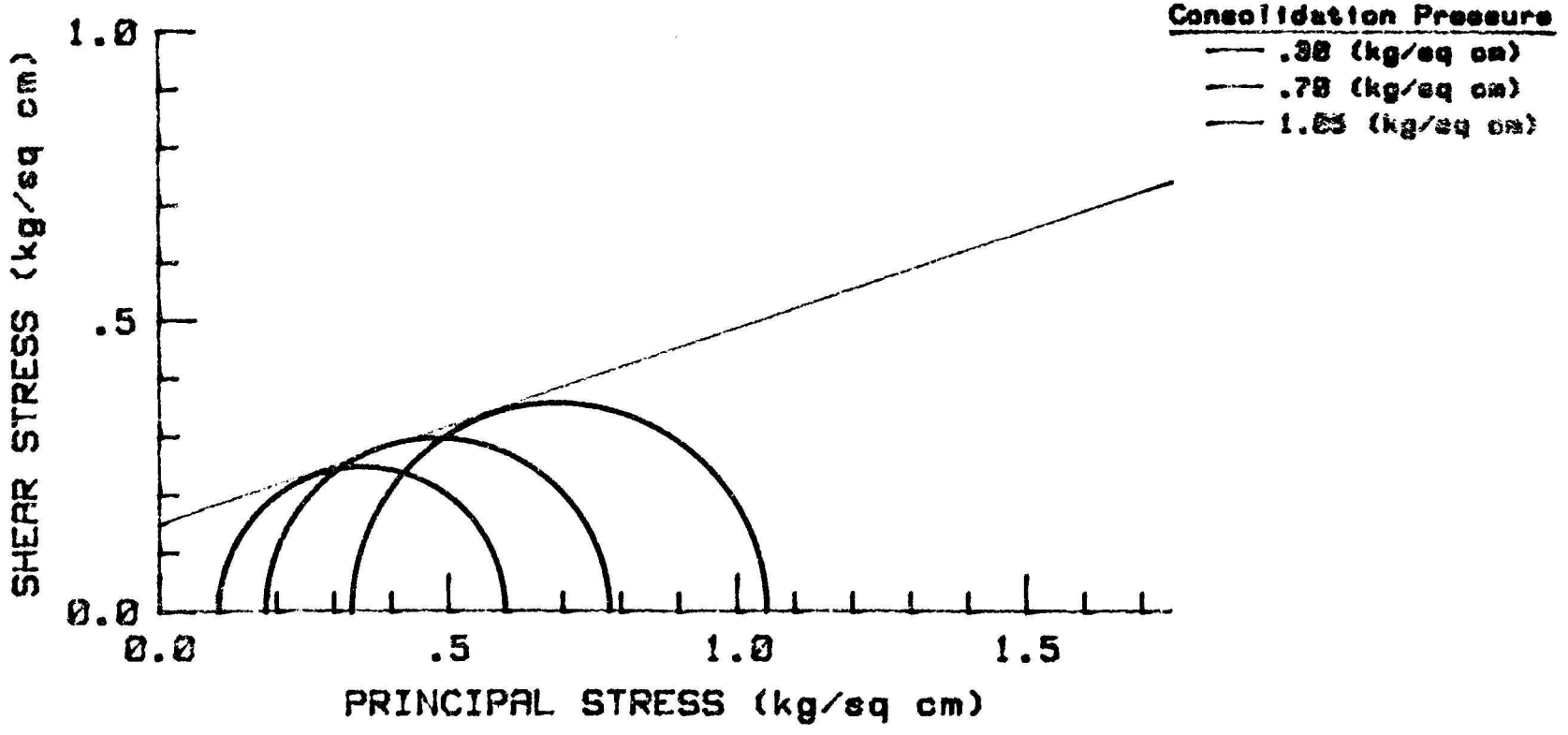

BATCHELLOR CREEK SITE 5
UNDISTURBED TRIAX. W/ BACKPRESSURE--SS & SR
EFFECTIVE STRESS ENVELOPE

ANGLE OF INTERNAL FRICTION = 29.6 Degrees
COHESION INTERCEPT = .10 kg/sq cm

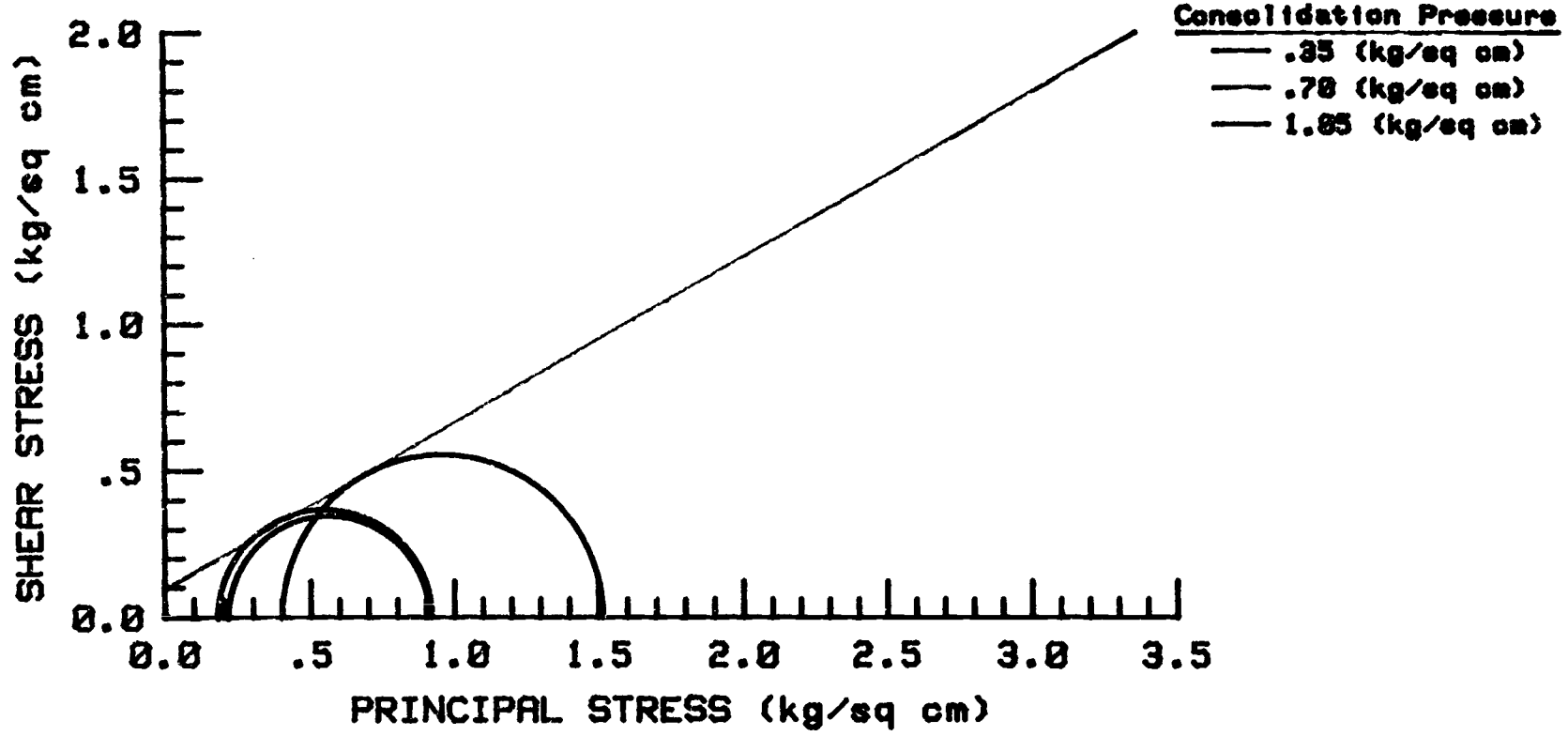

Strength testing summary of sample and test data

Site 6 - Box Canyon Creek

Effective Consolidation Pressure ($\sigma_3 - U_o$ in Kg/cm^2)	0.35	0.70	1.41
Natural Moisture Content (W_n in %)	42.1	45.4	45.0
Insitu Wet Unit Weight (γ in g/cm^3)	1.57	1.45	1.51
Insitu Dry Unit Weight (γ_d in g/cm^3)	1.10	1.00	1.04
Insitu Degree Saturation (S in %)	77.0	70.5	75.0
Cell Pressure during Test (σ_3 in Kg/cm^2)	2.46	3.13	2.46
Initial Pore Pressure (U_o in Kg/cm^2)	2.11	2.43	1.41
B-Pore Pressure Parameter during Test (Ratio)	0.95	0.96	0.98

Strength testing summary of effective stress strength parameters

Site 6 - Box Canyon Creek

For Mohr Envelope Derived from Stress-Strain Maximum Values

Effective Consolidation Pressure ($\sigma_3 - U_o$ in Kg/cm^2)		0.35	0.70	1.05
Deviator Stress at Failure ($\Delta\sigma_1$ in Kg/cm^2)		0.46	0.67	1.84
Pore Pressure at Failure (ΔU in Kg/cm^2)		0.21	0.40	0.61
Axial Strain at Failure (ϵ in %)		3.0	2.5	11.0
A-Pore Pressure Parameter at Failure (Ratio)		0.46	0.60	0.33
Effective Angle of Internal Friction (ϕ' in Degrees)	$\phi' =$	46.1		
Effective Cohesion Intercept (C' in Kg/cm^2)	$C' =$	-0.10		
Correlation Coefficient (r - dimensionless)	$r =$	.9928		

For Mohr Envelope Derived from Stress Ratio Maximum Values

Effective Consolidation Pressure ($\sigma_3 - U_o$ in Kg/cm^2)		0.35	0.70	1.05
Deviator Stress at Failure ($\Delta\sigma_1$ in Kg/cm^2)		0.58	0.72	1.81
Pore Pressure at Failure (ΔU in Kg/cm^2)		0.19	0.45	0.63
Axial Strain at Failure (ϵ in %)		12.5	10.0	9.0
A-Pore Pressure Parameter at Failure (Ratio)		0.33	0.62	0.35
Effective Angle of Internal Friction (ϕ' in Degrees)	$\phi' =$	46.1		
Effective Cohesion Intercept (C' in Kg/cm^2)	$C' =$	-0.08		
Correlation Coefficient (r-dimensionless)	$r =$	.9977		

For Mohr Envelope Derived from Effective Stress Path Plot

Effective Angle of Internal Friction (ϕ' in Degrees)	$\phi' =$	46.7
Effective Cohesion Intercept (C' in Kg/cm^2)	$C' =$	-0.10
Correlation Coefficient (r-dimensionless)	$r =$	.9933

BOX CANYON CREEK SITE 6
UNDISTURBED TRIAX. W/ BACKPRESSURE
DEVIATOR STRESS VS STRAIN

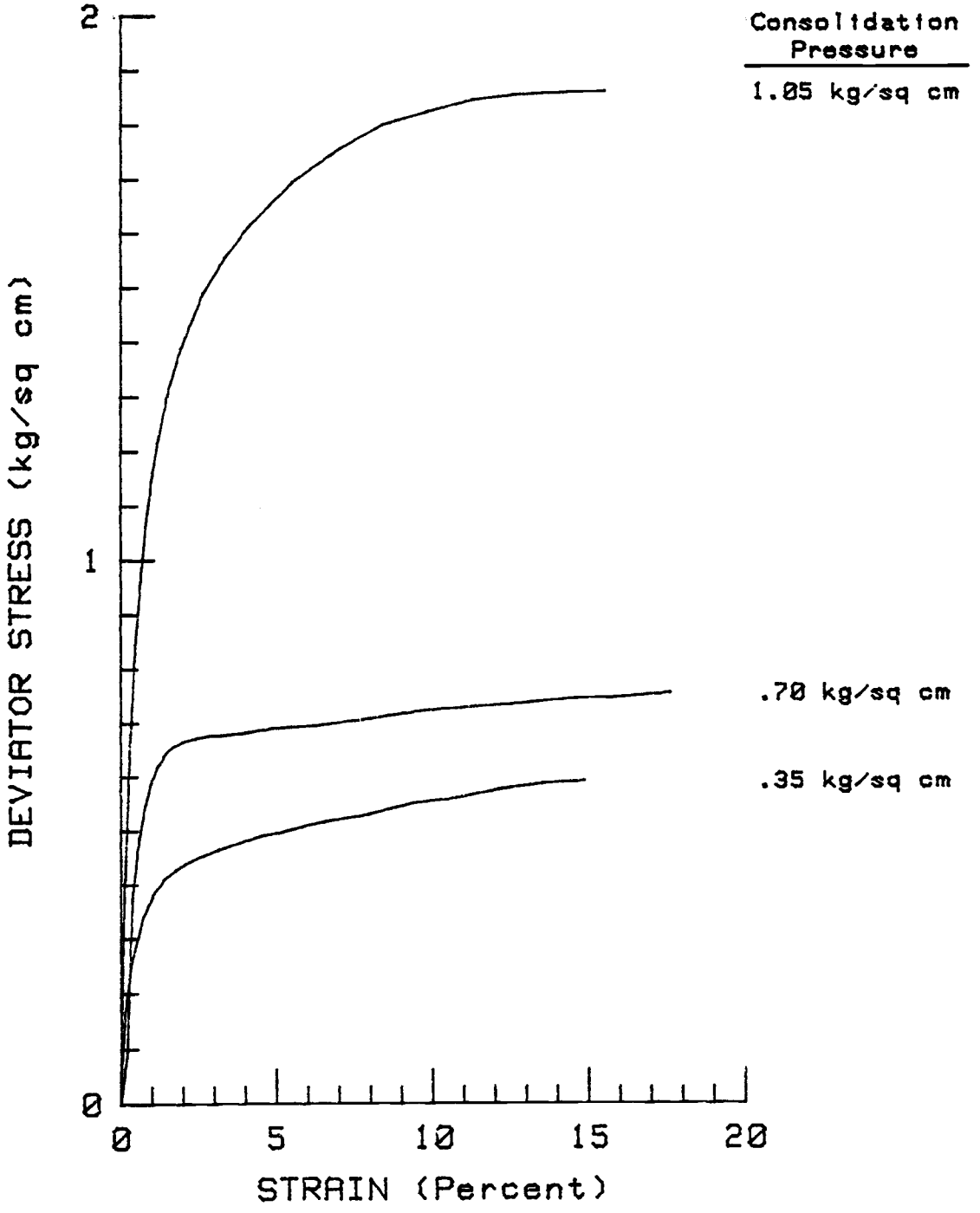

BOX CANYON CREEK SITE 6
UNDISTURBED TRIAX. W/ BACKPRESSURE
PORE WATER PRESSURE VS STRAIN

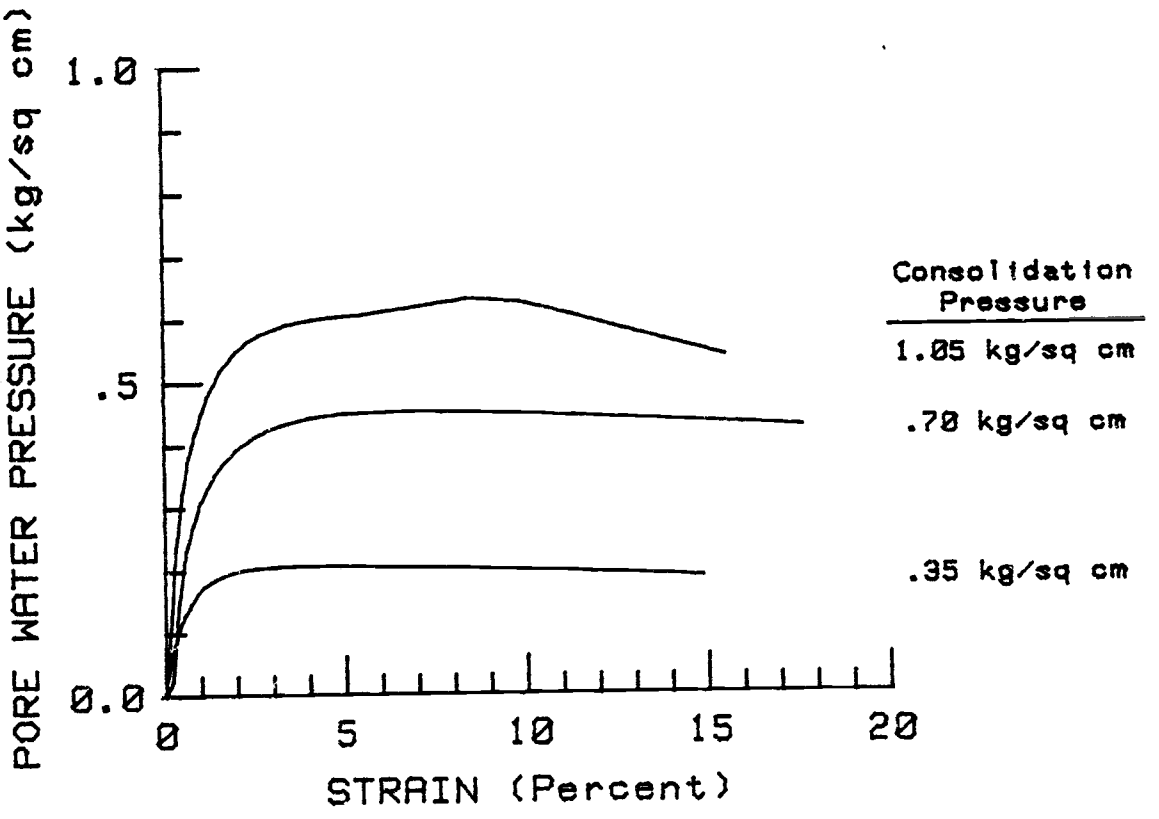

BOX CANYON CREEK SITE 6
UNDISTURBED TRIAX. W/ BACKPRESSURE
MAJOR PRINCIPAL STRESS RATIO VS STRAIN

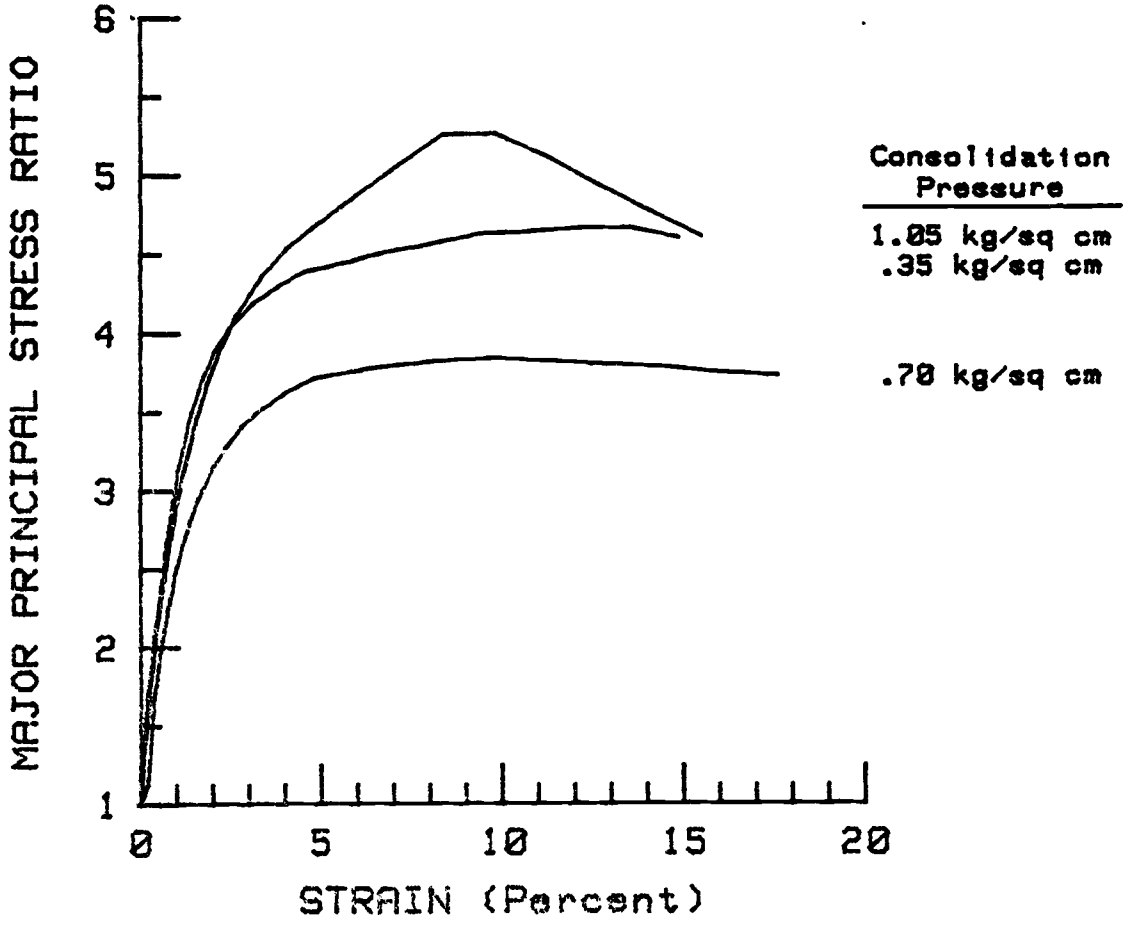

BOX CANYON CREEK SITE 6
UNDISTURBED TRIAX. W/ BACKPRESSURE
EFFECTIVE STRESS PATH PLOT

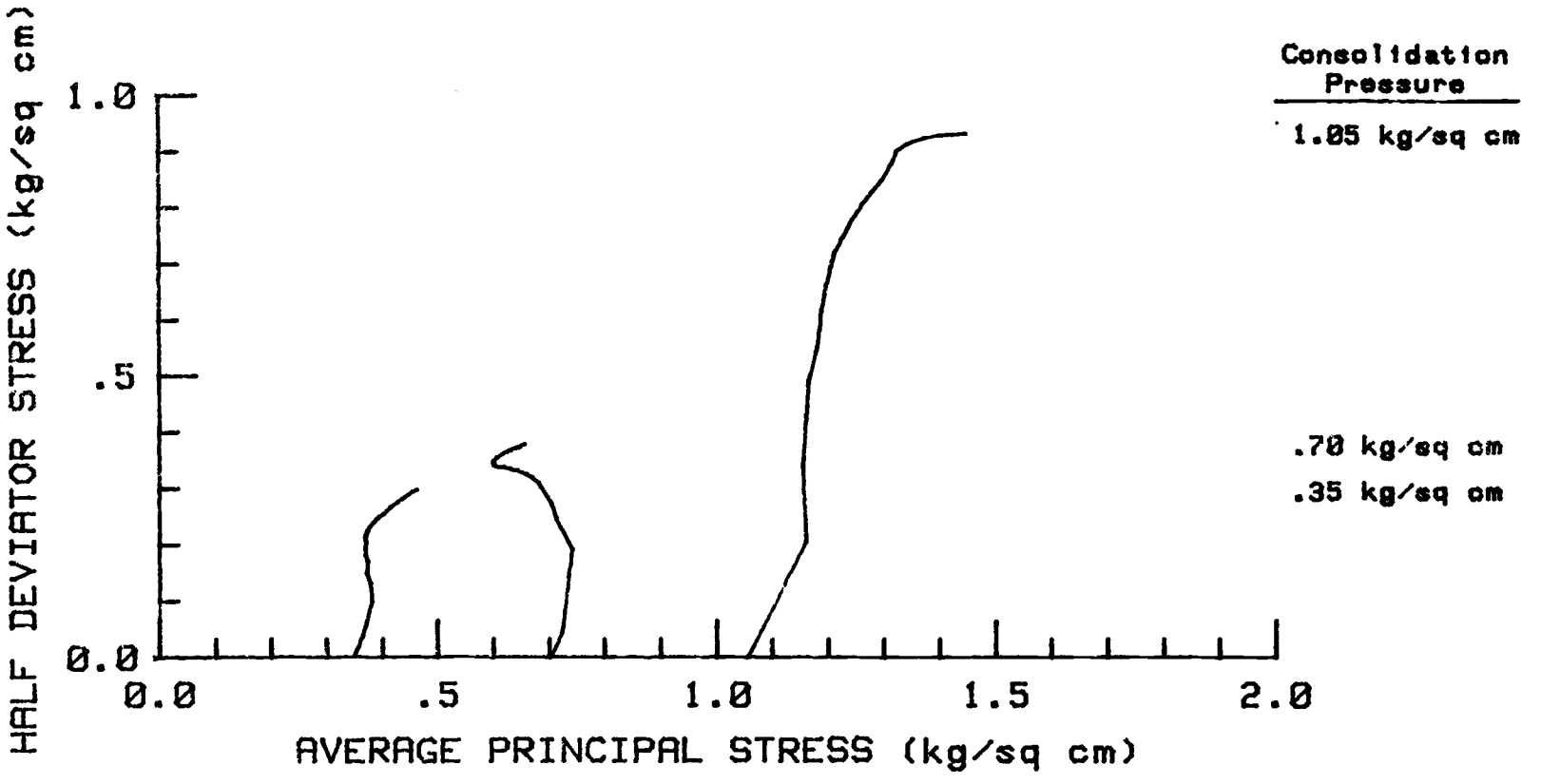

BOX CANYON CREEK SITE 6
UNDISTURBED TRIAX. W/ BACKPRESSURE--SS
EFFECTIVE STRESS ENVELOPE

ANGLE OF INTERNAL FRICTION = 46.6 Degrees
COHESION INTERCEPT =-.11 kg/sq cm

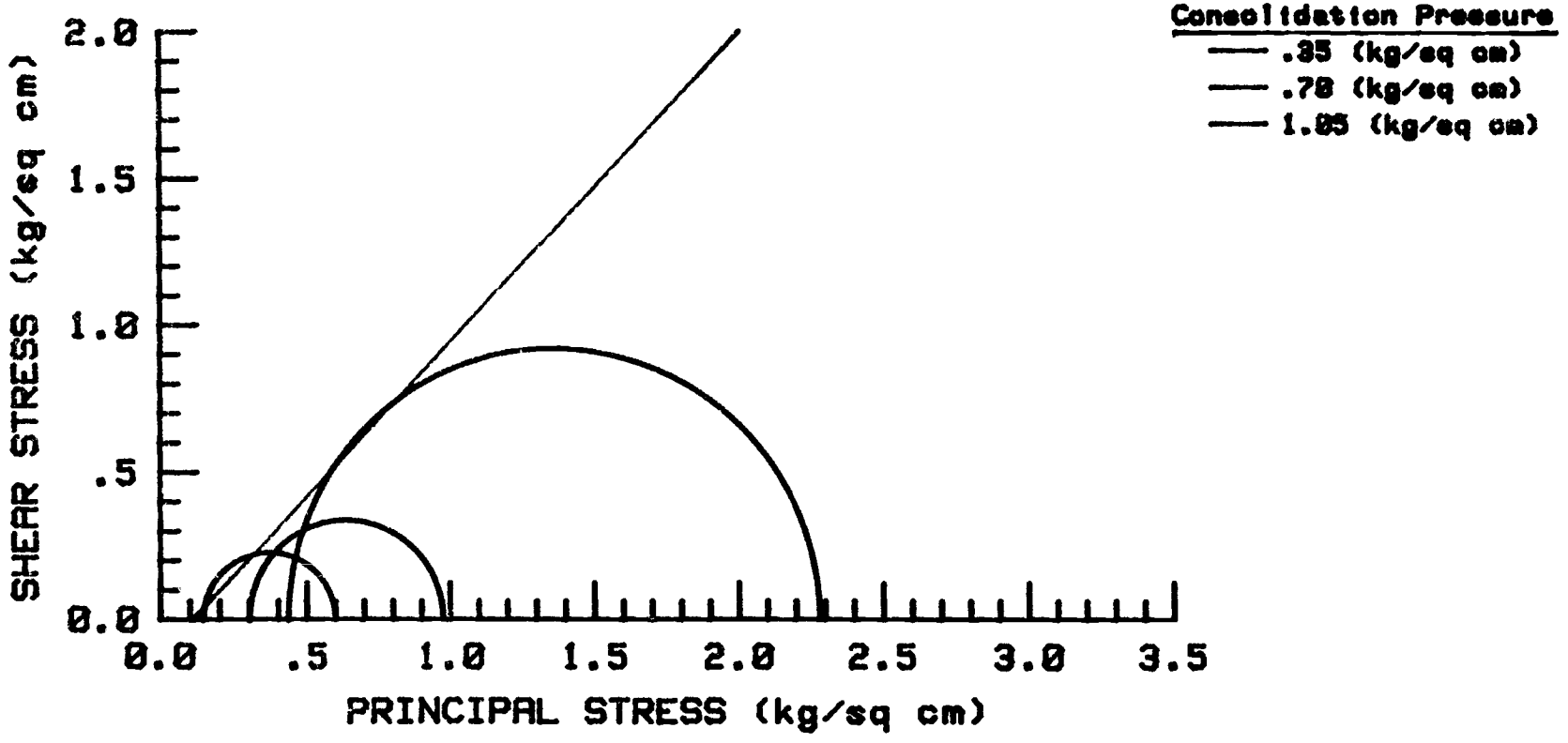

BOX CANYON CREEK SITE 6
UNDISTURBED TRIAX. W/ BACKPRESSURE--SR
EFFECTIVE STRESS ENVELOPE

ANGLE OF INTERNAL FRICTION = 46.9 Degrees
COHESION INTERCEPT =-.09 kg/sq cm

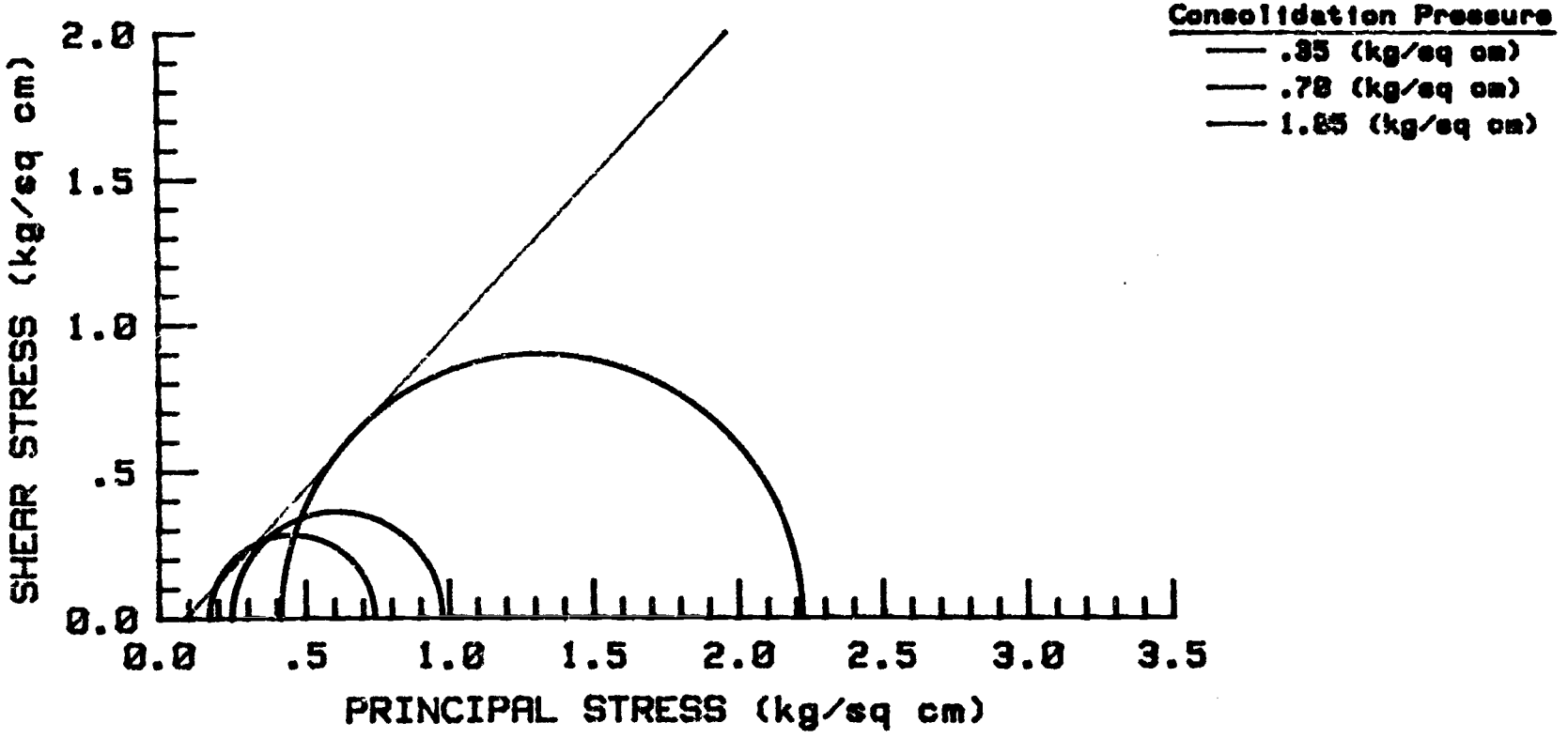

Strength testing summary of sample and test data

Site 7 - Quartzville Creek

Effective Consolidation Pressure ($\sigma_3 - U_o$ in Kg/cm^2)	0.35	0.70	1.41
Natural Moisture Content (W_n in %)	42.5	48.2	40.2
Insitu Wet Unit Weight (γ in g/cm^3)	1.44	1.55	1.48
Insitu Dry Unit Weight (γ_d in g/cm^3)	1.01	1.04	1.06
Insitu Degree Saturation (S in %)	67.2	80.5	68.1
Cell Pressure during Test (σ_3 in Kg/cm^2)	1.41	1.41	3.80
Initial Pore Pressure (U_o in Kg/cm^2)	1.06	0.71	2.75
B-Pore Pressure Parameter during Test (Ratio)	0.93	0.99	0.96

Strength testing summary of effective stress strength parameters

Site 7 - Quartzville Creek

For Mohr Envelope Derived from Stress-Strain Maximum Values

Effective Consolidation Pressure ($\sigma_3 - U_o$ in Kg/cm^2)		0.35	0.70	1.05
Deviator Stress at Failure ($\Delta\sigma_1$ in Kg/cm^2)		0.51	0.85	0.90
Pore Pressure at Failure (ΔU in Kg/cm^2)		0.22	0.40	0.63
Axial Strain at Failure (ϵ in %)		3.0	1.2	1.3
A-Pore Pressure Parameter at Failure (Ratio)		0.43	0.47	0.70
Effective Angle of Internal Friction (ϕ' in Degrees)	$\phi' =$	24.8		
Effective Cohesion Intercept (C' in Kg/cm^2)	$C' =$	0.11		
Correlation Coefficient (r - dimensionless)	$r =$	.9843		

For Mohr Envelope Derived from Stress Ratio Maximum Values

Effective Consolidation Pressure ($\sigma_3 - U_o$ in Kg/cm^2)		0.35	0.70	1.05
Deviator Stress at Failure ($\Delta\sigma_1$ in Kg/cm^2)		0.51	0.87	0.85
Pore Pressure at Failure (ΔU in Kg/cm^2)		0.22	0.46	0.80
Axial Strain at Failure (ϵ in %)		3.0	3.5	6.5
A-Pore Pressure Parameter at Failure (Ratio)		0.43	0.53	0.94
Effective Angle of Internal Friction (ϕ' in Degrees)	$\phi' =$	37.1		
Effective Cohesion Intercept (C' in Kg/cm^2)	$C' =$	0.03		
Correlation Coefficient (r-dimensionless)	$r =$	0.9988		

For Mohr Envelope Derived from Effective Stress Path Plot

Effective Angle of Internal Friction (ϕ' in Degrees)	$\phi' =$	38.1
Effective Cohesion Intercept (C' in Kg/cm^2)	$C' =$	0.0
Correlation Coefficient (r-dimensionless)	$r =$	.9984

QUARTZVILLE CREEK SITE 7
UNDISTURBED TRIAX. W/ BACKPRESSURE
DEVIATOR STRESS VS STRAIN

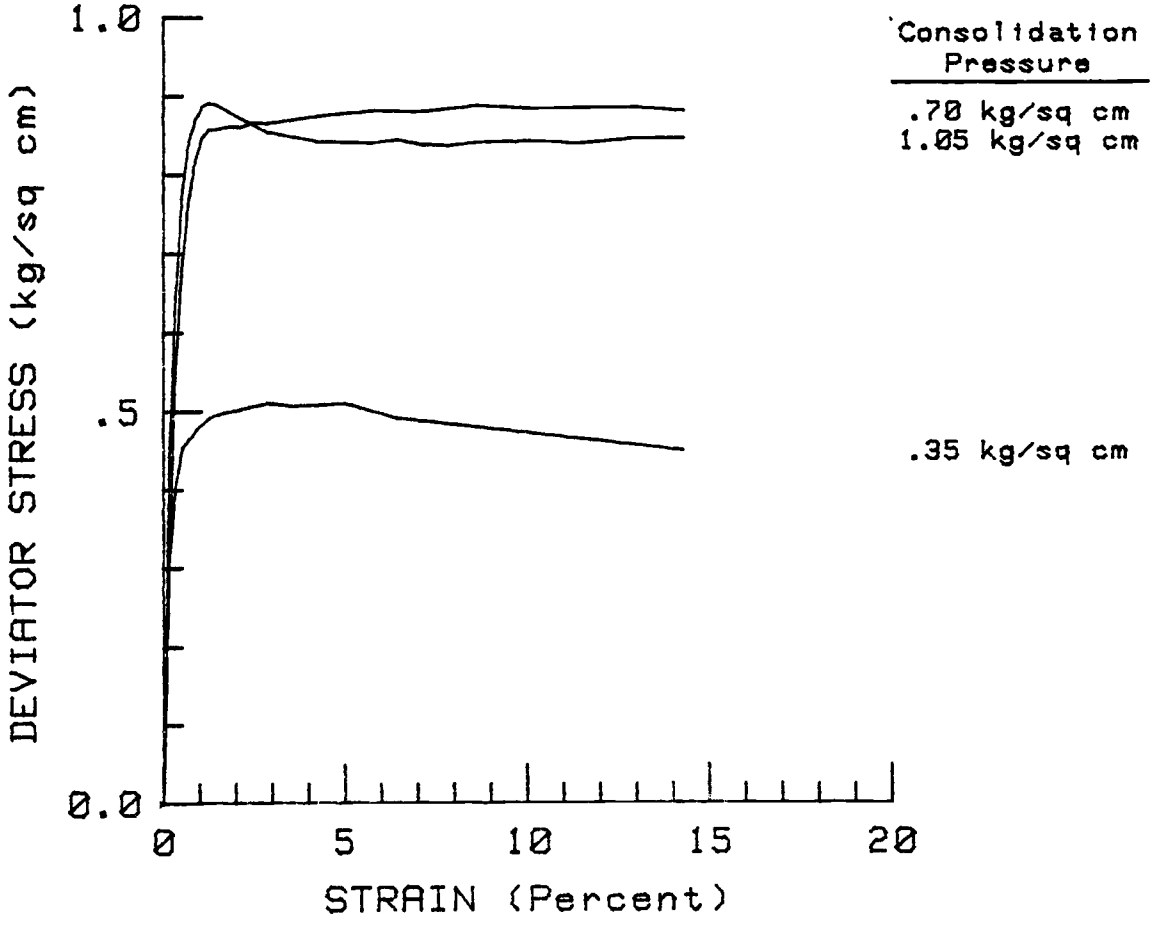

QUARTZVILLE CREEK SITE 7
UNDISTURBED TRIAX. W/ BACKPRESSURE
PORE WATER PRESSURE VS STRAIN

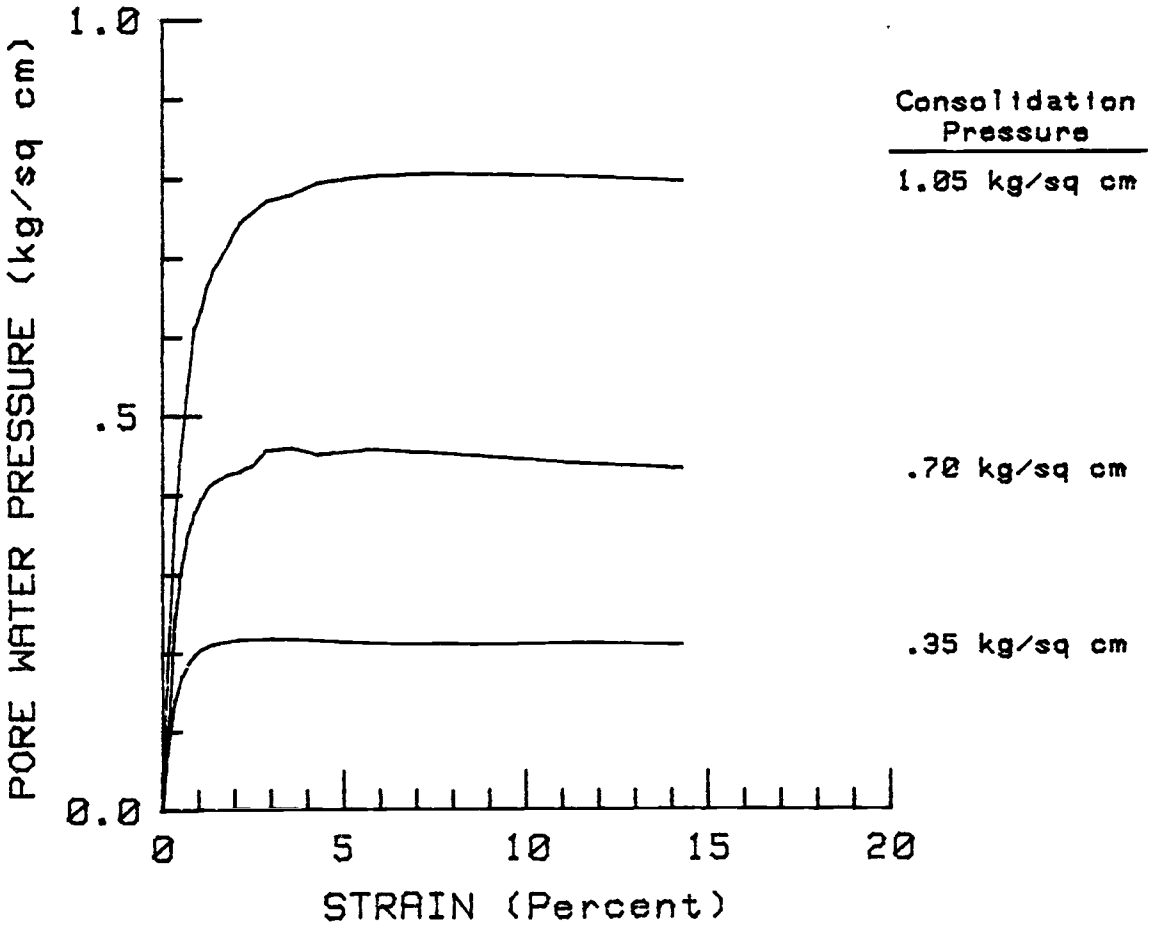

QUARTZVILLE CREEK SITE 7
UNDISTURBED TRIAX. W/ BACKPRESSURE
MAJOR PRINCIPAL STRESS RATIO VS STRAIN

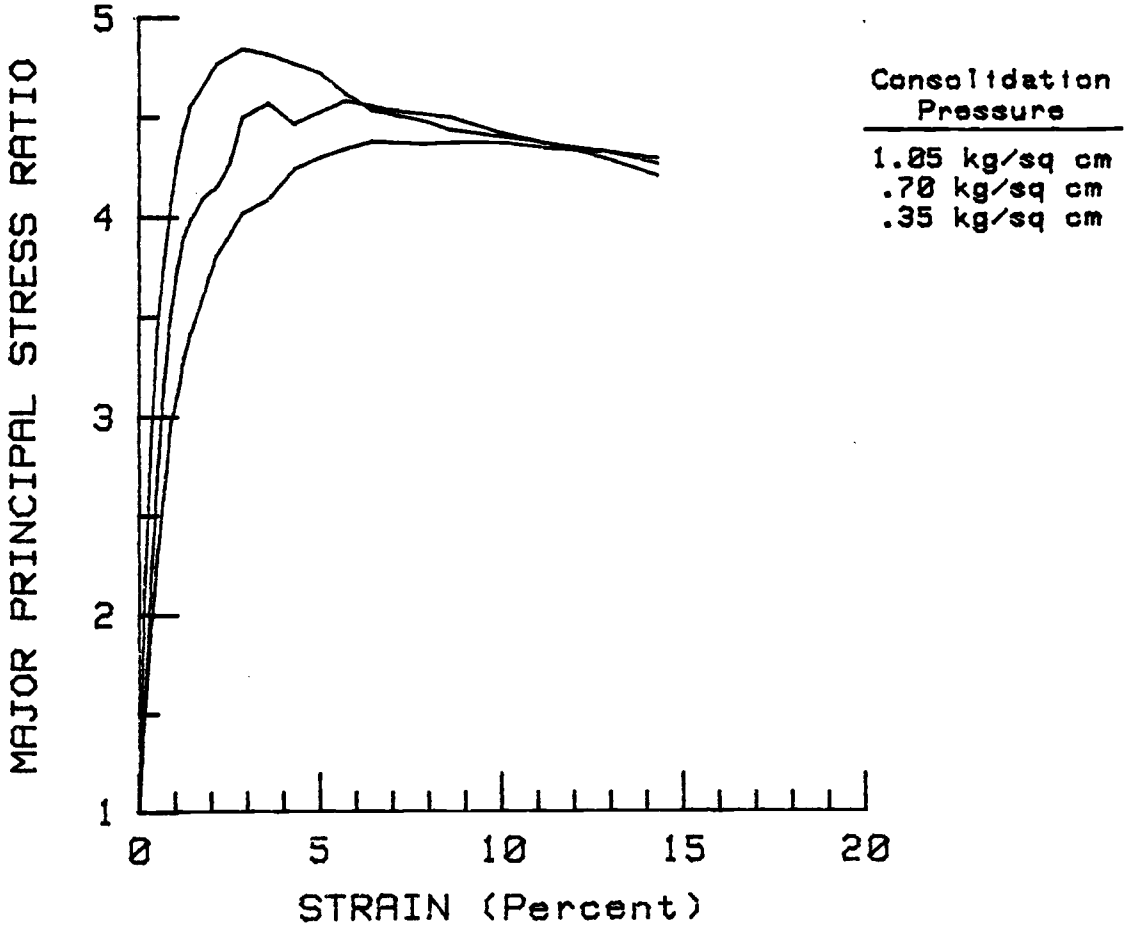

QUARTZVILLE CREEK SITE 7
UNDISTURBED TRIAX. W/ BACKPRESSURE
EFFECTIVE STRESS PATH PLOT

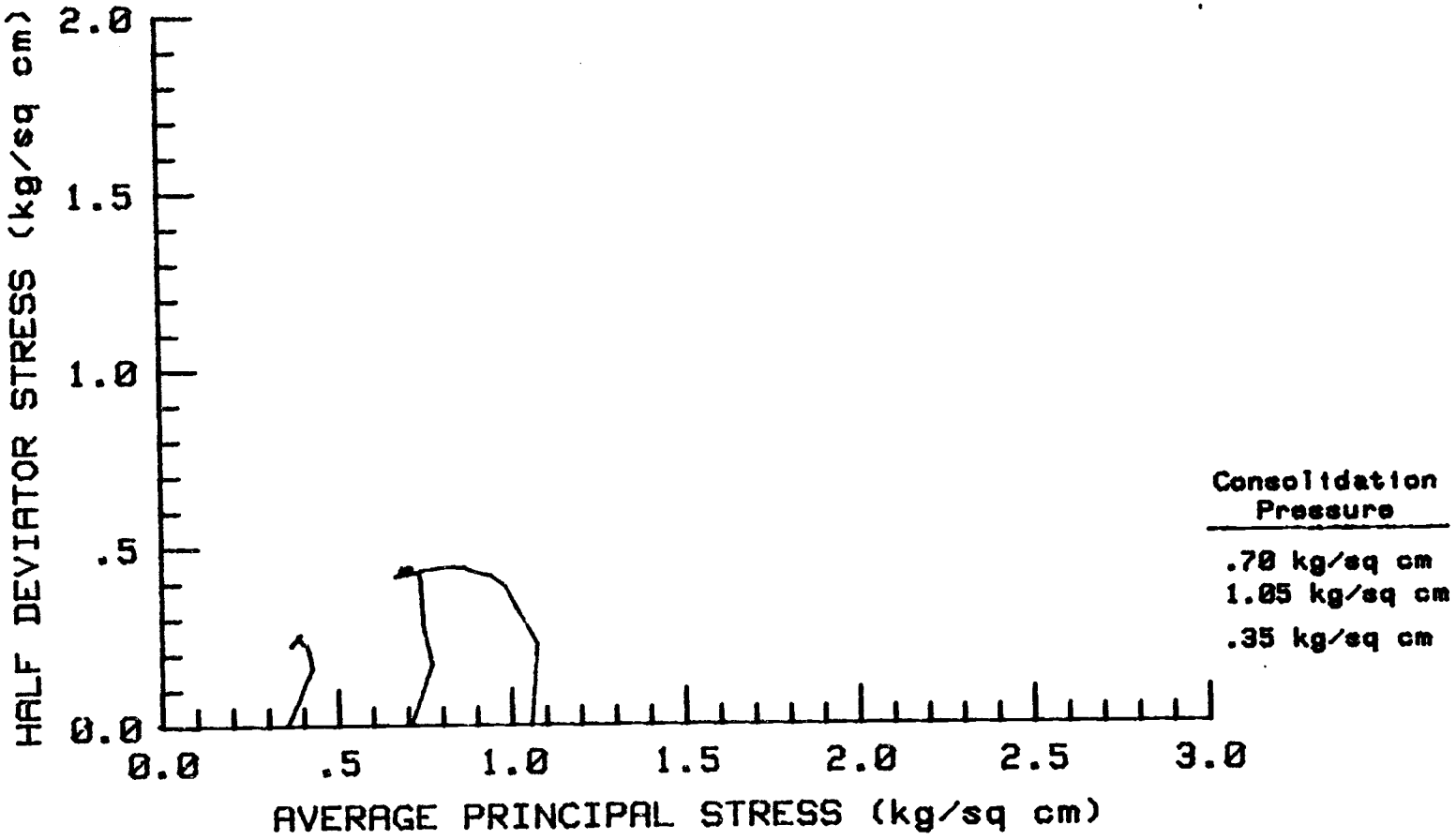

QUARTZVILLE CREEK SITE 7
UNDISTURBED TRIAX. W/ BACKPRESSURE--SS
EFFECTIVE STRESS ENVELOPE

ANGLE OF INTERNAL FRICTION = 24.9 Degrees
COHESION INTERCEPT = .11 kg/sq cm

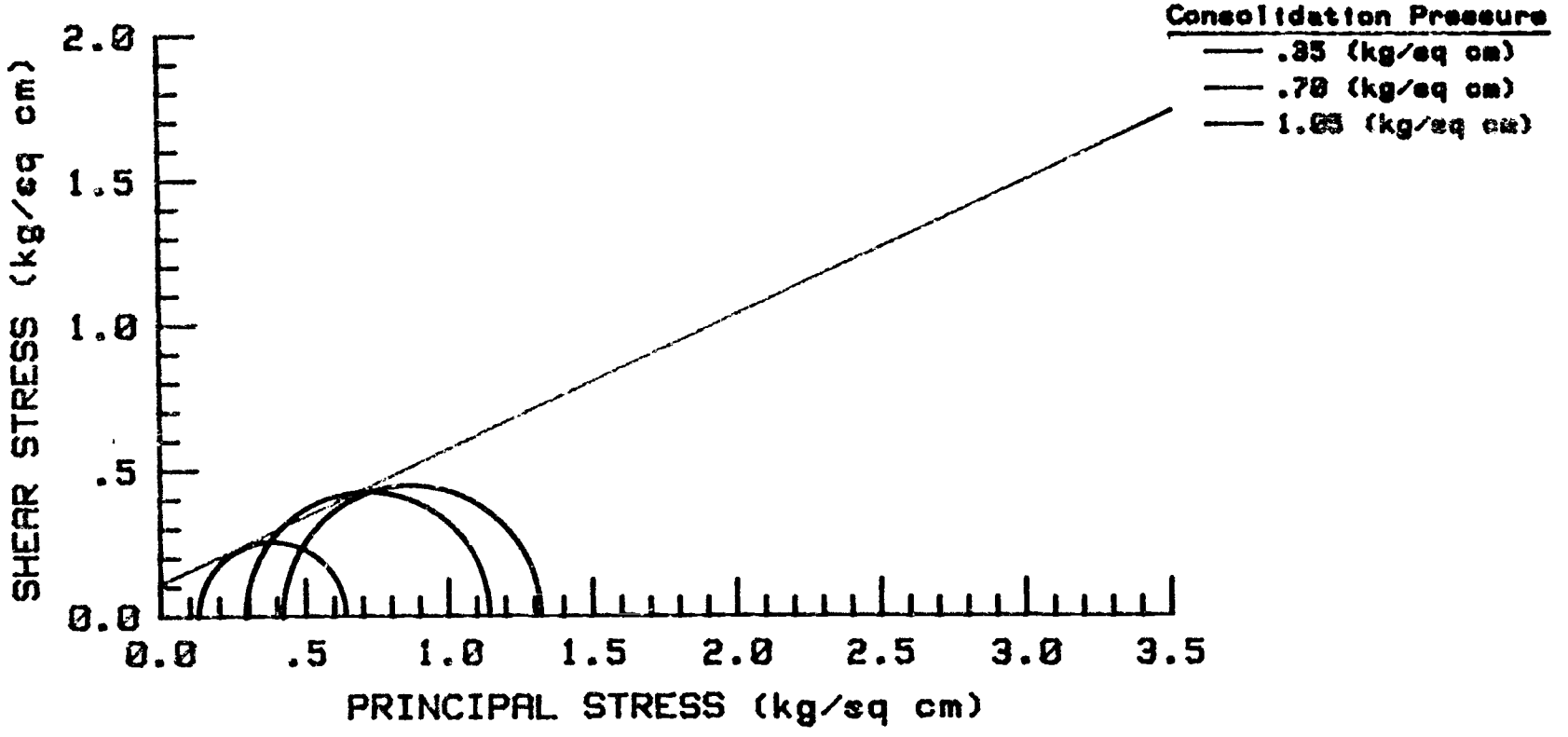

QUARTZVILLE CREEK SITE 7
UNDISTURBED TRIAX. W/ BACKPRESSURE--SR
EFFECTIVE STRESS ENVELOPE

ANGLE OF INTERNAL FRICTION = 37.8 Degrees
COHESION INTERCEPT = .02 kg/sq cm

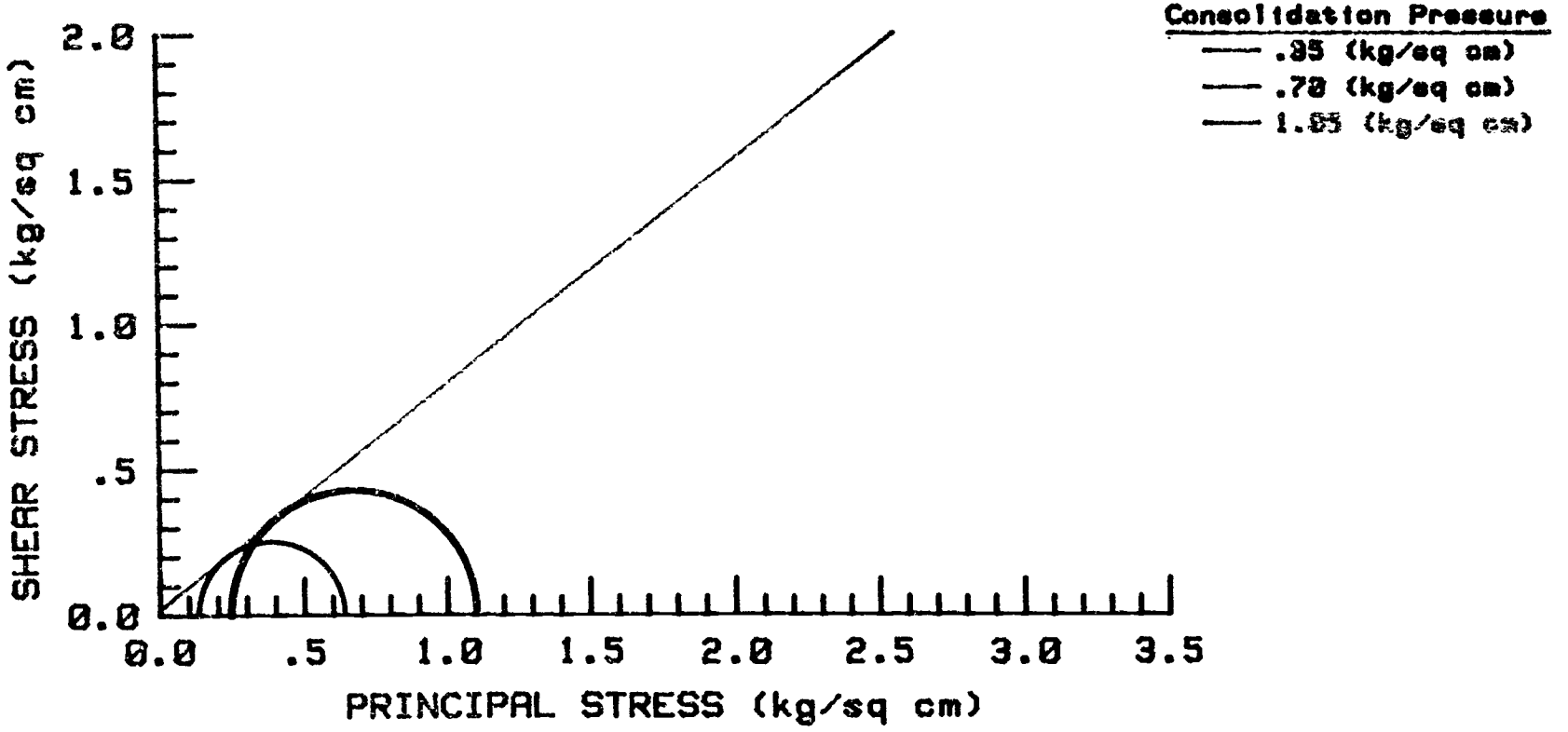

Strength testing summary of sample and test data

Site 8 - Fritz Creek

Effective Consolidation Pressure ($\sigma_3 - U_o$ in Kg/cm^2)	0.35	0.70	1.05
Natural Moisture Content (W_n in %)	45.5	40.0	53.3
Insitu Wet Unit Weight (γ in g/cm^3)	1.28	1.14	1.12
Insitu Dry Unit Weight (γ_d in g/cm^3)	0.88	0.81	0.73
Insitu Degree Saturation (S in %)	59.6	46.8	53.5
Cell Pressure during Test (σ_3 in Kg/cm^2)	3.17	2.11	3.52
Initial Pore Pressure (U_o in Kg/cm^2)	2.82	1.41	2.47
B-Pore Pressure Parameter during Test (Ratio)	0.86	0.90	0.93

Strength testing summary of effective stress strength parameters

Site 8 - Fritz Creek

For Mohr Envelope Derived from Stress-Strain Maximum Values

Effective Consolidation Pressure ($\sigma_3 - U_o$ in Kg/cm^2)		0.35	0.70	1.05
Deviator Stress at Failure ($\Delta\sigma_1$ in Kg/cm^2)		0.84	1.14	2.08
Pore Pressure at Failure (ΔU in Kg/cm^2)		0.18	0.40	0.62
Axial Strain at Failure (ϵ in %)		5.0	7.5	8.0
A-Pore Pressure Parameter at Failure (Ratio)		0.21	0.35	0.30
Effective Angle of Internal Friction (ϕ' in Degrees)	$\phi' =$	45.8		
Effective Cohesion Intercept (C' in Kg/cm^2)	$C' =$	-0.03		
Correlation Coefficient (r - dimensionless)	$r =$	.9966		

For Mohr Envelope Derived from Stress Ratio Maximum Values

Effective Consolidation Pressure ($\sigma_3 - U_o$ in Kg/cm^2)		0.35	0.70	1.05
Deviator Stress at Failure ($\Delta\sigma_1$ in Kg/cm^2)		0.72	1.14	1.98
Pore Pressure at Failure (ΔU in Kg/cm^2)		0.11	0.40	0.68
Axial Strain at Failure (ϵ in %)		2.5	7.5	4.5
A-Pore Pressure Parameter at Failure (Ratio)		0.15	0.35	0.34
Effective Angle of Internal Friction (ϕ' in Degrees)	$\phi' =$	56.3		
Effective Cohesion Intercept (C' in Kg/cm^2)	$C' =$	-0.26		
Correlation Coefficient (r-dimensionless)	$r =$	.9997		

For Mohr Envelope Derived from Effective Stress Path Plot

Effective Angle of Internal Friction (ϕ' in Degrees)	$\phi' =$	50.3
Effective Cohesion Intercept (C' in Kg/cm^2)	$C' =$	-0.11
Correlation Coefficient (r-dimensionless)	$r =$	.9901

FRITZ CREEK SITE 8
UNDISTRUBED TRIAX. W/ BACKPRESSURE
DEVIATOR STRESS VS STRAIN

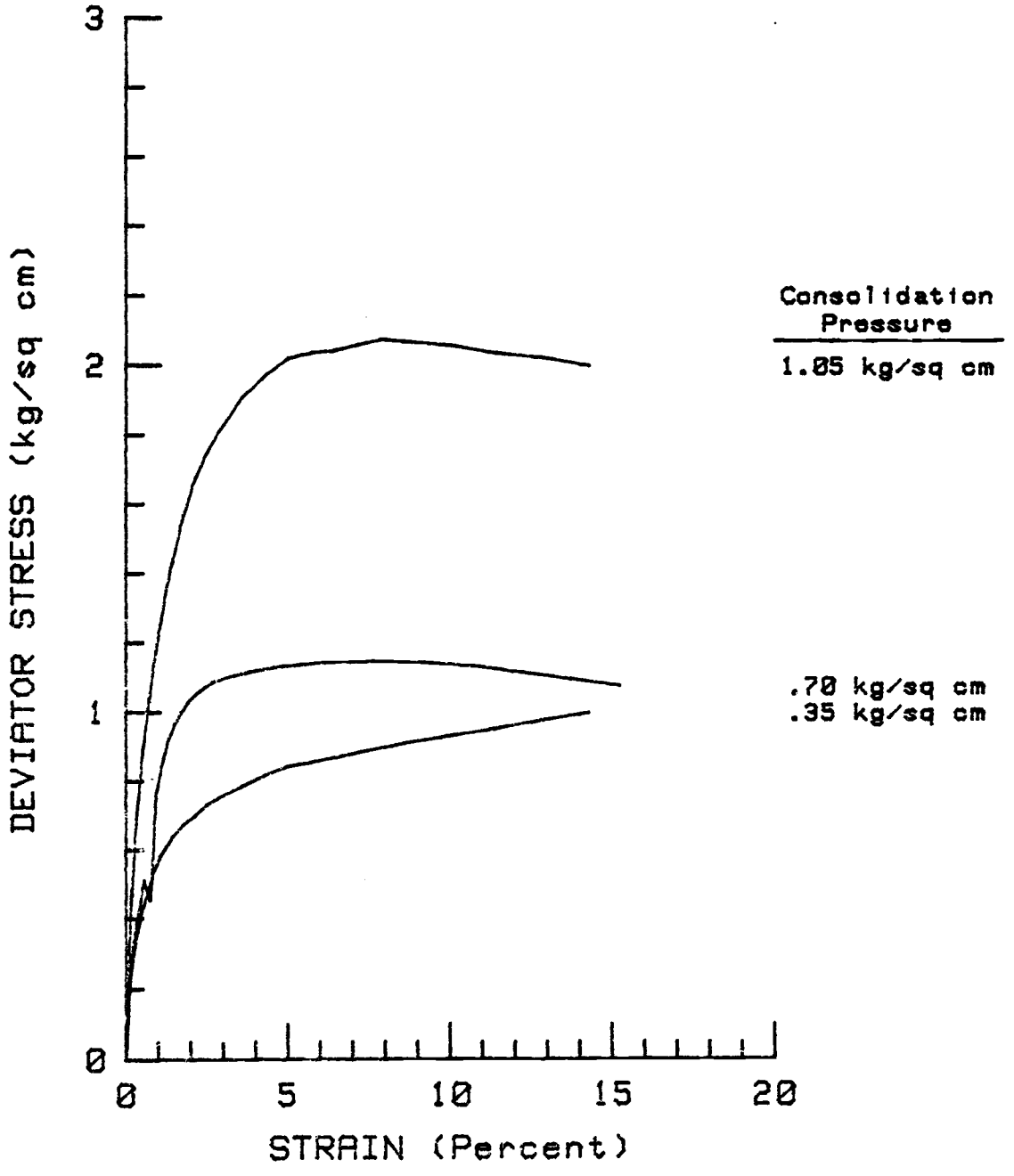

FRITZ CREEK SITE 8
UNDISTRUBED TRIAX. W/ BACKPRESSURE
PORE WATER PRESSURE VS STRAIN

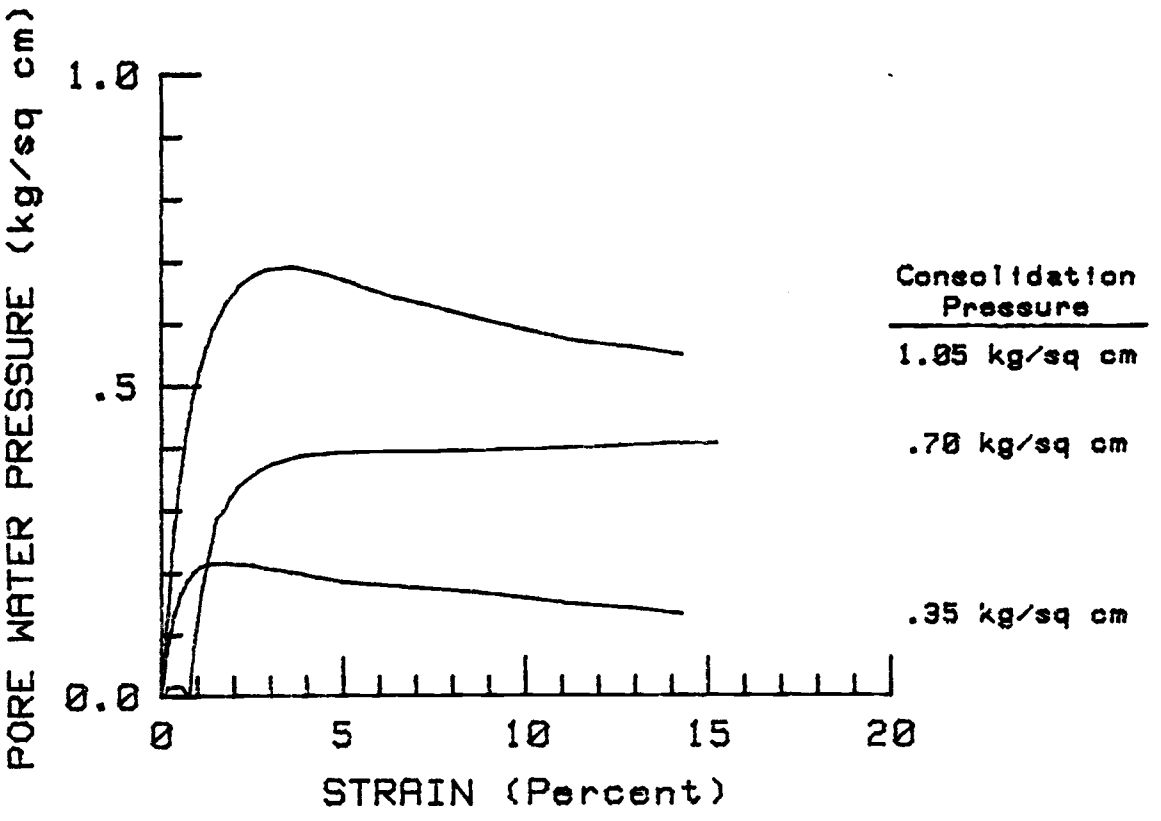

FRITZ CREEK SITE 8
UNDISTRUBED TRIAX. W/ BACKPRESSURE
MAJOR PRINCIPAL STRESS RATIO VS STRAIN

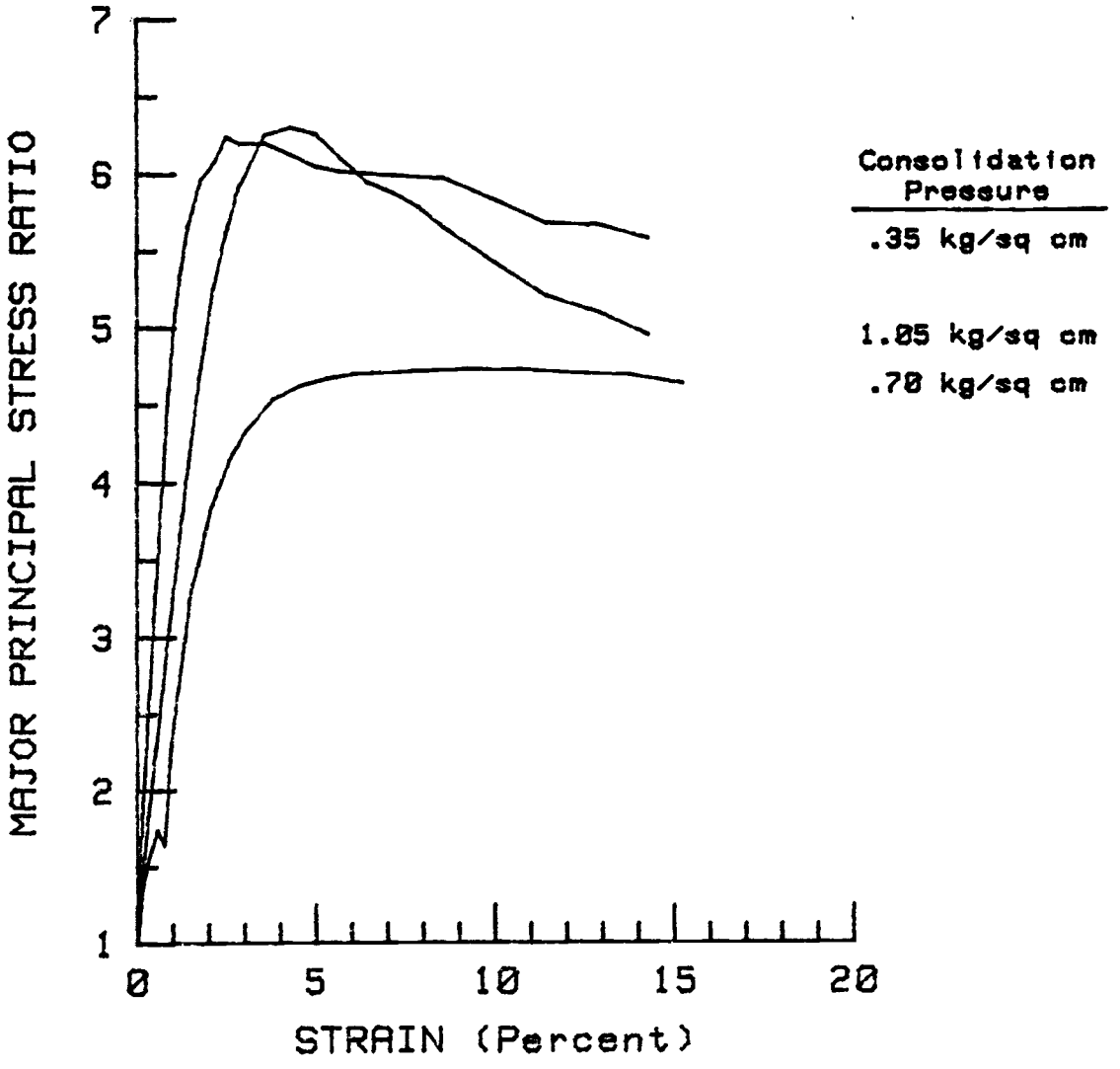

FRITZ CREEK SITE 8
UNDISTURBED TRIAX. W/ BACKPRESSURE
EFFECTIVE STRESS PATH PLOT

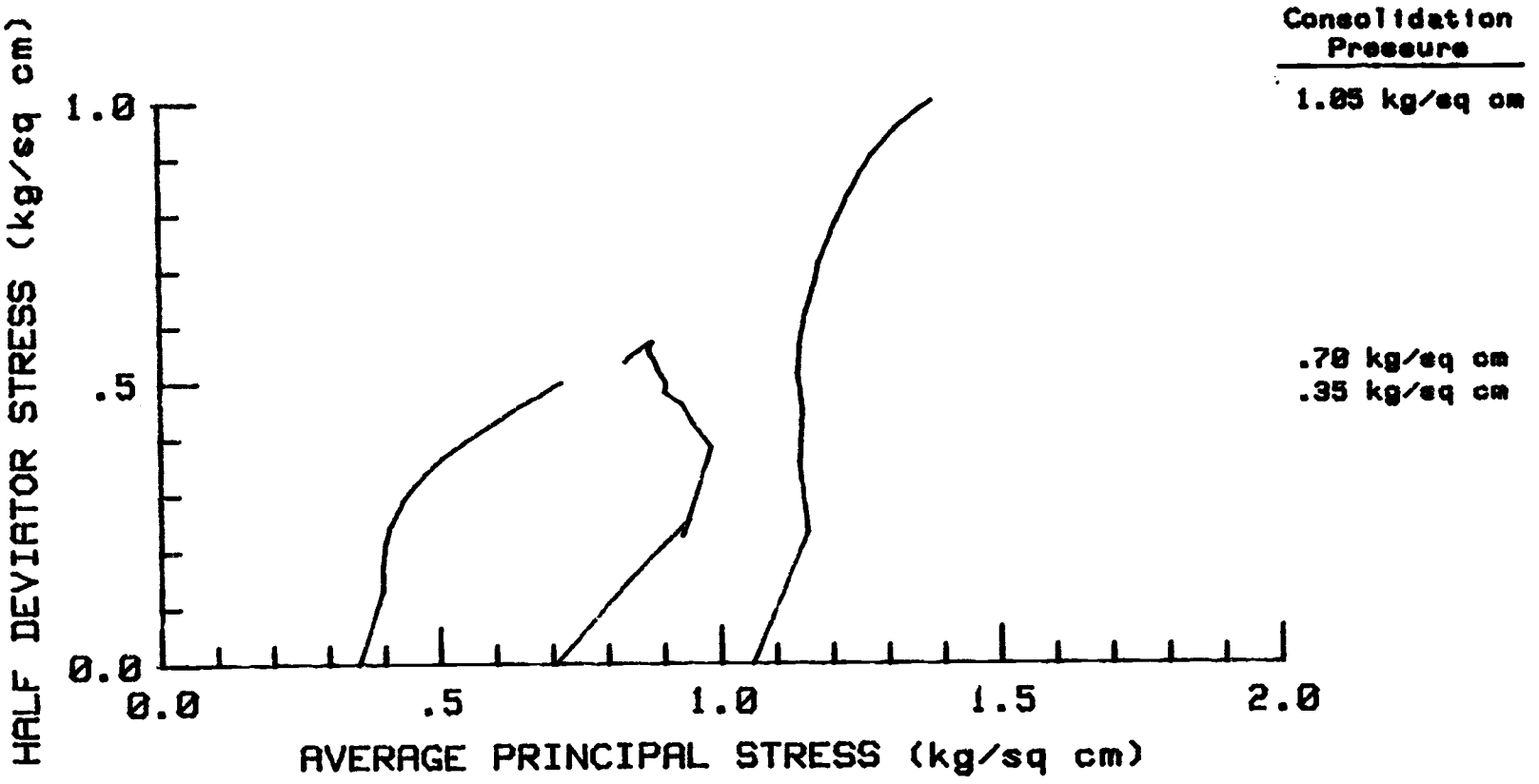

FRITZ CREEK SITE 8
UNDISTURBED TRIAX. W/ BACKPRESSURE--SS
EFFECTIVE STRESS ENVELOPE

ANGLE OF INTERNAL FRICTION = 45.4 Degrees
COHESION INTERCEPT =-.02 kg/sq cm

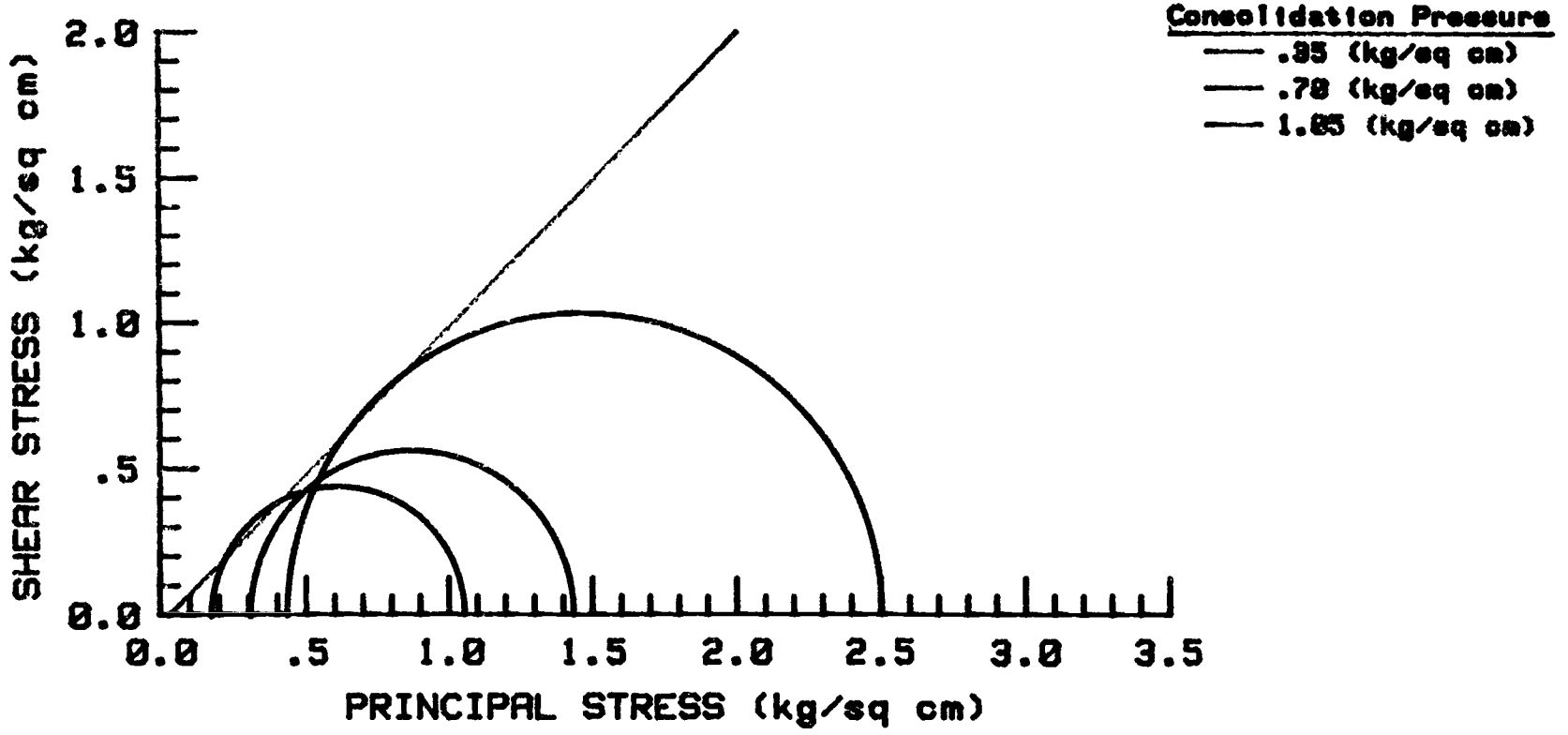

FRITZ CREEK SITE 8
UNDISTURBED TRIAX. W/ BACKPRESSURE--SR
EFFECTIVE STRESS ENVELOPE

ANGLE OF INTERNAL FRICTION = 57.6 Degrees
COHESION INTERCEPT =-.29 kg/sq cm

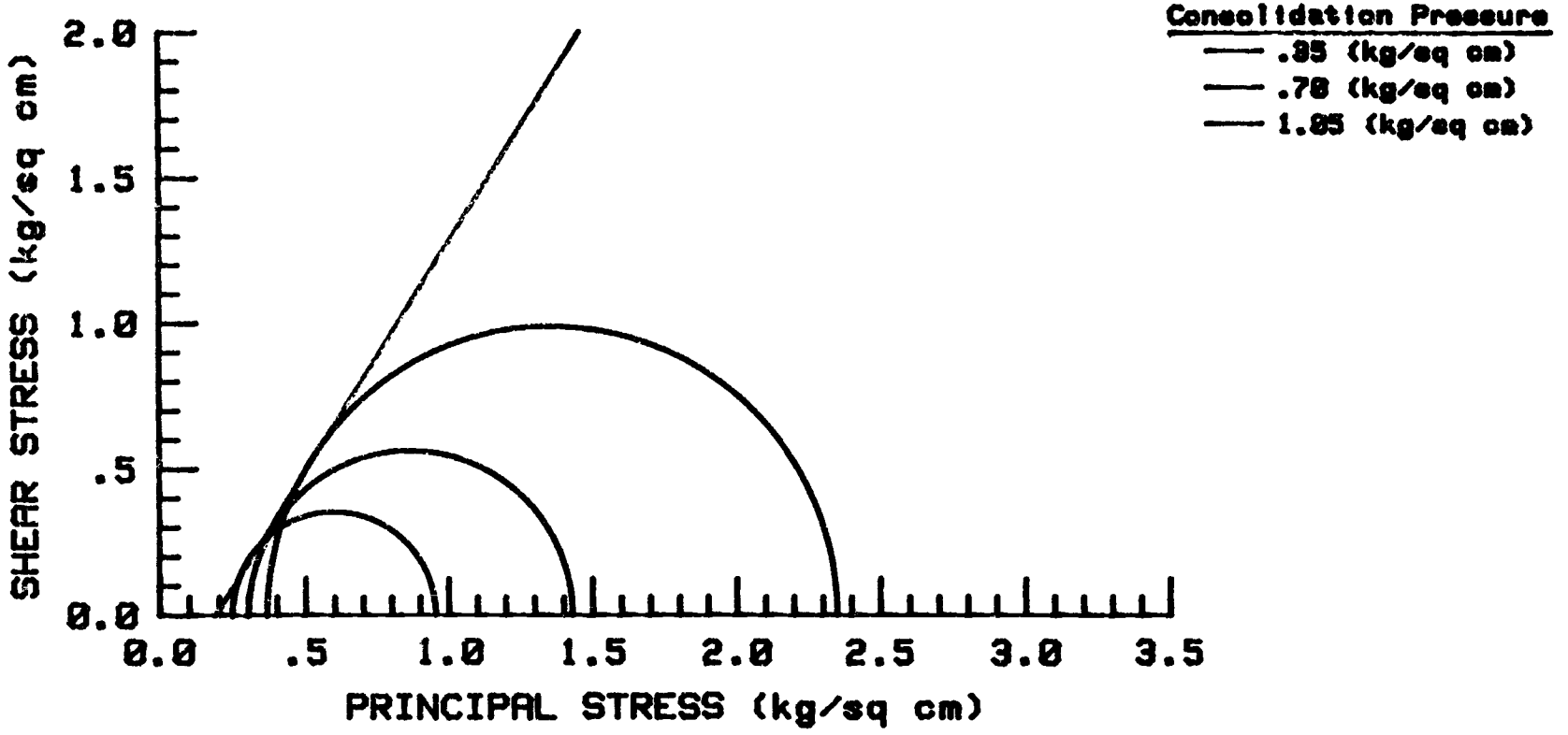

Strength testing summary of sample and test data

Site 9 - Lookout Creek

Effective Consolidation Pressure ($\sigma_3 - U_o$ in Kg/cm^2)	0.35	0.70	1.05
Natural Moisture Content (W_n in %)	31.5	43.7	32.6
Insitu Wet Unit Weight (γ in g/cm^3)	1.59	1.80	1.91
Insitu Dry Unit Weight (γ_d in g/cm^3)	1.21	1.25	1.44
Insitu Degree Saturation (S in %)	69.6	(103.1)	(102.0)
Cell Pressure during Test (σ_3 in Kg/cm^2)	1.41	3.52	2.81
Initial Pore Pressure (U_o in Kg/cm^2)	1.06	2.82	1.76
B-Pore Pressure Parameter during Test (Ratio)	0.98	0.94	0.96

Strength testing summary of effective stress strength parameters

Site 9 - Lookout Creek

For Mohr Envelope Derived from Stress-Strain Maximum Values

Effective Consolidation Pressure ($\sigma_3 - U_o$ in Kg/cm^2)		0.35	0.70	1.05
Deviator Stress at Failure ($\Delta\sigma_1$ in Kg/cm^2)		0.23	0.90	2.36
Pore Pressure at Failure (ΔU in Kg/cm^2)		0.24	0.40	0.23
Axial Strain at Failure (ϵ in %)		1.0	1.0	10
A-Pore Pressure Parameter at Failure (Ratio)		1.04	0.44	0.10
Effective Angle of Internal Friction (ϕ' in Degrees)	$\phi' =$	36.7		
Effective Cohesion Intercept (C' in Kg/cm^2)	$C' =$	-.01		
Correlation Coefficient (r - dimensionless)	$r =$	.9998		

For Mohr Envelope Derived from Stress Ratio Maximum Values

Effective Consolidation Pressure ($\sigma_3 - U_o$ in Kg/cm^2)		0.35	0.70	1.05
Deviator Stress at Failure ($\Delta\sigma_1$ in Kg/cm^2)		0.26	1.1	1.9
Pore Pressure at Failure (ΔU in Kg/cm^2)		0.28	0.44	0.6
Axial Strain at Failure (ϵ in %)		6.5	4.5	3
A-Pore Pressure Parameter at Failure (Ratio)		1.08	0.40	0.31
Effective Angle of Internal Friction (ϕ' in Degrees)	$\phi' =$	43.1		
Effective Cohesion Intercept (C' in Kg/cm^2)	$C' =$	-.01		
Correlation Coefficient (r-dimensionless)	$r =$	1.0000		

For Mohr Envelope Derived from Effective Stress Path Plot

Effective Angle of Internal Friction (ϕ' in Degrees)	$\phi' =$	43.3
Effective Cohesion Intercept (C' in Kg/cm^2)	$C' =$	0.01
Correlation Coefficient (r-dimensionless)	$r =$	.9999

LOOKOUT CREEK SITE 9
UNDISTURBED TRIAX. W/ BACKPRESSURE
DEVIATOR STRESS VS STRAIN

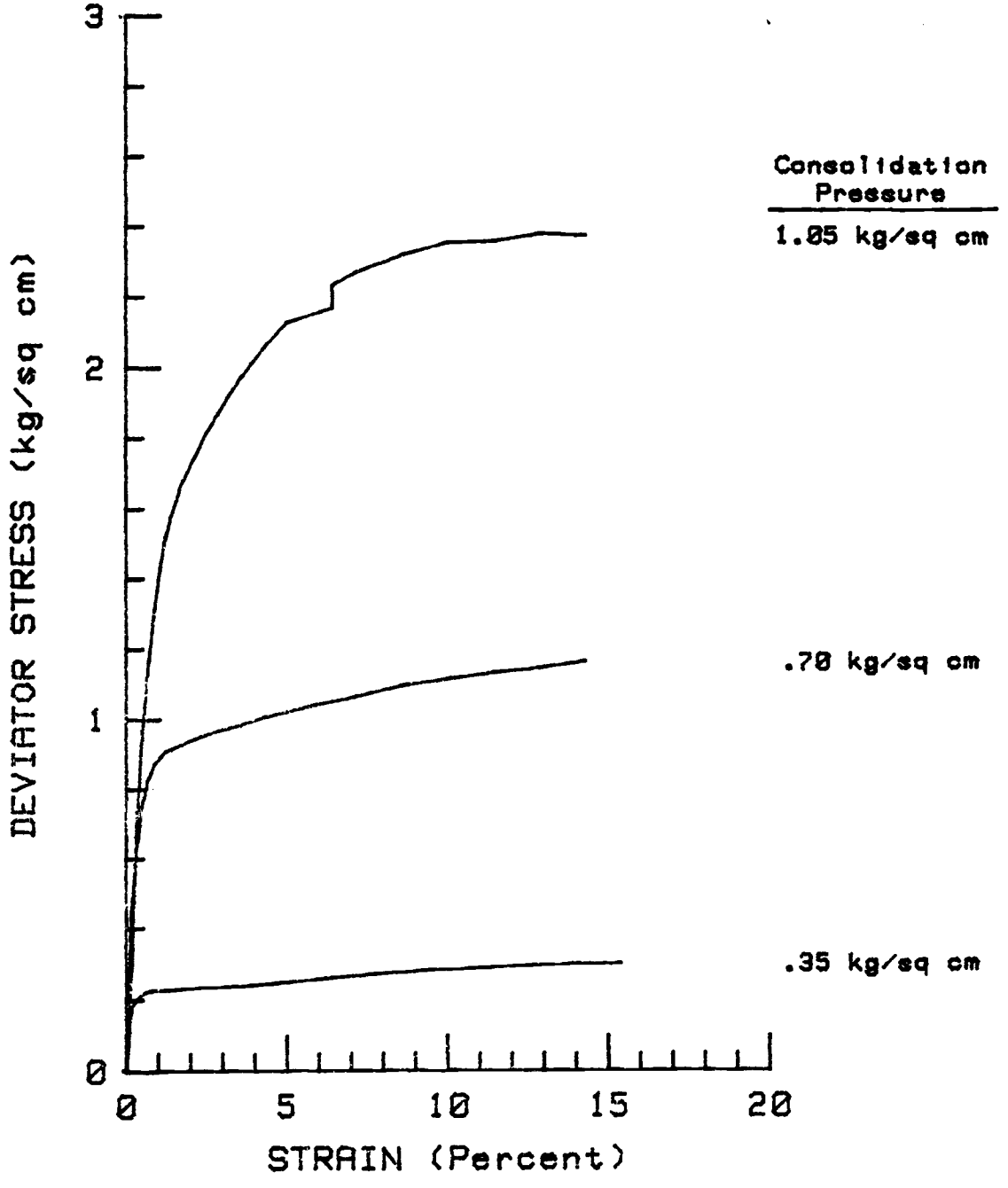

LOOKOUT CREEK SITE 9
UNDISTURBED TRIAX. W/ BACKPRESSURE
PORE WATER PRESSURE VS STRAIN

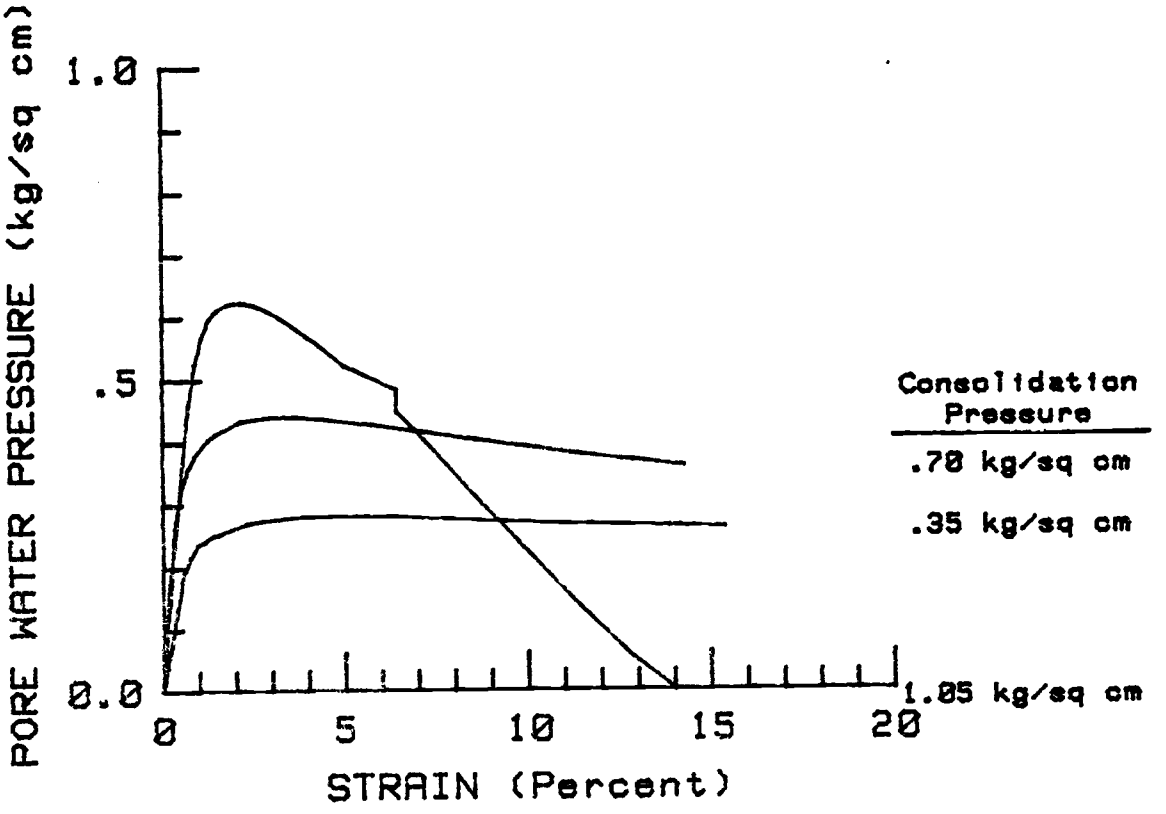

LOOKOUT CREEK SITE 9
UNDISTURBED TRIAX. W/ BACKPRESSURE
MAJOR PRINCIPAL STRESS RATIO VS STRAIN

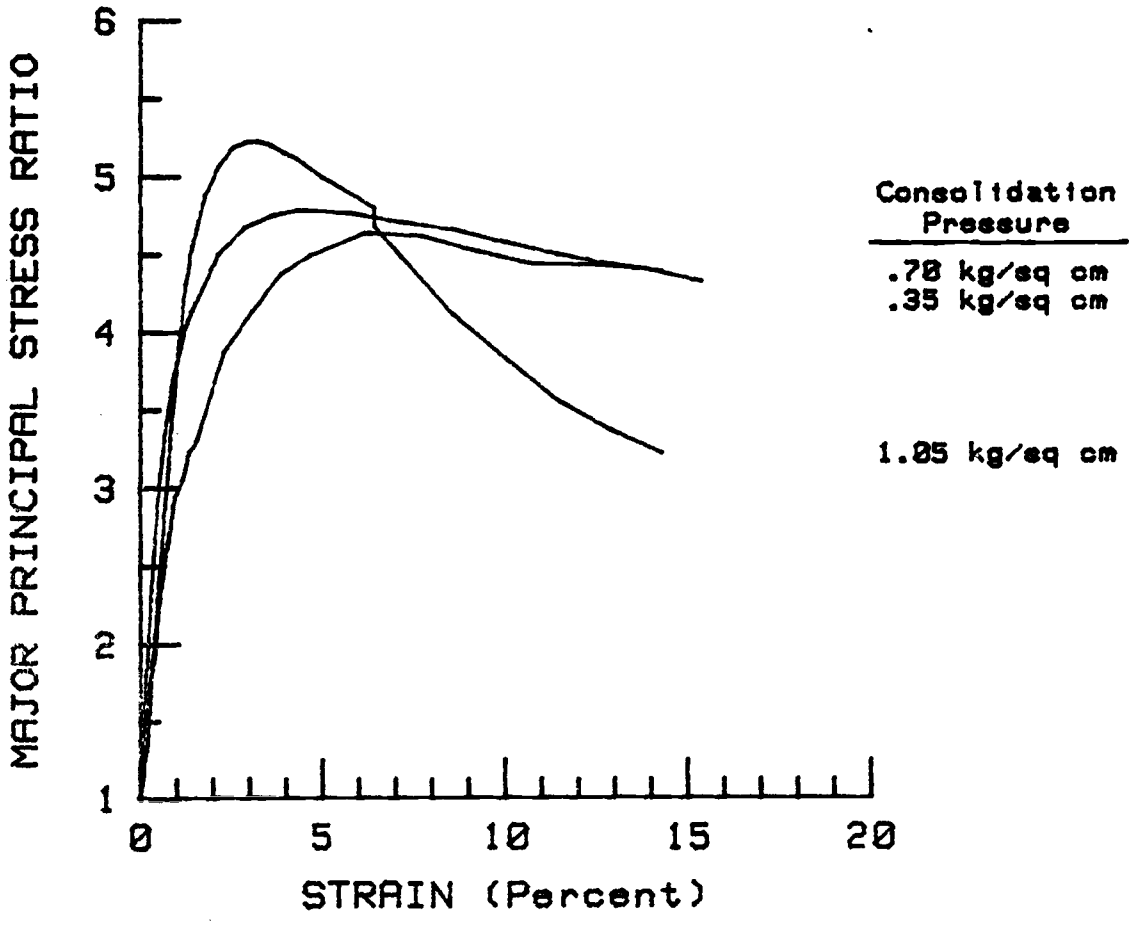

LOOKOUT CREEK SITE 9
UNDISTURBED TRIAX. W/ BACKPRESSURE
EFFECTIVE STRESS PATH PLOT

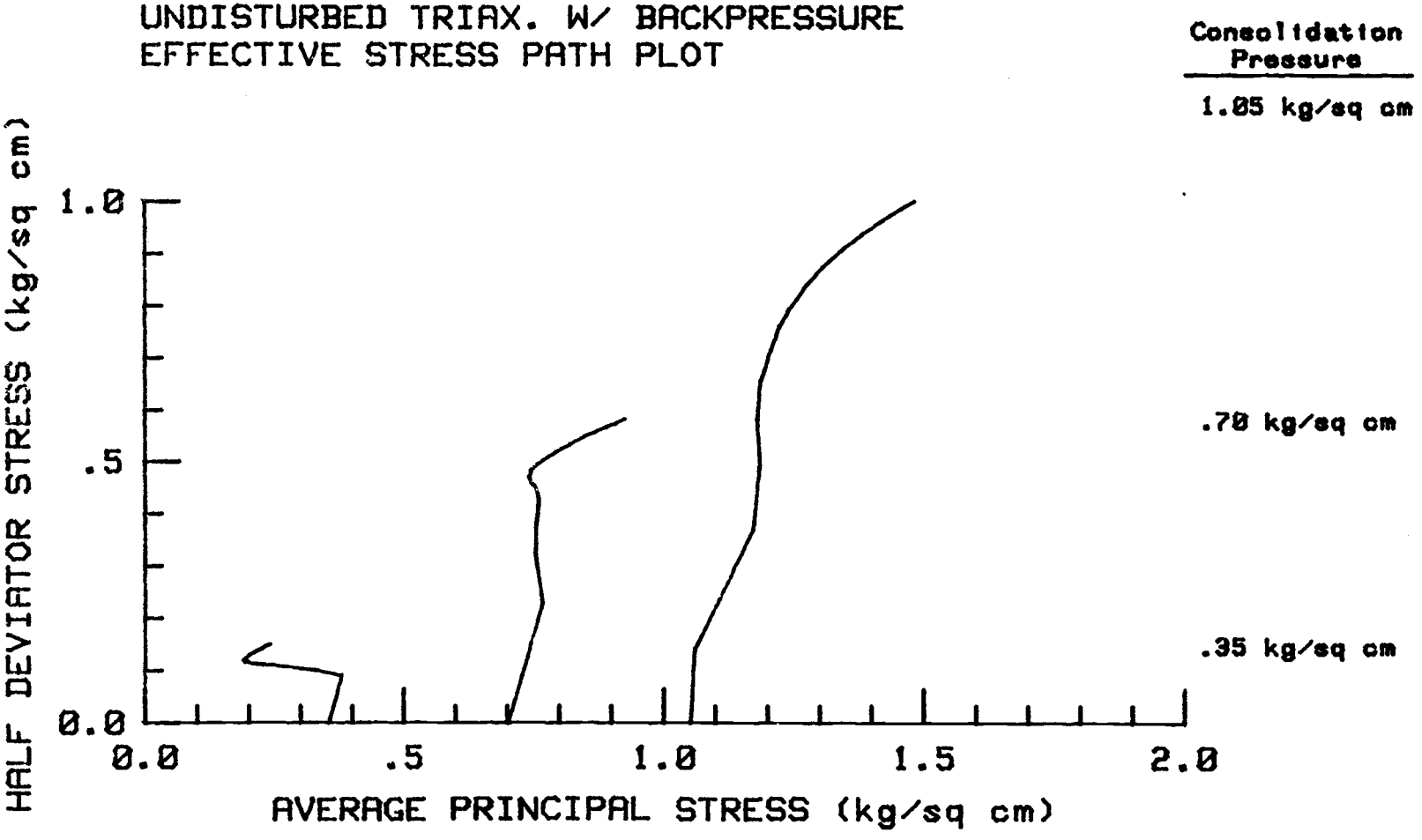

LOOKOUT CREEK SITE 9
UNDISTURBED TRIAX. W/ BACKPRESSURE--SS
EFFECTIVE STRESS ENVELOPE

ANGLE OF INTERNAL FRICTION = 36.8 Degrees
COHESION INTERCEPT =-.01 kg/sq cm

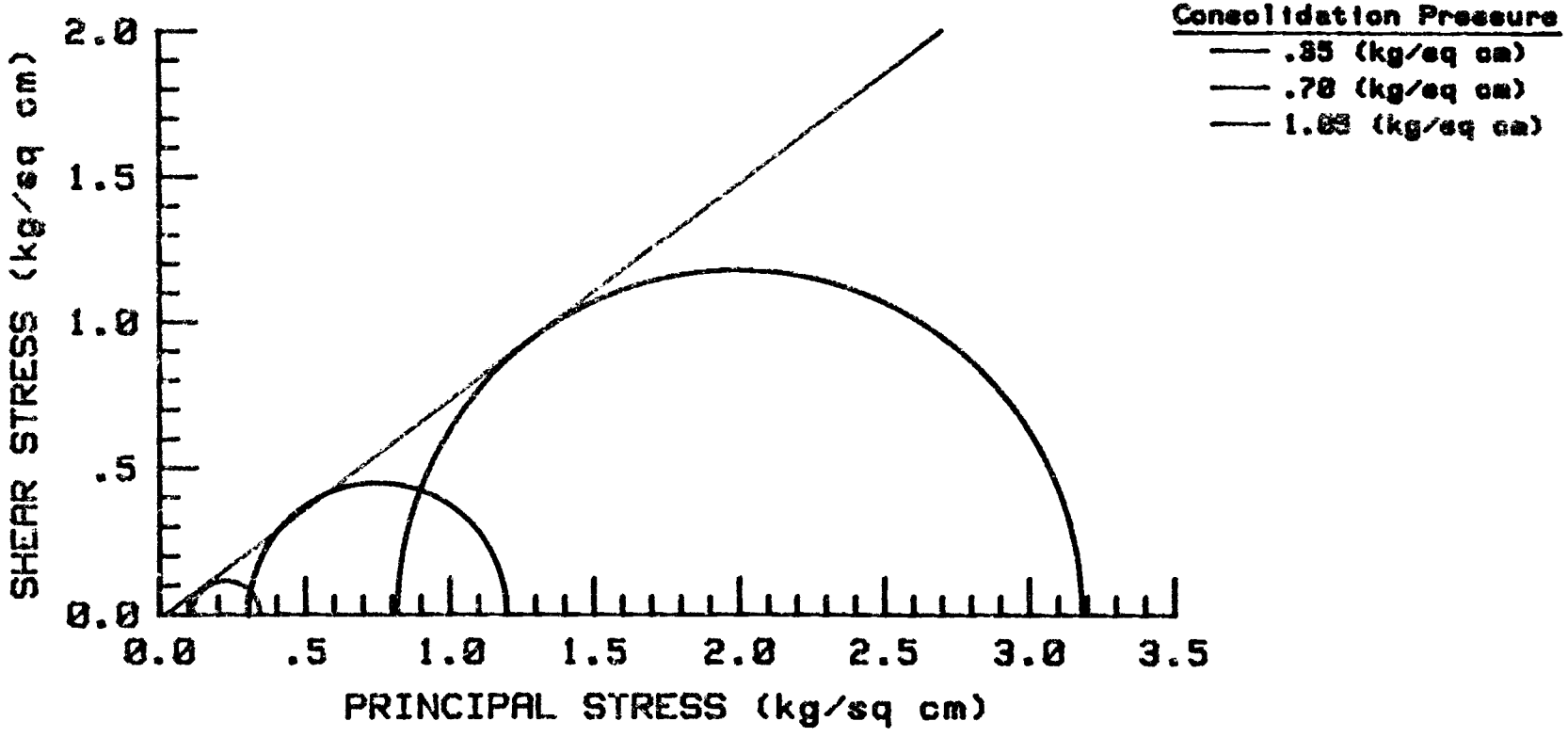

LOOKOUT CREEK SITE 9
UNDISTURBED TRIAX. W/ BACKPRESSURE--SR
EFFECTIVE STRESS ENVELOPE

ANGLE OF INTERNAL FRICTION = 43.4 Degrees
COHESION INTERCEPT =-.01 kg/sq cm

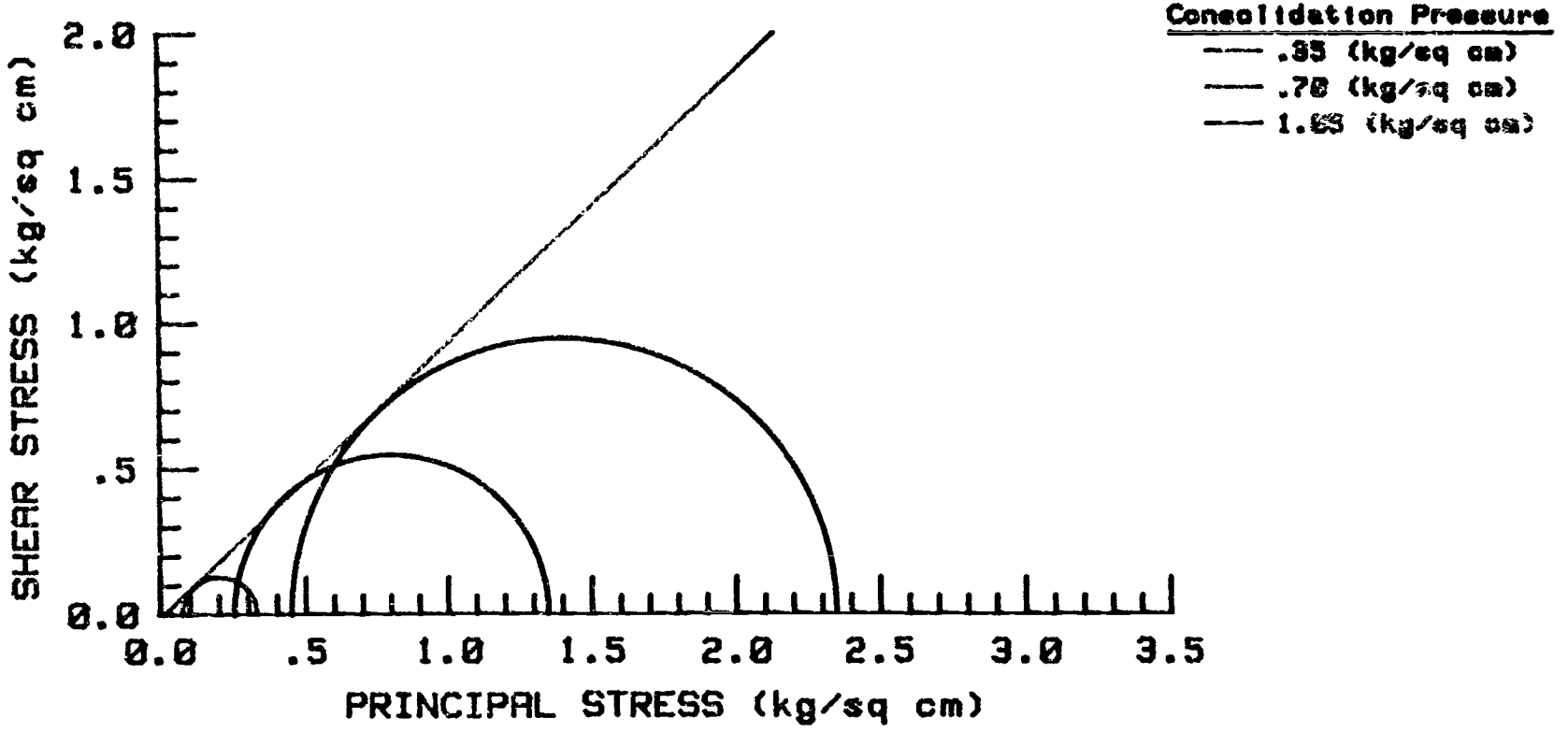

Strength testing summary of sample and test data

Site 10 - Alaska

Effective Consolidation Pressure ($\sigma_3 - U_o$ in Kg/cm^2)	0.35	0.70	1.05
Natural Moisture Content (W_n in %)	151.5	137.0	144.8
Insitu Wet Unit Weight (γ in g/cm^3)	1.33	1.33	1.27
Insitu Dry Unit Weight (γ_d in g/cm^3)	0.53	0.56	0.52
Insitu Degree Saturation (S in %)	99.9	97.3	93.2
Cell Pressure during Test (σ_3 in Kg/cm^2)	2.11	1.39	2.11
Initial Pore Pressure (U_o in Kg/cm^2)	1.76	0.69	1.06
B-Pore Pressure Parameter during Test (Ratio)	0.98	0.98	0.97

Strength testing summary of effective stress strength parameters

Site 10 - Alaska

For Mohr Envelope Derived from Stress-Strain Maximum Values

Effective Consolidation Pressure ($\sigma_3 - U_o$ in Kg/cm^2)		0.35	0.70	1.05
Deviator Stress at Failure ($\Delta\sigma_1$ in Kg/cm^2)		0.50	0.60	0.72
Pore Pressure at Failure (ΔU in Kg/cm^2)		0.25	0.52	0.72
Axial Strain at Failure (ϵ in %)		3.5	5.0	2.3
A-Pore Pressure Parameter at Failure (Ratio)		0.5	0.87	1.00
Effective Angle of Internal Friction (ϕ' in Degrees)	$\phi' =$	18.7		
Effective Cohesion Intercept (C' in Kg/cm^2)	C' =	0.15		
Correlation Coefficient (r - dimensionless)	r =	.9966		

For Mohr Envelope Derived from Stress Ratio Maximum Values

Effective Consolidation Pressure ($\sigma_3 - U_o$ in Kg/cm^2)		0.35	0.70	1.05
Deviator Stress at Failure ($\Delta\sigma_1$ in Kg/cm^2)		0.50	0.57	0.59
Pore Pressure at Failure (ΔU in Kg/cm^2)		0.25	0.54	0.78
Axial Strain at Failure (ϵ in %)		3.0	11.0	5.0
A-Pore Pressure Parameter at Failure (Ratio)		0.50	0.95	1.32
Effective Angle of Internal Friction (ϕ' in Degrees)	$\phi' =$	11.8		
Effective Cohesion Intercept (C' in Kg/cm^2)	C' =	0.19		
Correlation Coefficient (r-dimensionless)	r =	.9296		

For Mohr Envelope Derived from Effective Stress Path Plot

Effective Angle of Internal Friction (ϕ' in Degrees)	$\phi' =$	20.1
Effective Cohesion Intercept (C' in Kg/cm^2)	C' =	0.14
Correlation Coefficient (r-dimensionless)	r =	.9976

ALASKA SITE 10
UNDISTURBED TRIAX. W/ BACKPRESSURE
DEVIATOR STRESS VS STRAIN

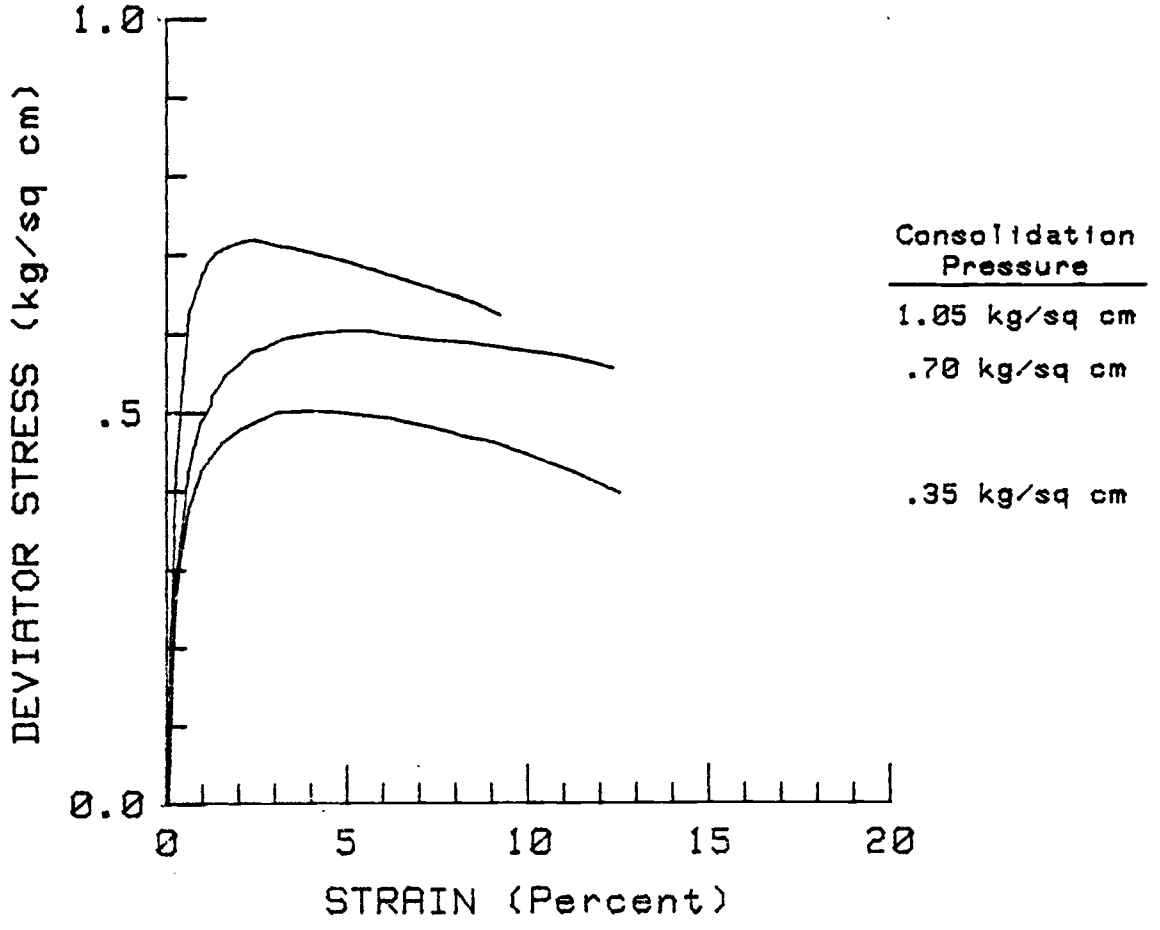

ALASKA SITE 10
UNDISTURBED TRIAX. W/ BACKPRESSURE
PORE WATER PRESSURE VS STRAIN

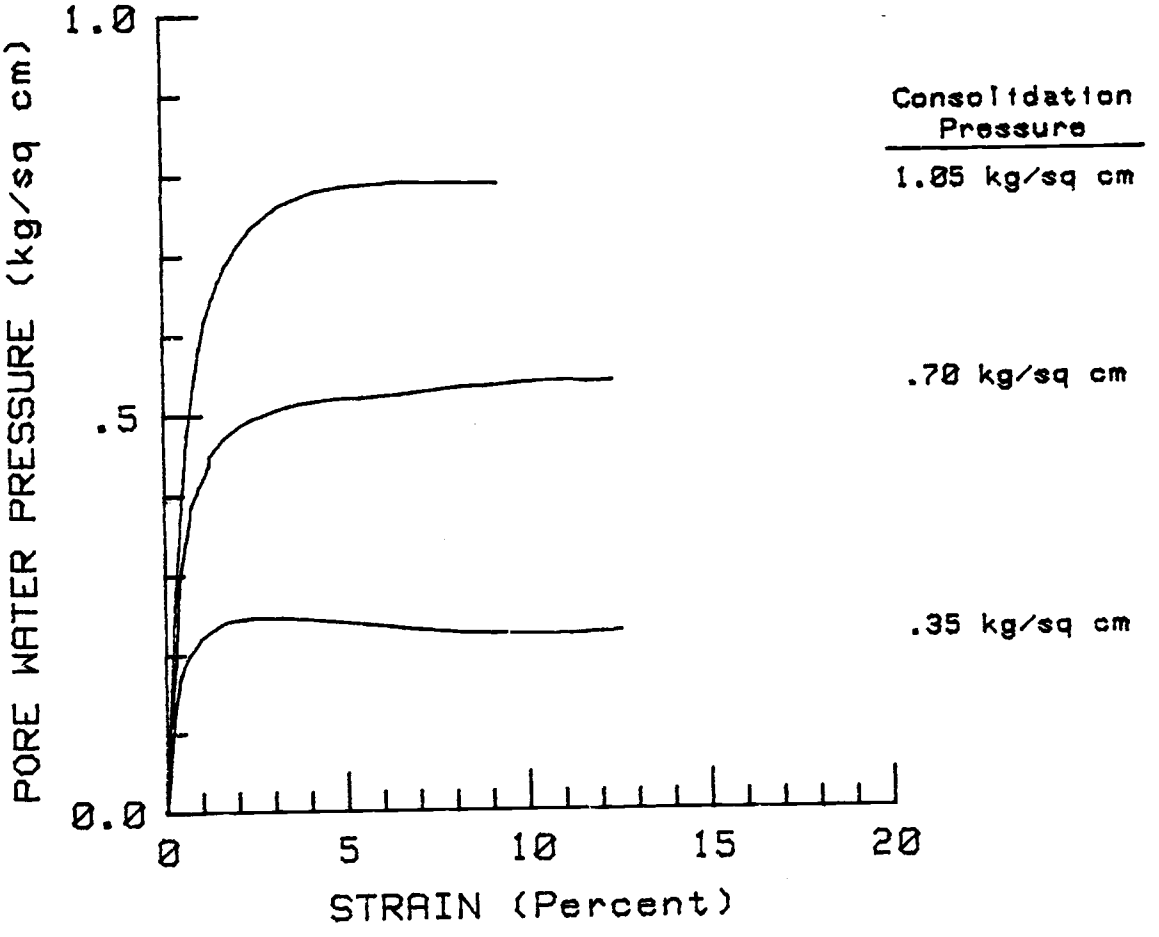

ALASKA SITE 10
UNDISTURBED TRIAX. W/ BACKPRESSURE
MAJOR PRINCIPAL STRESS RATIO VS STRAIN

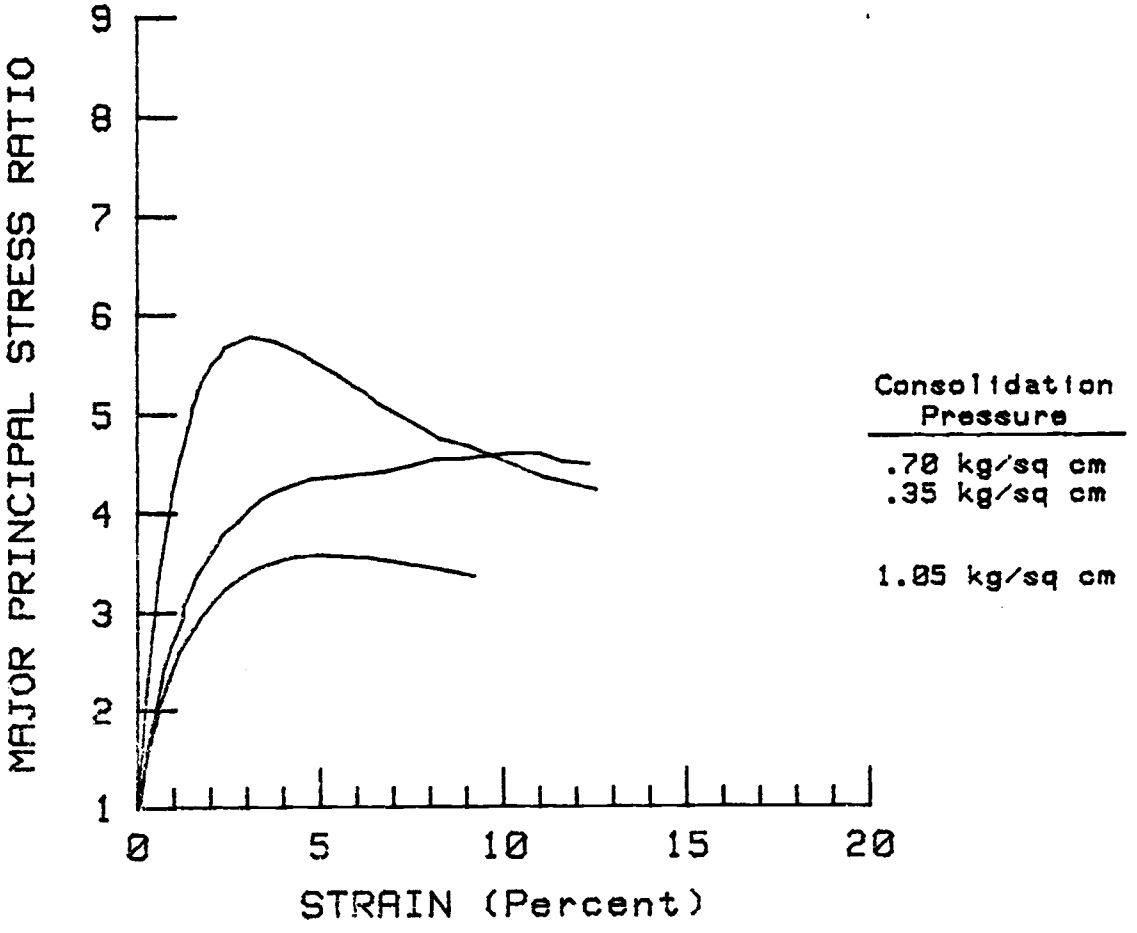

ALASKA SITE 10
UNDISTURBED TRIAX. W/ BACKPRESSURE
EFFECTIVE STRESS PATH PLOT

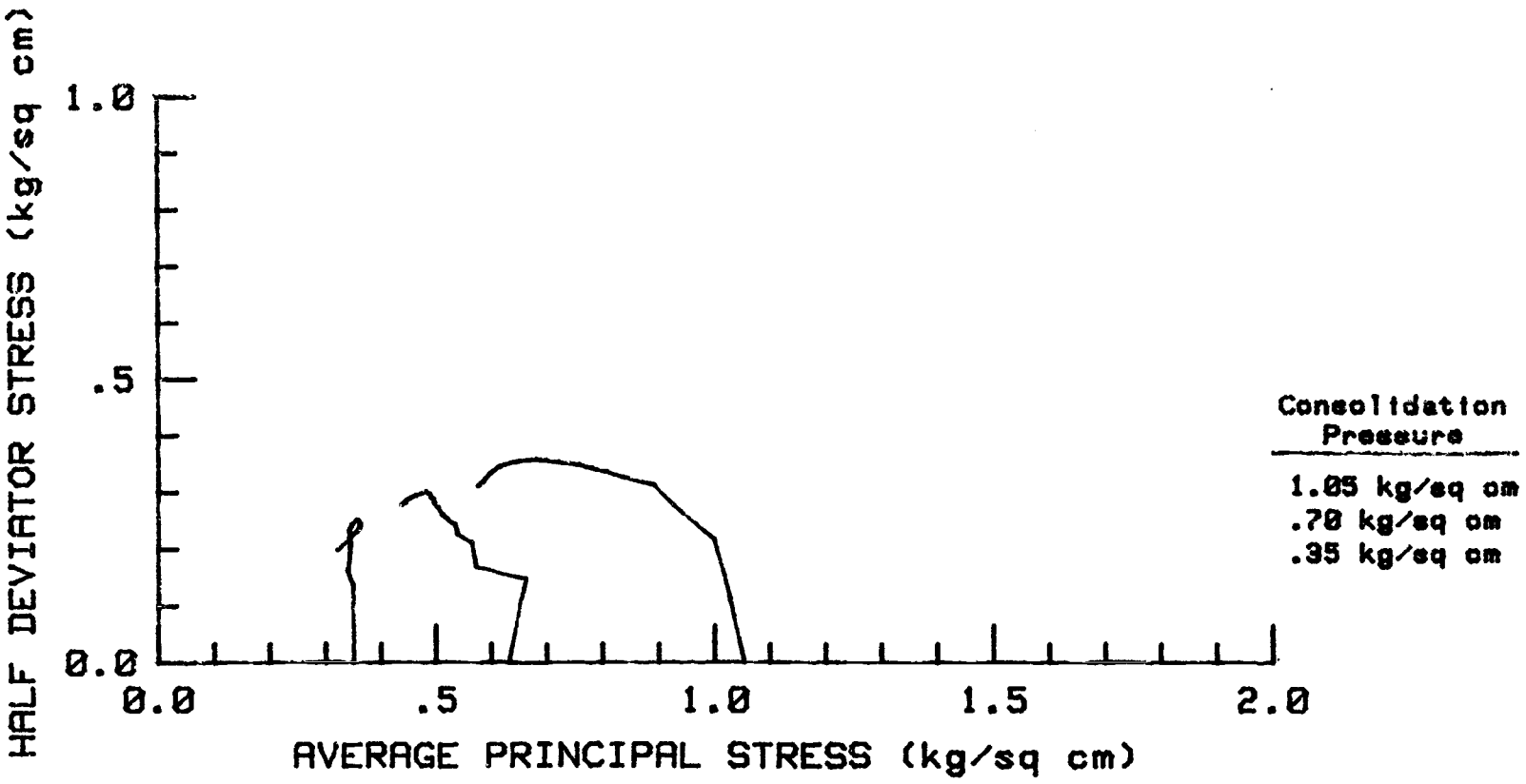

ALASKA SITE 18
UNDISTURBED TRIAX. W/ BACKPRESSURE--SR
EFFECTIVE STRESS ENVELOPE

ANGLE OF INTERNAL FRICTION = 11.8 Degrees
COHESION INTERCEPT = .19 kg/sq cm

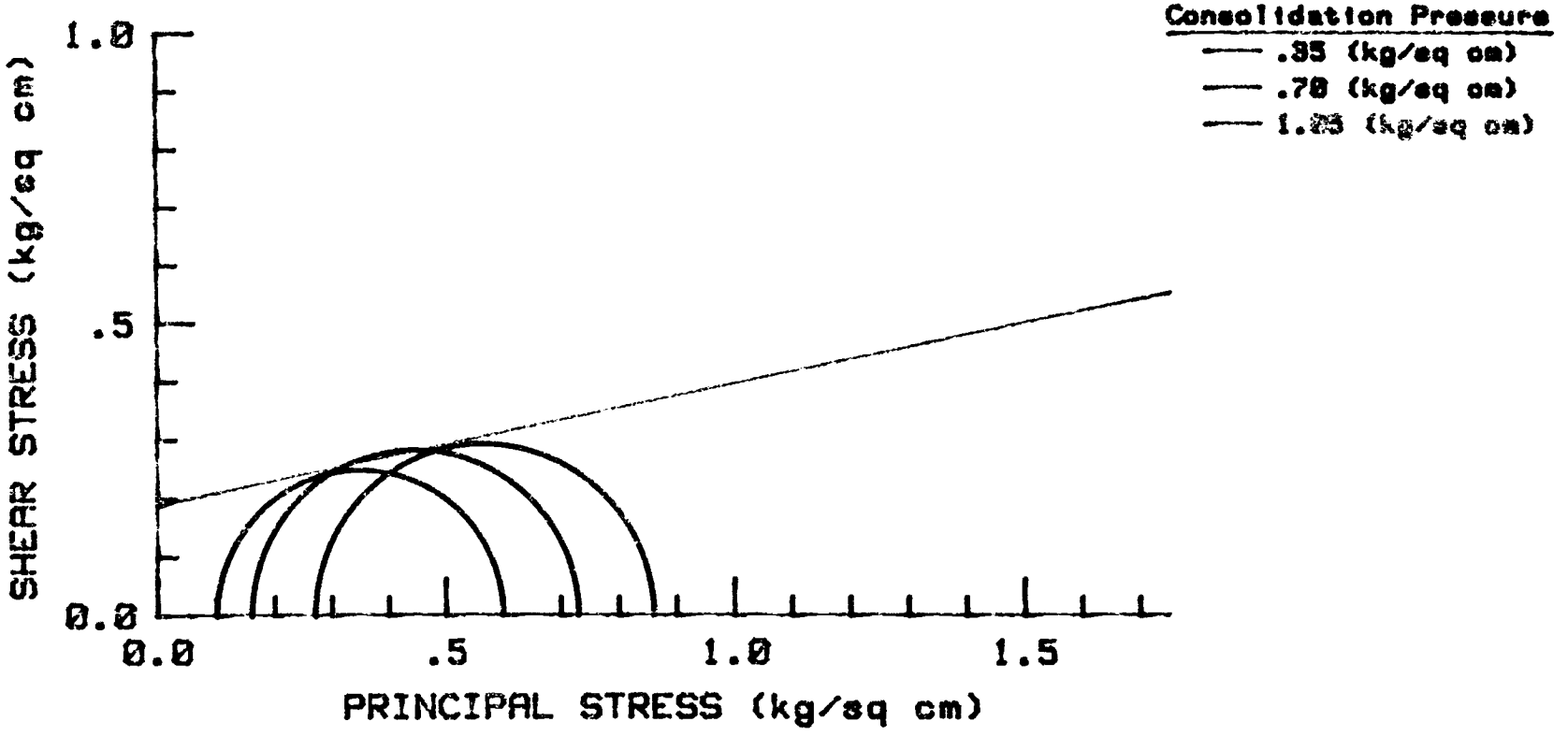

Strength testing summary of sample and test data

Site 11 - Alaska

Effective Consolidation Pressure ($\sigma_3 - U_o$ in Kg/cm^2)	0.35	0.70	1.05
Natural Moisture Content (W_n in %)	190.7	101.8	169.0
Insitu Wet Unit Weight (γ in g/cm^3)	1.25	1.35	1.29
Insitu Dry Unit Weight (γ_d in g/cm^3)	0.43	0.67	0.48
Insitu Degree Saturation (S in %)	97.3	90.1	98.2
Cell Pressure during Test (σ_3 in Kg/cm^2)	3.16	2.11	2.81
Initial Pore Pressure (U_o in Kg/cm^2)	2.81	1.41	1.76
B-Pore Pressure Parameter during Test (Ratio)	0.96	0.98	0.94

Strength testing summary of effective stress strength parameters

Site 11 - Alaska

For Mohr Envelope Derived from Stress-Strain Maximum Values				
Effective Consolidation Pressure ($\sigma_3 - U_o$ in Kg/cm^2)		0.35	0.70	1.05
Deviator Stress at Failure ($\Delta\sigma_1$ in Kg/cm^2)		0.73	1.0	1.43
Pore Pressure at Failure (ΔU in Kg/cm^2)		0.30	0.56	0.82
Axial Strain at Failure (ϵ in %)		3.0	7.0	5.0
A-Pore Pressure Parameter at Failure (Ratio)		0.41	0.56	0.57
Effective Angle of Internal Friction (ϕ' in Degrees)	$\phi' =$	41.5		
Effective Cohesion Intercept (C' in Kg/cm^2)	$C' =$	0.11		
Correlation Coefficient (r - dimensionless)	$r =$	.9990		
For Mohr Envelope Derived from Stress Ratio Maximum Values				
Effective Consolidation Pressure ($\sigma_3 - U_o$ in Kg/cm^2)		0.35	0.70	1.05
Deviator Stress at Failure ($\Delta\sigma_1$ in Kg/cm^2)		0.73	0.98	1.93
Pore Pressure at Failure (ΔU in Kg/cm^2)		0.3	0.57	0.82
Axial Strain at Failure (ϵ in %)		3.0	5.5	6.0
A-Pore Pressure Parameter at Failure (Ratio)		0.41	0.58	0.42
Effective Angle of Internal Friction (ϕ' in Degrees)	$\phi' =$	51.4		
Effective Cohesion Intercept (C' in Kg/cm^2)	$C' =$	0.04		
Correlation Coefficient (r-dimensionless)	$r =$	.9983		
For Mohr Envelope Derived from Effective Stress Path Plot				
Effective Angle of Internal Friction (ϕ' in Degrees)	$\phi' =$	43.2		
Effective Cohesion Intercept (C' in Kg/cm^2)	$C' =$	0.10		
Correlation Coefficient (r-dimensionless)	$r =$	1.0000		

ALASKA SITE 11
UNDISTURBED TRIAX. W/ BACKPRESSURE
DEVIATOR STRESS VS STRAIN

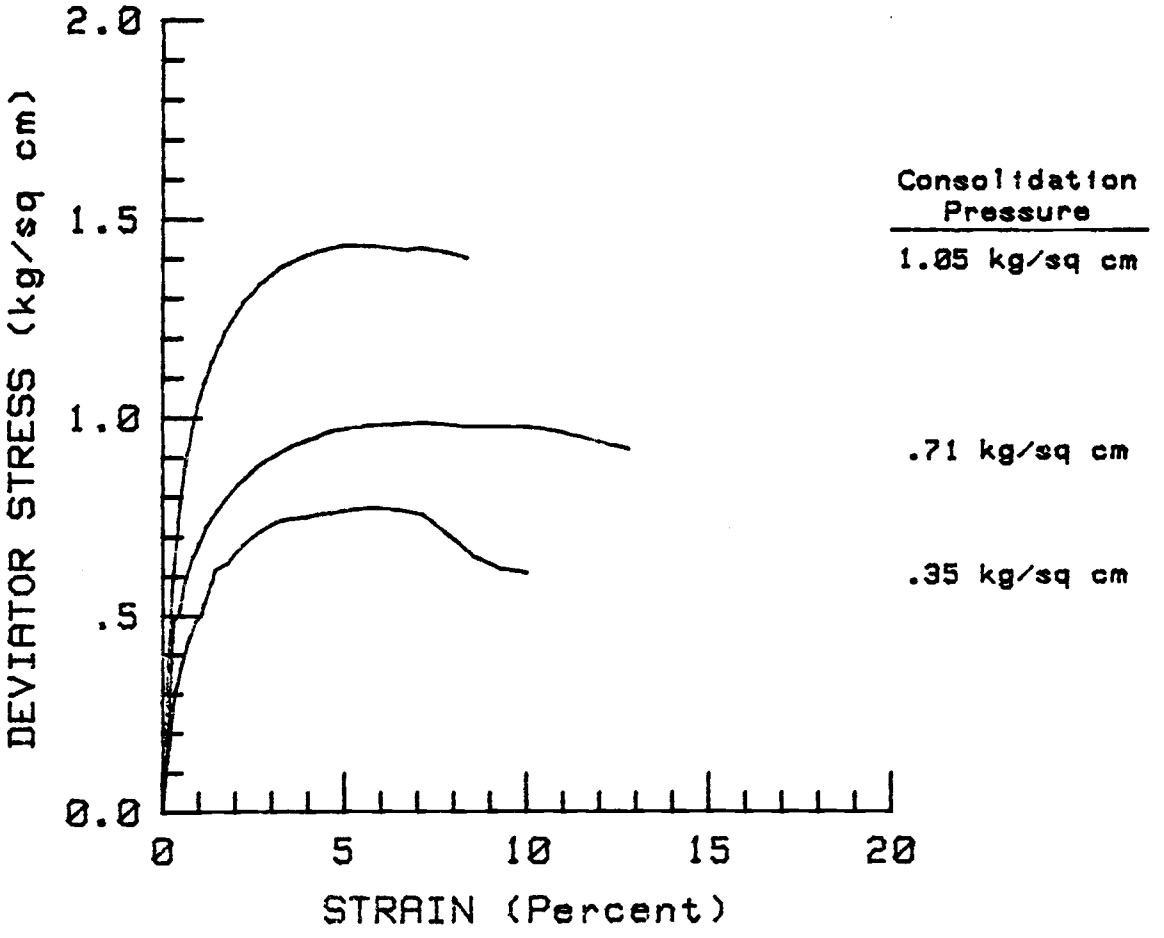

ALASKA SITE 11
UNDISTURBED TRIAX. W/ BACKPRESSURE
PORE WATER PRESSURE VS STRAIN

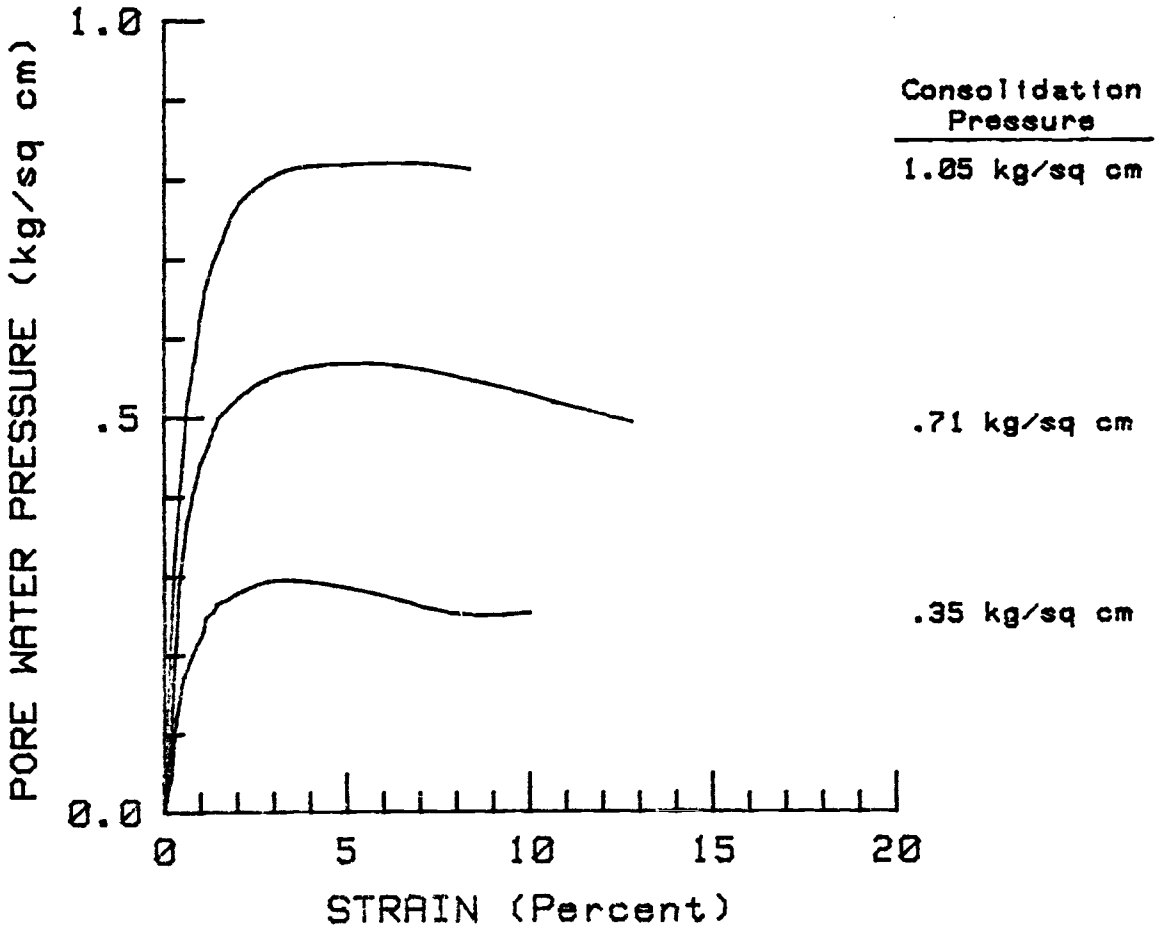

ALASKA SITE 11
UNDISTURBED TRIAX. W/ BACKPRESSURE
MAJOR PRINCIPAL STRESS RATIO VS STRAIN

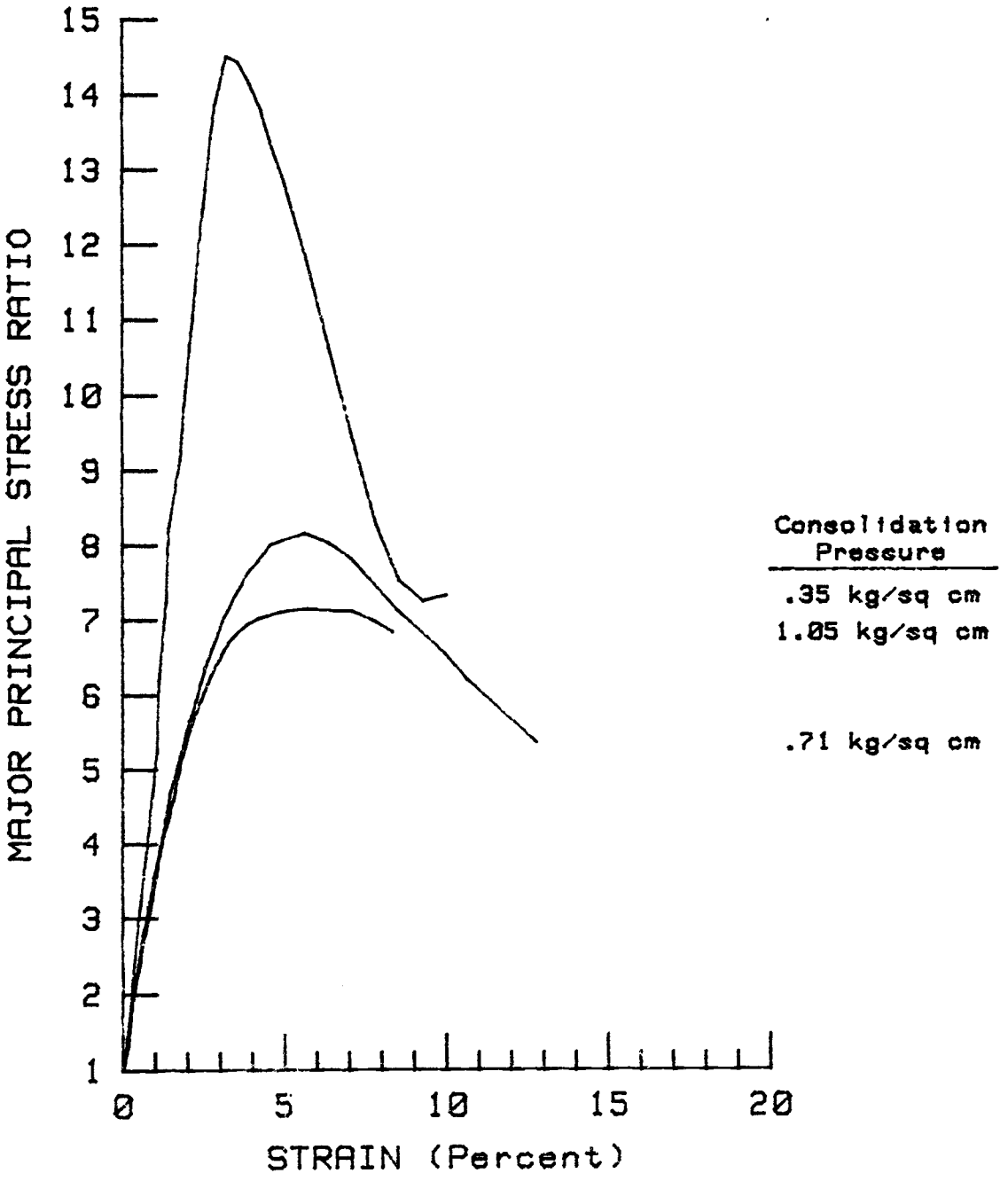

ALASKA SITE 11
UNDISTURBED TRIAX. W/ BACKPRESSURE
EFFECTIVE STRESS PATH PLOT

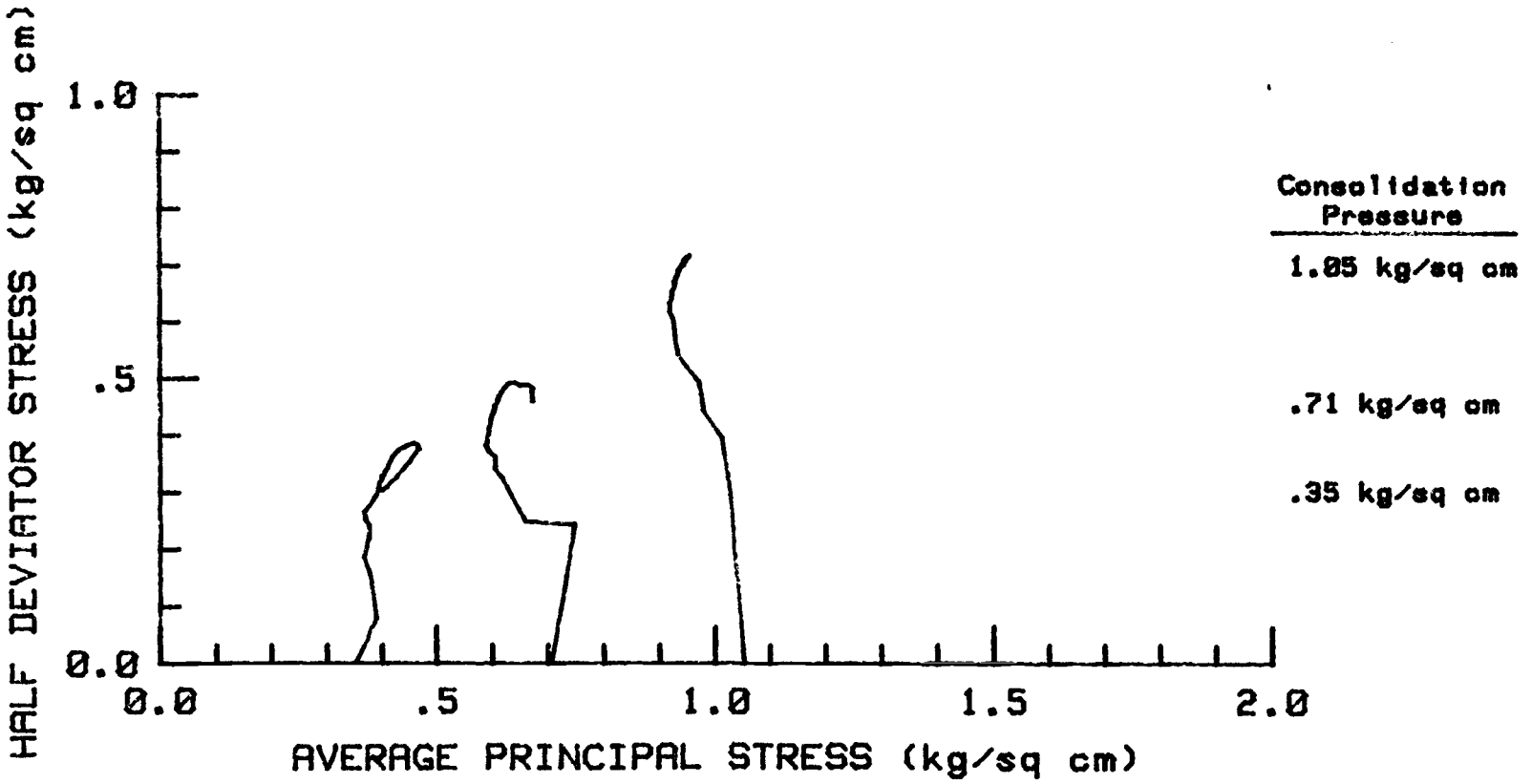

ALASKA SITE 11
UNDISTRBED TRIAX. W/ BACKPRESSURE
EFFECTIVE STRESS ENVELOPE

ANGLE OF INTERNAL FRICTION = 51.4 Degrees
COHESION INTERCEPT = .04 kg/sq cm

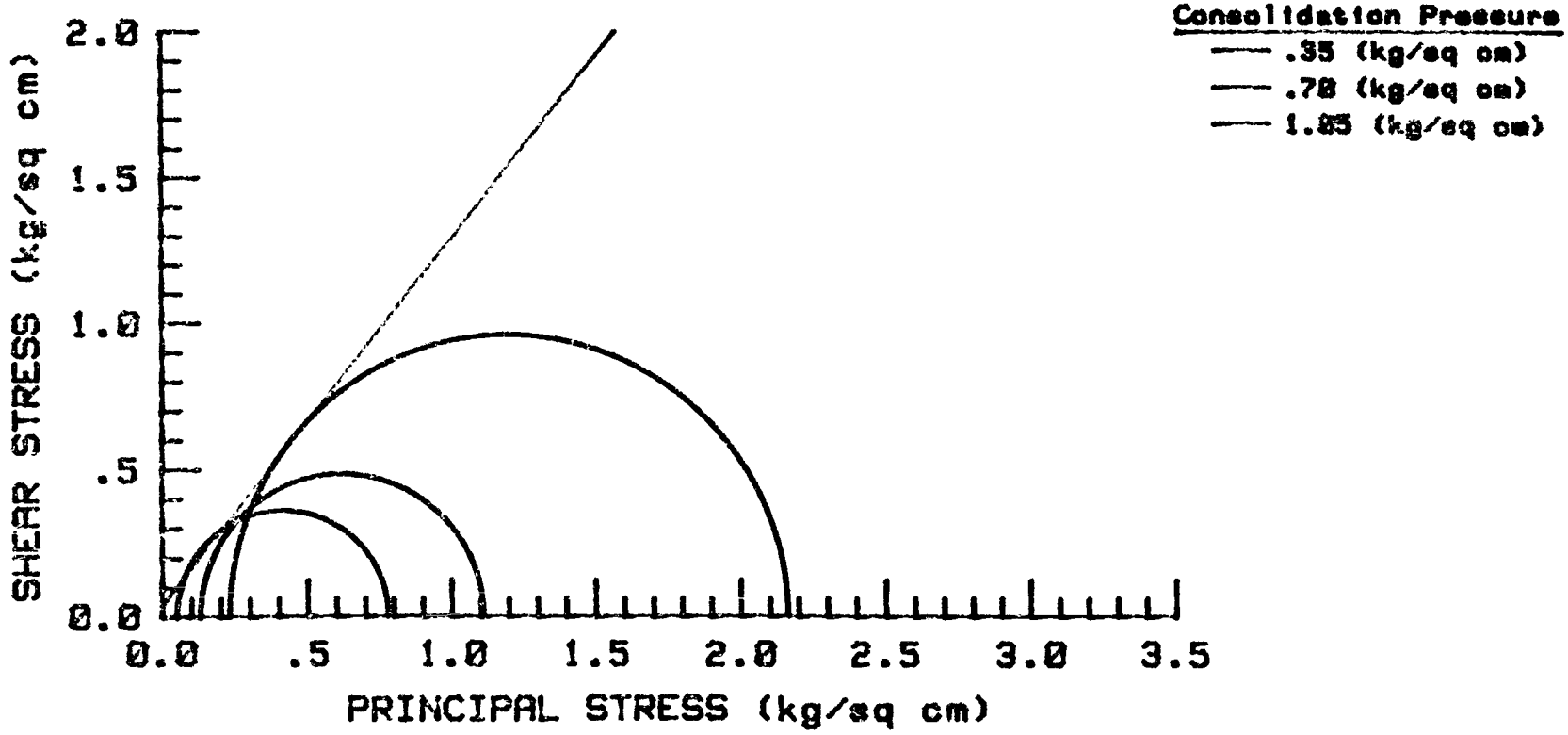

ALASKA SITE 11
UNDISTURBED TRIAX. W/ BACKPRESSURE
EFFECTIVE STRESS ENVELOPE

ANGLE OF INTERNAL FRICTION = 41.5 Degrees
COHESION INTERCEPT = .11 kg/sq cm

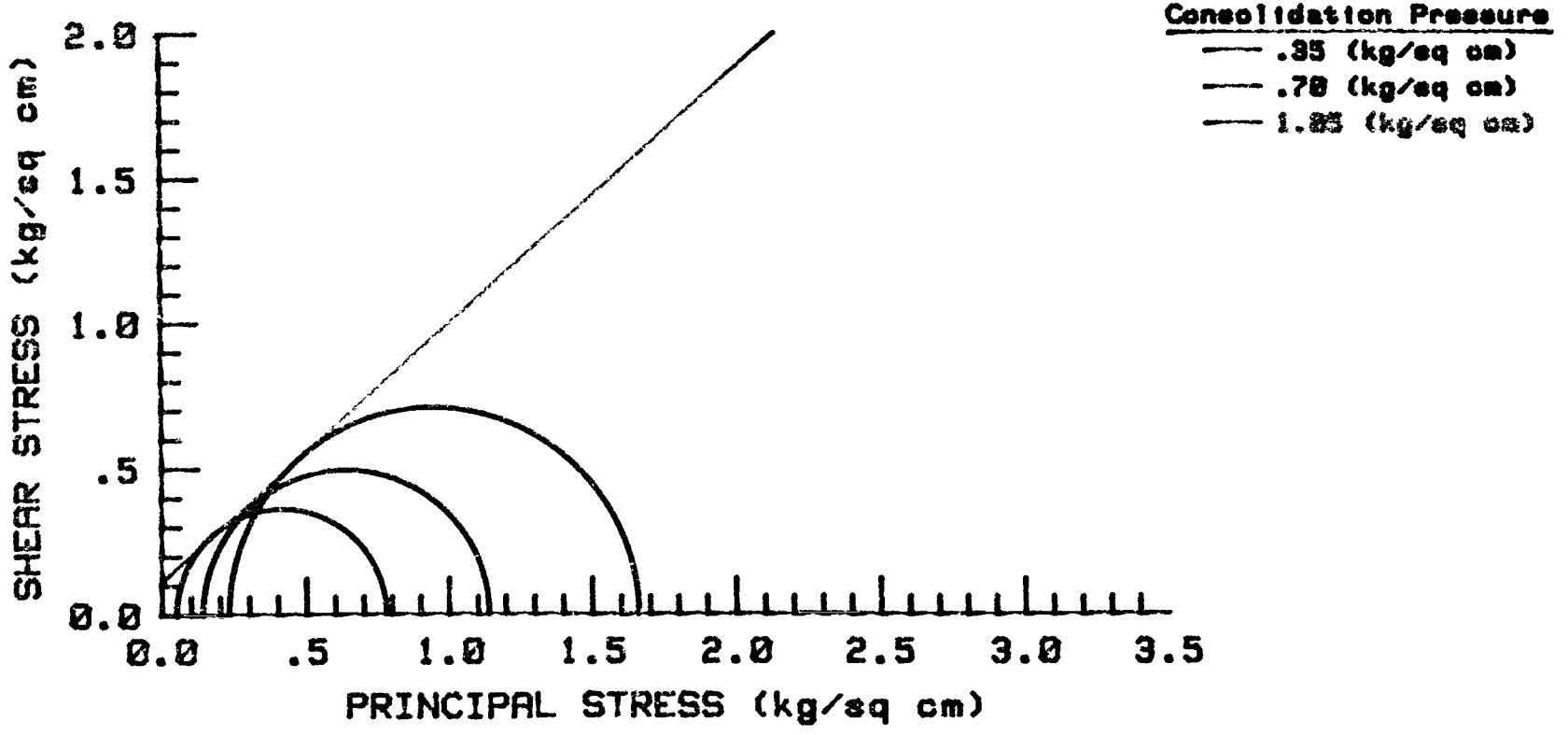

APPENDIX E

Laboratory Test Procedures -

Mineralogical Characterization

APPENDIX E

Laboratory Test Procedures - Mineralogical Characterization

Infrared Spectography

Fieldes and Furkert (1972) outlined an infrared absorption method for identifying components of whole soils without sample treatments other than air drying and grinding. The method used was as follows:

1. A large representative portion of soil sample was air dried at about 30° C to equilibrium.
2. This sample was ground and passed through a U.S. Standard Number 40 Sieve.
3. A subsample was ground and mixed thoroughly with 500 mg of KBr for several minutes with a hot dried mortar and pestle.
4. A 13 mm diameter disc was formed by pressing at 10,000 psi for several minutes in a specially machined die.
5. The discs were scanned from 4000 to 700 cm^{-1}, using a infrared absorption spectrometer.

Two discs were prepared for each sample, one with untreated dried soil, and the other treated with hydrogen peroxide for organic matter removal. Organic matter removal required that a soil slurry mixed with hydrogen peroxide be heated at low temperatures for several days until hydrogen peroxide - organic matter reactions

ceased. The slurry was then air dried and ground to a fine powder consistency.

The identification of allophane by this method is based on the 1620 cm^{-1} peak. As outlined by Fields and Farkert (1972), the type of allophane has an influence on the broad peak at about 1000 cm^{-1}. A siliceous allophane has a broad peak at 1080 cm^{-1}, normal allophane has a broad peak at 1030 cm^{-1}, and aluminum rich allophane has its broad peak at 980 cm^{-1}.

Transmission Electron Microscope

The preparation samples for transmission electron microscope (TEM) analysis was as related by John Hickman and Reid Glassman, both of the Department of Soil Science, Oregon State University. This sample preparation technique was based on much experience with preparation of volcanic ash soils for analysis with minimum mineralogical disturbance. Other treatments such as ultrasound separation or chemical dispersion may significantly alter the form and structure of these soils. Dispersion and separation of the clay fraction was as follows:

1. Whole soil samples at natural water content were wet sieved through a U. S. Standard Number 10 sieve.
2. The minus number 10 slurry was put into a capped 500 ml bottle. For each bottle of material, the pH was slightly

lowered by slowly adding 1 N-HCl into the solution until a pH of 4.5 was reached.

3. Each bottle of soil-HCl-distilled water slurry was gently agitated for twelve hours in a mechanical shaker.
4. The slurry was then passed through a U.S. Standard Number 270 sieve, and the minus Number 270 slurry retained.
5. pH was readjusted to 4.5.
6. Each bottle of slurry was agitated by hand shaking for a few seconds, then allowed to sit for 8 hours. Silt size particles will settle out of a 10 cm column during this time. Clay (< 2 mm) will be left in suspension.
7. Pour off and retain supernate.

Grid preparation was accomplished by preparing three carbon coated grids for each sample of supernate, each grid being a different dilution. These three dilutions were prepared in a 500 ml flask by:

1. Adding the soil-water mixture to distilled water in a 500 ml flask and diluting enough so that the solution was slightly cloudy. This diluted solution is dropped onto the first grid with a hyperdermic needle.
2. Pour out 250 ml of solution and add 250 ml of distilled water. Drop this more dilute solution onto grid number 2.

3. Pour out 250 ml of grid number 2 solution and add 250 ml of distilled water. Drop this very dilute solution onto grid number 3.

4. Air dry grids were stored in covered petrie dishes to prevent collection of dust.

This dilution technique assured adequate coverage of one of the grids without excessive concentrations of materials.

Several photographs representing general representative soil matrix were taken at 6500x magnification. Areas of further interest identified in the low magnification prints were magnified to 65000x by laboratory photographic techniques. At this magnification, a 50 A sphere would be .325 mm in diameter on the print.

Rapid Field and Laboratory Test for Allophane

This test was run in the laboratory according to a method outlined by Fieldes and Perrott (1966). This method required that a 10 mg portion of soil be placed on phenolphthalein paper and treated with a drop of 1 M NaF. The color reaction of the paper indicated the amount of allophanic activity the soil exhibits.

Phenolpthalein indicator paper is prepared by soaking strips of Whatman No. 42 filter paper in a solution composed of 1 g phenolpthalein dissolved in a 90% by volume ethyl alcohol solution. Dry

strips after soaking.

1 M NaF solution is prepared by maintaining a saturated aqueous NaF solution in the presence of excess undissolved NaF. This NaF solution solubolizes glass and therefore should be kept in a plastic bottle. This reagent is also very toxic, and should be handled with caution.

To test for allophanic activity, place a small amount of soil on horizontal phenolphthalein indicator paper. Allow 1 drop of saturated NaF solution to wet soil.

Subsoils containing large amounts of allophane quickly turn the indicator paper red. Colors resulting from this test on most soils will be red for more than 7% allophane, pink to red for 5 to 7%, and colorless for allophane percentages less than 5%.